POST-TRAUMATIC OSTEOARTHRITIS AFTER MENISCUS INJURY

EDITED BY: Andreas Martin Seitz, Tammy Haut Donahue, Fabio Galbusera, Jay Patel and Björn H. Drews

PUBLISHED IN: Frontiers in Bioengineering and Biotechnology

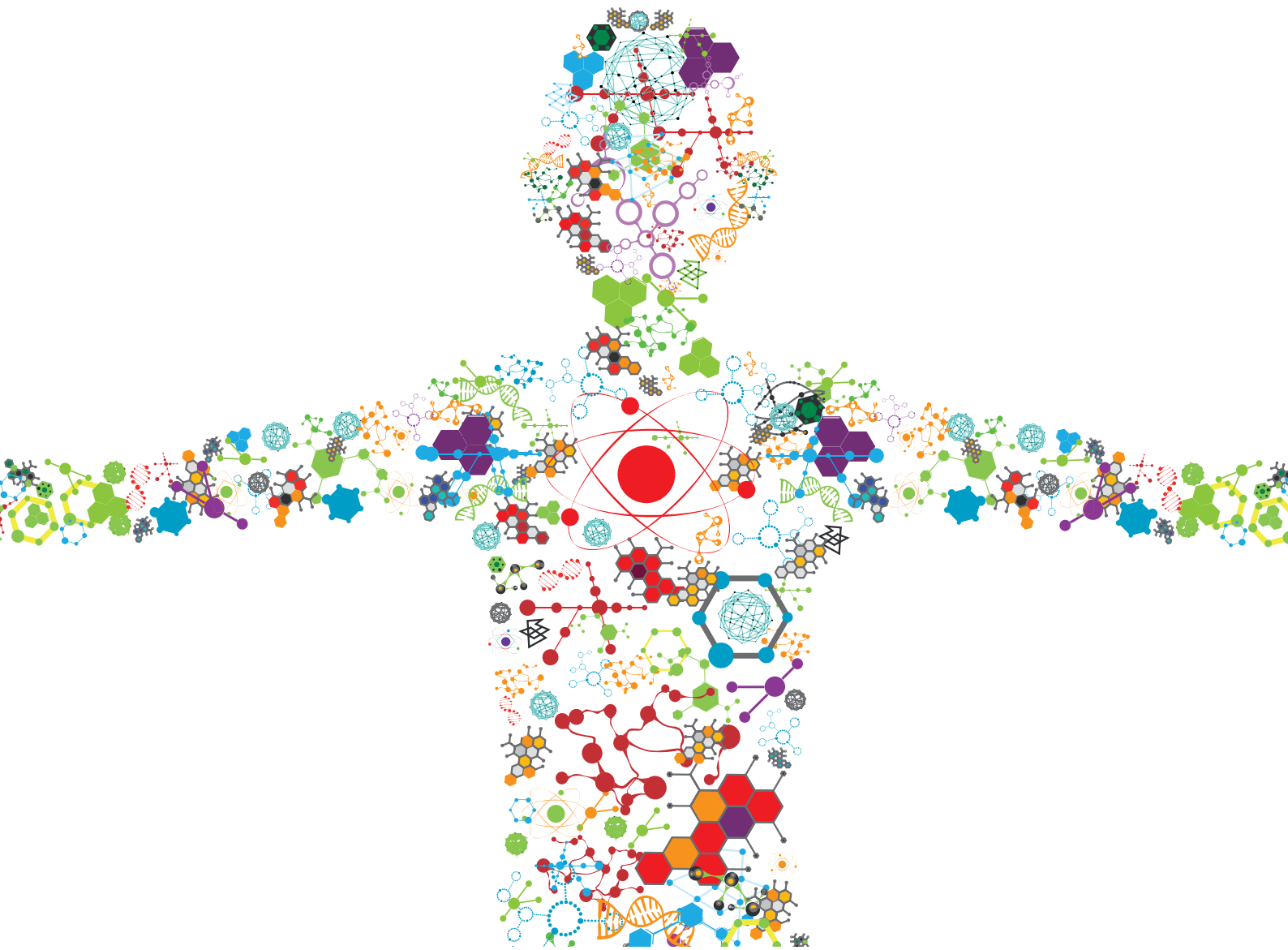

frontiers Research Topics

ISSN 1664-8714
ISBN 978-2-88976-019-0
DOI 10.3389/978-2-88976-019-0

About Frontiers

Frontiers is more than just an open-access publisher of scholarly articles: it is a pioneering approach to the world of academia, radically improving the way scholarly research is managed. The grand vision of Frontiers is a world where all people have an equal opportunity to seek, share and generate knowledge. Frontiers provides immediate and permanent online open access to all its publications, but this alone is not enough to realize our grand goals.

Frontiers Journal Series

The Frontiers Journal Series is a multi-tier and interdisciplinary set of open-access, online journals, promising a paradigm shift from the current review, selection and dissemination processes in academic publishing. All Frontiers journals are driven by researchers for researchers; therefore, they constitute a service to the scholarly community. At the same time, the Frontiers Journal Series operates on a revolutionary invention, the tiered publishing system, initially addressing specific communities of scholars, and gradually climbing up to broader public understanding, thus serving the interests of the lay society, too.

Dedication to Quality

Each Frontiers article is a landmark of the highest quality, thanks to genuinely collaborative interactions between authors and review editors, who include some of the world's best academicians. Research must be certified by peers before entering a stream of knowledge that may eventually reach the public - and shape society; therefore, Frontiers only applies the most rigorous and unbiased reviews.
Frontiers revolutionizes research publishing by freely delivering the most outstanding research, evaluated with no bias from both the academic and social point of view. By applying the most advanced information technologies, Frontiers is catapulting scholarly publishing into a new generation.

What are Frontiers Research Topics?

Frontiers Research Topics are very popular trademarks of the Frontiers Journals Series: they are collections of at least ten articles, all centered on a particular subject. With their unique mix of varied contributions from Original Research to Review Articles, Frontiers Research Topics unify the most influential researchers, the latest key findings and historical advances in a hot research area! Find out more on how to host your own Frontiers Research Topic or contribute to one as an author by contacting the Frontiers Editorial Office: frontiersin.org/about/contact

POST-TRAUMATIC OSTEOARTHRITIS AFTER MENISCUS INJURY

Topic Editors:
Andreas Martin Seitz, Ulm University Medical Center, Germany
Tammy Haut Donahue, University of Memphis, United States
Fabio Galbusera, Schulthess Klinik, Switzerland
Jay Patel, Emory University, United States
Björn H. Drews, St. Vinzenz Hospital, Germany

Citation: Seitz, A. M., Donahue, T. H., Galbusera, F., Patel, J., Drews, B. H., eds. (2022). Post-Traumatic Osteoarthritis After Meniscus Injury. Lausanne: Frontiers Media SA. doi: 10.3389/978-2-88976-019-0

Table of Contents

frontiers | Frontiers in Bioengineering and Biotechnology

EDITORIAL
published: 05 April 2022
doi: 10.3389/fbioe.2022.893800

Editorial: Post-Traumatic Osteoarthritis After Meniscus Injury

Jay M. Patel[1,2]*, *Tammy L. Haut Donahue*[3], *Fabio Galbusera*[4], *Björn H. Drews*[5] and *Andreas M. Seitz*[6]

[1]Department of Orthopaedics, Emory University, Atlanta, GA, United States, [2]Atlanta VA Medical Center, Decatur, GA, United States, [3]Department of Biomedical Engineering, University of Memphis, Memphis, TN, United States, [4]Schulthess Klinik, Zürich, Switzerland, [5]St. Vinzenz Hospital, Pfronten, Germany, [6]Institute of Orthopaedic Research and Biomechanics, Ulm University Medical Center, Ulm, Germany

Keywords: meniscus, osteoarthiritis, biomechanics, PTOA, meniscus repair

Editorial on the Research Topic

Post-Traumatic Osteoarthritis After Meniscus Injury

The menisci are fibrocartilaginous discs that are vital to load distribution and function of our knee joints. Due to their propensity for injury and relative lack of self-healing, these functions are often disrupted following traumatic injury. The result is the progression of post-traumatic osteoarthritis (PTOA), a huge burden on the population. In this Frontiers Research Topic, we bring together relevant contributions on various aspects of meniscal injury and PTOA progression, including meniscal function, metrics for studying PTOA, and repair considerations to prevent PTOA progression.

The meniscus has long been considered vital to distributing tibiofemoral loads in the joint (Lee et al., 2006). Sukopp et al. reviewed this literature, confirming that impaired knee joints (tears, meniscectomy, etc) consistently led to increased stresses. However, this review importantly noted that loading protocols were quite variable, and that future evaluation of load distribution may need better control to allow comparison across the field. Beyond load distribution, another meniscal function that has been up for debate is shock absorption. Classically, shock absorption had been cited as a key function of the menisci, until about 10 years ago (Andrews et al., 2011), when a nearly decade-long drop in Pubmed results for a search on "meniscus, shock absorption" is noted. Seitz et al. performed a robust evaluation of loss factors for intact, torn, and removed conditions, clearly demonstrating that there is indeed a shock absorbing function of the meniscus. Another important function of menisci is lubrication; de Roy et al. performed a study showing that both root injuries and meniscectomy do not affect whole joint friction. In the absence of changes to joint friction, patients may not "feel" a change that otherwise may result from catching or locking, and the initiation of PTOA under such conditions is likely associated with other functional deficits.

The effects of meniscal injury and removal on time-zero mechanics, as described previously, have been clearly linked to PTOA progression, especially in animal models involving destabilization of the medial meniscus (DMM) (Glasson et al., 2007; Bansal et al., 2020). Conversely, Haut Donahue et al. performed a morphological study on meniscus, cartilage, and bone health following a closed-joint traumatic injury model (resulting in ACL rupture), showing that even if the ACL was reconstructed after this injury, that the meniscus and cartilage still saw effects of damage. These new closed-joint models may better recreate the *in vivo* clinical situation, instead of the standard surgical DMM models. These models would also benefit from more standardized outcome metrics and guidance documents (Pfeifer et al., 2015), to truly evaluate the state of PTOA following meniscus injury, repair, and/or replacement. Trivedi et al. performed a systematic review of the outcome metrics of PTOA that were included in meniscus repair and replacement *in vivo* studies, showing that joint health is not always evaluated even if it is vital to determining the success of these approaches. Furthermore, new techniques

OPEN ACCESS

Edited and reviewed by:
Markus O. Heller, University of Southampton, United Kingdom

***Correspondence:**
Jay M. Patel
jay.milan.patel@emory.edu

Specialty section:
This article was submitted to Biomechanics, a section of the journal Frontiers in Bioengineering and Biotechnology

Received: *10 March 2022*
Accepted: *16 March 2022*
Published: *05 April 2022*

Citation:
Patel JM, Haut Donahue TL, Galbusera F, Drews BH and Seitz AM (2022) Editorial: Post-Traumatic Osteoarthritis After Meniscus Injury. Front. Bioeng. Biotechnol. 10:893800. doi: 10.3389/fbioe.2022.893800

are also being developed to analyze the state of articular cartilage, and could serve to identify early markers of PTOA that are not visible with current clinical imaging or arthroscopy. Gao et al. developed a novel confocal Raman microspectroscopy approach to spatially map glycosaminoglycan (GAG) loss, a technique that does not require tissue dissection or sampling, and that could be readily adapted toward non-destructive and potentially *in vivo* application (Gaifulina et al., 2021). Finally, in addition to establishing novel and consistent metrics for PTOA assessment, the identification of meniscal tears before PTOA initiation may be key to treating patients. Tack et al. utilized an MRI database from the Osteoarthritis Initiative, using a new neural network to identify meniscal tears. Combining these analytical advancements with technological innovations will give the field routes to identify both meniscal injuries and early markers of PTOA.

The multi-functional attributes of the meniscus, their influence on the progression of degenerative changes, and methods to evaluate early PTOA are all certainly of interest to the field. These findings, both inside and outside of this Research Topic, can also help to inform various repair and replacement techniques. For example, medial meniscus root tears are common yet present a huge mechanical burden due to a loss in load distribution and shock absorption (as noted by Sukopp et al., Seitz et al.). Repair of these root tears with transtibial techniques has shown promise (Pache et al., 2018); however, anatomic positioning of the repair site is also crucial. Floyd et al. show that non-anatomic repair of posterior medial meniscus root tears has consequences, including symptomatic extrusion, which may accelerate PTOA progression. Beyond root tears, research regarding the healing of the meniscal body post-injury is becoming increasingly common (Bansal et al., 2021), with the phrase "Save the Meniscus" commonly appearing in social medial and journal articles. Meniscus tear management often relies on the zone of tear; outer meniscus tears are repaired with suture and inner meniscus tears are typically treated with removal of the torn tissue (partial meniscectomy). This difference is often attributed to vascularity, however an opinion piece by Patel theorizes other factors that may be involved: circumferential disruption, obstruction by the dense matrix, and other joint factors (including inflammation). A couple of these factors were investigated by Andress et al., where anti-inflammatory modulation via compressive or tensile loading was confirmed with RNA-sequencing, verifying the role that loading (or lack thereof with disruption) may have in meniscal repair. Moreover, this contribution represents an exciting trend in meniscus research, combining omics and engineering to simultaneously study mechano-transduction and identify novel therapeutic targets. Finally, while identification of these therapeutic targets is important, implementing them *via* new scaffold technologies is also paramount. Dorthé et al. utilized a new technique called pneumatospinning, allowing the formation of thicker fiber mats that support fibrocartilage growth, and advancement over other nanofibrous scaffold fabrication techniques. This proof-of-concept study certainly warrants future exploration and may represent a method to better integrate with the native meniscal tissue.

As the meniscus research field continues to gain traction, this Frontiers Research Topic highlights new techniques in the field (Haut Donahue et al., Gao et al., Tack et al., Andress et al., Dorthé et al.), reviews the current state (Sukopp et al., Trivedi et al.), and establishes and/or challenges paradigms (Seitz et al., de Roy et al., Floyd et al., Patel), encompassing aspects of biomechanics, engineering, biology, and clinical management.

AUTHOR CONTRIBUTIONS

All authors listed have made a substantial, direct, and intellectual contribution to the work and approved it for publication.

REFERENCES

Andrews, S., Shrive, N., and Ronsky, J. (2011). The Shocking Truth about Meniscus. *J. Biomech.* 44, 2737–2740. doi:10.1016/j.jbiomech.2011.08.026

Bansal, S., Floyd, E. R., Kowalski, M., Aikman, E., Elrod, P., Burkey, K., et al. (2021). Meniscal Repair: The Current State and Recent Advances in Augmentation. *J. Orthop. Res.* 39, 1368–1382. doi:10.1002/jor.25021

Bansal, S., Miller, L. M., Patel, J. M., Meadows, K. D., Eby, M. R., Saleh, K. S., et al. (2020). Transection of the Medial Meniscus Anterior Horn Results in Cartilage Degeneration and Meniscus Remodeling in a Large Animal Model. *J. Orthop. Res.* 38, 2696–2708. doi:10.1002/jor.24694

Gaifulina, R., Nunn, A. D. G., Draper, E. R. C., Strachan, R. K., Blake, N., Firth, S., et al. (2021). Intra-operative Raman Spectroscopy and *Ex Vivo* Raman Mapping for Assessment of Cartilage Degradation. *Clin. Spectrosc.* 3, 100012. doi:10.1016/j.clispe.2021.100012

Glasson, S. S., Blanchet, T. J., and Morris, E. A. (2007). The Surgical Destabilization of the Medial Meniscus (DMM) Model of Osteoarthritis in the 129/SvEv Mouse. *Osteoarthritis and Cartilage* 15, 1061–1069. doi:10.1016/j.joca.2007.03.006

Lee, S. J., Aadalen, K. J., Malaviya, P., Lorenz, E. P., Hayden, J. K., Farr, J., et al. (2006). Tibiofemoral Contact Mechanics after Serial Medial Meniscectomies in the Human Cadaveric Knee. *Am. J. Sports Med.* 34, 1334–1344. doi:10.1177/0363546506286786

Pache, S., Aman, Z. S., Kennedy, M., Nakama, G. Y., Moatshe, G., Ziegler, C., et al. (2018). Meniscal Roots: Current Concepts Review. *Arch. Bone Jt. Surg.* 6 (4), 250–259. doi:10.22038/abjs.2018.26273.1694

Pfeifer, C. G., Fisher, M. B., Carey, J. L., and Mauck, R. L. (2015). Impact of Guidance Documents on Translational Large Animal Studies of Cartilage Repair. *Sci. Transl. Med.* 7, 310re9. doi:10.1126/scitranslmed.aac7019

Conflict of Interest: The authors declare that the research was conducted in the absence of any commercial or financial relationships that could be construed as a potential conflict of interest.

frontiers in Bioengineering and Biotechnology

ORIGINAL RESEARCH
published: 23 September 2021
doi: 10.3389/fbioe.2021.744065

The Natural History of Medial Meniscal Root Tears: A Biomechanical and Clinical Case Perspective

Edward R. Floyd[1], *Ariel N. Rodriguez*[2,3], *Kari L. Falaas*[4], *Gregory B. Carlson*[2], *Jorge Chahla*[5], *Andrew G. Geeslin*[6] *and Robert F. LaPrade*[2]*

[1]University of North Dakota School of Medicine and Health Sciences/Sanford Orthopedics & Sports Medicine, Fargo, ND, United States, [2]Twin Cities Orthopedics, Edina-Crosstown Surgery Center, Minneapolis, MN, United States, [3]Georgetown University School of Medicine, Washington, D.C., DC, United States, [4]University of Minnesota Medical School, Minneapolis, MN, United States, [5]Rush University Medical Center, Midwest Orthopaedics at Rush, Chicago, IL, United States, [6]Department of Orthopaedics and Rehabilitation, Larner College of Medicine, University of Vermont, Burlington, VT, United States

OPEN ACCESS

Edited by:
Andreas Martin Seitz, Ulm University Medical Center, Germany

Reviewed by:
Rene Verdonk, Ghent University, Belgium
Elmar Herbst, University of Muenster, Germany

***Correspondence:**
Robert F. LaPrade
lapradem dphd@gmail.com

Specialty section:
This article was submitted to Biomechanics, a section of the journal Frontiers in Bioengineering and Biotechnology

Received: *19 July 2021*
Accepted: *09 September 2021*
Published: *23 September 2021*

Citation:
Floyd ER, Rodriguez AN, Falaas KL, Carlson GB, Chahla J, Geeslin AG and LaPrade RF (2021) The Natural History of Medial Meniscal Root Tears: A Biomechanical and Clinical Case Perspective. Front. Bioeng. Biotechnol. 9:744065. doi: 10.3389/fbioe.2021.744065

Posterior medial meniscus root tears (PMMRTs) make up a relatively notable proportion of all meniscus pathology and have been definitively linked to the progression of osteoarthritis (OA). While known risk factors for development of OA in the knee include abnormal tibial coronal alignment, obesity and female gender, PMMRTs have emerged in recent years as another significant driver of degenerative disease. These injuries lead to an increase in average contact pressure in the medial compartment, along with increases in peak contact pressure and a decrease in contact area relative to the intact state. Loss of the root attachment impairs the function of the entire meniscus and leads to meniscal extrusion, thus impairing the force-dissipating role of the meniscus. Anatomic meniscus root repairs with a transtibial pullout technique have been shown biomechanically to restore mean and peak contact pressures in the medial compartment. However, nonanatomic root repairs have been reported to be ineffective at restoring joint pressures back to normal. Meniscal extrusion is often a consequence of nonanatomic repair and is correlated with progression of OA. In this study, the authors will describe the biomechanical basis of the natural history of medial meniscal root tears and will support the biomechanical studies with a case series including patients that either underwent non-operative treatment (5 patients) or non-anatomic repair of their medial meniscal root tears (6 patients). Using measurements derived from axial MRI, the authors will detail the distance from native root attachment center of the non-anatomic tunnels and discuss the ongoing symptoms of those patients. Imaging and OA progression among patients who were treated nonoperatively before presentation to the authors will be discussed as well. The case series thus presented will illustrate the natural history of meniscal root tears, the consequences of non-anatomic repair, and the findings of symptomatic meniscal extrusion associated with a non-anatomic repair position of the meniscus.

Keywords: meniscus, meniscus root tear, meniscus root repair, meniscal extrusion, osteoarthritis

INTRODUCTION

The meniscus plays a central role in protecting the overall health of the knee, and, while underappreciated in previous years, the maintenance of its integrity has emerged as a key factor in joint preservation (Sims et al., 2009; Yusuf et al., 2011; Driban et al., 2016; Foreman et al., 2020; Willinger et al., 2020). The current literature reports that 78% of patients under the age of 60 undergoing total knee arthroplasty (TKA) have sustained medial meniscal root tears (Choi and Park, 2015). However, lack of recognition, under-diagnosis, and neglect of meniscal root tears continue to be a preventable cause of osteoarthritis and TKA (LaPrade et al., 2014; Packer and Rodeo, 2009; Stärke et al., 2010a; Cinque et al., 2018).

A meniscal root tear may be defined as a complete radial tear within 1 cm of the anterior or posterior tibial attachment of the menisci or an avulsion of the attachment (LaPrade et al., 2014; Cinque et al., 2018; LaPrade et al., 2015a). Injuries causing meniscal root tears tend to occur during deep squatting or activities involving flexion, usually occurring concurrently with some type of rotation (LaPrade et al., 2014; Matheny et al., 2015). Injuries contributing to radial tears are often predicated by degenerative changes of the meniscus, which commonly occur in adults in their fourth or fifth decade of life and/or in obese individuals (Hwang et al., 2012; Brophy et al., 2019; Krych et al., 2020).

The association of medial meniscal root tears with progression to osteoarthritis of the knee has been well-documented in clinical studies. The circumferential fibers of the meniscus distribute vertically oriented compressive forces across the knee into axially directed "hoop stresses," thereby evenly distributing the load to the chondral surfaces (Athanasiou and Sanchez-Adams, 2009; Bansal et al., 2021). Meniscus root tears disrupt this biomechanical function, leading to increases in average contact pressure in the medial compartment (59–78%), secondary to a decrease in contact area (36–37% relative to the intact state) (Padalecki et al., 2014). These increases in average contact pressure may be greater in cases of concurrent varus deformity (Lim et al., 2008). The biomechanical consequences of a complete medial meniscus posterior root tear (MMPRT) are equivalent to those following a total medial meniscectomy (Allaire et al., 2008; Bedi et al., 2010). Root avulsions and radial tears up to 10 mm from the root attachment have been biomechanically validated to be functionally similar, resulting in significantly decreased contact areas at all flexion angles, as well as significantly increased mean and peak contact pressures (Padalecki et al., 2014; LaPrade et al., 2015b). This altered force profile in the knee may lead to meniscal extrusion and subsequent loss of articular cartilage (Athanasiou and Sanchez-Adams, 2009; Bedi et al., 2010).

This article will seek to explore the cause-effect and temporal relationship between meniscus root tears, meniscal extrusion, and development of the hallmarks of OA and its clinical implications. The authors will explain the anatomy and biomechanics for this natural history first, followed by case examples from the senior author's practice to provide illustration of the degenerative process following medial meniscus posterior root tears.

Anatomy

The meniscal root attachments play an integral role in anchoring the meniscus and preventing extrusion (LaPrade et al., 2014). Non-anatomical repair of the meniscal roots is reported to lead to osteoarthritic changes and may eventually necessitate TKA; thus, precise anatomic landmarks to guide arthroscopic meniscal root repair have been established (LaPrade et al., 2014; Johannsen et al., 2012a; Krych et al., 2017). The medial meniscus posterior root attachment (MPRA) is 9.6 mm posterior and 0.7 mm lateral to the medial tibial eminence (MTE) apex (or 11.5 ± 0.9 mm in direct distance) (LaPrade et al., 2014). The MPRA is 18.0 mm anterior to the posterior margin of the tibial plateau (James et al., 2014). The MPRA is 3.5 mm lateral to the articular cartilage inflection point of the medial plateau and 8.2 mm from the nearest point of the posterior cruciate ligament (PCL) footprint (Johannsen et al., 2012a). The footprint area of the MPRA is a mean of 30.4 mm^2. Three of the four meniscal roots, the posteromedial, posterolateral and anteromedial (PM, PL, and AM, respectively) also possess supplementary fibers which contribute significantly to the ultimate failure strength of each root attachment. Notably, the shiny white fibers (SWFs) of the PM root have been reported to account for up to 47.8% of the native root strength, and failure to incorporate these structures may impair the efficacy of current repair techniques (Ellman et al., 2014).

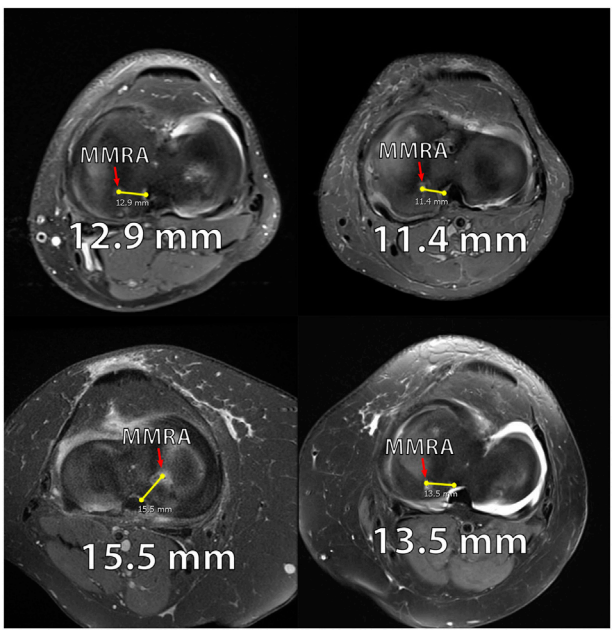

FIGURE 1 | Axial MRIs of 4 patients from the nonanatomic meniscal root reconstruction cohort. **(A)**: MRI of Nonanatomic Patient #1 displaying the medial meniscus root attachment 12.9 mm from anatomic attachment site (right knee). **(B)**: MRI of Nonanatomic Patient #5 displaying the medial meniscus root attachment 11.4 mm from anatomic attachment site (right knee). **(C)**: MRI of Nonanatomic Patient #4 displaying the medial meniscus root attachment 15.5 mm from anatomic attachment site (left knee). **(D)**. MRI of Nonanatomic Patient #6 displaying the medial meniscus root attachment 13.5 mm from anatomic attachment site (right knee).

Magnetic resonance imaging (MRI) is the gold standard to diagnose root tears with a specificity of 73% and sensitivity of 77% and NPV of 97% (Lee et al., 2014). A pathognomonic sign of meniscus root tear is the absence of an identifiable meniscus on sagittal sequence (referred to as the "ghost sign") (LaPrade et al., 2014; Cinque et al., 2018; Chahla et al., 2016). Other characteristic signs of meniscal tear include increased fluid accumulation around the meniscal root, >3 mm meniscal extrusion on a coronal image from the tibial articular edge, and "truncation signs" which are vertical line defects at the meniscal root attachment (James EWJ et al., 2017). Physical exam alone is often ineffective at diagnosing a posterior meniscus root tear, though palpable extrusion can sometimes be detected (Seil et al., 2011). A thorough history of pain with deep flexion, limited activity, and sometimes an popping sensation at the time of the inciting event can be helpful in diagnosing posterior meniscus root tear.

Biomechanics

In vitro, biomechanical studies report that a meniscal root tear is equivalent to a total meniscectomy. Allaire et al. (2008) demonstrated that there was no difference in contact pressures

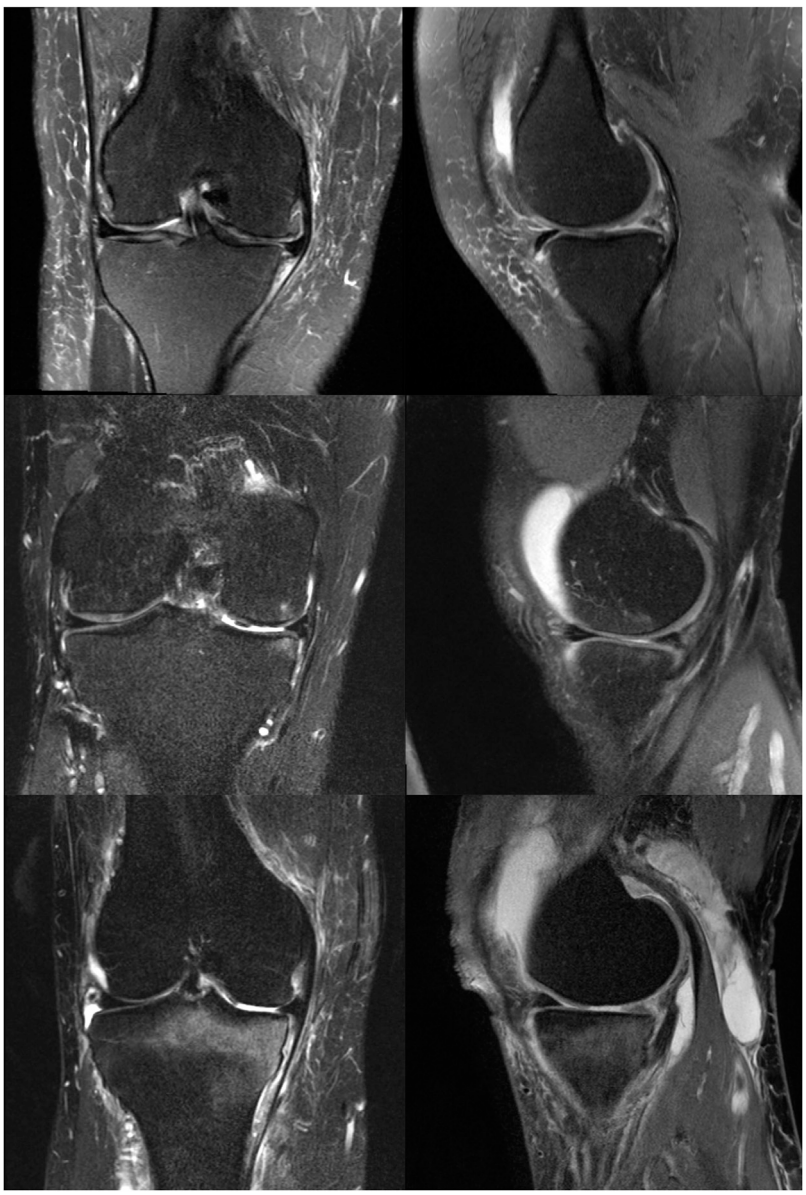

FIGURE 2 | Coronal and Sagittal MRIs of patients from the natural history cohort. **(A)**: Coronal and sagittal MRI of Natural History patient #1 illustrating medial meniscus extrusion and mild bony edema (right knee). **(B)**: Coronal and sagittal MRI of Natural History patient #3 illustrating mild medial meniscus extrusion and moderate bony edema (right knee). **(C)**: Coronal and sagittal MRI of Natural History Patient #6 illustrating mild medial meniscus extrusion and moderate to severe bony edema (right knee).

TABLE 1 | This table illustrates the distances between the tibial tunnel and the medial meniscus posterior root attachment. These measurements were taken using axial views of the MRIs of patients who underwent nonanatomic repair of the posterior medial meniscal root.

Patients with nonanatomic repairs	Tibial tunnel measured distance from anatomic medial meniscus posterior root attachment (mm)
Patient #1	12.9
Patient #2	8.2
Patient #3	14.0
Patient #4	15.5
Patient #5	11.4
Patient #6	13.5

between a meniscal root tear and a complete meniscectomy, suggesting their functional similarity (Allaire et al., 2008). The cadaver study found that a posterior root tear of the medial meniscus resulted in an increase of peak contact pressure of 25% in comparison to an intact meniscus. Furthermore, the authors found a 2.98° increase in external rotation and 0.84 mm increase of lateral tibial translation in knees with root tears. Contact pressure and rotation/translation were restored following repair.

Padalecki et al. examined the changes in average compartment pressures and contact area after medial meniscus root avulsions and radial tears at 3-, 6-, and 9 mm from the root, along with changes found after an anatomic repair. According to the authors' findings, the contact area for an intact meniscus ranges from 360 mm^2 at 90° to 450 mm^2 at 0°. Pooled findings across ROM conditions indicated that the actual contact area of the knee had an average 36% decrease for PMMR avulsions and 37% decrease for complete radial tears at 3-, 6-, and 9 mm from the root attachment. The authors found that average medial compartment contact pressures increased by 69% after root avulsions and 59–78% for radial tears near the root. For knee flexion angles greater than 0°, a meniscal root repair with a transtibial pullout technique restored contact pressures and area close to the normal range to be statistically indistinguishable (Padalecki et al., 2014).

One study reported that a 5 mm posteromedial fixation from the anatomic root attachment site (nonanatomic repair) resulted in increased average contact pressures and decreased contact area when compared to both the intact state and an anatomic repair (Packer and Rodeo, 2009). An anatomic root repair was reported to lead to significantly higher contact area, as well as lower average contact pressures across 0°, 30°, 60°, and 90° of flexion. Peak contact pressures were significantly increased for nonanatomic repairs by 59% relative to the intact state when pooled across all flexion angles, and peak contact pressures at 90° were significantly higher (+47%) for nonanatomic repairs in comparison to anatomic repairs (LaPrade et al., 2015b). These patients present in clinic with classic symptoms of OA, which include progressive pain and swelling.

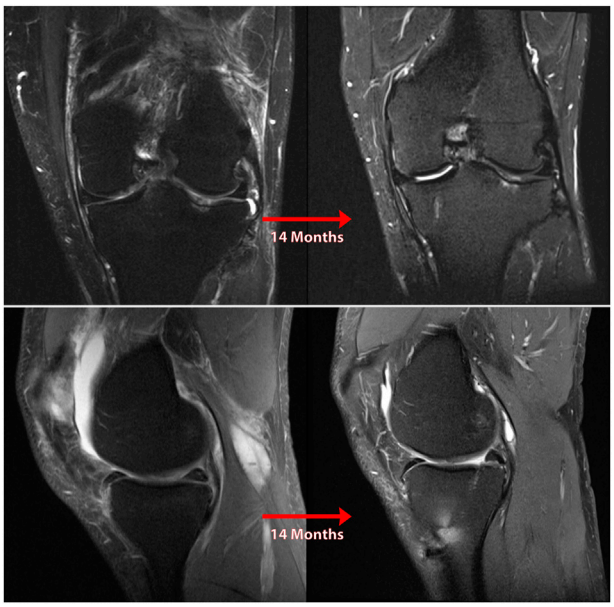

FIGURE 3 | Coronal **(A)** and sagittal **(B)** MR images of nonanatomic root repair patient #1 showing progression of osteoarthritis in the medial compartment of the knee over 14 months secondary to nonanatomic medial meniscus root repair (left knee). M = medial; L = lateral; A = anterior; P = Posterior.

Meniscal extrusion usually occurs secondary to medial meniscal root tears. As a consequence of extrusion, the torn meniscus may become adherent to the posteromedial joint capsule. Nonanatomic repairs may ultimately fail because they secure the meniscus in this non-functional, extruded position. Meniscal extrusion has been correlated with radiographic signs of osteoarthritis (Strauss et al., 2016). Despite the success of an anatomic repair under ideal circumstances, cyclic loading, representative of postoperative rehabilitation, or suture cut-out from the meniscal tissue, present ongoing problems even with correct surgical technique (LaPrade et al., 2015c). Use of an additional transtibial centralization suture may successfully

TABLE 2 | This table illustrates characteristics and timelines of the natural history of medial meniscus root tears. Cartilage degradation characteristics and extent of meniscal extrusion can be seen for each patient who had a neglected posterior medial meniscus root tear.

Natural history patients	Femorotibial joint space narrowing	Interval from injury (months)	Cartilage defect size	Cartilage defect grade	Meniscus extrusion
Natural History #1	Not applicable	60	Not applicable	Not applicable	Not applicable (unicompartmental arthroplasty)
Natural History #2	None	6	Not Measured	4	3 mm
Natural History #3	Not applicable	24	Not applicable	Not applicable	Not Applicable
Natural History #4	None	5	0.9 × 1.7 cm	4	3 mm
Natural History #5	None	15	Not measured	2	5 mm

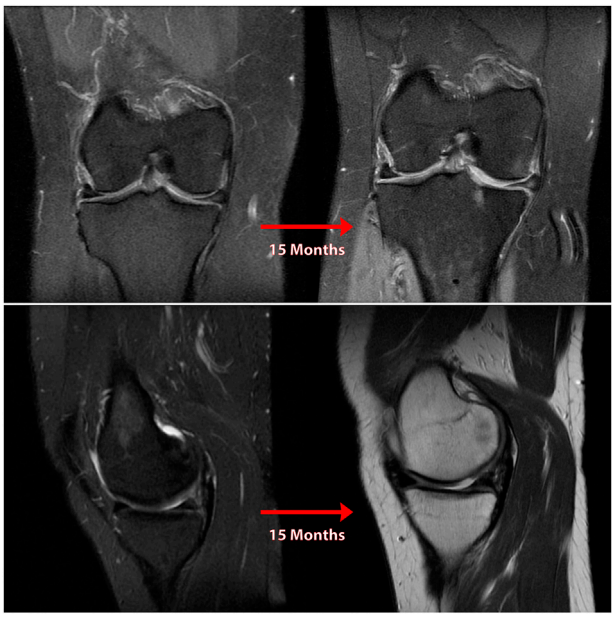

FIGURE 4 | Coronal **(A)** and sagittal **(B)** MR images of nonanatomic root repair patient #2 showing progression of osteoarthritis in the medial compartment of the knee over 15 months secondary to nonanatomic medial meniscus root repair (right knee). M = medial; L = lateral; A = anterior; P = Posterior.

treat meniscal extrusion and provides an additional point of fixation thereby protecting the repair (Daney et al., 2019; Dean et al., 2020a). Additional considerations include the effects of coronal malalignment; varus alignment has been linked to increased medial meniscus extrusion (Willinger et al., 2020).

Clinically, meniscectomy and non-operative treatment have shown inferior outcomes in preventing the progression of osteoarthritis (Stärke et al., 2010b; LaPrade et al., 2015b; Faucett et al., 2019). It has been reported in one study that, over 10 years, patients with medial meniscus root tears undergoing meniscectomy and nonoperative management progress to osteoarthritis at rates of 99.3 and 95.1%, respectively, in comparison to a significantly lower rate found following meniscus root repair (53.0%) (Faucett et al., 2019). However, the rate of osteoarthritis progression is variable and dependent on patient health and activity level. Another study reported that 87% of menisci treated non-operatively failed, with 31% of cases resulting in eventual total knee arthroplasty (TKA) (Krych et al., 2017). This results in the need for TKA or a subsequent surgery to release the extruded meniscus and return it to an anatomic location (LaPrade et al., 2015b; Choi and Park, 2015; Faucett et al., 2019).

Transtibial Two-Tunnel Pullout Repair

Indications for repair include healthy, active patients with PMMRTs. While age cutoffs have been sometimes applied, in the senior author's practice the relative health and activity level of the patient plays a large role in determining their potential benefit from an anatomic root repair. Advanced radiographic signs of OA is a counterindication.

If the meniscus root tear is scarred in an extruded position, an extensive peripheral release using scissor biters is performed first to separate the meniscus from the capsular wall (Dean et al., 2020b). An anatomic two tunnel transtibial pullout root repair is then performed to reposition the meniscus back into an anatomic position. In the transtibial pullout technique, the meniscal root is re-anchored to the tibial plateau by passing sutures through the meniscal root and retrieving them through transtibial tunnels (Dean et al., 2020b).

Initial incisions for the transtibial tunnels are made just medial to the tibial tubercle. The root attachment site is cleared to bleeding bone with a curette to facilitate healing (Dean et al., 2020b). The first tunnel is created along the posterior aspect of the posterior root attachment site using a tibial tunnel guide, while the second tunnel is created approximately 5 mm from the initial tunnel using an offset guide (Dean et al., 2020b). The torn meniscal root is repositioned into its anatomic location. A self-capture passer helps in passing two sutures or suture-tapes in a simple or vertical mattress configuration through the far posterior portion of the detached meniscal root, approximately 5 mm from the medial meniscus's lateral edge (Dean et al., 2020b). Lee et al. reports that using two sutures for repair showed improved outcomes for patients (Lee et al., 2014). As the sutures are passed through transtibial tunnels, care should be taken to avoid soft tissue bridging and a cannula may be used to facilitate suture shuttling (Dean et al., 2020b). The sutures are secured over a cortical fixation device on the anteromedial tibia with the knee flexed at 90° (Cinque et al., 2017). The posterior root of the medial meniscus should be visualized arthroscopically to confirm a secure repair.

CASES

Nonanatomic Repair

From the authors' practices, six patients who underwent revision root repair for initial nonanatomic posterior medial meniscus root tear (PMMRT) repairs were examined. (**Table 1**) These patients continued to exhibit painful symptoms and progression of osteoarthritis after a nonanatomic medial meniscus repair. The distance of the initial nonanatomic root repairs was measured on axial MRI, with measurements taken using an electronic image storage system client (IMPAX client 6 AGFA, Mortsel, Belgium) for picture archiving and communication system (PACS). The most proximal axial MRI slice was identified in which the transtibial root repair tunnel from the initial surgery could be seen. A line was then measured from the center of the nonanatomic tunnel to the center of the native PMMR attachment site, as determined by measurements given in Johannsen et al. (2012b).

The distances thus measured ranged from 8.2 to 14.0 mm, representing the distance from the initial tunnel to the anatomic attachment area (**Table 1**). Extrusion of the medial meniscus was noted in all cases. The interval of these patients from initial evaluation to revision ranged 5–17 months (date of initial surgery only available for patients 1, 2, 4 and 6). Patients were predominantly in their fifth decade.

FIGURE 5 | Coronal **(A and B)**, sagittal **(B)**, and axial **(C)** MR images of nonanatomic root repair patient #3 showing evidence of osteoarthritis in the medial compartment of the knee secondary to nonanatomic medial meniscus root repair (right knee). M = medial; L = lateral; A = anterior; P = Posterior.

For these patients, revision meniscus root repair was indicated. The extruded meniscus was released from the capsule, and an anatomic meniscus root repair was performed in the manner outlined above. Follow-up reports at 1 year were available for patients 1, 2 and 4. They reported improvement in symptoms and radiographic signs of osteoarthritis showed no progression. (See **Figures 1**–**8**).

Progression of Osteoarthritis in Untreated Meniscus Root Deficiency

Another five patients were examined who had identifiable PMMRTs at some point in the past and did not undergo meniscus root repair. Subsequent imaging demonstrated the progression of osteoarthritis (OA) following their untreated tear, following the known natural history of posterior meniscus root lesions. Information regarding these patients, in whom the natural history of OA progression can be observed following meniscus root tear, is given in **Table 2**.

Imaging studies verifying PMMRTs was available for each of these patients, whether from a prior provider or from the senior author's practice. The presence of a complete medial meniscus root tear without end-stage OA was verifiable on prior imaging for most of these patients, and new MRIs were obtained demonstrating the development of chondromalacia, full-thickness cartilage defects, meniscal extrusion, and joint space narrowing. Each of these patients is detailed below.

Patient 1, a 30-year-old male, suffered an iatrogenic PMMRT during posterior cruciate ligament (PCL) reconstruction, at which time the cartilage surfaces appeared healthy. The meniscus root was not repaired, and 5 years later severe medial compartment OA necessitated unicompartmental knee arthroplasty at the age of 29. The patient's course of treatment was complicated by an initially untreated PMMRT. (See **Figure 9**).

Patient 2, a 39-year-old male, suffered a PMMRT and was treated with partial medial meniscectomy (PMM). Within 6 months, the patient was highly symptomatic and an MRI at the authors' practice demonstrated grade III-IV chondromalacia of the MFC and medial tibial plateau (MTP) over a 15 × 18 mm area on both surfaces, in addition to a full-thickness radial tear a the far posterior PHMM.

Patient 3, a 43-year-old female, experienced a PMMRT and was seen in the senior author's practice. An MRI at the time of initial visit demonstrated normal, healthy cartilage surfaces. The patient declined treatment, and at 6 months after the initial visit, communicated that she was increasingly symptomatic with pain and functional limitation. Returning at 2 years after injury, new MRIs were obtained (See **Figure 10**) which demonstrated meniscal extrusion, abundant subchondral edema, loss of cartilage surface on the MFC and MTP weight-bearing areas

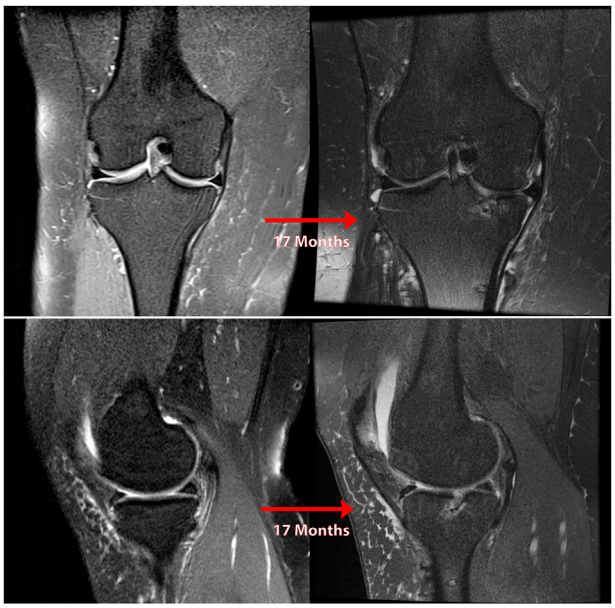

FIGURE 6 | Coronal **(A)** and sagittal **(B)** MR images of nonanatomic root repair patient #4 showing progression of osteoarthritis in the medial compartment of the knee over 17 months secondary to nonanatomic medial meniscus root repair (right knee). M = medial; L = lateral; A = anterior; P = Posterior.

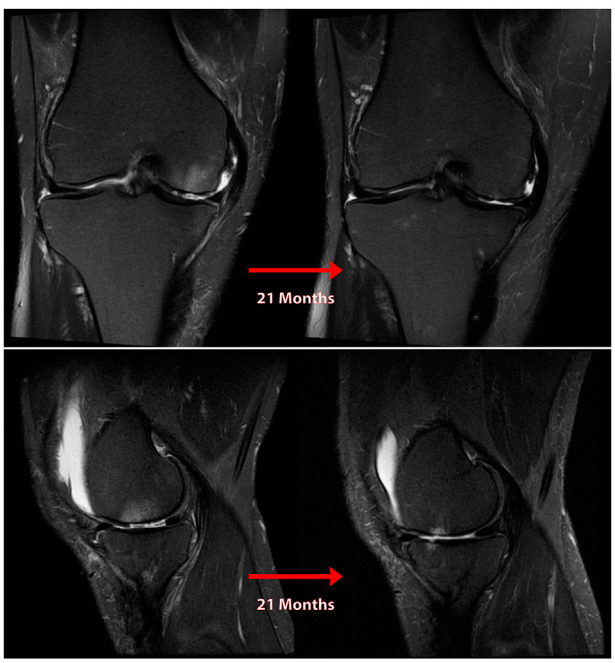

FIGURE 7 | Coronal **(A)** and sagittal **(B)** MR images of nonanatomic root repair patient #5 showing progression of osteoarthritis in the medial compartment of the knee over 21 months secondary to nonanatomic medial meniscus root repair (right knee). M = medial; L = lateral; A = anterior; P = Posterior.

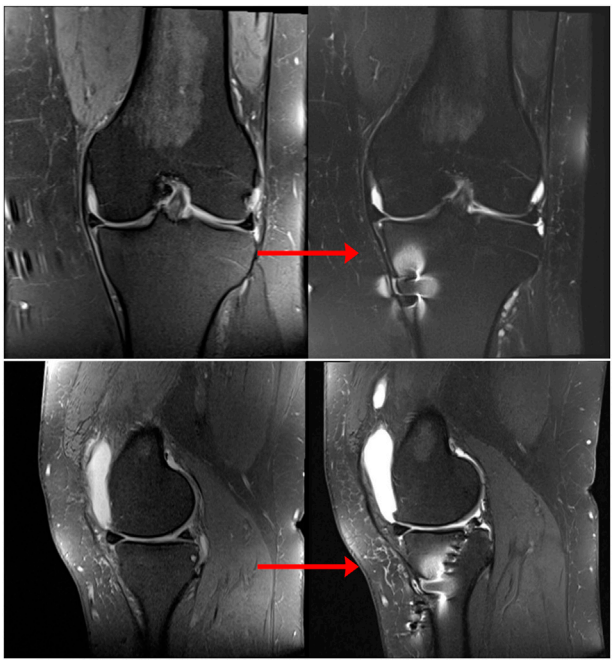

FIGURE 8 | Coronal **(A)** and sagittal **(B)** MR images of nonanatomic root repair patient #6 showing progression of osteoarthritis in the medial compartment of the knee over 12 months secondary to nonanatomic medial meniscus root repair (left knee). M = medial; L = lateral; A = anterior; P = Posterior.

and decreased medial joint space on standing Rosenberg radiographs.

Patient 4, a 57-year-old female, presented/experience pain for 5 months that began after going for a walk, radiographs and MRI showed preserved joint space and cartilage at the 4-month point. The patient's MRI at her office visit, however, revealed a full-thickness radial tear through the PHMM/root junction along with 3 mm of medial meniscus extrusion. Diffuse full-thickness chondral fissuring and signs of OA were noted on the weight-bearing surfaces of both the MTP and lateral femoral condyle (LFC). (See **Figure 11**).

Patient 5, a 49-year-old female, suffered a PMMRT after a biking injury. She was evaluated 4 weeks later and found to a medial meniscal root tear with some extrusion, along with mild chondromalacia of the medial compartment. On subsequent evaluation 15 months later, an MRI demonstrated grade II chondromalacia on the medial tibial plateau, patellofemoral and medial compartment OA, 5 mm of meniscal extrusion and a marked joint effusion in the absence of any ligamentous deficiency. Clinical evaluation revealed no other probable cause for this rapid progression to OA. (See **Figure 12**).

DISCUSSION

Appreciation of the deleterious effects of meniscal root tears has grown in recent years, as has knowledge of the biomechanical role

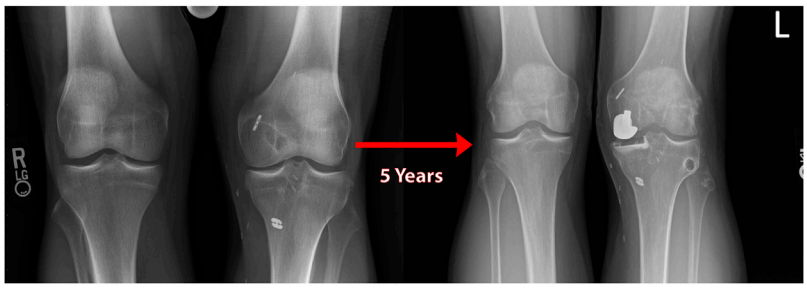

FIGURE 9 | Standing bilateral radiographs of the knee of natural history patient #1 showing results of a unilateral knee arthroplasty used to treat medial compartment osteoarthritis over 5 years following an iatrogenic medial meniscal root tear (left knee).

of the meniscus in the knee. While in the past, common practice involved complete or partial meniscectomy in treatment of many meniscal tears, advances in understanding of meniscal anatomy and of the importance of meniscal integrity in prevention of OA have led to increasing preference for repair over resection (8) (**Figure 13**). Meniscus root tears, in particular, have occupied a somewhat peculiar space, being underdiagnosed and often neglected.

However, biomechanical studies have demonstrated the clear link between posterior meniscal root tears and the progression of OA (Stärke et al., 2010b; Bansal et al., 2021). Long term high-level studies of meniscal root repair are still forthcoming; however, it is the authors' contention that biomechanical work validating the natural history of PMMRTs as equivalent to meniscectomy provides sufficient evidence to warrant repair in these injuries. In this study, we have presented a case series of patients who underwent nonanatomic PMMRT repairs and patients who presented with OA as a result of neglected medial meniscal root tears. In the author's practice, MRI is always obtained to evaluate if the meniscus is repairable. If the meniscus is repairable and the patient has a favorable profile for repair, the senior author will repair the meniscal root regardless of if it has a degenerative or traumatic etiology. All patients demonstrated a progression of medial compartment knee arthritis as predicted by previous biomechanical studies.

From a clinical standpoint, the observations made from biomechanical studies are borne out by the relatively fast development of OA after PMMRT, sometimes in a matter of months in the patients observed by these authors. As seen in this case series, unnecessary meniscectomy continues to be a significant driver of the development of OA in orthopedic practices all over the US. A case series of nonanatomic repairs of posterior medial meniscus root tears has not been presented previously, and these cases suggest that such repairs can reliably lead to a continuation or worsening of

FIGURE 10 | Coronal MRI of the knee of natural history patient #3 showing progression of osteoarthritis over 5 months following neglected medial meniscal root tear (right knee).

FIGURE 11 | Coronal **(A)** and sagittal **(B)** MR images of the knee of natural history patient #4 showing progression of osteoarthritis over 5 months following neglected medial meniscal root tear (left knee).

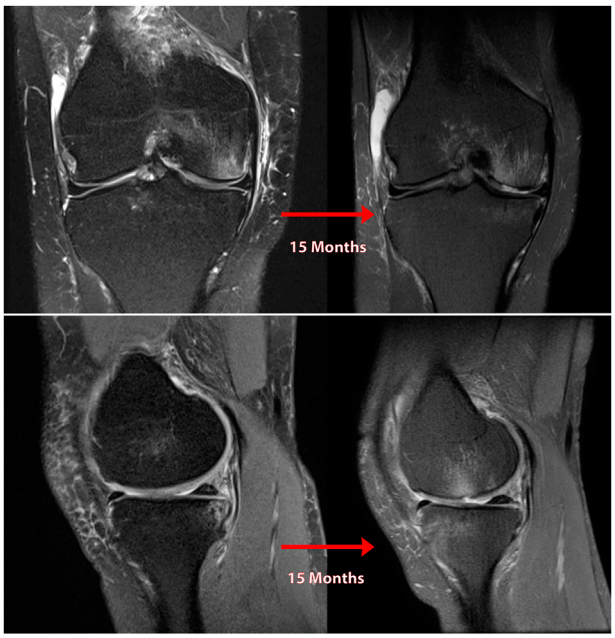

FIGURE 12 | Coronal **(A)** and sagittal **(B)** MR images of the knee of natural history patient #5 showing progression of osteoarthritis over 5 months following neglected medial meniscal root tear (right knee).

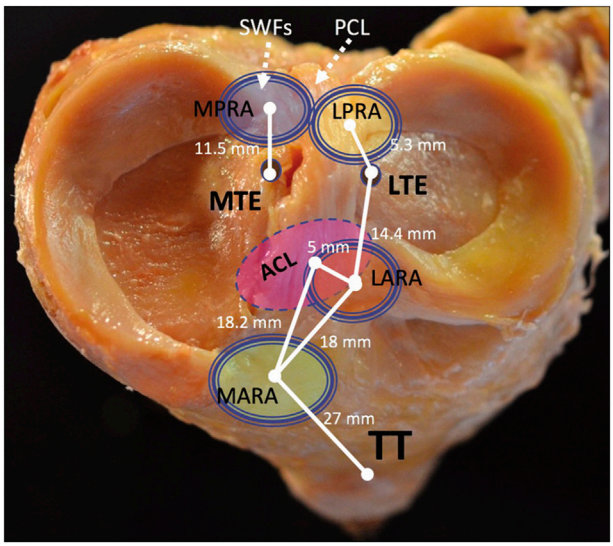

FIGURE 13 | The tibial plateau, medial and lateral menisci, and important points of arthroscopic anatomy. MPRA, medial posterior root attachment; LPRA, lateral posterior root attachment; LARA, lateral anterior root attachment; MARA, medial anterior root attachment; ACL, anterior cruciate ligament; TT, tibial tubercle; MTE, medial tibial eminence; LTE, lateral tibial eminence. Figure first appeared in: "LaPrade RF, Floyd ER, Carlson GB, Moatshe G, Chahla J, Monson JK. Meniscal Root Tears: Solving the Silent Epidemic. J Arthrosc Surg Sports Med 2021; 2 (1):47–57."

symptoms, and often require revision surgery. Meniscal extrusion after PMMRTs may partially explain the number of nonanatomic repairs seen nationwide; the meniscus often heals with scar tissue in the extruded position adjacent to the capsule and without some form of arthroscopic release is not readily reducible to anatomic position (DePhillipo et al., 2019). Biomechanical studies have given rationale, observed in the failure of the non-anatomic repairs presented here, that root repair which fail restore the anatomical position of the meniscus attachment are equivalent to meniscectomy (Stärke et al., 2010a; Padalecki et al., 2014; LaPrade et al., 2015b). Increased contact pressure in biomechanical studies may be correlated to progression of OA in untreated PMMRTs.

As noted above, indications for PMMRT repair can be dependent on the patient's age and activity status. Radiographic absence of arthritis and active lifestyle should be counterbalanced against patients' age alone. Younger patients without significant cartilage defects or joint space narrowing and MRI evidence of meniscal root tear should be considered good candidates for this surgery.

Limitations of this report include complex histories and not examining the potential relation between patient weight, alignment, and progression of symptoms. For some patients who presented without a clear inciting event, the actual duration of time may be uncertain in which the weight-bearing cartilage surfaces were exposed to increased contact forces due to PMMRT. An additional limitation may be selection bias in presenting primarily patients from a private sports medicine practice in the midwestern United States. However, the senior author's practice is a tertiary referral practice which serves patients from across and outside of the United States; therefore, any selection bias may be more socioeconomic than geographical.

CONCLUSION

Root tears of the posterior medial meniscus can be potentially debilitating injuries, leading to pain, limitation of activity, and decreased quality of life. Biomechanical studies have suggested an additional link between PMMRTs and the progression of OA, and a high incidence of untreated PMMRTs has been reported among younger patients undergoing TKA. Anatomic reduction of the meniscus root attachment and restoration of the native root position restores the integrity of the knee and prevents progression of this natural history. A heightened awareness for this injury pattern is necessary with prompt MRI if history and exam suggest a possible meniscal root tear. Magnetic resonance imaging requires careful scrutiny by surgeons to ensure identification of these tears. At the time of surgery, specific attention to the posterior meniscal roots and including probing the structures at the time of knee arthroscopy is recommended. In appropriately selected patients, repair of a meniscus root tear should be performed with a validated repair construct (i.e., two sutures secured through transtibial tunnels) with consideration of a peripheral release to anatomically reduce the meniscus.

DATA AVAILABILITY STATEMENT

The original contributions presented in the study are included in the article/Supplementary Material, further inquiries can be directed to the corresponding author.

AUTHOR CONTRIBUTIONS

All authors listed have made a substantial, direct, and intellectual contribution to the work and approved it for publication.

FUNDING

Ossur Research Grant for Sports Medicine Fellowship-Related research at Twin Cities Orthopedics.

REFERENCES

Allaire, R., Muriuki, M., Gilbertson, L., and Harner, C. D. (2008). Biomechanical Consequences of a Tear of the Posterior Root of the Medial Meniscus. *The J. Bone Jt. Surgery-American Volume* 90 (9), 1922–1931. doi:10.2106/jbjs.g.00748

Athanasiou, K. A., and Sanchez-Adams, J. (2009). Engineering the Knee Meniscus. *Synth. Lectures Tissue Eng.* 1 (1), 1–97. doi:10.2200/s00186ed1v01y200903tis001

Bansal, S., Floyd, E. R., Kowalski, M., Aikman, E., Elrod, P., Burkey, K., et al. (2021). Meniscal Repair: The Current State and Recent Advances in Augmentation. *J. Orthop. Res.* 39 (7), 1368–1382. doi:10.1002/jor.25021

Bedi, A., Kelly, N. H., Baad, M., Fox, A. J., Brophy, R. H., Warren, R. F., et al. (2010). Dynamic Contact Mechanics of the Medial Meniscus as a Function of Radial Tear, Repair, and Partial Meniscectomy. *J. Bone Jt. Surgery-American Volume* 92 (6), 1398–1408. doi:10.2106/jbjs.i.00539

Brophy, R. H., Wojahn, R. D., Lillegraven, O., and Lamplot, J. D. (2019). Outcomes of Arthroscopic Posterior Medial Meniscus Root Repair. *J. Am. Acad. Orthopaedic Surgeons* 27 (3), 104–111. doi:10.5435/jaaos-d-17-00065

Chahla, J., Moulton, S. G., LaPrade, C. M., Dean, C. S., and LaPrade, R. F. (2016). Posterior Meniscal Root Repair: The Transtibial Double Tunnel Pullout Technique. *Arthrosc. Tech.* 5 (2), e291–e296. doi:10.1016/j.eats.2016.01.006

Choi, E.-S., and Park, S.-J. (2015). Clinical Evaluation of the Root Tear of the Posterior Horn of the Medial Meniscus in Total Knee Arthroplasty for Osteoarthritis. *Knee Surg. Relat. Res.* 27 (2), 90–94. doi:10.5792/ksrr.2015.27.2.90

Cinque, M. E., Chahla, J., Moatshe, G., Faucett, S. C., Krych, A. J., and LaPrade, R. F. (2018). Meniscal Root Tears: a Silent Epidemic. *Br. J. Sports Med.* 52 (13), 872–876. doi:10.1136/bjsports-2017-098942

Cinque, M. E., Geeslin, A. G., Chahla, J., Dornan, G. J., and LaPrade, R. F. (2017). Two-Tunnel Transtibial Repair of Radial Meniscus Tears Produces Comparable Results to Inside-Out Repair of Vertical Meniscus Tears. *Am. J. Sports Med.* 45 (10), 2253–2259. doi:10.1177/0363546517704425

Daney, B. T., Aman, Z. S., Krob, J. J., Storaci, H. W., Brady, A. W., Nakama, G., et al. (2019). Utilization of Transtibial Centralization Suture Best Minimizes Extrusion and Restores Tibiofemoral Contact Mechanics for Anatomic Medial Meniscal Root Repairs in a Cadaveric Model. *Am. J. Sports Med.* 47 (7), 1591–1600. doi:10.1177/0363546519844250

Dean, R. S., DePhillipo, N. N., Monson, J. K., and LaPrade, R. F. (2020). Peripheral Stabilization Suture to Address Meniscal Extrusion in a Revision Meniscal Root Repair: Surgical Technique and Rehabilitation Protocol. *Arthrosc. Tech.* 9 (8), e1211–e1218. doi:10.1016/j.eats.2020.04.022

Dean, R. S., DePhillipo, N. N., Monson, J. K., and LaPrade, R. F. (2020). Peripheral Stabilization Suture to Address Meniscal Extrusion in a Revision Meniscal Root Repair: Surgical Technique and Rehabilitation Protocol. *Arthrosc. Tech.* 9 (8), e1211–e1218. doi:10.1016/j.eats.2020.04.022

DePhillipo, N. N., Kennedy, M. I., Chahla, J., and LaPrade, R. F. (2019). Type II Medial Meniscus Root Repair with Peripheral Release for Addressing Meniscal Extrusion. *Arthrosc. Tech.* 8 (9), e941–e946. doi:10.1016/j.eats.2019.05.001

Driban, J. B., Stout, A. C., Duryea, J., Lo, G. H., Harvey, W. F., Price, L. L., et al. (2016). Coronal Tibial Slope Is Associated with Accelerated Knee Osteoarthritis: Data from the Osteoarthritis Initiative. *BMC Musculoskelet. Disord.* 17, 299. doi:10.1186/s12891-016-1158-9

Ellman, M. B., LaPrade, C. M., Smith, S. D., Rasmussen, M. T., Engebretsen, L., Wijdicks, C. A., et al. (2014). Structural Properties of the Meniscal Roots. *Am. J. Sports Med.* 42 (8), 1881–1887. doi:10.1177/0363546514531730

Faucett, S. C., Geisler, B. P., Chahla, J., Krych, A. J., Kurzweil, P. R., Garner, A. M., et al. (2019). Meniscus Root Repair vs Meniscectomy or Nonoperative Management to Prevent Knee Osteoarthritis after Medial Meniscus Root Tears: Clinical and Economic Effectiveness. *Am. J. Sports Med.* 47 (3), 762–769. doi:10.1177/0363546518755754

Foreman, S. C., Liu, Y., Nevitt, M. C., Neumann, J., Joseph, G. B., Lane, N. E., et al. (2020). Meniscal Root Tears and Extrusion Are Significantly Associated with the Development of Accelerated Knee Osteoarthritis: Data from the Osteoarthritis Initiative. *Cartilage*, 1947603520934525.

Hwang, B.-Y., Kim, S.-J., Lee, S.-W., Lee, H.-E., Lee, C.-K., Hunter, D. J., et al. (2012). Risk Factors for Medial Meniscus Posterior Root Tear. *Am. J. Sports Med.* 40 (7), 1606–1610. doi:10.1177/0363546512447792

James Ewj, A. M., Cinque, M. E., Chahla, J., and LaPrade, R. F. (2017). An Evidence-Based Approach to the Diagnosis and Treatment of Meniscal Root Tears. *Minerva Ortop Traumatol.* 68 (2), 81–90. doi:10.23736/s0394-3410.17.03805-x

James, E. W., LaPrade, C. M., Ellman, M. B., Wijdicks, C. A., Engebretsen, L., and LaPrade, R. F. (2014). Radiographic Identification of the Anterior and Posterior Root Attachments of the Medial and Lateral Menisci. *Am. J. Sports Med.* 42 (11), 2707–2714. doi:10.1177/0363546514545863

Johannsen, A. M., Civitarese, D. M., Padalecki, J. R., Goldsmith, M. T., Wijdicks, C. A., and LaPrade, R. F. (2012). Qualitative and Quantitative Anatomic Analysis of the Posterior Root Attachments of the Medial and Lateral Menisci. *Am. J. Sports Med.* 40 (10), 2342–2347. doi:10.1177/0363546512457642

Johannsen, A. M., Civitarese, D. M., Padalecki, J. R., Goldsmith, M. T., Wijdicks, C. A., and LaPrade, R. F. (2012). Qualitative and Quantitative Anatomic Analysis of the Posterior Root Attachments of the Medial and Lateral Menisci. *Am. J. Sports Med.* 40 (10), 2342–2347. doi:10.1177/0363546512457642

Krych, A. J., Bernard, C. D., Kennedy, N. I., Tagliero, A. J., Camp, C. L., Levy, B. A., et al. (2020). Medial versus Lateral Meniscus Root Tears: Is There a Difference in Injury Presentation, Treatment Decisions, and Surgical Repair Outcomes?. *Arthrosc. J. Arthroscopic Relat. Surg.* 36 (4), 1135–1141. doi:10.1016/j.arthro.2019.11.098

Krych, A. J., Reardon, P. J., Johnson, N. R., Mohan, R., Peter, L., Levy, B. A., et al. (2017). Non-operative Management of Medial Meniscus Posterior Horn Root Tears Is Associated with Worsening Arthritis and Poor Clinical Outcome at 5-year Follow-Up. *Knee Surg. Sports Traumatol. Arthrosc.* 25 (2), 383–389. doi:10.1007/s00167-016-4359-8

LaPrade, C. M., Ellman, M. B., Rasmussen, M. T., James, E. W., Wijdicks, C. A., Engebretsen, L., et al. (2014). Anatomy of the Anterior Root Attachments of the Medial and Lateral Menisci. *Am. J. Sports Med.* 42 (10), 2386–2392. doi:10.1177/0363546514544678

LaPrade, C. M., Foad, A., Smith, S. D., Turnbull, T. L., Dornan, G. J., Engebretsen, L., et al. (2015). Biomechanical Consequences of a Nonanatomic Posterior Medial Meniscal Root Repair. *Am. J. Sports Med.* 43 (4), 912–920. doi:10.1177/0363546514566191

LaPrade, C. M., James, E. W., Cram, T. R., Feagin, J. A., Engebretsen, L., and LaPrade, R. F. (2015). Meniscal Root Tears. *Am. J. Sports Med.* 43 (2), 363–369. doi:10.1177/0363546514559684

LaPrade, R. F., Floyd, E. R., Carlson, G. B., Moatshe, G., Chahla, J., and Monson, J. K. (2021) Meniscal Root Tears: Solving the Silent Epidemic. *J. Arthroscopic Surg. Sports Med.* 2, 47-57. doi:10.25259/jassm_55_2020

LaPrade, R. F., LaPrade, C. M., Ellman, M. B., Turnbull, T. L., Cerminara, A. J., and Wijdicks, C. A. (2015). Cyclic Displacement after Meniscal Root Repair Fixation. *Am. J. Sports Med.* 43 (4), 892–898. doi:10.1177/0363546514562554

Lee, D. W., Ha, J. K., and Kim, J. G. (2014). Medial Meniscus Posterior Root Tear: a Comprehensive Review. *Knee Surg. Relat. Res.* 26 (3), 125–134. doi:10.5792/ksrr.2014.26.3.125

Lim, B. W., Hinman, R. S., Wrigley, T. V., and Bennell, K. L. (2008). Varus Malalignment and its Association with Impairments and Functional Limitations in Medial Knee Osteoarthritis. *Arthritis Rheum.* 59 (7), 935–942. doi:10.1002/art.23820

Matheny, L. M., Ockuly, A. C., Steadman, J. R., and LaPrade, R. F. (2015). Posterior Meniscus Root Tears: Associated Pathologies to Assist as Diagnostic Tools. *Knee Surg. Sports Traumatol. Arthrosc.* 23 (10), 3127–3131. doi:10.1007/s00167-014-3073-7

Packer, J. D., and Rodeo, S. A. (2009)., 28. viii, 259–283. doi:10.1016/j.csm.2008.10.011Meniscal Allograft Transplantation*Clin. Sports Med.*2

Padalecki, J. R., Jansson, K. S., Smith, S. D., Dornan, G. J., Pierce, C. M., Wijdicks, C. A., et al. (2014). Biomechanical Consequences of a Complete Radial Tear Adjacent to the Medial Meniscus Posterior Root Attachment Site. *Am. J. Sports Med.* 42 (3), 699–707. doi:10.1177/0363546513499314

Seil, R., Dück, K., and Pape, D. (2011). A Clinical Sign to Detect Root Avulsions of the Posterior Horn of the Medial Meniscus. *Knee Surg. Sports Traumatol. Arthrosc.* 19 (12), 2072–2075. doi:10.1007/s00167-011-1550-9

Sims, E. L., Carland, J. M., Keefe, F. J., Kraus, V. B., Guilak, F., and Schmitt, D. (2009). Sex Differences in Biomechanics Associated with Knee Osteoarthritis. *J. Women Aging* 21 (3), 159–170. doi:10.1080/08952840903054856

Stärke, C., Kopf, S., Gröbel, K.-H., and Becker, R. (2010). The Effect of a Nonanatomic Repair of the Meniscal Horn Attachment on Meniscal Tension: a Biomechanical Study. *Arthrosc. J. Arthroscopic Relat. Surg.* 26 (3), 358–365. doi:10.1016/j.arthro.2009.08.013

Stärke, C., Kopf, S., Gröbel, K.-H., and Becker, R. (2010). The Effect of a Nonanatomic Repair of the Meniscal Horn Attachment on Meniscal Tension: A Biomechanical Study. *Arthrosc. J. Arthroscopic Relat. Surg.* 26 (3), 358–365. doi:10.1016/j.arthro.2009.08.013

Strauss, E. J., Day, M. S., Ryan, M., and Jazrawi, L. (2016). Evaluation, Treatment, and Outcomes of Meniscal Root Tears: A Critical Analysis Review. *JBJS Rev.* 4 (8). doi:10.2106/JBJS.RVW.15.00082

Willinger, L., Lang, J. J., von Deimling, C., Diermeier, T., Petersen, W., Imhoff, A. B., et al. (2020). Varus Alignment Increases Medial Meniscus Extrusion and Peak Contact Pressure: a Biomechanical Study. *Knee Surg. Sports Traumatol. Arthrosc.* 28 (4), 1092–1098. doi:10.1007/s00167-019-05701-1

Yusuf, E., Bijsterbosch, J., Slagboom, P. E., Rosendaal, F. R., Huizinga, T. W. J., and Kloppenburg, M. (2011). Body Mass index and Alignment and Their Interaction as Risk Factors for Progression of Knees with Radiographic Signs of Osteoarthritis. *Osteoarthritis and Cartilage* 19 (9), 1117–1122. doi:10.1016/j.joca.2011.06.001

Conflict of Interest: The authors declare that the research was conducted in the absence of any commercial or financial relationships that could be construed as a potential conflict of interest.

Publisher's Note: All claims expressed in this article are solely those of the authors and do not necessarily represent those of their affiliated organizations, or those of the publisher, the editors and the reviewers. Any product that may be evaluated in this article, or claim that may be made by its manufacturer, is not guaranteed or endorsed by the publisher.

frontiers in Bioengineering and Biotechnology

ORIGINAL RESEARCH
published: 28 October 2021
doi: 10.3389/fbioe.2021.744197

Non-Destructive Spatial Mapping of Glycosaminoglycan Loss in Native and Degraded Articular Cartilage Using Confocal Raman Microspectroscopy

Tianyu Gao[1], *Alexander J. Boys*[1], *Crystal Zhao*[2], *Kiara Chan*[1], *Lara A. Estroff*[1,3] *and Lawrence J. Bonassar*[2,4]*

[1]Department of Materials Science and Engineering, Cornell University, Ithaca, NY, United States, [2]Sibley School of Mechanical and Aerospace Engineering, Cornell University, Ithaca, NY, United States, [3]Kavli Institute at Cornell for Nanoscale Science, Ithaca, NY, United States, [4]Meinig School of Biomedical Engineering, Cornell University, Ithaca, NY, United States

Articular cartilage is a collagen-rich tissue that provides a smooth, lubricated surface for joints and is also responsible for load bearing during movements. The major components of cartilage are water, collagen, and proteoglycans. Osteoarthritis is a degenerative disease of articular cartilage, in which an early-stage indicator is the loss of proteoglycans from the collagen matrix. In this study, confocal Raman microspectroscopy was applied to study the degradation of articular cartilage, specifically focused on spatially mapping the loss of glycosaminoglycans (GAGs). Trypsin digestion was used as a model for cartilage degradation. Two different scanning geometries for confocal Raman mapping, cross-sectional and depth scans, were applied. The chondroitin sulfate coefficient maps derived from Raman spectra provide spatial distributions similar to histological staining for glycosaminoglycans. The depth scans, during which subsurface data were collected without sectioning the samples, can also generate spectra and GAG distributions consistent with Raman scans of the surface-to-bone cross sections. In native tissue, both scanning geometries demonstrated higher GAG content at the deeper zone beneath the articular surface and negligible GAG content after trypsin degradation. On partially digested samples, both scanning geometries detected an ~100 μm layer of GAG depletion. Overall, this research provides a technique with high spatial resolution (25 μm pixel size) to measure cartilage degradation without tissue sections using confocal Raman microspectroscopy, laying a foundation for potential *in vivo* measurements and osteoarthritis diagnosis.

Keywords: confocal Raman microspectroscopy, articular cartilage, osteoarthritis, glycosaminoglycans, cartilage degradation model

OPEN ACCESS

Edited by:
Tammy Haut Donahue,
University of Massachusetts Amherst, United States

Reviewed by:
Thierry Hoc,
Ecole Centrale de Lyon, France
Amin Komeili,
University of Guelph, Canada

***Correspondence:**
Lawrence J. Bonassar
lb244@cornell.edu

Specialty section:
This article was submitted to Biomechanics, a section of the journal Frontiers in Bioengineering and Biotechnology

Received: *19 July 2021*
Accepted: *24 September 2021*
Published: *28 October 2021*

Citation:
Gao T, Boys AJ, Zhao C, Chan K, Estroff LA and Bonassar LJ (2021) Non-Destructive Spatial Mapping of Glycosaminoglycan Loss in Native and Degraded Articular Cartilage Using Confocal Raman Microspectroscopy. Front. Bioeng. Biotechnol. 9:744197. doi: 10.3389/fbioe.2021.744197

1 INTRODUCTION

Osteoarthritis (OA) is a degenerative disease that mainly affects articular cartilage and related joint tissues. Articular cartilage is the tissue at the end of long bones that provides a smooth surface and lubricated joint motion, as well as a mechanically robust structure for load bearing. Structurally, articular cartilage is composed of three layers: a thin surface layer that contains a dense collagen fiber network that is oriented parallel to the articular surface and with low proteoglycan content; a middle

zone that has relatively disorganized collagen fibers and a higher proteoglycan content; and, adjacent to the bone, a deep zone that contains collagen fibers oriented perpendicular to the bone surface and has the highest proteoglycan content (Muir et al., 1970). During the progression of OA, the major organic components of cartilage extracellular matrix (ECM), the collagen network and proteoglycans, are gradually degraded by enzymes released during the inflammatory response (Mort and Billington, 2001; Martel-Pelletier et al., 2016). This degradation causes roughening of the articular surface, leading to mechanically induced ECM degradation and death of chondrocytes (cells that renew and maintain the ECM). Over time, the cartilage becomes severely eroded, causing thickening of subchondral bone and eventually direct bone-on-bone contact within the joint space. Clinically, OA is diagnosed by radiographic methods, such as Kellgren-Lawrence scores (Kellgren and Lawrence, 1957), in which joint space narrowing is considered the main diagnostic indicator. Notably, joint-space narrowing is indicative of advanced disease. As such, X-ray techniques cannot detect OA at its early stages. In early stage OA, the cartilage structure remains intact while chemical degradation of ECM components is happening close to the articular surface. The major hallmark for early stage OA is the depletion of subsurface glycosaminoglycans (GAGs), such as aggrecan (Lark et al., 1995). This work addresses the need for an analytical technique able to detect these chemical changes in cartilage composition that are indicative of early stage OA. Specifically, we use Raman microspectroscopy to spatially map the removal of proteoglycans from bovine cartilage.

Experimental studies of early-stage cartilage disease typically utilize histological stains to demonstrate cartilage quality (Pritzker et al., 2006). For instance, the scoring system presented by the Osteoarthritis Research Society International (OARSI) is fully developed based on compositional and structural information in histology sections, including proteoglycan reduction and surface discontinuity. Typical histology stains such as Safranin-O and Alcian Blue (for proteoglycans) or Picrosirius Red (for collagen) are utilized to demonstrate the distribution of the main biochemical components. These techniques are effective for qualitative assessment of the distribution of matrix components but are inherently not quantitative. Fourier transform infrared (FTIR) microspectroscopy has also been applied for more quantitative analysis of degraded cartilage. Concentrations of biomolecules can be measured quantitatively using FTIR, based on the absorption spectra of the tissue (Camacho et al., 2001; Rieppo et al., 2010; Khanarian et al., 2014). However, both histology and FTIR microspectroscopy require tissue removal and subsequent processing including fixation, dehydration, sectioning, and mounting. As such, their utility for clinical diagnosis and disease monitoring is limited. Magnetic resonance imaging (MRI) is used clinically for assessing cartilage quality (Alhadlaq et al., 2004; Goodwin et al., 2004; Potter et al., 2009; Bron et al., 2013). Although MRI collects information about thickness, surface characterization, and biochemical components, it is limited in spatial resolution (~100 μm), which limits its ability to track the zonal compositional changes in the early stages of OA that are on the length scale of 150 μm (Glover and Mansfield, 2002).

Raman microspectroscopy is capable of measuring structural information non-destructively, with an adequate resolution (<1 μm) to collect signals related to biochemical composition and structure (Bergholt et al., 2016b). This method is based on reflective vibrational spectroscopy and has been applied to several kinds of tissue such as ligaments, cartilage, osteochondral junctions, or bones, of which the major components are quite limited (water, collagen, proteoglycans, minerals) (Morris et al., 2002; Raghavan et al., 2010a; Raghavan et al., 2010b; Takahashi et al., 2014; Boys et al., 2019; Das Gupta et al., 2020). Unlike FTIR, the Raman signal of water does not have a strong overlap with ECM components, and as such, this technique can be applied to hydrated or even submerged tissue (Gamsjaeger et al., 2014; Irwin et al., 2021). Raman microspectroscopy has been applied to cartilage samples resulting in composition maps with a ~0.3 μm spatial resolution. Chondrocytes are visible and the distribution of major components of cartilage (water, collagen, GAG, cytoplasm, DNA) can be detected (Bergholt et al., 2016b). The normalized values of each component in Raman maps are also quantitatively related to the absolute biochemical concentration from the articular surface to the deep zone of the cartilage (Albro et al., 2018). However, most studies using Raman microspectroscopy were performed on healthy cartilage samples. The ability of Raman microspectroscopy to measure biochemical distributions within degraded or damaged cartilage has received much less attention. In previous work, mapping of the depth-dependent composition of cartilage was accomplished by sectioning the tissue and scanning from the articular surface to the bone (Bergholt et al., 2016b; Albro et al., 2018). While this technique is quantitative, sectioning the tissue clinically from a patient for compositional analysis can cause secondary damage to the osteoarthritic joint.

The objective of this study is to examine the effectiveness of confocal Raman microspectroscopy for mapping the composition of degraded cartilage. To achieve this objective, two scanning geometries were applied: 1) scanning from the cut face (referred to as cross-section scan), which enables quantification throughout the tissue depth, but cannot be accomplished clinically; 2) scanning confocally at the articular surface (referred to as depth scan), which has a limited depth of penetration, but could be applied *in vivo*. To assess the ability of confocal Raman microspectroscopy to image GAG loss from the articular surface, we used an established model of trypsin-induced degradation (Bonassar et al., 1995; Griffin et al., 2014; DiDomenico et al., 2019). We assessed the extent to which GAG distribution maps achieved by this confocal Raman microspectroscopy technique are comparable to traditional methods such as histology. The outcomes of this study will provide new methods and data for the development of confocal Raman microspectroscopy as a technique for non-destructive, high-resolution cartilage compositional analysis.

2 MATERIALS AND METHODS

2.1 Cartilage Sample Preparation and Trypsin Degradation

Cartilage samples were harvested from neonatal bovine tibial plateaus (six animals) acquired from an abattoir (Gold Medal Packing, Rome, NY). Cylindrical cartilage samples were

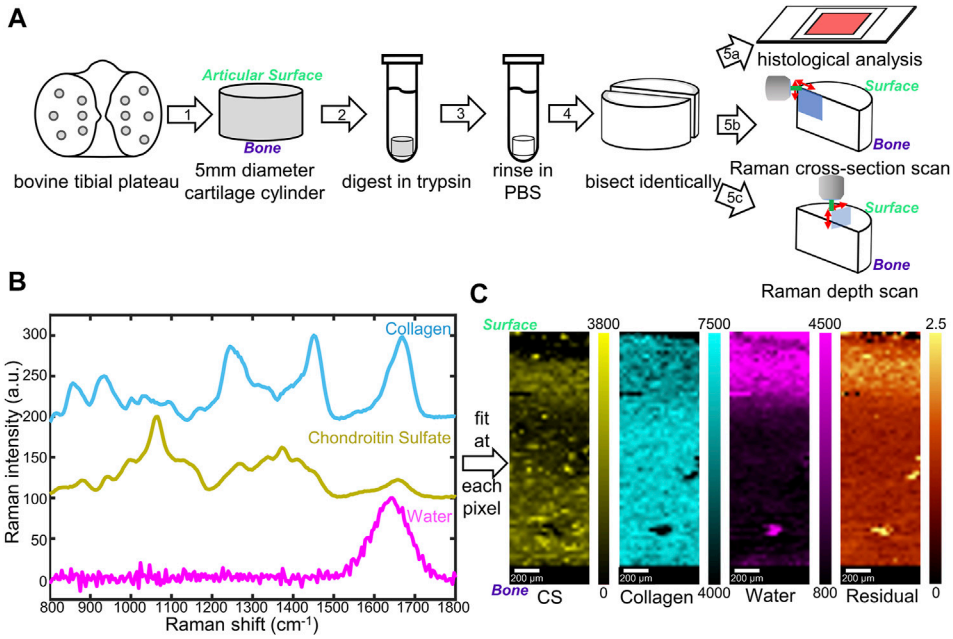

FIGURE 1 | (A) Schematic diagram of sample preparation and characterization. Cylindrical cartilage samples (5 mm) were collected from a bovine tibial plateau (1), digested in trypsin (2), rinsed (3), and bisected (4) for histological stains (5a) as well as Raman microspectroscopy (5b, c). Two Raman scanning geometries, cross-section scan (5b) and depth scan (5c), have been applied. **(B)** Reference Raman spectra collected for individual components in cartilage: top (blue) lyophilized rat tail collagen, middle (yellow) shark cartilage chondroitin sulfate (CS) powder; bottom (magenta) deionized water. **(C)** Representative Raman coefficient maps, and residual generated by fitting the three reference spectra in **(B)** to spectra obtained from native cartilage samples.

harvested by applying 5 mm biopsy punches to the articular surface of the contact zone between the tibial plateau and the femoral condyle to obtain full-thickness samples (**Figure 1A**, Step 1).

Cylindrical cartilage samples were randomly divided into three different groups: native group, fully digested group, and partially digested group. For the native group, samples were incubated in phosphate buffered saline (PBS, Invitrogen, Grand Island, NY) for 2 h. For the fully digested group, samples were incubated in a 0.25 wt% trypsin solution (lyophilized powder from bovine pancreas, ≥10,000 BAEE units/mg protein, Sigma-Aldrich, St. Louis, MO) for 2 h to completely remove proteoglycans (Bonassar et al., 1995). For the partially digested group, samples were incubated in a 0.000625 wt% trypsin solution for 0.5 h. All the samples were then rinsed in 10 mL PBS at 4°C for 1 h. Each sample was cut with a razor blade into two semi-cylindrical pieces, one was used for Raman analysis, the other was used for biochemical analysis.

2.2 Raman Data Collection

2.2.1 Sample Preparation

All cartilage samples were anchored in 2 wt% low melting point agarose gel (gelling temperature 25 ± 5°C, Fisher Bioreagents) in Petri dishes (diameter 40 mm, height 12 mm) to prevent movement during confocal Raman mapping. The gel solution was preheated to 80°C in a water bath then cooled until 35°C before added to the Petri dishes. For tissue anchoring, a thin layer of the gel solution was added to each Petri dish at 35°C. Cartilage samples were then partially submerged in the solution, with the measuring surfaces exposed and facing upwards. The measuring surface of a sample is the articular-surface-to-bone cut face for the cross-section scan and is the articular surface for the depth scan. The dishes were cooled at 4°C until completely gelled. PBS was then added into the dishes to submerge the tissue samples.

2.2.2 Raman Mapping

For scanning at the cross-section (*cross-section scan*), samples were mounted in the confocal Raman microscope to enable measurements along the articular surface-to-subchondral bone cut face of the sample (**Figure 1A**, Step 5b). The pixel size for cross-section scans was 30 × 30 μm.

For scanning at the articular surface (*depth scan*), samples were mounted in the confocal Raman microscope to enable measurements along the articular surface of the sample (**Figure 1A**, Step 5c). Depth-dependent information was collected by changing the working distance between the objective and the articular surface. The pixel size for depth scans was 25 × 25 μm.

All the confocal Raman spectra were collected with a WITec Alpha300R Confocal Raman microscope through a 40x dipping lens. A 532 nm green laser with a 62 mW power was used as the excitation source.

2.2.3 Spectral Analysis

Using the WITec Project FIVE software (Version 5.2 PLUS, WITec, Ulm, Germany), spectra collected from cartilage

samples were baseline subtracted via the Shape function of the WITec Project FIVE software (Shape size parameter: 400) and cropped to 800–1,800 cm^{-1} fingerprint area, then normalized to the maximum intensity of their $-CH_2$ bending peaks (~1,445 cm^{-1}). The mineralized region close to the subchondral bone was confirmed by calculating the 906–986 cm^{-1} phosphate peak areas and masked out manually.

Three different constituents, collagen (Col), chondroitin sulfate (CS), and water, were chosen as standards for the analysis. Collagen from rat tail tendons was extracted, purified, and lyophilized as described previously (Iannucci et al., 2019), as the collagen standard sample. Chondroitin sulfate powder from shark cartilage (Sigma-Aldrich) was used as the CS standard. Deionized purified water was used as the water standard. For each reference, 12 Raman spectra were collected using a 532 nm laser at 62 mW through a 50× objective. Spectra were baselined as described above, cropped to 800–1,800 cm^{-1} fingerprint region, and normalized to their highest peaks (~1,670 cm^{-1} for collagen, ~1,060 cm^{-1} for CS, and ~1,640 cm^{-1} for water). The average of the 12 spectra for each standard was considered as final reference spectra (**Figure 1B**).

The three reference spectra (Col, CS, and water) were used for non-negative fitting through the WITec True Component analysis. Briefly, the reference spectra were input through the Component Spectra Drop action, and fitting was performed using the linear combination based, Basis Analysis function. At each pixel, the spectrum collected from a sample was fit by linear combination of the three reference spectra. By amalgamating all the pixels, fitting coefficient maps, as well as residual images, were generated via WITec Project FIVE software.

2.3 Biochemical Analysis of Glycosaminoglycan Content

Dimethylmethylene Blue (DMMB) assay was applied to quantitatively measure the GAG content within the cartilage (Farndale et al., 1986). Cartilage samples (n = 8) were collected as described above. The first 1 mm to the articular surface and the last 1 mm to the bone were removed. Samples were randomly separated into two groups, each including four samples. One group was fully digested with trypsin, and the other group was treated with PBS (as described above). Both groups were then rinsed for 1 h, frozen overnight, and lyophilized for 48 h. The lyophilized samples were then subjected to biochemical analyses for GAGs using a method previously reported (Ballyns et al., 2008; DiDomenico et al., 2019). Briefly, samples were digested by 0.125 mg/mL papain (buffered aqueous suspension, Sigma-Aldrich) at 60°C for 16 h and mixed with 16 mg/L DMMB solution (pH = 1.5) in a well plate. The absorbance was measured at 525 nm using a plate reader (Biotek Synergy HT). GAG content of the sample was calibrated by comparing the absorbance of samples to the standard curve, which was determined by polynomial fitting of the absorbance data from GAG standards.

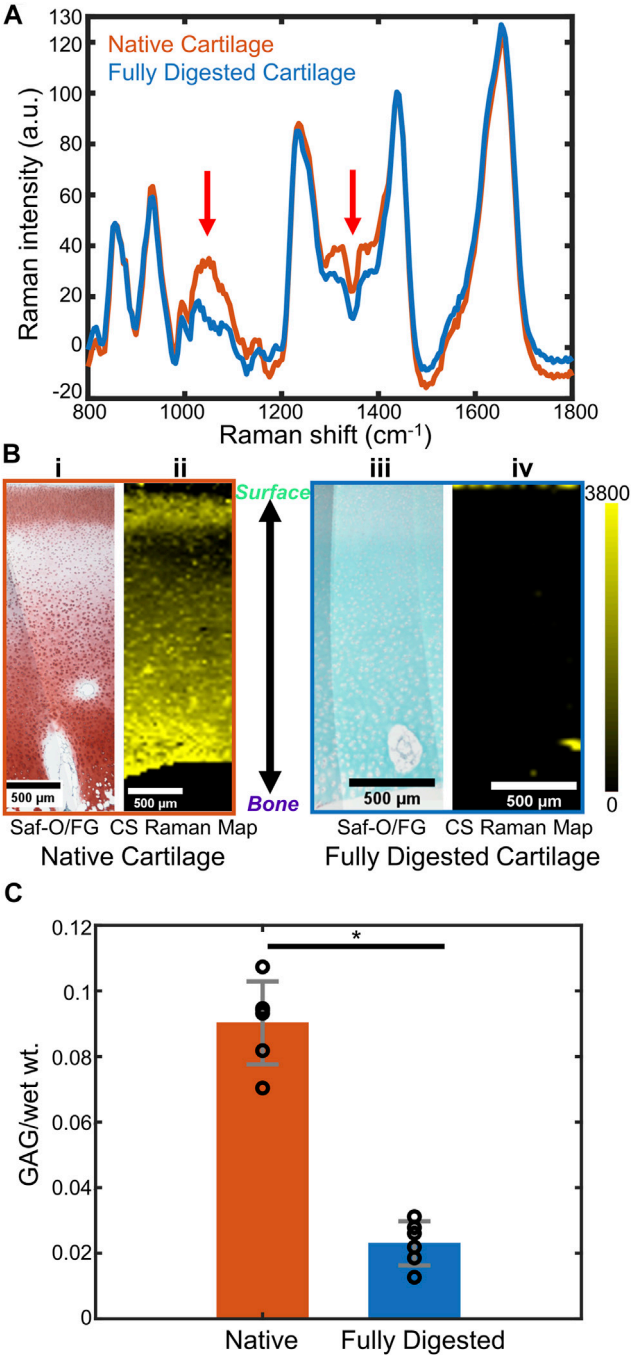

FIGURE 2 | (A) Representative Raman spectra of native bovine cartilage and fully trypsin-digested bovine cartilage. (Spectra are obtained by averaging a 15-pixel by 15-pixel area at the center of the respective Raman images. Red arrows: GAG-related spectral regions). **(B) (i)** Safranin-O stained histology section of native cartilage, articular surface at the top of the image. **(ii)** CS coefficient map for the same region as **(i)**. **(iii)** Safranin-O stained histology section of fully trypsin-digested cartilage, articular surface at the top of the image. **(iv)** CS coefficient map for the same region as **(iii)**. **(C)** DMMB biochemical assay to determine the GAG content (GAG/wet wt.) of native cartilage and fully digested cartilage (n = 6, *: p < 0.01). Abbreviations: Saf-O, Safranin-O; FG, Fast Green; CS, chondroitin sulfate.

2.4 Histology

Semi-cylindrical cartilage samples were fixed in 10 v/v% formalin solution for 24 h, then in 70 v/v% ethanol for 24 h. Samples were embedded in paraffin and sectioned along the surface-to-bone cut face. Sections were dehydrated and deparaffinized using ethanol and xylene, then stained with Weigert's hematoxylin for 10 min. For GAG visualization, the sections were counterstained with 0.001% fast green solution for 5 min and stained with 0.1% Safranin-O for 8 min. Slides were imaged with a Nikon Eclipse TE2000-S microscope (Nikon Instruments, Melville, NY) and a SPOT RT camera (Diagnostic Instruments, Sterling Heights, MI).

2.5 Statistical Analysis

To measure the statistical significance, quantitative data from the biochemical analysis were expressed as mean ± standard deviation. The pairwise comparisons of the biochemical data were analyzed *via* a one-way ANOVA test. Quantitative data from depth distribution measurements for native and digested cartilage were expressed as mean ± standard deviation. The pairwise comparisons were analyzed via mixed model analysis. Fitting coefficient data from cross-section scans and depth scans at different depths were analyzed through a mixed-model approach. Estimated values and confidence intervals were compared between different scanning geometries and between native and digested tissue. All analyses were performed using the IBM SPSS software platform.

3 RESULTS

3.1 Raman Microspectroscopy of Native and Fully Digested Cartilage

To achieve a controlled amount of GAG degradation in cartilage samples, we used a trypsin digestion model to mimic the degradation in early stage OA (**Figure 1A**). Trypsin cleaves the core protein of aggrecan, the largest source of GAG in cartilage, but does not degrade the collagen helix (Bornstein et al., 1966; Anderson, 1969). In order to map the distribution of ECM components in trypsin-degraded bovine cartilage, confocal Raman mapping was applied along the surface-to-bone cut face of semi-cylindrical bovine cartilage samples. The main components (collagen, GAGs, and water) in all the samples, both native and fully digested, were mapped (700 μm by 2,200 μm) from the articular surface to the subchondral bone (**Figure 1C**).

In a single spectrum taken from the middle zone of the native cartilage (**Figure 2A**), diagnostic peaks were observed in the 800–1,800 cm^{-1} fingerprint region, including ~857 cm^{-1} proline peak, ~935 cm^{-1} collagen triple helices, ~1,060 cm^{-1} sulfate peak (from GAGs), ~1,245 cm^{-1} amide III peak, ~1,445 cm^{-1} -CH_2 bending peak, and ~1,668 cm^{-1} amide I peak (Pavlou et al., 2018). These peaks were also observed in the spectrum from fully digested cartilage, excluding the 1,000–1,200 and 1,300–1,450 cm^{-1} regions, which had a reduction of peak intensity compared to the spectrum of the native tissue. These regions were consistent with the main peaks of chondroitin sulfate (**Figure 1B**), indicating a reduction in the GAG content of the tissue.

The Raman maps were generated from the fitting coefficients for the reference spectra at each pixel and compared to Safranin-O stained histological sections. Safranin-O staining on native cartilage (**Figure 2Bi**) demonstrated a thin layer of cartilage with low GAG content at the articular surface and a relatively GAG-rich region in the deep zone. Similar distributions were observed in the Raman map of CS fitting coefficients (**Figure 2Bii**). For fully digested samples, however, the lack of pink-red Safranin-O staining throughout the section indicated the absence of proteoglycans in this sample (**Figure 2Biii**). The Raman map of the CS fitting coefficients showed a similar depletion of the GAG within the tissue (**Figure 2Biv**).

To quantitatively demonstrate the effect of the trypsin digestion on removal of GAGs from the cartilage samples, a DMMB biochemical analysis was performed on the bulk tissue (**Figure 2C**, $n = 6$ for each group). Based upon the DMMB assay, the fully digested cartilage demonstrated a ~75% loss of total GAG components after trypsin digestion as compared to the native cartilage GAG content ($p < 0.01$).

3.2 Subsurface Confocal Raman Microspectroscopy of Native and Fully Digested Cartilage

Confocal Raman mapping was applied to native and fully digested tissue samples under the depth scan method (**Figure 3A**), in which depth-dependent information was collected confocally by moving the objective towards the articular surface and focusing into the tissue. For native tissue, the Raman map indicated a thin layer without CS at the articular surface of cartilage and a higher CS content at the deeper region. The Raman map of fully digested cartilage, however, demonstrated negligible CS content throughout the tissue. The collagen, on the other hand, is shown to be evenly distributed across the imaged area for both native and fully digested cartilage samples. Linear depth scans were performed starting from the articular surface and moving deeper into the tissue in 30 μm increments down to 300 μm. These scans were compared to those obtained by scanning at the cut face of cartilage from the surface to the deeper zone. Both scanning geometries were applied to native and fully digested tissue. Representative spectra at 300 μm below the articular surface collected via both geometries (**Figure 3B**) demonstrate similar spectra for native cartilage samples, showing that confocal spectra collection is possible within 300 μm of the surface. In fully digested cartilage samples, the spectra showed weaker signals in 1,000–1,200 and 1,300–1,450 cm^{-1} GAG regions and high similarity between the two different scanning geometries.

When the CS fitting coefficients are plotted as a function of distance from the articular surface (**Figure 3C**), in native tissue, a depth-dependent increase was seen when scanning below the surface ($p < 0.01$). Similar trends in GAG content of native tissue were observed by both scanning geometries: low at the articular surface and high at deeper regions ($p = 0.111$). For fully digested tissue, both scanning geometries show negligible GAG concentrations throughout the 300 μm scanning region.

3.3 Confocal Raman Mapping of Partially Digested Cartilage

To model early-stage OA in which GAG depletion occurs only near the articular surface, we used a much lower concentration of

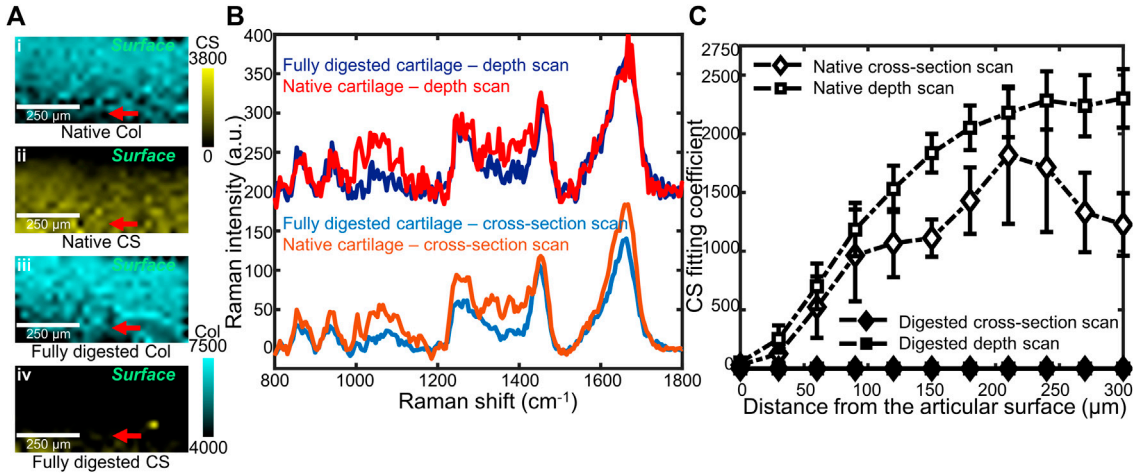

FIGURE 3 | (A) Representative coefficient maps of CS and collagen (Col) obtained by confocal Raman depth scans on native (i,ii), and fully digested (iii,iv) articular cartilage. Red arrows: the 300 μm depth position at which spectra in **(B)** were obtained. **(B)** Representative Raman spectra of native cartilage and fully digested cartilage, all taken from 300 μm beneath the articular surface. Both cross-section scan and depth scan have been used, and a 200 a.u. offset was applied to each depth scan spectrum for clarity. **(C)** CS coefficient plotted as a function of distance from the articular surface, up to 300 μm beneath the surface. Data from two cross-section scans (native and digested) as well as two depth scans (native and digested) are plotted (n = 4).

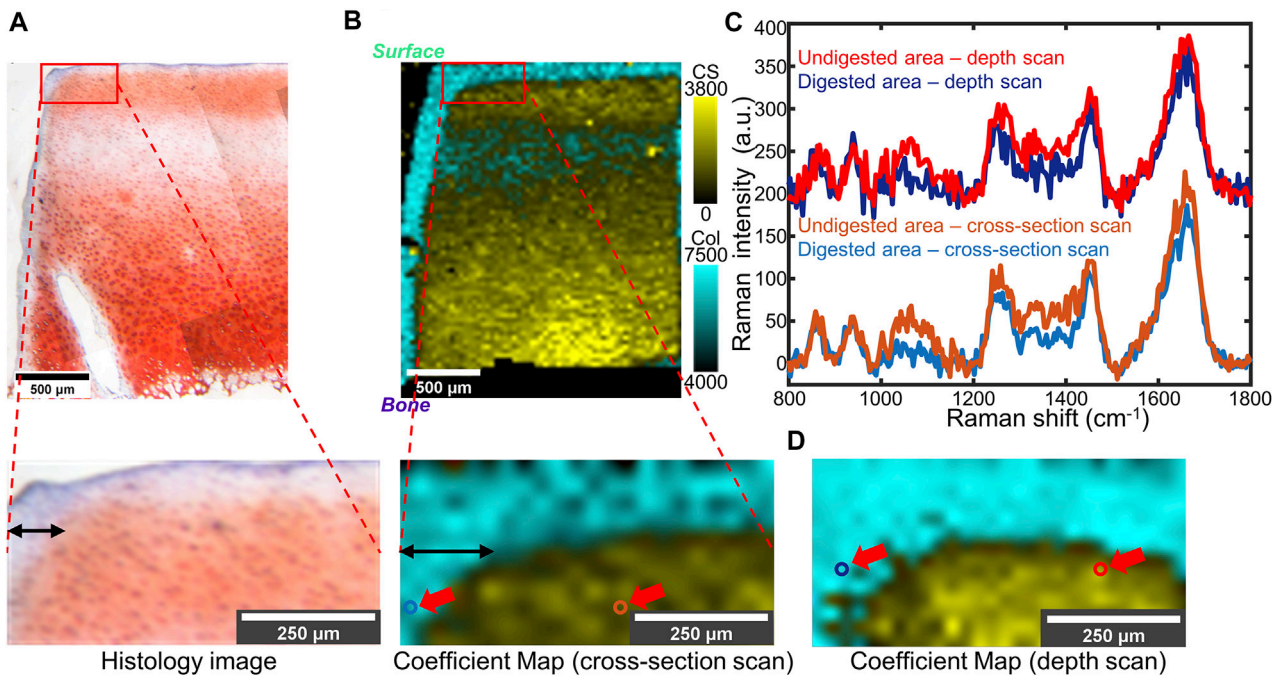

FIGURE 4 | (A) Top: Light microscope image of partially trypsin-digested cartilage tissue stained by Safranin-O. Bottom: Higher-magnification of the area of interest (the red box). **(B)** Top: Overlaid coefficient map of CS and collagen took in the same region as **(A)**, taken by cross-section scan. Bottom: Higher magnification of the area of interest (the red box). **(C)** Point spectra collected from digested or undigested areas of the same sample. The collection points are shown as colored circles (indicated by red arrows) in (**B**, bottom) and **(D)**. A 200 a.u. offset was applied to each depth scan spectrum for clarity. **(D)** Overlaid coefficient map of the same sample as **(B)**, taken by depth scan. In **(B)** and **(D)**: Cyan: collagen; Yellow: CS.

trypsin for a shorter digestion time. Confocal Raman mappings, both cross-section and depth scans, were applied to the partially digested bovine cartilage. Histological analysis with Safranin-O staining (**Figure 4A**) revealed a region of GAG depletion extending around 100 μm from the trypsin-exposed surfaces (**Figure 4A**, the top and left). The cross-section Raman scan

showed a similar distribution (**Figure 4B**), with a ~100 μm narrow band with high collagen coefficients but low CS coefficients observed at the trypsin-exposed surfaces. The CS coefficient map obtained from a depth scan recapitulated the distribution of collagen and GAGs observed in cross-section Raman maps and the histology image (**Figure 4D**). A curved interface between GAG-depleted and CS-rich regions was observed in all three analyses. The point spectra taken from the digested region and the undigested region demonstrate evident differences in the GAG-related regions (1,000–1,200 and 1,300–1,450 cm^{-1}) (**Figure 4C**), which are consistent with the zonal differences observed in the histology images and the Raman maps.

4 DISCUSSION

In this study, data collected from confocal Raman microspectroscopy were used to spatially map GAG loss in a trypsin digestion model of cartilage degradation. Cross-section Raman scans at the cut face of cartilage and confocal depth scans at the articular surface were applied to native and digested cartilage samples. The resulting maps successfully imaged the GAG distribution in partially degraded cartilage, a model for early stages of OA, with a pixel size of 25 μm.

Our research demonstrates that confocal Raman microspectroscopy has the potential to be utilized for compositional analysis of cartilage degradation. Although several analytical techniques have been utilized on tissues like cartilage which is made of only a few major components, they all have limitations. Traditional measurements for proteoglycan distribution in ECM are mostly performed via histological stains, such as Safranin-O or Alcian blue. However, fixation and sectioning of samples may lead to artifacts or inconsistencies between different sections. The staining outcome also varies among samples, making it unsuitable for quantitative analysis (Rosenberg, 1971; Király et al., 1996; Puchtler et al., 1988). Overall, despite being widely utilized in analyses of degraded cartilage, such methods reveal only qualitative distribution of each biochemical component within a sample. Spectroscopic techniques, like FTIR imaging, can yield more quantitative results (Rieppo et al., 2010). However, FTIR-based imaging techniques require specific sample preparation, including thin-sectioning, dehydration, optional embedding, and mounting on non-IR absorbing slides (Taylor and Donnelly, 2020). In contrast, Raman microspectroscopy can be utilized for quantitative analysis on thicker, unfixed, hydrated, or even submerged samples, because water does not have strong contributions to Raman signals, especially in the fingerprint region (Albro et al., 2018). Raman microspectroscopy has also been reported to be non-detrimental to cells (Gamsjaeger et al., 2014; Akiva et al., 2016; Bergholt et al., 2017), making it potentially available for analyzing tissue *in vivo* (Zeng et al., 2008; Duraipandian et al., 2014).

In this study, Raman spectra were collected via cross-section scans and depth scans. In cross-section scans, spectra were collected along the cut face of articular cartilage from the surface to the deep zone. Since the scans are at the cut face of the sample, cross-section scans can image the entire tissue from the articular surface to subchondral bone. For depth scans, however, spectra were collected confocally as optical slices of different depths by moving the objective and the focal plane. Spectral intensities decrease with depth into the tissue due to light absorption and scattering. However, these effects are similar across spectra, enabling quantitative comparisons by normalizing peaks of interest to reference peaks. Notably, these two scanning geometries yield similar results within the first 300 μm from the tissue surface (**Figure 4**). A previous study indicates that the superficial zone thickness is less than 250 μm for human, bovine, and canine cartilage (Panula et al., 1998; Quinn et al., 2013). Hence, obtaining reliable spectra from 300 μm beneath the articular surface enables detection of the GAG-rich region, where GAG depletion first occurs in early stage OA. Since the depth scan does not require cutting of the sample, it can be applied to intact tissue. In early stage OA, GAG depletion occurs at the surface layer of articular cartilage (Lark et al., 1995; Pritzker et al., 2006). Imaging from a 300 μm layer beneath the surface will be informative to assess early stage OA. Therefore, this technique has the potential to be applied under circumstances when tissue biopsies are saved or even through Raman-compatible arthroscopic probes (Bergholt et al., 2017).

In our study, both histology and biochemical analysis demonstrate a considerable GAG reduction in trypsin-digested tissue. Raman spectra and maps show similar results (Farndale et al., 1982; Chandrasekhar et al., 1987), with negligible coefficients of chondroitin sulfate detected, as indicated by near 0 values of CS fitting coefficients (**Figures 2A,B**). The results show that proteoglycan reduction can be measured by confocal Raman mapping. High-resolution Raman maps of GAG content recapitulate the distribution seen in histology. In native tissue, both geometries indicated low GAG concentration at the articular surface and an increase of GAG concentration at the deeper zone. In fully digested tissue both methods showed negligible GAG concentration throughout the samples. The distribution is consistent with previous work, in which the GAG distribution is determined by histology (Silverberg et al., 2014). The Raman coefficient maps, which showed a significant reduction in chondroitin sulfate content but no change in collagen content (**Figures 3Ai,iii**), are consistent with literature studies that show trypsin exposure removed proteoglycans but did not damage the collagen network (Bonassar et al., 1995; DiDomenico et al., 2019). Considering that the Raman spectral intensity of each component of ECM is assumed to be proportional to its concentration, this semi-quantitative method effectively compares the GAG distribution among samples with different levels of degradation (**Figures 2Bii,iv**; **Figures 4B,D**) (Albro et al., 2018).

The partially digested articular cartilage samples were used as a model for early-stage OA in which GAG depletion happens primarily near the surface but in the absence of surface fibrillation. Such degradation corresponds to OARSI grade 1 or 2 (Pritzker et al., 2006). In our study, Raman microspectroscopy detected GAG removal by trypsin degradation near the edge of samples in a thin band with a

thickness around 100 μm. Notably, the resolution of Raman microscopy (25 μm pixel size) is better than other *in vivo* techniques like GAG-specific MRI. These Raman maps are also consistent with the Safranin-O staining of these tissues. Nonetheless, a slight difference in the thickness of the digestion edge was noticeable between Safranin-O staining (~100 μm) and Raman maps (~150 μm). This difference could be either due to the different sensitivity between Raman mapping and the Safranin-O dye or due to the deformation of histological samples under formalin fixation and sectioning.

While these results are promising, we still have some limitations for interpreting our data. For each sample, the time for spectral collection is long, typically for several hours. With the limitation of the confocal Raman microscope, spectra collected from regions more than 300 μm below the articular surface are noisy and unsuitable for reference fitting. A higher penetration depth might be possible by increasing the laser power. A 532 nm laser with 200 mW power (Boys et al., 2019) and a 785 nm laser with 250 mW power (Bergholt et al., 2017) have been reported to not damage cells in submerged microscopy systems. A too high laser power, however, can damage organic tissue and therefore there is a tradeoff between depth penetration and tissue integrity. Other Raman methods, such as Spatially Offset Raman Spectroscopy (SORS) and Transmission Raman Spectroscopy (TRS) were reported to give better signals for sub-surface spectra collection (Vardaki et al., 2015; Ghita et al., 2016; Matousek and Stone, 2016). Despite their applications for imaging other tissue such as bone (Matousek et al., 2006; Cui et al., 2020), to the best of our knowledge, these techniques have not been reported for cartilage imaging.

Additionally, although the non-negative spectral fitting was successful, it is important to note that the reference spectra were collected from dry forms of the biomacromolecules. As compared to dry forms, in hydrated cartilage tissue, biomacromolecules like collagen and GAGs have different tertiary and quaternary structures due to the hydration of these molecules and intermolecular interactions. For example, the Raman signature of collagen is strongly dependent on the size and orientation of collagen fibers, the aggregation of aggrecan can affect its spectra, and the hydration of chondroitin sulfate also alters the Raman signature (Bansil et al., 1978; Ellis et al., 2009; Masic et al., 2011; Galvis et al., 2013). In future work, obtaining hydrated reference spectra may yield more nuanced maps of macromolecule orientation and confirmation in the hydrated cartilage tissue. Some features of the Raman fingerprint area can also indicate detailed differences among compositions, such as chondroitin-4-sulfate (C4S) and chondroitin-6-sulfate (C6S) (Ellis et al., 2009). Nevertheless, more advanced analysis techniques are required to decompose spectra of similar molecules from the Raman spectra of the cartilage tissue.

This study collected data from the articular surface and on hydrated tissue. This technique has the potential to be incorporated into a fiber-optic Raman device, creating an optical fiber-based confocal Raman detection unit for an arthroscope (Esmonde-White et al., 2011; Bergholt et al., 2016a; Bergholt et al., 2017; Kandel et al., 2020). Since *in vivo* Raman spectra have been reported to be collected from human skin, lung, and bone (Matousek et al., 2006; Zeng et al., 2008), such a device may advance the analysis for *in vivo* animal models and diagnoses of early stage OA. Here, we have only applied this technique to a simplified enzymatic digestion model of bovine cartilage. Human cartilage, in contrast, is reported to be thicker in general but has a similar thickness in the superficial zone (Rieppo et al., 2003; Taylor et al., 2012). A higher composition of non-GAG solid content is also observed in human cartilage (Démarteau et al., 2006). Therefore, Raman maps that have different distribution or higher collagen content are expected to be acquired when human samples are studied, while superficial zone (50–100 μm thick for bovine cartilage) and transition zone (100–200 μm thick for bovine cartilage) of the samples (Mansfield and Winlove, 2017) can still be covered. Naturally occurring OA could be more complex, possibly including a roughened surface or thinner cartilage layer, which may result in lowered reflection or signal contribution from bone autofluorescence, leading to difficulties in analyzing Raman data. Other biomolecules, like hemoglobin and lipids, can also cause excessive background signals or distortions in Raman spectra, leading to further difficulties. This effect may prove challenging for *in vivo* imaging, where the bathing medium is synovial fluid that may contain components that complicate the interpretation of Raman data.

5 CONCLUSION

This work investigated the ability of confocal Raman microspectroscopy to determine the GAG distribution within trypsin-degraded bovine articular cartilage. We applied two different scan geometries using Raman microspectroscopy, cross-section scans and depth scans, on a trypsin digestion cartilage model for component analysis. The spatial distributions of major components (e.g., collagen, CS) within the articular cartilage obtained from Raman maps were qualitatively similar to the spatial distributions revealed by histology. Native bovine cartilage samples had lower GAG content at the articular surface, with an increase in GAG content at the deeper zone. Fully trypsin-digested samples show negligible GAG content throughout the entire tissue. We found that both scan geometries can provide similar Raman spectra when measuring beneath the articular surface. In cross-section scans, the data were collected from the exposed articular-surface-to-bone cut face. The depth scan enables depth-dependent spectra collection at the articular surface by moving the focal plane beneath the tissue surface, providing a data collection method that does not require sectioning of the tissue. In partially digested samples, zonal GAG depletion was detected by both scanning geometries. A thin digestion region at a ~100 μm scale was observed. Regional compositional differences were shown both in point spectra and in Raman maps and recapitulate the results shown in histology. This work demonstrates that confocal Raman microscopy is capable of high-resolution compositional analysis for degraded articular cartilage. The results lay a foundation for non-invasive

measurements of cartilage composition for *in vivo* studies and clinical early-stage OA diagnosis.

DATA AVAILABILITY STATEMENT

The raw data supporting the conclusion of this article will be made available by the authors, without undue reservation.

AUTHOR CONTRIBUTIONS

TG, AB, LE, and LB contributed to conception and design of this study. TG, AB, CZ, and KC took part in the acquisition and analysis of the data. All the authors contributed to interpretation of data and discussion. TG wrote the draft of the manuscript. All authors contributed to the article and approved the submitted version.

FUNDING

This work was supported by NSF CMMI 1927197 and NIH F31 AR070009. This work also made use of the Cornell Center for Materials Research Shared Facilities which are supported through the NSF MRSEC program (DMR-1719875).

ACKNOWLEDGMENTS

The authors greatly acknowledge Jennie A. M. R. Kunitake (Department of Materials Science and Engineering, Cornell University) for providing technical support on software operation and spectral analysis. The authors would also like to thank Cornell University Animal Health Diagnostic Center for the support on histology stains and analysis.

REFERENCES

Akiva, A., Kerschnitzki, M., Pinkas, I., Wagermaier, W., Yaniv, K., Fratzl, P., et al. (2016). Mineral Formation in the Larval Zebrafish Tail Bone Occurs via an Acidic Disordered Calcium Phosphate Phase. *J. Am. Chem. Soc.* 138, 14481–14487. doi:10.1021/jacs.6b09442

Albro, M. B., Bergholt, M. S., St-Pierre, J. P., Vinals Guitart, A., Zlotnick, H. M., Evita, E. G., et al. (2018). Raman Spectroscopic Imaging for Quantification of Depth-dependent and Local Heterogeneities in Native and Engineered Cartilage. *Npj Regen. Med.* 3, 3. doi:10.1038/s41536-018-0042-7

Alhadlaq, H. A., Xia, Y., Moody, J. B., and Matyas, J. R. (2004). Detecting Structural Changes in Early Experimental Osteoarthritis of Tibial Cartilage by Microscopic Magnetic Resonance Imaging and Polarised Light Microscopy. *Ann. Rheum. Dis.* 63, 709–717. doi:10.1136/ard.2003.011783

Anderson, A. J. (1969). Effects of Lysosomal Collagenolytic Enzymes, Anti-inflammatory Drugs and Other Substances on Some Properties of Insoluble Collagen. *Biochem. J.* 113, 457–463. doi:10.1042/bj1130457

Ballyns, J. J., Gleghorn, J. P., Niebrzydowski, V., Rawlinson, J. J., Potter, H. G., Maher, S. A., et al. (2008). Image-Guided Tissue Engineering of Anatomically Shaped Implants via MRI and Micro-CT Using Injection Molding. *Tissue Eng. A* 14, 1195–1202. doi:10.1089/ten.tea.2007.0186

Bansil, R., Yannas, I., and Stanley, H. (1978). Raman Spectroscopy: A Structural Probe of Glycosaminoglycans. *Biochim. Biophys. Acta Gen. Subj.* 541, 535–542. doi:10.1016/0304-4165(78)90163-0

Bergholt, M. S., Albro, M. B., and Stevens, M. M. (2017). Online Quantitative Monitoring of Live Cell Engineered Cartilage Growth Using Diffuse Fiber-Optic Raman Spectroscopy. *Biomaterials* 140, 128–137. doi:10.1016/j.biomaterials.2017.06.015

Bergholt, M. S., Lin, K., Wang, J., Zheng, W., Xu, H., Huang, Q., et al. (2016a). Simultaneous Fingerprint and High-Wavenumber Fiber-Optic Raman Spectroscopy Enhances Real-Timein Vivodiagnosis of Adenomatous Polyps during Colonoscopy. *J. Biophoton* 9, 333–342. doi:10.1002/jbio.201400141

Bergholt, M. S., St-Pierre, J.-P., Offeddu, G. S., Parmar, P. A., Albro, M. B., Puetzer, J. L., et al. (2016b). Raman Spectroscopy Reveals New Insights into the Zonal Organization of Native and Tissue-Engineered Articular Cartilage. *ACS Cent. Sci.* 2, 885–895. doi:10.1021/acscentsci.6b00222

Bonassar, L. J., Frank, E. H., Murray, J. C., Paguio, C. G., Moore, V. L., Lark, M. W., et al. (1995). Changes in Cartilage Composition and Physical Properties Due to Stromelysin Degradation. *Arthritis Rheum.* 38, 173–183. doi:10.1002/art.1780380205

Bornstein, P., Kang, A. H., and Piez, K. A. (1966). The Limited Cleavage of Native Collagen with Chymotrypsin, Trypsin, and Cyanogen Bromide*. *Biochemistry* 5, 3803–3812. doi:10.1021/bi00876a010

Boys, A. J., Kunitake, J. A. M. R., Henak, C. R., Cohen, I., Estroff, L. A., and Bonassar, L. J. (2019). Understanding the Stiff-To-Compliant Transition of the Meniscal Attachments by Spatial Correlation of Composition, Structure, and Mechanics. *ACS Appl. Mater. Inter.* 11, 26559–26570. doi:10.1021/acsami.9b03595

Bron, E. E., van Tiel, J., Smit, H., Poot, D. H. J., Niessen, W. J., Krestin, G. P., et al. (2013). Image Registration Improves Human Knee Cartilage T1 Mapping with Delayed Gadolinium-Enhanced MRI of Cartilage (dGEMRIC). *Eur. Radiol.* 23, 246–252. doi:10.1007/s00330-012-2590-3

Camacho, N. P., West, P., Torzilli, P. A., and Mendelsohn, R. (2001). FTIR Microscopic Imaging of Collagen and Proteoglycan in Bovine Cartilage. *Biopolymers* 62, 1–8. doi:10.1002/1097-0282(2001)62:1<1:aid-bip10>3.0.co;2-o

Chandrasekhar, S., Esterman, M. A., and Hoffman, H. A. (1987). Microdetermination of Proteoglycans and Glycosaminoglycans in the Presence of Guanidine Hydrochloride. *Anal. Biochem.* 161, 103–108. doi:10.1016/0003-2697(87)90658-0

Cui, H., Glidle, A., and Cooper, J. M. (2020). Highly Efficient Spatially Offset Raman Spectroscopy to Profile Molecular Composition in Bone. *IEEE Access* 8, 62905–62911. doi:10.1109/ACCESS.2020.2984170

Das Gupta, S., Finnilä, M. A. J., Karhula, S. S., Kauppinen, S., Joukainen, A., Kröger, H., et al. (2020). Raman Microspectroscopic Analysis of the Tissue-specific Composition of the Human Osteochondral junction in Osteoarthritis: A Pilot Study. *Acta Biomater.* 106, 145–155. doi:10.1016/j.actbio.2020.02.020

Démarteau, O., Pillet, L., Inaebnit, A., Borens, O., and Quinn, T. M. (2006). Biomechanical Characterization and *In Vitro* Mechanical Injury of Elderly Human Femoral Head Cartilage: Comparison to Adult Bovine Humeral Head Cartilage. *Osteoarthritis Cartilage* 14, 589–596. doi:10.1016/j.joca.2005.12.011

DiDomenico, C. D., Kaghazchi, A., and Bonassar, L. J. (2019). Measurement of Local Diffusion and Composition in Degraded Articular Cartilage Reveals the Unique Role of Surface Structure in Controlling Macromolecular Transport. *J. Biomech.* 82, 38–45. doi:10.1016/j.jbiomech.2018.10.019

Duraipandian, S., Bergholt, M., Zheng, W., and Huang, Z. (2014). *Quantitative Fiber-Optic Raman Spectroscopy for Tissue Raman Measurements*. Editors A. Mahadevan-Jansen and W. Petrich (San Francisco, CA), 89390V. doi:10.1117/12.2039576

Ellis, R., Green, E., and Winlove, C. P. (2009). Structural Analysis of Glycosaminoglycans and Proteoglycans by Means of Raman Microspectrometry. *Connect. Tissue Res.* 50, 29–36. doi:10.1080/03008200802398422

Esmonde-White, K. A., Esmonde-White, F. W. L., Morris, M. D., and Roessler, B. J. (2011). Fiber-optic Raman Spectroscopy of Joint Tissues. *Analyst* 136, 1675–1685. doi:10.1039/C0AN00824A

Farndale, R., Buttle, D., and Barrett, A. (1986). Improved Quantitation and Discrimination of Sulphated Glycosaminoglycans by Use of

Dimethylmethylene Blue. *Biochim. Biophys. Acta Gen. Subj.* 883, 173–177. doi:10.1016/0304-4165(86)90306-5

Farndale, R. W., Sayers, C. A., and Barrett, A. J. (1982). A Direct Spectrophotometric Microassay for Sulfated Glycosaminoglycans in Cartilage Cultures. *Connect. Tissue Res.* 9, 247–248. doi:10.3109/03008208209160269

Galvis, L., Dunlop, J. W. C., Duda, G., Fratzl, P., and Masic, A. (2013). Polarized Raman Anisotropic Response of Collagen in Tendon: Towards 3D Orientation Mapping of Collagen in Tissues. *PLoS One* 8, e63518. doi:10.1371/journal.pone.0063518

Gamsjaeger, S., Klaushofer, K., and Paschalis, E. P. (2014). Raman Analysis of Proteoglycans Simultaneously in Bone and Cartilage. *J. Raman Spectrosc.* 45, 794–800. doi:10.1002/jrs.4552

Ghita, A., Matousek, P., and Stone, N. (2016). Exploring the Effect of Laser Excitation Wavelength on Signal Recovery with Deep Tissue Transmission Raman Spectroscopy. *Analyst* 141, 5738–5746. doi:10.1039/C6AN00490C

Glover, P., and Mansfield, S. P. (2002). Limits to Magnetic Resonance Microscopy. *Rep. Prog. Phys.* 65, 1489–1511. doi:10.1088/0034-4885/65/10/203

Goodwin, D. W., Wadghiri, Y. Z., Zhu, H., Vinton, C. J., Smith, E. D., and Dunn, J. F. (2004). Macroscopic Structure of Articular Cartilage of the Tibial Plateau: Influence of a Characteristic Matrix Architecture on MRI Appearance. *Am. J. Roentgenology* 182, 311–318. doi:10.2214/ajr.182.2.1820311

Griffin, D. J., Vicari, J., Buckley, M. R., Silverberg, J. L., Cohen, I., and Bonassar, L. J. (2014). Effects of Enzymatic Treatments on the Depth-dependent Viscoelastic Shear Properties of Articular Cartilage. *J. Orthop. Res.* 32, 1652–1657. doi:10.1002/jor.22713

Iannucci, L. E., Boys, A. J., McCorry, M. C., Estroff, L. A., and Bonassar, L. J. (2019). Cellular and Chemical Gradients to Engineer the Meniscus-to-Bone Insertion. *Adv. Healthc. Mater.* 8, 1800806. doi:10.1002/adhm.201800806

Irwin, R. M., Gao, T., Boys, A. J., Ortved, K., Cohen, I., and Bonassar, L. J. (2021). Microscale Strain Mapping Demonstrates the Importance of Interface Slope in the Mechanics of Cartilage Repair. *J. Biomech.* 114, 110159. doi:10.1016/j.jbiomech.2020.110159

Kandel, S., Querido, W., Falcon, J. M., Reiners, D. J., and Pleshko, N. (2020). Approaches forIn SituMonitoring of Matrix Development in Hydrogel-Based Engineered Cartilage. *Tissue Eng. C: Methods* 26, 225–238. doi:10.1089/ten.tec.2020.0014

Kellgren, J. H., and Lawrence, J. S. (1957). Radiological Assessment of Osteo-Arthrosis. *Ann. Rheum. Dis.* 16, 494–502. doi:10.1136/ard.16.4.494

Khanarian, N. T., Boushell, M. K., Spalazzi, J. P., Pleshko, N., Boskey, A. L., and Lu, H. H. (2014). FTIR-I Compositional Mapping of the Cartilage-To-Bone Interface as a Function of Tissue Region and Age. *J. Bone Miner Res.* 29, 2643–2652. doi:10.1002/jbmr.2284

Király, K., Lammi, M., Arokoski, J., Lapveteläinen, T., Tammi, M., Helminen, H., et al. (1996). Safranin O Reduces Loss of Glycosaminoglycans from Bovine Articular Cartilage during Histological Specimen Preparation. *Histochem. J.* 28, 99–107. doi:10.1007/BF02331414

Lark, M. W., Bayne, E. K., and Lohmander, L. S. (1995). Aggrecan Degradation in Osteoarthritis and Rheumatoid Arthritis. *Acta Orthopaedica Scand.* 66, 92–97. doi:10.3109/17453679509157660

Mansfield, J. C., and Winlove, C. P. (2017). Lipid Distribution, Composition and Uptake in Bovine Articular Cartilage Studied Using Raman Micro-spectrometry and Confocal Microscopy. *J. Anat.* 231, 156–166. doi:10.1111/joa.12624

Martel-Pelletier, J., Barr, A. J., Cicuttini, F. M., Conaghan, P. G., Cooper, C., Goldring, M. B., et al. (2016). Osteoarthritis. *Nat. Rev. Dis. Primers* 2, 1–18. doi:10.1038/nrdp.2016.72

Masic, A., Bertinetti, L., Schuetz, R., Galvis, L., Timofeeva, N., Dunlop, J. W. C., et al. (2011). Observations of Multiscale, Stress-Induced Changes of Collagen Orientation in Tendon by Polarized Raman Spectroscopy. *Biomacromolecules* 12, 3989–3996. doi:10.1021/bm201008b

Matousek, P., Draper, E. R. C., Goodship, A. E., Clark, I. P., Ronayne, K. L., and Parker, A. W. (2006). Noninvasive Raman Spectroscopy of Human Tissue *In Vivo*. *Appl. Spectrosc.* 60, 758–763. doi:10.1366/000370206777886955

Matousek, P., and Stone, N. (2016). Development of Deep Subsurface Raman Spectroscopy for Medical Diagnosis and Disease Monitoring. *Chem. Soc. Rev.* 45, 1794–1802. doi:10.1039/C5CS00466G

Morris, M. D., Carden, A., Rajachar, R. M., and Kohn, D. H. (2002). "Effects of Applied Load on Bone Tissue as Observed by Raman Spectroscopy," in *Biomedical Vibrational Spectroscopy II*. (International Symposium on Biomedical Optics, 2002, San Jose, CA, United States), 47–54. doi:10.1117/12.460798

Mort, J. S., and Billington, C. J. (2001). Articular Cartilage and Changes in Arthritis: Matrix Degradation. *Arthritis Res.* 3, 337. doi:10.1186/ar325

Muir, H., Bullough, P., and Maroudas, A. (1970). The Distribution of Collagen in Human Articular Cartilage with Some of its Physiological Implications. *J. Bone Jt. Surg. Br. volume* 52-B, 554–563. doi:10.1302/0301-620X.52B3.554

Panula, H. E., Hyttinen, M. M., Arokoski, J. P. A., Långsjö, T. K., Pelttari, A., Kiviranta, I., et al. (1998). Articular Cartilage Superficial Zone Collagen Birefringence Reduced and Cartilage Thickness Increased before Surface Fibrillation in Experimental Osteoarthritis. *Ann. Rheum. Dis.* 57, 237–245. doi:10.1136/ard.57.4.237

Pavlou, E., Zhang, X., Wang, J., and Kourkoumelis, N. (2018). Raman Spectroscopy for the Assessment of Osteoarthritis. *Ann. Jt.* 3, 83. doi:10.21037/aoj.2018.09.10

Potter, H. G., Black, B. R., and Chong, L. R. (2009). New Techniques in Articular Cartilage Imaging. *Clin. Sports Med.* 28, 77–94. doi:10.1016/j.csm.2008.08.004

Pritzker, K. P. H., Gay, S., Jimenez, S. A., Ostergaard, K., Pelletier, J.-P., Revell, P. A., et al. (2006). Osteoarthritis Cartilage Histopathology: Grading and Staging. *Osteoarthritis Cartilage* 14, 13–29. doi:10.1016/j.joca.2005.07.014

Puchtler, H., Meloan, S. N., and Waldrop, F. S. (1988). Are Picro-Dye Reactions for Collagens Quantitative? *Histochemistry* 88, 243–256. doi:10.1007/BF00570280

Quinn, T. M., Häuselmann, H.-J., Shintani, N., and Hunziker, E. B. (2013). Cell and Matrix Morphology in Articular Cartilage from Adult Human Knee and Ankle Joints Suggests Depth-Associated Adaptations to Biomechanical and Anatomical Roles. *Osteoarthritis Cartilage* 21, 1904–1912. doi:10.1016/j.joca.2013.09.011

Raghavan, M., Sahar, N. D., Wilson, R. H., Mycek, M.-A., Pleshko, N., Kohn, D. H., et al. (2010a). "Polarized Raman Spectroscopy of Bone Tissue: Watch the Scattering," in *Photonic Therapeutics and Diagnostics VI*. (SPIE BiOS, 2010, San Francisco, California, United States), 754848. doi:10.1117/12.841977

Raghavan, M., Sahar, N. D., Wilson, R. H., Mycek, M.-A., Pleshko, N., Kohn, D. H., et al. (2010b). Quantitative Polarized Raman Spectroscopy in Highly Turbid Bone Tissue. *J. Biomed. Opt.* 15, 037001. doi:10.1117/1.3426310

Rieppo, J., Halmesmaki, E., Siitonen, U., Laasanen, M., Toyras, J., Kiviranta, I., et al. (2003). Histological Differences of Human, Bovine and Porcine Cartilage. *Trans. Orthop. Res. Soc.* 28, 589.

Rieppo, L., Saarakkala, S., Närhi, T., Holopainen, J., Lammi, M., Helminen, H. J., et al. (2009). Quantitative Analysis of Spatial Proteoglycan Content in Articular Cartilage with Fourier Transform Infrared Imaging Spectroscopy: Critical Evaluation of Analysis Methods and Specificity of the Parameters. *Microsc. Res. Tech.* 73, NA. doi:10.1002/jemt.20789

Rosenberg, L. (1971). Chemical Basis for the Histological Use of Safranin O in the Study of Articular Cartilage. *J. Bone Jt. Surg.* 53, 69–82. doi:10.2106/00004623-197153010-00007

Silverberg, J. L., Barrett, A. R., Das, M., Petersen, P. B., Bonassar, L. J., and Cohen, I. (2014). Structure-Function Relations and Rigidity Percolation in the Shear Properties of Articular Cartilage. *Biophysical J.* 107, 1721–1730. doi:10.1016/j.bpj.2014.08.011

Takahashi, Y., Sugano, N., Takao, M., Sakai, T., Nishii, T., and Pezzotti, G. (2014). Raman Spectroscopy Investigation of Load-Assisted Microstructural Alterations in Human Knee Cartilage: Preliminary Study into Diagnostic Potential for Osteoarthritis. *J. Mech. Behav. Biomed. Mater.* 31, 77–85. doi:10.1016/j.jmbbm.2013.02.014

Taylor, E. A., and Donnelly, E. (2020). Raman and Fourier Transform Infrared Imaging for Characterization of Bone Material Properties. *Bone* 139, 115490. doi:10.1016/j.bone.2020.115490

Taylor, S. D., Tsiridis, E., Ingham, E., Jin, Z., Fisher, J., and Williams, S. (2012). Comparison of Human and Animal Femoral Head Chondral Properties and

Geometries. *Proc. Inst. Mech. Eng. H* 226, 55–62. doi:10.1177/0954411911428717

Vardaki, M. Z., Gardner, B., Stone, N., Matousek, P., and Matousek, P. (2015). Studying the Distribution of Deep Raman Spectroscopy Signals Using Liquid Tissue Phantoms with Varying Optical Properties. *Analyst* 140, 5112–5119. doi:10.1039/C5AN01118C

Zeng, H., Zhao, J., Short, M., Mclean, D. I., Lam, S., Mcwilliams, A., et al. (2008). Raman Spectroscopy for *In Vivo* Tissue Analysis and Diagnosis, from Instrument Development to Clinical Applications. *J. Innov. Opt. Health Sci.* 1, 95–106. doi:10.1142/S1793545808000054

Conflict of Interest: The authors declare that the research was conducted in the absence of any commercial or financial relationships that could be construed as a potential conflict of interest.

Publisher's Note: All claims expressed in this article are solely those of the authors and do not necessarily represent those of their affiliated organizations, or those of the publisher, the editors and the reviewers. Any product that may be evaluated in this article, or claim that may be made by its manufacturer, is not guaranteed or endorsed by the publisher.

frontiers in Bioengineering and Biotechnology

ORIGINAL RESEARCH
published: 02 December 2021
doi: 10.3389/fbioe.2021.747217

A Multi-Task Deep Learning Method for Detection of Meniscal Tears in MRI Data from the Osteoarthritis Initiative Database

Alexander Tack[1]*, *Alexey Shestakov*[1], *David Lüdke*[1] and *Stefan Zachow*[1,2]

[1]Dept. for Visual and Data-Centric Computing, Zuse Institute Berlin, Berlin, Germany, [2]Charité–University Medicine, Berlin, Germany

We present a novel and computationally efficient method for the detection of meniscal tears in Magnetic Resonance Imaging (MRI) data. Our method is based on a Convolutional Neural Network (CNN) that operates on complete 3D MRI scans. Our approach detects the presence of meniscal tears in three anatomical sub-regions (anterior horn, body, posterior horn) for both the Medial Meniscus (MM) and the Lateral Meniscus (LM) individually. For optimal performance of our method, we investigate how to preprocess the MRI data and how to train the CNN such that only relevant information within a Region of Interest (RoI) of the data volume is taken into account for meniscal tear detection. We propose meniscal tear detection combined with a bounding box regressor in a multi-task deep learning framework to let the CNN implicitly consider the corresponding RoIs of the menisci. We evaluate the accuracy of our CNN-based meniscal tear detection approach on 2,399 Double Echo Steady-State (DESS) MRI scans from the Osteoarthritis Initiative database. In addition, to show that our method is capable of generalizing to other MRI sequences, we also adapt our model to Intermediate-Weighted Turbo Spin-Echo (IW TSE) MRI scans. To judge the quality of our approaches, Receiver Operating Characteristic (ROC) curves and Area Under the Curve (AUC) values are evaluated for both MRI sequences. For the detection of tears in DESS MRI, our method reaches AUC values of 0.94, 0.93, 0.93 (anterior horn, body, posterior horn) in MM and 0.96, 0.94, 0.91 in LM. For the detection of tears in IW TSE MRI data, our method yields AUC values of 0.84, 0.88, 0.86 in MM and 0.95, 0.91, 0.90 in LM. In conclusion, the presented method achieves high accuracy for detecting meniscal tears in both DESS and IW TSE MRI data. Furthermore, our method can be easily trained and applied to other MRI sequences.

Keywords: knee joint, meniscal lesions, convolutional neural networks–CNN, residual learning, explainable AI (XAI), multi-task deep learning, bounding box regression, object detection

OPEN ACCESS

Edited by:
Fabio Galbusera, Galeazzi Orthopedic Institute (IRCCS), Italy

Reviewed by:
Andrea Cina, Galeazzi Orthopedic Institute (IRCCS), Italy
Jonas Schwer, University of Ulm, Germany
Fuyuan Liao, Xi'an Technological University, China

***Correspondence:**
Alexander Tack
tack@zib.de

Specialty section:
This article was submitted to Biomechanics, a section of the journal Frontiers in Bioengineering and Biotechnology

Received: *25 July 2021*
Accepted: *15 October 2021*
Published: *02 December 2021*

Citation:
Tack A, Shestakov A, Lüdke D and Zachow S (2021) A Multi-Task Deep Learning Method for Detection of Meniscal Tears in MRI Data from the Osteoarthritis Initiative Database. Front. Bioeng. Biotechnol. 9:747217. doi: 10.3389/fbioe.2021.747217

1 INTRODUCTION

Menisci are hydrated fibrocartilaginous soft tissues within the knee joint that absorb shocks, provide lubrication, and allow for joint stability during movement (Markes et al., 2020). In patients with symptomatic osteoarthritis, meniscal damage is also found very frequently with a prevalence of up to 91% (Bhattacharyya et al., 2003). Meniscal tears are usually caused by trauma and degeneration

(Beaufils and Pujol, 2017) and might lead to a loss of function, early osteoarthritis, tibiofemoral osteophytes, and cartilage loss (Ding et al., 2007; Snoeker et al., 2021). Magnetic Resonance Imaging (MRI) is commonly used for the noninvasive assessment of meniscal morphology since MRI provides a three-dimensional view of the knee joint with high contrast between soft tissues. Hence, MRI is the recognized screening tool for diagnostic assessment before performing therapeutic arthroscopy or any other treatment (Crawford et al., 2007). Among other factors, a proper treatment concept for meniscal damage depends highly on the type of tear and its location (Englund et al., 2001; Beaufils and Pujol, 2017). An appropriate medical intervention can delay further development of arthritic changes, improve quality of life, and reduce healthcare expenditures. However, in practice, the optimal treatment is not always apparent (Khan et al., 2014; Kise et al., 2016), while an improper procedure might even lead to an acceleration of osteoarthritis progression (Roemer et al., 2017). For this reason, an accurate and reliable diagnosis of meniscal tears in view of their location, type, and orientation is important.

The diagnosis of meniscal tears in MRI is a time consuming and tedious procedure. These defects are often difficult to detect due to their small sizes and arbitrary orientations. It is frequently necessary to go back and forth in the MRI slices and switch view directions for a thorough assessment of occurrences and spatial extents of pathological changes. In addition, the meniscal representation in the image data depends on the chosen MRI sequence. What appears clearly visible in one sequence may be barely noticeable in another due to insufficient contrast. Computer-Aided Diagnosis (CAD) attempts to overcome some of these limitations. CAD tools can be employed to increase the sensitivity and specificity of physicians in detecting and classifying meniscal tears (Bien et al., 2018; Pedoia et al., 2019; Kunze et al., 2020). Moreover, CAD could speed up the diagnosis, reduce the number of unintentionally missed defects, avoid unnecessary interventions (e.g., arthroscopic interventions), and lead to fewer treatment delays. Several CAD approaches for an automated detection of meniscal tears in MRI data have been proposed in recent years. A distinction can be made between methods that evaluate the 2D contents of cross-sectional images often coming from a set of curated slices (2D approaches) and those that evaluate 3D image information in the MRI data volume (3D approaches). In the context of image analysis by means of Convolutional Neural Networks (CNNs), we distinguish between 2D CNNs and 3D CNNs. In the case of the 2D approaches, there exists a pseudo-3D variant in which sets of (neighboring) sectional images are included in the evaluation. In these pseudo-3D variants, 2D CNNs are employed to encode 2D slices of a 3D MRI dataset. Afterwards, the respective 2D encodings are condensed (e.g., by global max- or average-pooling), concatenated, and passed to a classifier.

Roblot et al. (2019) proposed a method to detect meniscal tears from a curated set of sagittal 2D MRI slices. Their approach is based on the 2D "faster R-CNN" (Ren et al., 2015) and comprises three steps: Firstly, the positions of both meniscal horns are detected; secondly, the presence of a tear is classified; and thirdly, the respective tear orientation is determined. The method yields an Area Under the Curve (AUC) of the Receiver Operating Characteristic (ROC) of 0.92 for the detection of the meniscal horns' positions, an AUC of 0.94 for detecting the presence of meniscal tears, and an AUC of 0.83 for the determination of the tear orientations. Couteaux et al. (2019) presented a similar method, also detecting meniscal tears from a curated set of sagittal 2D MRI slices. They employed a masked region-based 2D CNN (He et al., 2017) to locate the anterior and the posterior horns of the Medial Meniscus (MM) as well as the Lateral Meniscus (LM). Their method yields on average an AUC of 0.906 for all three tasks, i.e. the location of the respective region, the detection of meniscal tears, and the classification of the tear orientation.

Processing of all MRI slices instead of individually selected ones was performed by Bien et al. (2018) who proposed a 2D CNN for the detection of meniscal tears. Their method achieves an AUC of 0.847. Pedoia et al. (2019) adopted a method that combined a 2D CNN for meniscus segmentation with a 3D CNN for detection and severity assessment of meniscal tears. This approach was able to differentiate between tears and no tears with an AUC of 0.89. Tsai et al. (2020) proposed a so-called "Efficiently-Layered Network" for detection of meniscal tears, reaching an AUC of 0.904 and 0.913 for two different datasets. Azcona et al. (2020) demonstrated the use of a 2D CNN as a pseudo-3D variant for detection of torn menisci. Their method relies on transfer learning while using data augmentation and reaches an AUC of 0.934. Fritz et al. (2020) presented a deep 3D CNN to detect tears in MRI data for MM and LM, respectively. Their method reaches AUC values of 0.882, 0.781, and 0.961 for the detection of medial, lateral, and overall meniscal tears. Rizk et al. (2021) also proposed a 3D CNN for meniscal tear detection in MRI data for MM and LM individually. Their approach yields an AUC of 0.93 for MM and 0.84 for LM.

A common limitation among many of the methods listed above is their strong reliance on segmentations of the menisci (or at least of bounding boxes), which can be challenging to obtain due to the inhomogeneous appearance of pathological menisci in MRI data as well as an insufficient contrast to adjacent tissues (Rahman et al., 2020). Furthermore, some approaches merely operate on 2D slices. A major limitation of such methods is that the trained 2D CNNs cannot take whole MRI volumes into account, thus possibly missing important feature correlations in 3D space. Besides, an appropriate selection of curated slices requires expert knowledge. Therefore, the applicability of these methods to 3D volumes is unclear since they were not trained on 3D data. Finally, none of the presented methods is able to detect meniscal tears for all anatomical sub-regions of the menisci individually, i.e., the anterior horn, the meniscal body, and the posterior horn.

Our motivation is to detect meniscal tears in MRI data more accurately than previous methods in terms of correctness and localization. For this purpose, we present a method that detects tears in anatomical sub-regions of both the MM and the LM. We design our study in a manner that allows for a comparison of different possible approaches. Moreover, the study shows our progression in addressing the task of meniscal tear detection in

3D MR images. We investigate how to handle best the input data such that the least pre-processing is required for inference and the best accuracy is achieved. Furthermore, we show that our proposed method generalizes well to different MRI sequences. We employ two ResNet architectures (He et al., 2016; Yu et al., 2017) to classify meniscal tears in each sub-region of the MM and the LM, respectively, utilizing three different approaches.

In a first approach (i), we train a 3D CNN on the complete 3D MRI dataset as input. We call it *Full-scale* approach within the remainder of this article.

Since large input data requires a lot of GPU memory, longer time for training and inference, and contains image information not necessarily needed for an assessment of meniscal tears, we decided to crop the data to the Regions of Interest (RoI) of both menisci in an automated pre-processing step that requires segmentations of sufficient quality for training and testing (Tack et al., 2018). Hence, in a second approach (ii), a 3D CNN is trained on these cropped MRIs detecting meniscal tears more accurately than in our first approach. We refer to the second approach as *BB-crop* approach.

We enhanced the performance of our first approach by adding a bounding box regression task. Thus, our final approach (iii) trains a CNN to detect meniscal tears in complete 3D MRI, combined with an additional bounding box regression task leading to an auxiliary loss (the *BB-loss* approach). Framing the problem of meniscal tear detection in this multi-task learning setting – simultaneously solving meniscal tear detection and meniscal bounding box regression – allows our model to implicitly learn to focus on the meniscal regions. Furthermore, segmentation masks are only required during training. Hence, our final approach requires the least data pre-processing at inference time and achieves the best results.

This study presents a method that detects meniscal tears in 3D MRI data on a sub-region level, i.e., the anterior horn, the meniscal body, and the posterior horn for both MM and LM. Formulating the problem in a multi-task learning setting, by adding the information of the location of the menisci as an auxiliary loss to our 3D CNN, state-of-the-art results are achieved. In order to provide an explanation to our CNN's decision, SmoothGrad saliency maps (Smilkov et al., 2017) are computed and visualized. That way a visual guidance can be given to the clinical domain experts for confirming the results of our approach.

2 MATERIALS AND METHODS

In **section 2.1** of this chapter, the data to our method is presented. Thereafter, in **sections 2.2** we introduce our data pre-processing and bounding box generation. Section **2.3** is a description of the model architectures utilized in our approach and of their respective components. The particular configuration of our three approaches is illustrated in detail in **sections 2.4**, **2.5**, and **2.6**, followed by an explanation of our experimental set-up and training in **section 2.7**. Finally, a statistical evaluation is summarized in **section 2.8** and a method for saliency maps is proposed in **section 2.9**.

TABLE 1 | Demographics: In this study, 2,399 DESS and 2,396 IW TSE MRI scans from the OAI database are analyzed. In these data, slightly more normal than diseased medial menisci (MM) and lateral menisci (LM) are contained. Here, normal is defined as no conspicuous features with respect to the MOAKS scoring system in any sub-region.

	DESS	IW TSE
Number of MR images	2,399	2,396
In-plane resolution	0.36 mm × 0.36 mm	0.36 mm × 0.36 mm
Usual slice dimension	384 × 384	442 × 448
Slice thickness	0.7 mm	3 mm
Number of slices	160	35 to 43
Side (left; right)	1104; 1295	1104; 1292
Sex (female; male)	1489; 910	1487; 909
Age [years]	61.88 ± 8.87	61.89 ± 8.86
BMI [kg/m^2]	29.01 ± 4.79	29.08 ± 4.79
MM (% normal)	60.0%	59.9%
LM (% normal)	80.0%	79.9%

2.1 Data from the OAI Database

The publicly available database of the Osteoarthritis Initiative (OAI)[1] was established to provide researchers with resources to promote the prevention and treatment of knee osteoarthritis. We use 2,399 sagittal Double Echo Steady-State (DESS) 3D MRI scans from the OAI database acquired using Siemens Trio 3.0 Tesla scanners (Peterfy et al., 2006). Additionally, 2,396 sagittal Intermediate-Weighted Turbo Spin-Echo (IW TSE) MRI scans are investigated for the same patients. The demographics of our study are shown in **Table 1**.

The OAI database includes multiple reading studies of respective osteoarthritis characteristics, which can be assessed in medical image data. As a gold standard, we utilize labels from MOAKS (Hunter et al., 2011) image reading studies performed by clinical experts. In the MOAKS scoring system, the menisci are divided into three anatomical sub-regions: anterior horn, body, posterior horn. We consider a sub-region as not containing a tear if the MOAKS score is "normal" or indicates a signal abnormality (which is not extending through the meniscal surface and, hence, is no tear). We considered any other type of abnormality (radial, horizontal, vertical, etc.) as a meniscal tear (c.f. **Supplementary Table S1**). Examples of the MRI sequences, signal abnormalities, and meniscal tears are shown in **Figure 1**.

2.2 Data Pre-processing and Localization of Menisci

In a first step of our pre-processing, the intensities of all MR images are scaled to a range of [0, 1] using min-max normalization. Following that, a standardization is applied to each MR image $\mathcal{I}_i$ according to:

$$\tilde{\mathcal{I}}_i = \frac{\mathcal{I}_i - \mu}{\sigma}, \tag{1}$$

where μ is the mean intensity and σ is the standard deviation of the training population of normalized scans. Leveraging meniscal

[1]https://nda.nih.gov/oai/

FIGURE 1 | Examples of normal menisci, signal abnormalities, and subjects with meniscal tears shown for DESS as well as IW TSE MRI data. For a summary of different types of meniscal tears per sub-region the reader is referred to **Supplementary Table S1**.

segmentations generated by the method of Tack et al. (2018) RoIs spanning the MM and LM are created for DESS MRI data (see **Figure 2**). RoIs are computed by querying the minimum and maximum position of the menisci along each dimension of the binary segmentation masks: $x_{\min}$, $x_{\max}$, $y_{\min}$, $y_{\max}$, $z_{\min}$, $z_{\max}$. The bounding boxes are uniquely defined as the 3D center coordinate

$$BB_{center} = \begin{bmatrix} (x_{max} - x_{min})/2 + x_{min} \\ (y_{max} - y_{min})/2 + y_{min} \\ (z_{max} - z_{min})/2 + z_{min} \end{bmatrix}, \quad (2)$$

and with the respective height ($x_{\max} - x_{\min}$), width ($y_{\max} - y_{\min}$), and depth ($z_{\max} - z_{\min}$). These values are represented as relative

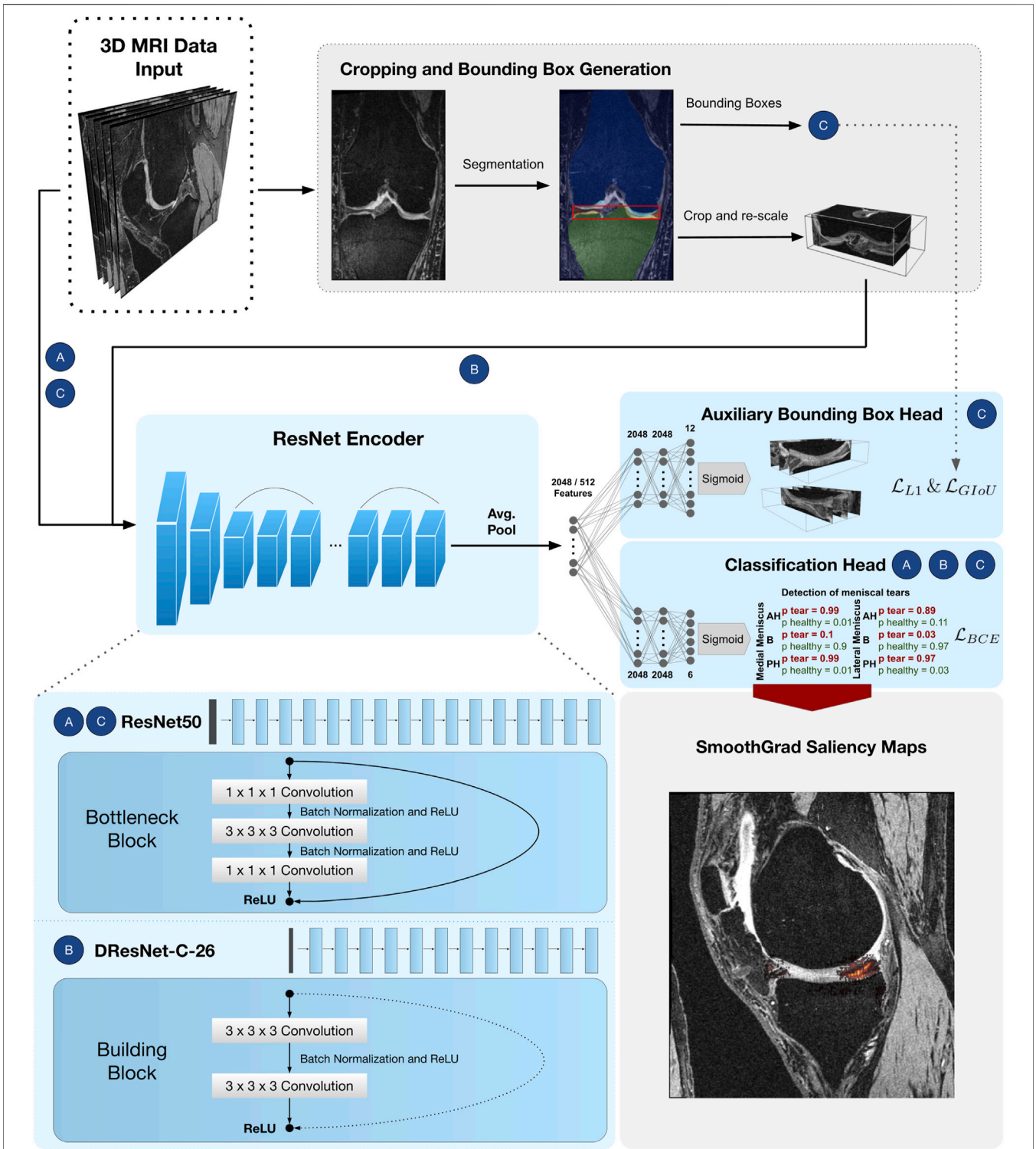

FIGURE 2 | CNN pipeline for detection of meniscal tears in six sub-regions. Approach *Full-scale* uses a ResNet50 encoder followed by a classifier head with $\mathcal{L}_{BCE}$ for classification of meniscal tears in 3D MRI data **(A)**. Approach *BB-crop* reduces the 3D MRI input to the meniscal RoI and uses a DRN-C-26 encoder followed by a classifier head with $\mathcal{L}_{BCE}$ to detect meniscal tears **(B)**. Approach *BB-loss* uses a ResNet50 encoder followed by a classifier head with $\mathcal{L}_{BCE}$ as well as another bounding box regression head with $\mathcal{L}_{L1}$ and $\mathcal{L}_{GIoU}$ in order to predict bounding boxes of the menisci in the 3D MRI data **(C)**. The ResNet50 is made up of an initial convolutional layer followed by max-pooling before 16 ResNet bottleneck blocks with residual connections are stacked. The DRN-C-26 starts with the same convolutional layer but is immediately followed by ten residual building blocks and, lastly, two building blocks without a residual connection. After average pooling, the encoders generate 2048 and 512 features, respectively. Finally, SmoothGrad saliency maps are presented as overlaid heatmaps on top of the respective MR image to highlight these regions that mostly influenced the detection of tears (bottom right corner).

image coordinates. Hence, a bounding box is defined by 6 floating values: $[BB^{x}_{center}, BB^{y}_{center}, BB^{z}_{center}, height, width, depth]$.

For the IW TSE data 600 segmentations are generated in a semi-automated fashion using Amira ZIB Edition[2] (Reddy, 2017). These masks are defined as voxel-wise annotations of the tissue belonging to the respective meniscus. The method of Tack et al. (2018) was originally developed and evaluated on DESS MRI data. Since the DESS and IW TSE MRI sequences differ significantly in the image resolution (number of slices), that could pose an issue, we have decided to train the self-adapting nnU-net framework (Isensee et al., 2021) on these 600 training datasets. The nnU-net offers 2D and 3D architectures with 3D architectures usually yielding better results (Isensee et al., 2021). For this reason, we have used a 3D variant of the nnU-net that employs 3D convolutions in an encoder-decoder framework with skip-connections. For the IW TSE data, the nnU-net has been automatically configured to have an input size of 24 × 256 × 256 pixels and seven layers of 3D convolutions (Isensee et al., 2021). We train the nnU-net with data augmentation such as random rotations and random cropping using a dice similarity coefficient loss (Isensee et al., 2021) until convergence is reached. Hereby, the dice similarity coefficient is computed between the output of the nnU-net and the respective hand-labelled target segmentation masks. Afterwards, the nnU-net is employed to segment all 2,396 IW TSE MRI scans to yield the respective meniscal RoIs. In order to achieve this, multiple patches of the MRI with a size of 24 × 256 × 256 pixels are being processed by the nnU-net. These patches overlap by half of the patch size in each dimension. Afterwards, the nnU-net framework merges all patches to a final 3D segmentation mask employing a majority voting for every pixel.

2.3 Model Architecture

Two distinct models, which are based on 3D counterparts of ResNet architectures (He et al., 2016; Yu et al., 2017) are introduced. ResNets have been widely applied to the medical domain and provide good properties due to the employed skip connections. In theory, the residual connections allow the design of very deep ResNets without exhibiting problems of vanishing gradients (Ide and Kurita, 2017). We have chosen 3D counterparts of 2D ResNets since 3D convolutions are able to comprehend three-dimensional context inherently. It has previously been shown in the context of musculoskeletal MRI analysis that 3D convolutions are more powerful than concatenation of 2D slices as well as a provision of multiple 2D slices as input to a CNN that employs 2D convolutions (Ambellan et al., 2019; Tack and Zachow, 2019). We adapt these 3D ResNet architectures to the three different approaches and their associated input volume sizes. Each model consists of a ResNet encoder followed by one or two Multi-Layer Perceptron (MLP) heads. The *BB-crop* approach has a dilation ResNet-C-26 architecture with an MLP head for the multi-label classification. The *Full-scale* approach has a ResNet50 encoder with a classifier MLP head, and the *BB-loss* approach consists of a ResNet50 encoder with two MLP heads. The performance of the classification task is improved in the BB-loss approach by solving additionally a second task, which is to learn a bounding box regression simultaneously. Again, the first MLP head is employed for multi-label classification. The second MLP head is responsible for the bounding box regression task. All ResNets comprise of a series of convolutional layers, each followed by batch normalization (Ioffe and Szegedy, 2015) and a Rectified Linear Unit (ReLU) activation function (Agarap, 2018).

Our approaches that will be presented in the following sections are designed based on (a selection of) encoders and MLP heads:

ResNet50 Encoder

He et al. (2016) proposed a residual layer connection as a way to train deep neural networks without suffering from vanishing gradients. One of their proposed architectures is the ResNet50, with a total of 50 convolutional layers (see **Figure 2**). The network comprises an initial convolutional layer with kernel size 7 × 7 × 7 followed by a max-pooling layer with kernel size 3 × 3 × 3 and stride 2. The following residual layers are grouped in so-called "bottleneck blocks" (see **Figure 2**), which are constructed of three convolutional layers. The first and the last are convolutional layers, with kernel size 1 × 1 × 1, where the first one downsamples the number of volume features, and the last one applies feature upsampling. Between these layers, there is a convolutional layer with kernel size 3 × 3 × 3. The bottleneck blocks are arranged in four groups of sizes 3, 4, 6, and 3, where each group starts with a stride of 2 in the first convolutional layer to downsample the feature volumes' spatial dimensions. Finally, the residual blocks are terminated with a global average pooling (Lin et al., 2013) over the 2048 individual 3D feature volumes coming from the last layer of the ResNet encoder. Computing the average value of each feature map via global average pooling results in a 1D tensor with 2048 features.

Dilation ResNet-C-26 Encoder

The DRN-C-26 is a dilated residual CNN architecture with 26 layers introduced by Yu et al. (2017). The original ResNet downsamples the input images by a factor of 32. Downsampling our cropped and uneven sized image volumes by such an amount would result in a loss of information about small and salient parts caused by less expressive feature maps. However, simply reducing the convolutional stride restricts the receptive field of subsequent layers. For this reason, Yu et al. (2017) presented an approach with which downsampling could be reduced while sustaining a sufficiently large receptive field and improving classification results. To construct the DRN-C-26 Yu et al. (2017) applied the following changes to the ResNet18 (He et al., 2016) made of so-called ResNet "building blocks" with two convolutional layers with kernel size 3 × 3 × 3 (see **Figure 2**). First, the convolutional stride in the last two groups is replaced by dilation. Second, the initial max-pooling layer is replaced by two

[2]https://amira.zib.de

residual building blocks. Lastly, to reduce aliasing artefacts, a decrease in dilation is added with two final building blocks without residual connections. Again, the residual blocks of the DRN-C-26 are followed by a global average pooling over the 512 feature maps of the last ResNet layer, resulting in a 1D tensor with 512 features.

MLP Heads

The features obtained by the respective ResNet encoders are passed through a simple three-layered feed-forward network, also known as MLP, to achieve the respective classifications and regressions. As shown in **Figure 2**, the MLP input dimension matches the feature dimensions of the CNN (i.e., 2048 neurons in case of ResNet50 and 512 neurons for a DRN-C-26). The hidden layers of all MLP's consist of 2048 neurons. The classifier head has six output nodes. In the *BB-loss* setting, an additional three-layered MLP with twelve output nodes was added to perform a bounding box regression.

2.4 *Full-Scale* Approach: Detection of Meniscal Tears in Complete MRI Scans

In our first and most straightforward approach, the complete 3D MRI is provided as input to the CNN. The CNN consists of a ResNet50 encoder followed by an MLP head. The outputs of the MLP after a sigmoid activation represent the probabilities for the six meniscal sub-regions to contain a tear.

The CNN is trained by minimizing the binary cross-entropy loss $\mathcal{L}_{BCE}$ for a given batch of N samples. With a target matrix $\mathbf{Y} \in \mathbb{Z}_2^{N\times C}$ and an output matrix $\hat{\mathbf{Y}} \in \mathbb{R}^{N\times C}$ for all C meniscal sub-region labels the definition of $\mathcal{L}_{BCE}$ is:

$$\mathcal{L}_{BCE} = \frac{1}{N}\sum_{c=1}^{C}\sum_{i=1}^{N} w_c\,[y_{i,c} log\,(\sigma\,(\hat{y}_{i,c})) + (1 - y_{i,c}) log\,(1 - \sigma\,(\hat{y}_{i,c}))], \tag{3}$$

where w_c is an inverse weighting of label frequencies and $\sigma(\cdot)$ is a sigmoid activation function. The *Full-scale* approach is visualized under A) in **Figure 2**.

2.5 *BB-Crop* Approach: Detection of Meniscal Tears in Cropped MRI Datasets

Cropping 3D MRI data to the meniscal RoI is expected to provide two desirable properties. First, it provides smaller volumes reducing the required GPU memory as well as the run time. Second, the *Full-scale* 3D MR images can be considered noisy as they provide additional and unnecessary information about surrounding anatomical structures. By cropping the data to the RoI of the menisci, this unnecessary information is suppressed. Leveraging the RoI generated as described in **section 2.2** the 3D MR images are cropped with a 5% margin around the menisci. Each cropped image is then resampled with trilinear interpolation to the closest multiples of 16, given the biggest bounding box in the training set. **Figure 2** visualizes the cropping and resampling process. Consequently, the cropped and resampled images have a size of (64, 64, 176) for the DESS data and (16, 64, 176) for the IW TSE data. *BB-crop* utilizes a Dilation Resnet-C-26 encoder followed by an MLP classifier head. The CNN is trained by minimizing the $\mathcal{L}_{BCE}$ as given in **Eq. 3**. The framework is visualized under B) in **Figure 2**.

2.6 *BB-Loss* Approach: Detection of Meniscal Tears in Complete MRI Scans Enhanced by Regression of Meniscal Bounding Boxes

The *BB-crop* approach requires segmentation of both menisci (or at least the determination of a meniscal region) in training and testing. Since generating segmentations is time-consuming (the method of Tack et al. (2018) requires approximately 5 min of run time), it is beneficial to avoid this step. Moreover, this approach heavily relies on high-quality bounding boxes in training and inference, which are difficult to obtain and strongly influence the performance quality. Thus, the motivation for our final *BB-loss* approach is to detect meniscal tears in 3D MRI data without extensive pre-processing requirements such as segmenting the menisci or computing bounding boxes for meniscal regions. Instead, the location of the menisci is added as an additional loss term for the training. The encoder is kept identical to the *Full-scale* approach, namely a ResNet-50 encoder. Furthermore, an identical MLP head is utilized for the meniscal tear detection. Additionally, we show that the meniscal position information helps the CNN to focus on these regions in the image yielding better results. A second MLP head is employed in the *BB-loss* approach to regress the coordinates of the meniscal RoI. By incorporating this knowledge as a loss in the training process, the locations of the menisci must not be explicitly provided at test time. The total loss in the *BB-loss* setting is computed considering the multi-label classification and the bounding box regression task. For detection of meniscal tears $\mathcal{L}_{BCE}$ is employed (**Eq. 3**). In the bounding box regression the outputs of the MLP head are 6 coordinates d for the MM and LM, respectively. Utilizing a sigmoid activation function, these values are given as relative positions within the image in a range of [0, 1] of the respective dimension. For a detailed description of the bounding box generation procedure, we refer the reader to **section 2.2**. The first component of the bounding box loss is an L1-term $\mathcal{L}_{L1}$ defined as

$$\mathcal{L}_{L1} = \|B - \hat{B}\|, \tag{4}$$

with a predicted bounding box $\hat{B}$ and a target bounding box B that is derived from the automated segmentation masks. These $N \times 2d$ matrices contain N rows with medial and lateral bounding box values. Where $b_{n,i}$ and $\hat{b}_{n,i}$ describe the nth element of the batch and the ith value of the concatenated bounding boxes. With this formulation the loss is given as

$$\mathcal{L}_{L1} = \frac{1}{N}\sum_{n=1}^{N}\sum_{i=1}^{2d} |b_{n,i} - \hat{b}_{n,i}|. \tag{5}$$

The second component of the bounding box loss is a modified Intersection over Union (IoU) term, more specifically the Generalized-IoU (GIoU) $\mathcal{L}_{GIoU}$ (Rezatofighi et al., 2019) defined as:

$$\mathcal{L}_{GIoU} = 1 - IoU + \frac{|C \setminus (B \cup \hat{B})|}{|C|}, \quad (6)$$

where C is a convex hull enclosing the predicted and the target box. The operator $|\cdot|$ computes the box volume. The convex hull is the smallest possible region that encloses both the output and the target bounding boxes. It can be defined as a bounding box, fully characterised by the 6 coordinates elaborated above. It is computed by taking the minimum and maximum extent of both the target bounding box and the predicted bounding box coordinates along the x-, y- and z-axis. The numerator of the third term of the $\mathcal{L}_{GIoU}$ is the convex hull volume subtracted by the volume of B and $\hat{B}$, and the denominator is the volume of the convex hull. Hence, the third term of the $\mathcal{L}_{GIoU}$ can be considered as the relative volume of the convex hull not covered by the union of predicted and target bounding box. The IoU is defined as $\frac{|B \cap \hat{B}|}{|B \cup \hat{B}|}$, that is, the ratio of the intersecting voxels of B and $\hat{B}$ to their union. The $\mathcal{L}_{GIoU}$ is computed for each meniscal RoI and averaged for the given batch. The overall loss $\mathcal{L}$ for the *BB-loss* approach is given as

$$\mathcal{L} = \mathcal{L}_{BCE} + \mathcal{L}_{L1} + \mathcal{L}_{GIoU}. \quad (7)$$

The *BB-loss* approach is visualized under C) in **Figure 2**.

2.7 Experimental Setup and Training of CNNs

The given MRI data of the OAI are randomly split into 50% training data, 15% validation data and 35% testing data. Hence, our two experiments have 1200/359/840 and 1197/359/840 training/validation/testing scans for the DESS data and the IW TSE data, respectively. We implemented the CNNs of all approaches in PyTorch 1.9. Convolutional weights are initialized using a normal distribution as in He et al. (2015) tailored towards our deep neural networks with asymmetric ReLU activation functions. While, batch normalization weights and biases are initialized constant with 1 and 0. We train our CNNs on an Nvidia A100 GPU with 40 GB memory. Training our three ResNets, separate learning rates and dropout probabilities for the ResNet-encoders and the MLP-heads are introduced. Suitable learning rate, dropout and batch size hyper-parameters are found using the validation data of the DESS scans. The learning rate values for all parts (ResNet encoder, classifier head and bounding box head) are evaluated in an interval of $[1e-5, 0.01]$. Dropout percentages are varied in an interval of [0.1, 0.9]. Further, the training batch size limited by the input size is varied from 2 to 64 for the *BB-crop* approach. Due to a larger input volume in approach *Full-scale* and *BB-loss* batch size was kept constant at a value of 4. For a complete summary of our hyper-parameter values, please refer to **Supplementary Table S2**. Training is performed using the ADAM optimizer (Kingma and Ba, 2014) with $\beta_1 = 0.9$, $\beta_2 = 0.999$ and $\epsilon = 1e-08$ with a learning rate decay of 0.5 every 50 epochs. Training on the IW TSE sequence is not performed from scratch, instead, both ResNet encoder and MLP weights are fine-tuned. In both DRN-C-26 and ResNet50 cases, we use the CNNs that achieve the lowest validation loss on the DESS sequence.

On-the-fly data augmentation is performed during training. Specifically, this means, random cropping around the RoI, horizontal flips, rotations, Gaussian noise, and intensity scaling are applied with 50% probability. For the *Full-scale* approach, we perform random cropping of up to 10% along coronal, 20% sagittal and 20% axial direction. In the *BB-crop* approach, random crops are performed by uniformly cropping within a 20% margin around the menisci. The *BB-loss* approach uniformly samples possible crops around the menisci. All cropped images are resampled with trilinear interpolation to attain consistent sizes per approach and dataset. Input images for the *Full-scale* and *BB-loss* approach are sampled for the DESS sequence data to (160, 384, 384) and for IW TSE images to (44, 448, 448). The *BB-crop* approach resamples to (64, 64, 176) and (16, 64, 176), respectively. The added Gaussian noise is pixel-wise sampled as $\epsilon \in \mathcal{N}(0.1, 0.5)$. The random rotation is uniformly sampled from $\mathcal{U}(-5°, +5°)$ and image intensity is scaled by a uniformly sampled multiplication factor $b \in \mathcal{U}(0.9, 1.1)$.

2.8 Statistical Assessment of Detection Quality

For all experiments, we plot the true positive rate (TPR = sensitivity) against the false positive rate (FPR = 1–specificity) at various decision thresholds to create ROC curves (Brown and Davis, 2006). Additionally, we compute the ROC AUC to assess the quality of our classifiers. The quality of our predicted bounding boxes is assessed by computing the IoU with the target bounding boxes. We consider IoU values over 0.5 as successful localization of the menisci since this is a common value in object detection tasks (Girshick et al., 2014).

2.9 SmoothGrad Saliency Map Visualizations for Areas Addressed by the CNN

Gradient saliency maps (Simonyan et al., 2013) (otherwise called pixel attribution maps or sensitivity maps) highlight pixel regions in the input image that mostly influenced a neural network's decision. To attain such pixel attributions, one computes the derivative of the final linear layer in a neural network with respect to the input via back-propagation. More formally, a gradient saliency map S_c for a sub-region c for which our neural network f yields a detection of meniscal tears is calculated as:

$$S_c(\tilde{\mathcal{I}}_i) = \frac{\partial f_c(\tilde{\mathcal{I}}_i)}{\partial \tilde{\mathcal{I}}_i}. \quad (8)$$

For our two most promising approaches *BB-crop* and *BB-loss*, these maps are computed by applying a slight enhancement to the original mechanism - the SmoothGrad method (Smilkov et al., 2017). Similar to the SmoothGrad approach of Smilkov et al. (2017) we augmented the input image slightly, introducing noise, such that through averaging, the saliency maps of different noise levels are smoothed out. We apply Gaussian distributed noise $\epsilon \in \mathcal{N}(0.1, 0.5)$, random horizontal flips, uniformly sampled rotations $r \in \mathcal{U}(-5°, +5°)$ and uniformly sampled pixel intensity shift with a multiplication factor $b \in \mathcal{U}(0.9, 1.1)$. Each image is augmented 20 times with a probability of 50% per augmentation, and the resulting maps are averaged.

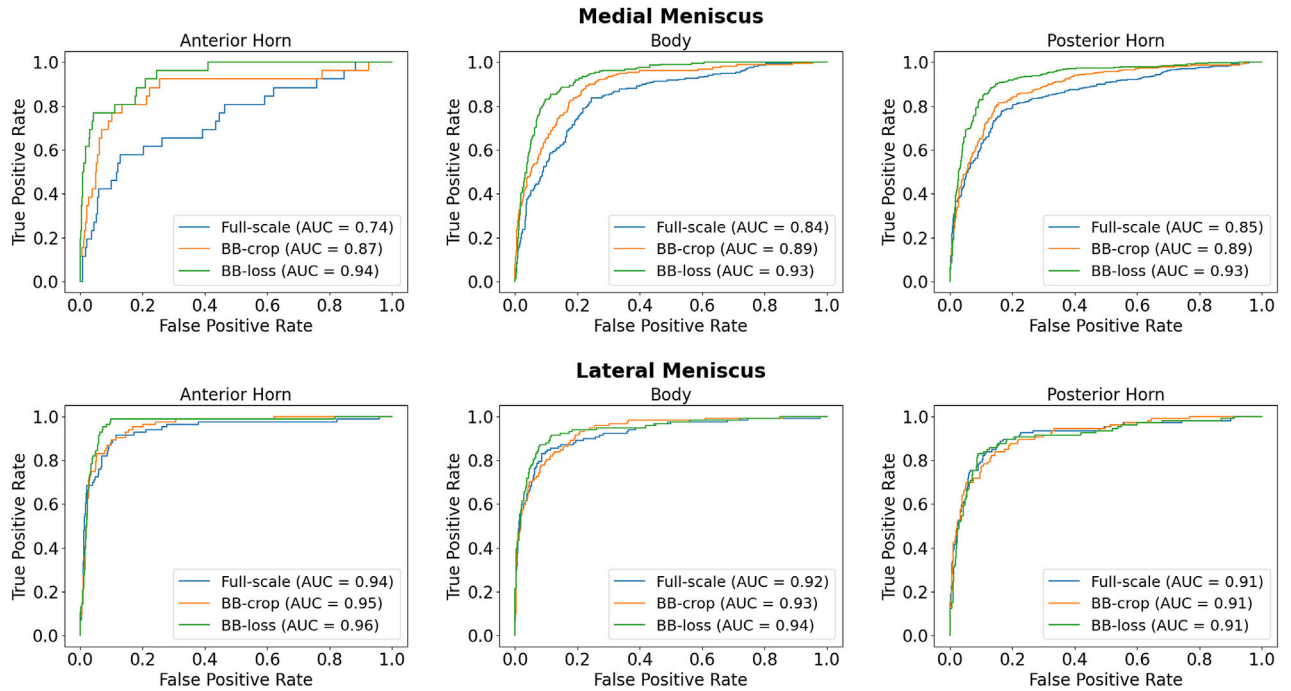

FIGURE 3 | ROC curves for detection of meniscal tears in DESS MRI data.

TABLE 2 | ROC AUC results for medial menisci (MM) and lateral menisci (LM) in DESS MRI data.

	MM			LM		
Method	**Anterior**	**Body**	**Posterior**	**Anterior**	**Body**	**Posterior**
Full-scale	0.74	0.84	0.85	0.94	0.92	0.91
BB-crop	0.87	0.89	0.89	0.95	0.93	**0.91**
BB-loss	**0.94**	**0.93**	**0.93**	**0.96**	**0.94**	**0.91**

The best results for each anatomical sub-region are highlighted in bold.

3 RESULTS

We applied all approaches to DESS as well as IW TSE data from the OAI database. Each of our approaches detects meniscal tears for the MM and the LM. In particular, tears are detected in the three anatomical sub-regions anterior horn, meniscal body, and posterior horn. All results are presented in this section.

3.1 Detection of Meniscal Tears in DESS MRI Data

Employing the *Full-scale* approach, the AUC values are 0.74, 0.84, 0.85 for the anterior horn, body, and posterior horn of the MM. For the LM, the AUC values are 0.94, 0.92, 0.91. The *BB-crop* approach usually yields higher AUC values, being 0.87, 0.89, 0.89 and 0.95, 0.93, 0.91. The *BB-loss* gives the highest AUC values, being 0.94, 0.93, 0.93 and 0.96, 0.94, 0.91. The ROC curves employing all three approaches are shown in **Figure 3**. In addition, all ROC AUC results are summarized in **Table 2**.

3.2 Detection of Meniscal Tears in IW TSE MRI Data

Employing the *Full-scale* approach, the AUC values are 0.82, 0.87, 0.82 for the anterior horn, body, and posterior horn of the MM. For the LM, the AUC values are 0.88, 0.85, 0.85. The *BB-crop* approach usually yields higher AUC values, being 0.84, 0.89, 0.86, and 0.92, 0.90, 0.90. The *BB-loss* gives similar AUC values, being 0.84, 0.88, 0.86, and 0.95, 0.91, 0.90. The ROC curves of all approaches are shown in **Figure 4**. Further, all AUC values are summarized in **Table 3**.

3.3 Localization of Menisci via the *BB-Loss* Approach

To investigate the bounding box regression quality of the proposed method we evaluate the distribution of the IoU values for the predicted bounding boxes (**Figure 5**). For the DESS dataset (our primary benchmark), we observed a very high quality of MM and LM bounding box predictions. With the values being close to normally distributed around a mean value of 0.71 (95% confidence interval (CI): 0.71–0.72) and standard deviation of 0.13. With the IoU threshold of 0.5, we conclude that 95% of the resulted bounding boxes are identified correctly. Unfortunately, we observed a clear decrease in the object detection performance in the IW TSE dataset. With a mean value of 0.58 (95% CI: 0.57–0.59) and a standard deviation of 0.14. Applying the same detection threshold as above we testify, that only around 76% of menisci were detected correctly, with the overall quality of the bounding boxes being more widely spread.

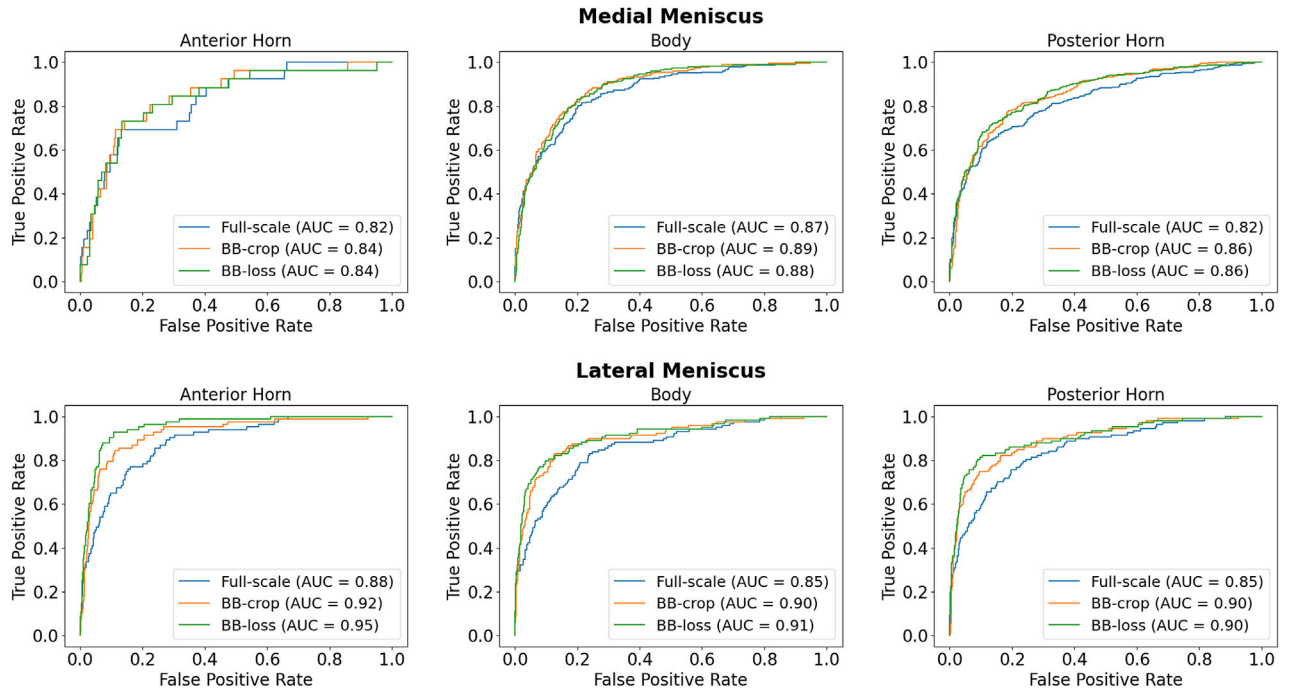

FIGURE 4 | ROC curves for detection of meniscal tears in IW TSE MRI data.

TABLE 3 | ROC AUC results for medial menisci (MM) and lateral menisci (LM) in IW TSE data.

	MM			LM		
Method	**Anterior**	**Body**	**Posterior**	**Anterior**	**Body**	**Posterior**
Full-scale	0.82	0.87	0.82	0.88	0.85	0.85
BB-crop	**0.84**	**0.89**	**0.86**	0.92	0.90	**0.90**
BB-loss	**0.84**	0.88	**0.86**	**0.95**	**0.91**	**0.90**

The best results for each anatomical sub-region are highlighted in bold.

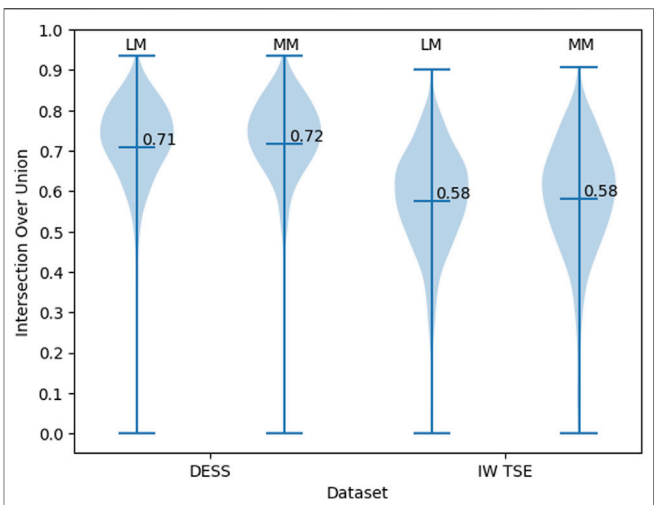

FIGURE 5 | The distribution of the IoU values for the bounding boxes of MM and LM in DESS and IW TSE MRI data.

3.4 Visualization of Areas Addressed by the CNN

Figure 6 shows SmoothGrad saliency maps for the *BB-crop* and *BB-loss* approach overlaid to MR images. Examples are shown for randomly selected test cases, displaying different kinds of meniscal tears for DESS and IW TSE data. The RoIs for the *BB-loss* approach were extracted using predicted bounding boxes and the respective close-ups are shown. Red arrows point at the location of meniscal defects. Most saliency maps obtained this way display a plausible localization of the meniscal tears. The plausibility of these maps was qualitatively evaluated by their correspondence to the target labels of the regions in which the tears could also be confirmed with the help of visual inspection of the image data. SmoothGrad saliency maps are capable of highlighting more than just one affected sub-region, i.e., in the presence of defects in multiple sub-regions of one meniscus, one similarly observes these being correctly highlighted. With the Dilation ResNet-C-26 employed in the *BB-crop* approach, we observed that this CNN yields smoother and less noisy SmoothGrad saliency maps. However, in many cases, ResNet-50 saliency maps targeted the affected region better, but did not outline this region sharply.

3.5 Detection Performance—Different Sub-regions and Defect Types

Even though the occurrence of defects varies between meniscal sub-regions (see **Supplementary Figure S2**), we observe only minimal differences between AUC values of

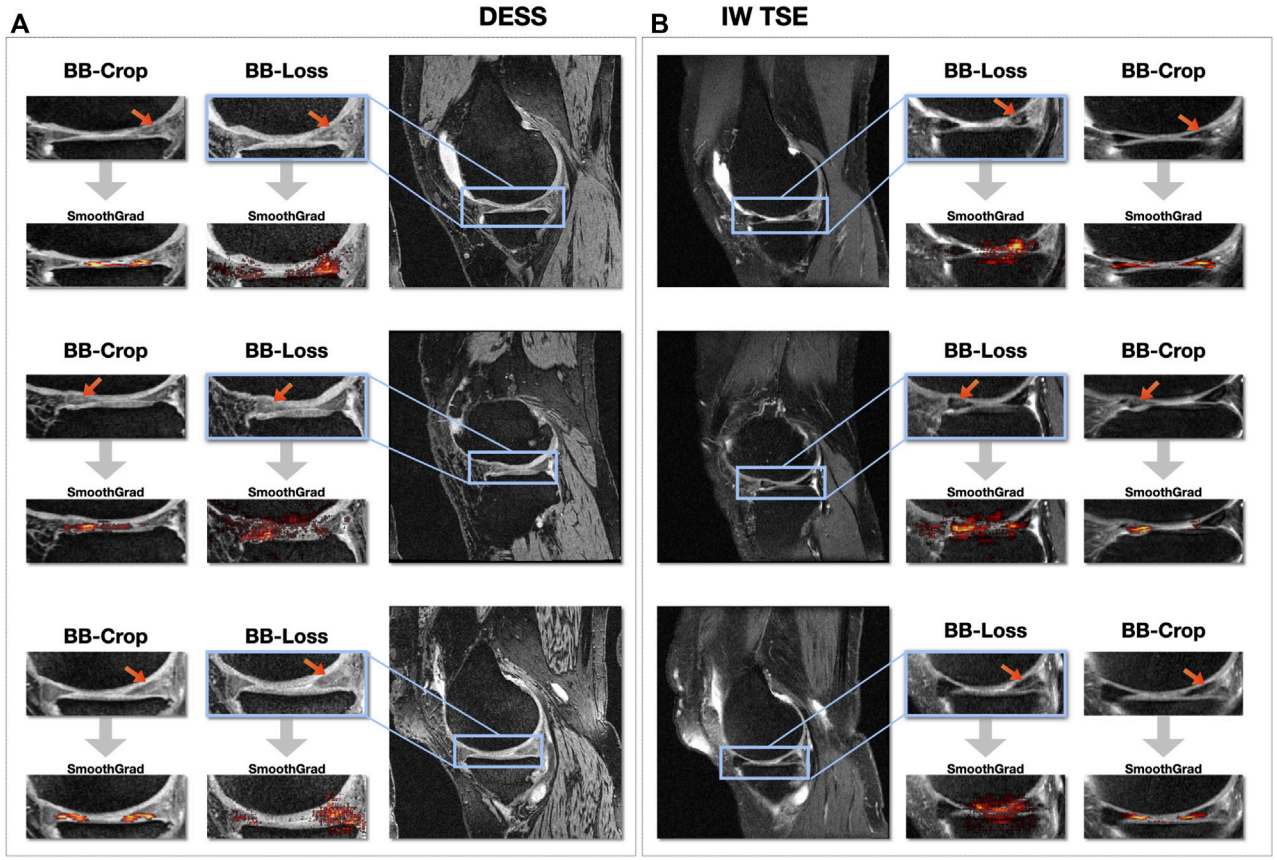

FIGURE 6 | SmoothGrad saliency maps overlaid over DESS MRI data **(A)** and IW TSE MRI data **(B)**.

sub-regions in DESS MRI data (c.f. **Table 2**). However, we analyzed the false positive classifications and found that for all sub-regions, signal abnormalities were more often misclassified than normal menisci were (see **Supplementary Figure S1**). The misclassification rate of signal abnormalities is highest for the posterior horn of the lateral meniscus, the region with the least AUC for the DESS data. Conversely, the lowest signal abnormality misclassification rate is prevalent in the posterior horn of the medial meniscus, the sub-region with the highest number of signal abnormalities (**Supplementary Table S1**).

The least common types of tears occurring in the data are radial and vertical tears, amounting to 72 and 69, respectively. Vertical tears were most challenging for our method to detect in DESS data and led to the most false negative results (see **Supplementary Figure S2**). Radial meniscal tears were the ones yielding the second highest rate of misclassifications.

4 DISCUSSION

The primary goal of our work was to develop a method that provides an efficient, robust and automated way to detect and better locate meniscal tears in MRI data, that is, the detection of tears with respect to the anatomical regions in which they occur. We devised a procedure that utilizes a 3D CNN to process arbitrary 3D MRI data without the need for any extensive pre-processing.

Many previously proposed methods already yield a high accuracy in the detection of meniscal tears. To compare our results to the related work, we focus our assessment on the results of our *BB-loss* approach on the DESS MRI data. Our method detects meniscal tears in anatomical sub-regions of MM and LM. However, it has not been explicitly trained for menisci tear detection in the entire knee as well as the two menisci. Therefore, to obtain the respected values, we performed max operations on our CNNs' outputs. A comparison of the different approaches with their respective detection AUC is summarized in **Table 4**. Our *BB-loss* approach achieved state-of-the-art results in detecting meniscal tears in the medial and lateral meniscus with an AUC of 0.94 and 0.93. For the task of meniscal tear detection in the entire knee *BB-loss* approach had an AUC of 0.94 is second to the approach of Fritz et al. (2020). However, the proposed methods from the related work still leave a desire for a more precise spatial assignment of the findings. For instance, localizing tears per meniscus or in anatomical sub-regions thereof. For tear detection per meniscus, our method performs better than related

TABLE 4 | Comparison of our results on DESS MRI data to the related work. The "3D data" column indicates whether the method is trained on and applied to complete 3D MR images. The explainable AI "XAI" column indicates if concepts of saliency maps are employed in order to highlight the areas responsible for the CNNs' decisions.

	Roblot et al. (2019)*	Couteaux et al. (2019)*	Bien et al. (2018)	Pedoia et al. (2019)	Tsai et al. (2020)	Azcona et al. (2020)	Fritz et al. (2020)	Rizk et al. (2021)	Ours: *Full-scale*	Ours: *BB-crop*	Ours: *BB-loss*
3D data	×	×	✓	✓	✓	✓	✓	✓	✓	✓	✓
XAI	×	✓	✓	×	✓	×	✓	✓	✓	✓	✓
Anywhere	0.94	0.906	0.847	0.89	0.904 and 0.913	0.934	**0.961**	–	0.81	0.89	0.94
Any MM	–	–	–	–	–	–	0.882	0.93	0.79	0.89	**0.94**
Any LM	–	–	–	–	–	–	0.781	0.84	0.87	0.92	**0.93**
MM-AH	✓	✓	–	–	–	–	–	–	0.85	0.84	**0.94**
MM-B	–	–	–	–	–	–	–	–	0.82	0.89	**0.93**
MM-PH	✓	✓	–	–	–	–	–	–	0.78	0.89	**0.93**
LM-AH	✓	✓	–	–	–	–	–	–	0.90	0.95	**0.96**
LM-B	–	–	–	–	–	–	–	–	0.86	0.92	**0.94**
LM-PH	✓	✓	–	–	–	–	–	–	0.88	**0.91**	**0.91**

**Roblot et al. (2019) and Couteaux et al. (2019) detected meniscal tears in 2D slices for AH and PH, but reported overall results only.*
The best methods for the respective task are highlighted in bold.

work (Fritz et al., 2020; Rizk et al., 2021). However, the novelty of our method is the detection of tears for each anatomical sub-region of the menisci in 3D MRI data, providing an anatomically more detailed localization.

With AUC values being consistently higher than 0.90 for DESS MRI data, our approach achieves excellent detection quality for all meniscal sub-regions using uncropped 3D MRI volumes. We also show that our method generalizes well to other MRI sequences, that is, from DESS to IW TSE data. IW TSE data provides a more challenging setting with a higher slice thickness in the mediolateral direction. Moreover, for certain meniscal defects, such as horizontal tears in the meniscal body, a lower resolution in the acquired MR image direction significantly reduces the visibility of the features required for an accurate classification. The result could be improved by using an input image with an isotropic resolution. Such an image can be obtained by either upsampling an existing image or, even better—acquiring a new image, at a higher resolution.

Signal abnormalities are still a challenge. In cases where menisci with tears are to be distinguished from menisci without tears, signal abnormalities are currently regarded as the latter. A fine-grained differentiation between tears and signal abnormalities is likewise a challenge to our method, primarily through the ambiguous image appearance. Potentially, more training data, as present for the region with the most signal abnormalities—the MM posterior horn, would allow our CNN to better learn to distinguish signal abnormalities from tears.

We expected our model to generalize to all meniscal pathologies but observed problems detecting vertical and radial tears. However, these tears were less common in the available training data, and we believe that more data on such cases would enable our method to detect vertical and radial tears with higher accuracy. Furthermore, coronal and axial imaging sequence orientation could provide additional insights (Bien et al., 2018), possibly improving the detection of otherwise barely visible tears.

One major limitation that we see is that our method still requires a localization of the menisci in training. However, other segmentation approaches or (non-automatic) approaches could be applied to attain bounding boxes, possibly improving results by providing more accurate bounding boxes for training.

5 CONCLUSIONS AND FUTURE WORK

We present a method in an efficient and fully automated multi-task learning setting that accurately detects meniscal tears on a sub-region level in MM and LM. Our method yields the best results on sagittal DESS MRI data and generalizes well to sagittal IW TSE data. Further, visual support for clinical detection of meniscal tears is provided by SmoothGrad saliency maps highlighting regions that mainly contributed to the decision.

Future work could comprise an analysis of anomaly detection (normal vs. signal abnormality vs. torn menisci) or a classification of different types of tears (horizontal, radial, complex, etc.). Since some of these types occur only rarely for specific sub-regions, deep learning-based methods probably require a lot more image data or data generated with generative models. Also, new issues of class imbalances will arise for the classification of tear types.

From the method perspective, the choice of an encoder provides opportunities for improvement. For instance, recent self-attention mechanisms, so-called "transformer" architectures (Vaswani et al., 2017; Dosovitskiy et al., 2020) are worth an investigation. Since transformers typically require a vast amount of training data, they might not necessarily lead to better accuracy, but the self-attention maps (Caron et al., 2021) may result in a more meaningful explanatory power than classical methods of saliency mapping. Also, generative adversarial networks have been recently employed for explaining the decision of CNN's (Katzmann et al., 2021; Shih et al., 2021). As deep learning methods become more precise in localizing meniscal tears coupled with further sophisticated concepts on explainability,

CAD tools will become practical for clinical decision support. In future work, we plan to investigate whether our method better assists physicians in their diagnostic tasks.

DATA AVAILABILITY STATEMENT

Publicly available datasets were analyzed in this study. This data can be found here: https://nda.nih.gov/oai/ for the MR images analyzed in this study as well as the medical image annotations from the NIH OAI archive. The employed segmentation masks of all MM and LM will be made publicly available at https://pubdata.zib.de upon publication of this paper.

ETHICS STATEMENT

The studies involving human participants were reviewed and approved by the OAI coordinating center and by each OAI clinical site. The patients/participants provided their written informed consent to participate in this study.

AUTHOR CONTRIBUTIONS

AT, AS, DL, and SZ designed the study. AT, AS, and DL implemented the proposed methods. AT, AS, and DL collected the data, performed the statistical evaluation and executed the experiments. SZ obtained the funding resources for this project. AT, AS, DL, and SZ drafted and wrote the manuscript.

FUNDING

The authors gratefully acknowledge the financial support by the German federal ministry of education and research (BMBF) within the research network on musculoskeletal diseases, grant no. 01EC1408B (Overload/PrevOP). Furthermore, the authors are funded by the Deutsche Forschungsgemeinschaft (DFG, German Research Foundation) within research project ZA 592/4-1.

ACKNOWLEDGMENTS

The Osteoarthritis Initiative is a public-private partnership comprised of five contracts (N01-AR-2-2258; N01-AR-2-2259; N01-AR-2-2260; N01-AR-2-2261; N01-AR-2-2262) funded by the National Institutes of Health, a branch of the Department of Health and Human Services, and conducted by the OAI Study Investigators. Private funding partners include Merck Research Laboratories; Novartis Pharmaceuticals Corporation, GlaxoSmithKline; and Pfizer, Inc. Private sector funding for the OAI is managed by the Foundation for the National Institutes of Health. This manuscript was prepared using an OAI public use data set and does not necessarily reflect the opinions or views of the OAI investigators, the NIH, or the private funding partners.

SUPPLEMENTARY MATERIAL

The Supplementary Material for this article can be found online at: https://www.frontiersin.org/articles/10.3389/fbioe.2021.747217/full#supplementary-material

REFERENCES

Agarap, A. F. (2018). *Deep Learning Using Rectified Linear Units (Relu)*. New York: arXiv preprint, arXiv:1803.08375.

Ambellan, F., Tack, A., Ehlke, M., and Zachow, S. (2019). Automated Segmentation of Knee Bone and Cartilage Combining Statistical Shape Knowledge and Convolutional Neural Networks: Data from the Osteoarthritis Initiative. *Med. Image Anal.* 52, 109–118. doi:10.1016/j.media.2018.11.009

Azcona, D., McGuinness, K., and Smeaton, A. F. (2020). "A Comparative Study of Existing and New Deep Learning Methods for Detecting Knee Injuries Using the Mrnet Dataset," in Proceedings of the 2020 International Conference on Intelligent Data Science Technologies and Applications (IDSTA), Valencia, Spain, October 2020 (IEEE), 149–155.

Beaufils, P., and Pujol, N. (2017). Management of Traumatic Meniscal Tear and Degenerative Meniscal Lesions. Save the Meniscus. *Orthopaedics Traumatol. Surg. Res.* 103, S237–S244. doi:10.1016/j.otsr.2017.08.003

Bhattacharyya, T., Gale, D., Dewire, P., Totterman, S., Gale, M. E., McLaughlin, S., et al. (2003). The Clinical Importance of Meniscal Tears Demonstrated by Magnetic Resonance Imaging in Osteoarthritis of the Knee. *JBJS* 85, 4–9. doi:10.2106/00004623-200301000-00002

Bien, N., Rajpurkar, P., Ball, R. L., Irvin, J., Park, A., Jones, E., et al. (2018). Deep-learning-assisted Diagnosis for Knee Magnetic Resonance Imaging: Development and Retrospective Validation of Mrnet. *PLoS Med.* 15, e1002699. doi:10.1371/journal.pmed.1002699

Brown, C. D., and Davis, H. T. (2006). Receiver Operating Characteristics Curves and Related Decision Measures: A Tutorial. *Chemometrics Intell. Lab. Syst.* 80, 24–38. doi:10.1016/j.chemolab.2005.05.004

Caron, M., Touvron, H., Misra, I., Jégou, H., Mairal, J., Bojanowski, P., et al. (2021). *Emerging Properties in Self-Supervised Vision Transformers*. New York: arXiv preprint arXiv:2104.14294.

Couteaux, V., Si-Mohamed, S., Nempont, O., Lefevre, T., Popoff, A., Pizaine, G., et al. (2019). Automatic Knee Meniscus Tear Detection and Orientation Classification with Mask-Rcnn. *Diagn. Interv. Imaging* 100, 235–242. doi:10.1016/j.diii.2019.03.002

Crawford, R., Walley, G., Bridgman, S., and Maffulli, N. (2007). Magnetic Resonance Imaging versus Arthroscopy in the Diagnosis of Knee Pathology, Concentrating on Meniscal Lesions and Acl Tears: a Systematic Review. *Br. Med. Bull.* 84, 5–23. doi:10.1093/bmb/ldm022

Ding, C., Martel-Pelletier, J., Pelletier, J.-P., Abram, F., Raynauld, J.-P., Cicuttini, F., et al. (2007). Meniscal Tear as an Osteoarthritis Risk Factor in a Largely Non-osteoarthritic Cohort: a Cross-Sectional Study. *J. Rheumatol.* 34, 776–784.

Dosovitskiy, A., Beyer, L., Kolesnikov, A., Weissenborn, D., Zhai, X., Unterthiner, T., et al. (2020). *An Image Is worth 16x16 Words: Transformers for Image Recognition at Scale*. New York: arXiv preprint arXiv:2010.11929.

Englund, M., Roos, E. M., Roos, H., and Lohmander, L. (2001). Patient-relevant Outcomes Fourteen Years after Meniscectomy: Influence of Type of Meniscal Tear and Size of Resection. *Rheumatology* 40, 631–639. doi:10.1093/rheumatology/40.6.631

Fritz, B., Marbach, G., Civardi, F., Fucentese, S. F., and Pfirrmann, C. W. (2020). Deep Convolutional Neural Network-Based Detection of Meniscus Tears: Comparison with Radiologists and Surgery as Standard of Reference. *Skeletal Radiol.* 49, 1207–1217. doi:10.1007/s00256-020-03410-2

Girshick, R., Donahue, J., Darrell, T., and Malik, J. (2014). "Rich Feature Hierarchies for Accurate Object Detection and Semantic Segmentation," in Proceedings of the IEEE conference on computer vision and pattern recognition, Columbus, OH, USA, June 2014, 580–587.

He, K., Gkioxari, G., Dollár, P., and Girshick, R. (2017). "Mask R-Cnn," in Proceedings of the IEEE international conference on computer vision, October, 2017, 2961–2969.

He, K., Zhang, X., Ren, S., and Sun, J. (2016). "Deep Residual Learning for Image Recognition," in Proceedings of the IEEE conference on computer vision and pattern recognition, Las Vegas, NV, USA, June 2016, 770–778.

He, K., Zhang, X., Ren, S., and Sun, J. (2015). "Delving Deep into Rectifiers: Surpassing Human-Level Performance on Imagenet Classification," in Proceedings of the IEEE international conference on computer vision, Santiago, Chile, December 2015, 1026–1034.

Hunter, D. J., Guermazi, A., Lo, G. H., Grainger, A. J., Conaghan, P. G., Boudreau, R. M., et al. (2011). Evolution of Semi-quantitative Whole Joint Assessment of Knee Oa: Moaks (Mri Osteoarthritis Knee Score). *Osteoarthritis and Cartilage* 19, 990–1002. doi:10.1016/j.joca.2011.05.004

Ide, H., and Kurita, T. (2017). "Improvement of Learning for Cnn with Relu Activation by Sparse Regularization," in Proceedings of the International Joint Conference on Neural Networks (IJCNN), Anchorage, AK, USA, May 2017 (IEEE), 2684–2691. doi:10.1109/ijcnn.2017.7966185

Ioffe, S., and Szegedy, C. (2015). "Batch Normalization: Accelerating Deep Network Training by Reducing Internal Covariate Shift," in Proceedings of the International conference on machine learning, Lille, France, July 2015, (PMLR), 448–456.

Isensee, F., Jaeger, P. F., Kohl, S. A., Petersen, J., and Maier-Hein, K. H. (2021). Nnu-Net: a Self-Configuring Method for Deep Learning-Based Biomedical Image Segmentation. *Nat. Methods* 18, 203–211. doi:10.1038/s41592-020-01008-z

Katzmann, A., Taubmann, O., Ahmad, S., Mühlberg, A., Sühling, M., and Groß, H.-M. (2021). Explaining Clinical Decision Support Systems in Medical Imaging Using Cycle-Consistent Activation Maximization. *Neurocomputing* 458, 141–156. doi:10.1016/j.neucom.2021.05.081

Khan, M., Evaniew, N., Bedi, A., Ayeni, O. R., and Bhandari, M. (2014). Arthroscopic Surgery for Degenerative Tears of the Meniscus: a Systematic Review and Meta-Analysis. *Cmaj* 186, 1057–1064. doi:10.1503/cmaj.140433

Kingma, D. P., and Ba, J. (2014). *Adam: A Method for Stochastic Optimization*. New York: arXiv preprint arXiv:1412.6980.

Kise, N. J., Risberg, M. A., Stensrud, S., Ranstam, J., Engebretsen, L., and Roos, E. M. (2016). Exercise Therapy versus Arthroscopic Partial Meniscectomy for Degenerative Meniscal Tear in Middle Aged Patients: Randomised Controlled Trial with Two Year Follow-Up. *bmj* 354. doi:10.1136/bjsports-2016-i3740rep

Kunze, K. N., Rossi, D. M., White, G. M., Karhade, A. V., Deng, J., Williams, B. T., et al. (2020). Diagnostic Performance of Artificial Intelligence for Detection of Anterior Cruciate Ligament and Meniscus Tears: A Systematic Review. *Arthrosc. J. Arthroscopic Relat. Surg.* 37 (2), 771–781. doi:10.1016/j.arthro.2020.09.012

Lin, M., Chen, Q., and Yan, S. (2013). *Network in Network*. New York: arXiv preprint arXiv:1312.4400.

Markes, A. R., Hodax, J. D., and Ma, C. B. (2020). Meniscus Form and Function. *Clin. Sports Med.* 39, 1–12. doi:10.1016/j.csm.2019.08.007

Pedoia, V., Norman, B., Mehany, S. N., Bucknor, M. D., Link, T. M., and Majumdar, S. (2019). 3d Convolutional Neural Networks for Detection and Severity Staging of Meniscus and Pfj Cartilage Morphological Degenerative Changes in Osteoarthritis and Anterior Cruciate Ligament Subjects. *J. Magn. Reson. Imaging* 49, 400–410. doi:10.1002/jmri.26246

Peterfy, C., Gold, G., Eckstein, F., Cicuttini, F., Dardzinski, B., and Stevens, R. (2006). Mri Protocols for Whole-Organ Assessment of the Knee in Osteoarthritis. *Osteoarthritis and Cartilage* 14, 95–111. doi:10.1016/j.joca.2006.02.029

Rahman, M. M., Dürselen, L., and Seitz, A. M. (2020). Automatic Segmentation of Knee Menisci–A Systematic Review. *Artif. Intelligence Med.* 105, 101849. doi:10.1016/j.artmed.2020.101849

Reddy, G. V. (2017). *Automatic Classification of 3D MRI Data Using Deep Convolutional Neural Networks*. Master's thesis (Germany: Otto-von-Guericke-Universität Magdeburg).

Ren, S., He, K., Girshick, R., and Sun, J. (2015). Faster R-Cnn: Towards Real-Time Object Detection with Region Proposal Networks. *Adv. Neural Inf. Process. Syst.* 28, 91–99.

Rezatofighi, H., Tsoi, N., Gwak, J., Sadeghian, A., Reid, I., and Savarese, S. (2019). "Generalized Intersection over union: A Metric and a Loss for Bounding Box Regression," in Proceedings of the IEEE/CVF Conference on Computer Vision and Pattern Recognition, Long Beach, CA, USA, June 2019, 658–666.

Rizk, B., Brat, H., Zille, P., Guillin, R., Pouchy, C., Adam, C., et al. (2021). Meniscal Lesion Detection and Characterization in Adult Knee Mri: A Deep Learning Model Approach with External Validation. *Physica Med.* 83, 64–71. doi:10.1016/j.ejmp.2021.02.010

Roblot, V., Giret, Y., Antoun, M. B., Morillot, C., Chassin, X., Cotten, A., et al. (2019). Artificial Intelligence to Diagnose Meniscus Tears on Mri. *Diagn. Interv. Imaging* 100, 243–249. doi:10.1016/j.diii.2019.02.007

Roemer, F. W., Kwoh, C. K., Hannon, M. J., Hunter, D. J., Eckstein, F., Grago, J., et al. (2017). Partial Meniscectomy Is Associated with Increased Risk of Incident Radiographic Osteoarthritis and Worsening Cartilage Damage in the Following Year. *Eur. Radiol.* 27, 404–413. doi:10.1007/s00330-016-4361-z

Shih, S.-M., Tien, P.-J., and Karnin, Z. (2021). "Ganmex: One-Vs-One Attributions Using gan-based Model Explainability," in Proceedings of the International Conference on Machine Learning, Vienna, Austria on Virtual, July 2021 (PMLR), 9592–9602.

Simonyan, K., Vedaldi, A., and Zisserman, A. (2013). *Deep inside Convolutional Networks: Visualising Image Classification Models and Saliency Maps*. New York: arXiv preprint arXiv:1312.6034.

Smilkov, D., Thorat, N., Kim, B., Viégas, F., and Wattenberg, M. (2017). *Smoothgrad: Removing Noise by Adding Noise*. New York: arXiv preprint arXiv:1706.03825.

Snoeker, B., Ishijima, M., Kumm, J., Zhang, F., Turkiewicz, A., and Englund, M. (2021). Are Structural Abnormalities on Knee Mri Associated with Osteophyte Development? Data from the Osteoarthritis Initiative. *Osteoarthritis and Cartilage* S1063-4584 (21), 00841–00844.

Tack, A., Mukhopadhyay, A., and Zachow, S. (2018). Knee Menisci Segmentation Using Convolutional Neural Networks: Data from the Osteoarthritis Initiative. *Osteoarthritis and Cartilage* 26, 680–688. doi:10.1016/j.joca.2018.02.907

Tack, A., and Zachow, S. (2019). "Accurate Automated Volumetry of Cartilage of the Knee Using Convolutional Neural Networks: Data from the Osteoarthritis Initiative," in Proceedings of the 2019 IEEE 16th International Symposium on Biomedical Imaging (ISBI 2019), Venice, Italy, April 2019 (IEEE), 40–43.

Tsai, C.-H., Kiryati, N., Konen, E., Eshed, I., and Mayer, A. (2020). "Knee Injury Detection Using Mri with Efficiently-Layered Network (Elnet)," in Proceedings of the Medical Imaging with Deep Learning, July, 2020, Montreal, Canada (PMLR), 784–794.

Vaswani, A., Shazeer, N., Parmar, N., Uszkoreit, J., Jones, L., Gomez, A. N., et al. (2017). "Attention Is All You Need," in Advances in neural information processing systems (NIPS 2017), Long Beach, CA, USA, December 2017, 5998–6008.

Yu, F., Koltun, V., and Funkhouser, T. (2017). "Dilated Residual Networks," in Proceedings of the IEEE conference on computer vision and pattern recognition, Honolulu, HI, USA, July 2017, 472–480.

Conflict of Interest: The authors declare that the research was conducted in the absence of any commercial or financial relationships that could be construed as a potential conflict of interest.

frontiers in Bioengineering and Biotechnology

SYSTEMATIC REVIEW
published: 03 December 2021
doi: 10.3389/fbioe.2021.765596

Influence of Menisci on Tibiofemoral Contact Mechanics in Human Knees: A Systematic Review

*Matthias Sukopp, Florian Schall, Steffen P. Hacker, Anita Ignatius, Lutz Dürselen and Andreas M. Seitz**

Institute of Orthopaedic Research and Biomechanics, Center of Trauma Research Ulm, Ulm University Medical Center, Ulm, Germany

Purpose: Menisci transfer axial loads, while increasing the load-bearing tibiofemoral contact area and decreasing tibiofemoral contact pressure (CP). Numerous clinical and experimental studies agree that an increased CP is one predominant indicator for post-traumatic osteoarthritis (PTOA) of the knee joint. However, due to the immense variability in experimental test setups and wide range of treatment possibilities in meniscus surgery, it is difficult to objectively assess their impact on the CP determination, which is clearly crucial for knee joint health. Therefore, the aim of this systematic review is to investigate the influence of different meniscal injuries and their associated surgical treatments on the CP. Secondly, the influence of different test setups on CP measurements is assessed. On the basis of these results, we established the basis for recommendations for future investigations with the aim to determine CPs under different meniscal states.

Methods: This review was conducted in accordance with the PRISMA guidelines. Studies were identified through a systematic literature search in Cochrane, PubMed and Web of Science databases. Literature was searched through pre-defined keywords and medical subject headings.

Results: This review indicates a significant increase of up to 235% in peak CP when comparing healthy joints and intact menisci with impaired knee joints, injured or resected menisci. In addition, different test setups were indicated to have major influences on CP: The variety of test setups ranged from standard material testing machines, including customized setups *via* horizontal and vertical knee joint simulators, through to robotic systems. Differences in applied axial knee joint loads ranged from 0 N up to 2,700 N and resulted unsurprisingly in significantly different peak CPs of between 0.1 and 12.06 MPa.

Conclusion: It was shown that untreated traumatic meniscal tears result in an increased CP. Surgical repair intervention were able to restore the CP comparable to the healthy, native condition. Test setup differences and particularly axial joint loading variability also led to major CP differences. In conclusion, when focusing on CP measurements in the knee joint, transparent and traceable *in vitro* testing conditions are essential to allow researchers to make a direct comparison between future biomechanical investigations.

Keywords: tibiofemoral contact, contact pressure, systematic review, meniscus injuries, osteoarthritis, PTOA

OPEN ACCESS

Edited by:
Bernardo Innocenti, Université libre de Bruxelles, Belgium

Reviewed by:
Emanuela Bologna, University of Palermo, Italy
Francesco Travascio, University of Miami, United States

****Correspondence:***
Andreas M. Seitz
andreas.seitz@uni-ulm.de

Specialty section:
This article was submitted to Biomechanics, a section of the journal Frontiers in Bioengineering and Biotechnology

Received: *27 August 2021*
Accepted: *21 October 2021*
Published: *03 December 2021*

Citation:
Sukopp M, Schall F, Hacker SP, Ignatius A, Dürselen L and Seitz AM (2021) Influence of Menisci on Tibiofemoral Contact Mechanics in Human Knees: A Systematic Review. Front. Bioeng. Biotechnol. 9:765596. doi: 10.3389/fbioe.2021.765596

INTRODUCTION

Traumatic meniscus injuries are one of the most predominant risk factors for post-traumatic osteoarthritis (PTOA) (Cooper et al., 2000; Wilder et al., 2002; Roos, 2005), resulting in a considerable socioeconomic burden globally (Felson and Zhang, 1998). The semilunar, fibrocartilaginous knee joint menisci play a crucial role in load-bearing and load transmission within the knee joint (Walker and Erkman, 1975; Fukubayashi and Kurosawa, 1980). During knee joint movements, the wedge-shaped menisci actively increase the load-bearing contact area by compensating the incongruency of the articular surfaces of the tibia and femur, resulting in a decreased tibiofemoral contact pressure (CP) (Walker and Erkman, 1975).

A typical meniscus injury mechanism is external tibial rotation in combination with axial loading during knee flexion (Nielsen and Yde, 1991), which frequently occurs during sports activities like football, basketball, soccer, and skiing (Baker et al., 1985). Depending on the injury mechanism, various types of meniscal tears can occur and they are categorized in accordance to their location and shape. In the outer third zone—the so-called vascularized, "red" zone—the gold standard of meniscal tear treatment is suturing (Rankin et al., 2002; Makris et al., 2011), while repair in the avascular, "white" zone is commonly not indicated, because of a poor healing potential. Therefore, tears that are localized in this avascular zone are predominantly treated by (partial) meniscectomy (Makris et al., 2011) or being replaced using different substitutes (Linke et al., 2006; de Groot, 2010; Stein et al., 2019). In more severe cases, like permeating root or radial tears, which are described to be biomechanically equivalent to a total meniscectomy, the major function of the meniscus is completely lost (Allaire et al., 2008). In such cases, the CP is dramatically increased, which will lead, when untreated, in the long term to the development of premature knee joint PTOA (Felson et al., 2000; Heckelsmiller et al., 2017).

Experimentally, the CP is normally determined during *in vitro* experiments use a large variety of test setups, ranging from customized setups that are integrated in a standard material testing machine, horizontal, and vertical rigs (Oxford-rig) and robotic systems. The knee joint motion during the tests is achieved either *via* an actuator (passive movement) or actively by simulating muscle forces, for example, the quadriceps muscle for extension. In most investigations, the CP is measured between the menisci and the tibial plateau by means of a pressure sensitive film (**Figure 1**). However, due to the immense variability in experimental test setups, including the respective loading regimes, and wide range of treatment possibilities in meniscus surgery, it is sometimes difficult to objectively assess their mutable impact on the CP determination, which is clearly crucial for knee joint health. Therefore, the main aim of the present systematic review was to investigate the influence of the intact, injured, repaired, or resected meniscal state on the CP. Secondly, we evaluated the impact of different test setups and conditions—for example, variabilities in axial force, knee alignment and muscle simulation on the CP. This overview of currently available testing conditions, which have been used to investigate the impact of different meniscal states on CP measurements, allowed us to establish the basis for recommendations that allow for transparent and reproducible test conditions for future biomechanical CP studies.

METHODS

Search Strategy

This review was conducted in accordance with the PRISMA guidelines (Moher et al., 2009). A comprehensive and systematic review of the literature was performed to identify studies investigating the meniscal influence on the tibiofemoral contact mechanics in human knee joints. For the literature research, the Cochrane, PubMed and Web of Science databases were used. The literature search strategy was developed using a combination of keywords and medical subject heading (MeSH; **Table 1**), which were extended to maximize the inclusion of potentially relevant studies.

Study Selection

The results of the database searches were transferred into Endnote (Clarivate Analytics, PA, United States), where the references were automatically updated and duplicates removed. All titles and abstracts of the identified publications were screened. Papers containing *in vitro* tibiofemoral CP data and those investigating healthy, non-degenerated menisci, meniscal interventions, meniscal tears, repair or replacement or meniscectomy and their influence on the CP were included. Per requirement, the CP must also be clearly assignable to the respectively used knee flexion angles (0, 30, and 60°). Studies with computational/simulation approaches, studies in which the focus was other than on human knee joints, gender impact studies and those investigating knees with pathological alterations were excluded. Additionally, the reference lists of the selected publications were screened to include relevant studies that were missed during the previously described selection process.

All publications that included CPs were evaluated graphically, indicating axial loads, meniscal states, interventions, knee joint compartment and the respective peak CP. Only studies directly reporting CP values were investigated and analyzed. The detailed selection process of the study selection is given in **Figure 2**. The full text of the remaining articles was then analyzed and data from eligible studies were extracted.

RESULTS

Following removal of duplicates and exclusions made based on the exclusion criteria, the strategic search resulted in 89 publications (**Figure 2**; **Supplementary Material**). Of these, 34 publications were additionally evaluated graphically. These publications are listed in more detail in the diagrams below

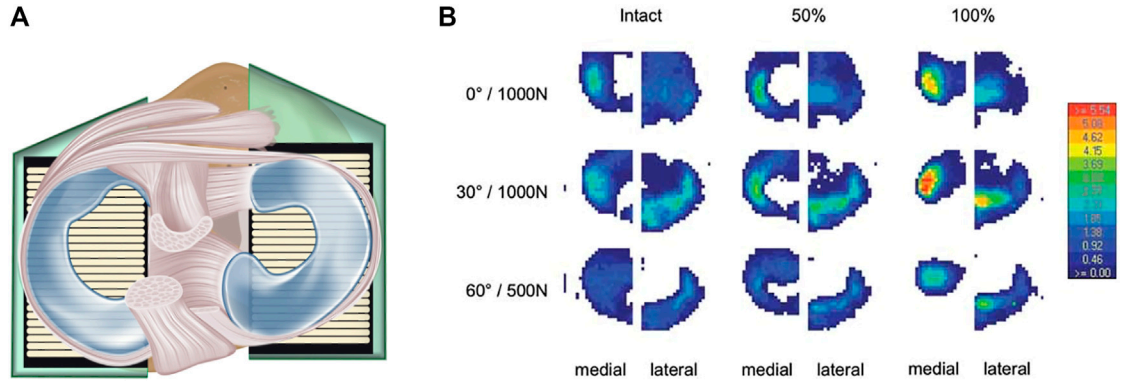

FIGURE 1 | (A) Axial view. Schematic drawing of a knee joint with intact menisci, including an equipped pressure-sensitive foil sensor between the menisci and the tibia to measure tibiofemoral contact mechanics *in vitro*. The femur is removed to allow better visibility of the sensor placement inside the knee. **(B)** Example of a tibiofemoral contact measurement: "Contact pressure at the tibial plateau of a representative knee. The pattern of the sensors shows the lateral and medial compartments under intact, 50 and 100% partial resection state at two flexion angles (0 and 30°) under an axial load of 1,000 N and at 60° flexion under 500 N, respectively. The anterior aspect of the joint is pointing upwards. The legend on the right side indicates the pressure in MPa." Reprinted with permission from Seitz et al. (2019).

TABLE 1 | Queries and search results for Cochrane, PubMed and Web of Science with the number of publications found.

Database	Query	Items found
Cochrane-PubMed-Web of Science	(knee*) AND (contact*) AND (mechanic*) AND (menisc*) AND (pressure)	93
	(knee*) AND (analysis*) AND (pressure*)	1,495
	(knee*) AND (contact pressure*) AND (tibiofemoral*)	174
	(knee joint*) AND (biomechanics*) AND (contact*)	604
	(knee joint*) AND (contact*) AND (pressure*)	640
	(knee*) AND (contact mechanism*)	428
	MeSH: (knee*) AND MeSH: (contact*) AND MeSH: (mechanic*) AND MeSH: (menisc*) AND MeSH: (pressure*)	125

(**Figures 3–7**). The remaining 55 publications could not be graphed because no graphing information was provided. Nonetheless, they were evaluated in the text in the following chapters. The following subdivisions were used for detailed comparisons: *Meniscal states, test setups, loading application* and *muscle force simulation*.

Meniscal states

From a biomechanical point of view, a reduced tibiofemoral contact area caused by meniscal tears (**Figure 8**) or partial or total meniscectomy (**Figure 9**) can potentially lead to premature gonarthrosis. Therefore, we investigated the effects of meniscal injuries and their surgical treatments on the tibiofemoral CP in this chapter.

Meniscal Tears

Forkel et al. found, that an isolated root tear of the lateral meniscus led to an increased peak CP by 23% compared to the intact meniscal state, while a meniscus root tear with an associated transection of the meniscofemoral ligament led to an increase of 225% compared to the intact state. Furthermore, they showed that an anatomic transtibial fixation of the tear or alternatively with a transtibial fixation *via* an anterior cruciate ligament tunnel restores the CP values in the lateral compartment to that comparable to the intact state (Forkel et al., 2014). Schillhammer et al. measured a 50% increase in CP in the case of a posterior horn detachment (Schillhammer et al., 2012). Furthermore, the authors showed that the peak CP in the lateral compartment can be reduced to the intact level by means of a transtibial tunnel repair (Schillhammer et al., 2012). Marzo and others investigated a 32% increase in CP in the medial compartment after simulating a posterior root tear of the medial meniscus (Marzo and Gurske-Deperio, 2009). They concluded, that such a tear can cause the meniscus to extrude out of the joint, leading to a loss of the ability to absorb hoop stresses, finally resulting in an increased peak CP (Allaire et al., 2008; Marzo and Gurske-Deperio, 2009). Repair of the meniscus after a posterior horn tear of the medial meniscus with a transosseous suture (Marzo and Kumar, 2007) restored the hoop stress resistance of the meniscus with a peak CP similar to healthy knee joints (Allaire et al., 2008; Marzo and Gurske-Deperio, 2009). Furthermore, Chen et al. (1996) and Paletta et al. (1997) corroborated these results. Therefore, it can be concluded that a transtibial suture repair of a posterior meniscus root tear is able to restore the CP to that comparable to the intact meniscus situation.

Zhang et al. investigated the treatment of a radial meniscus tear in the medial meniscus with an all-inside meniscal repair

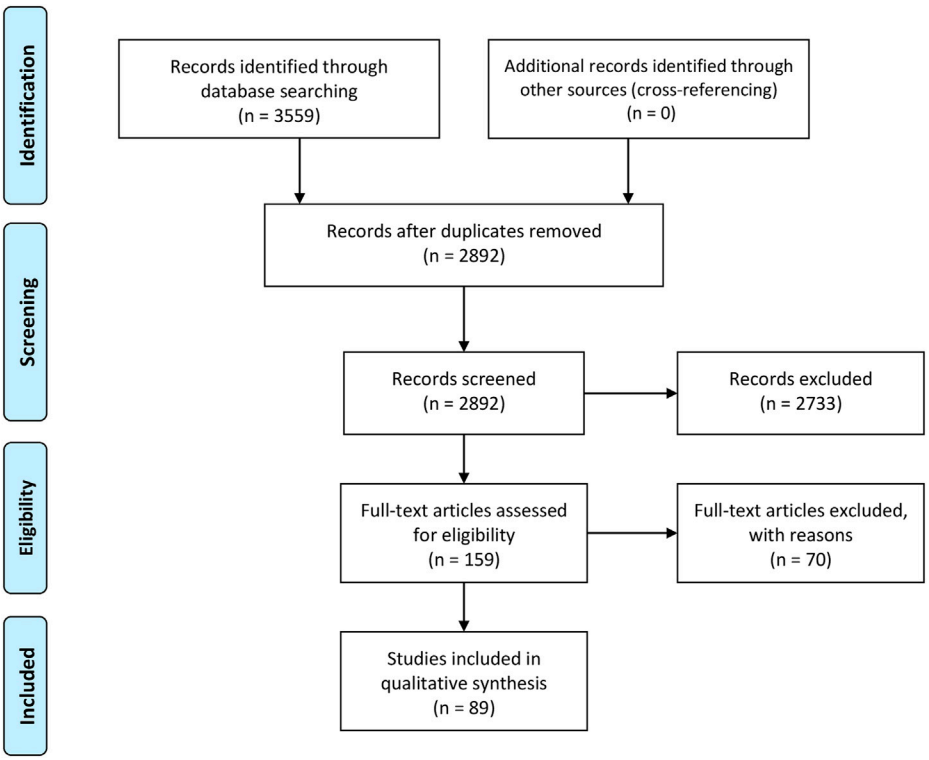

FIGURE 2 | Flow diagram of the study selection process; according to the PRISMA guideline, last update: 2021/08/01.

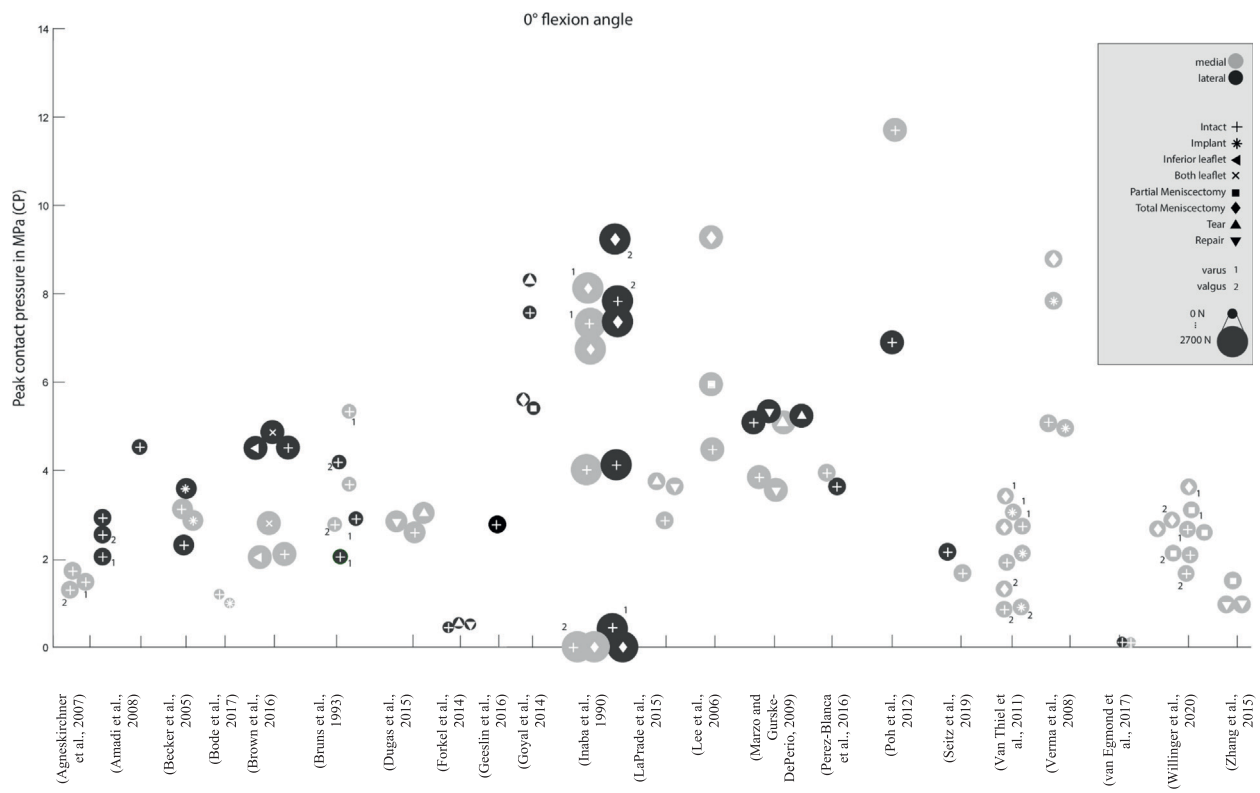

FIGURE 3 | Peak contact pressure at 0° knee joint flexion. Differentiation between lateral, medial and meniscal states. Data point size represents the magnitude of the applied axial load ranging from 0 N to 2,700 N. (Data extracted from written values).

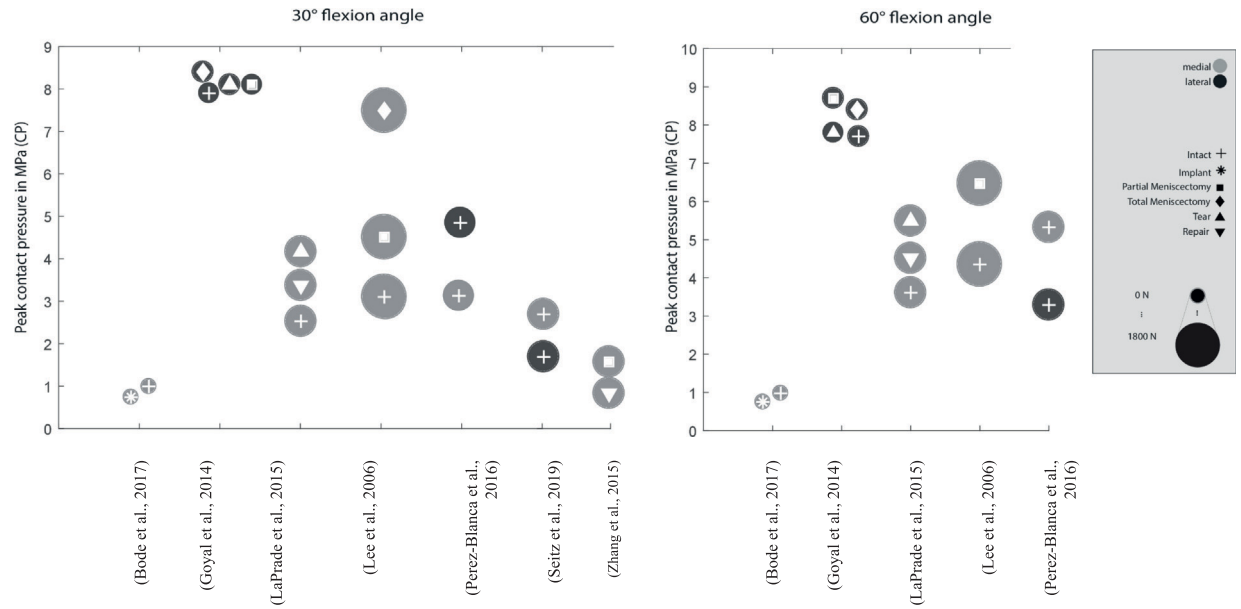

FIGURE 4 | Peak contact pressure at 30° and 60° knee joint flexion. Differentiation between lateral, medial and meniscal states. Data point size represents the magnitude of the applied axial load ranging from 0 N to 1,800 N. (Data extracted from written values)

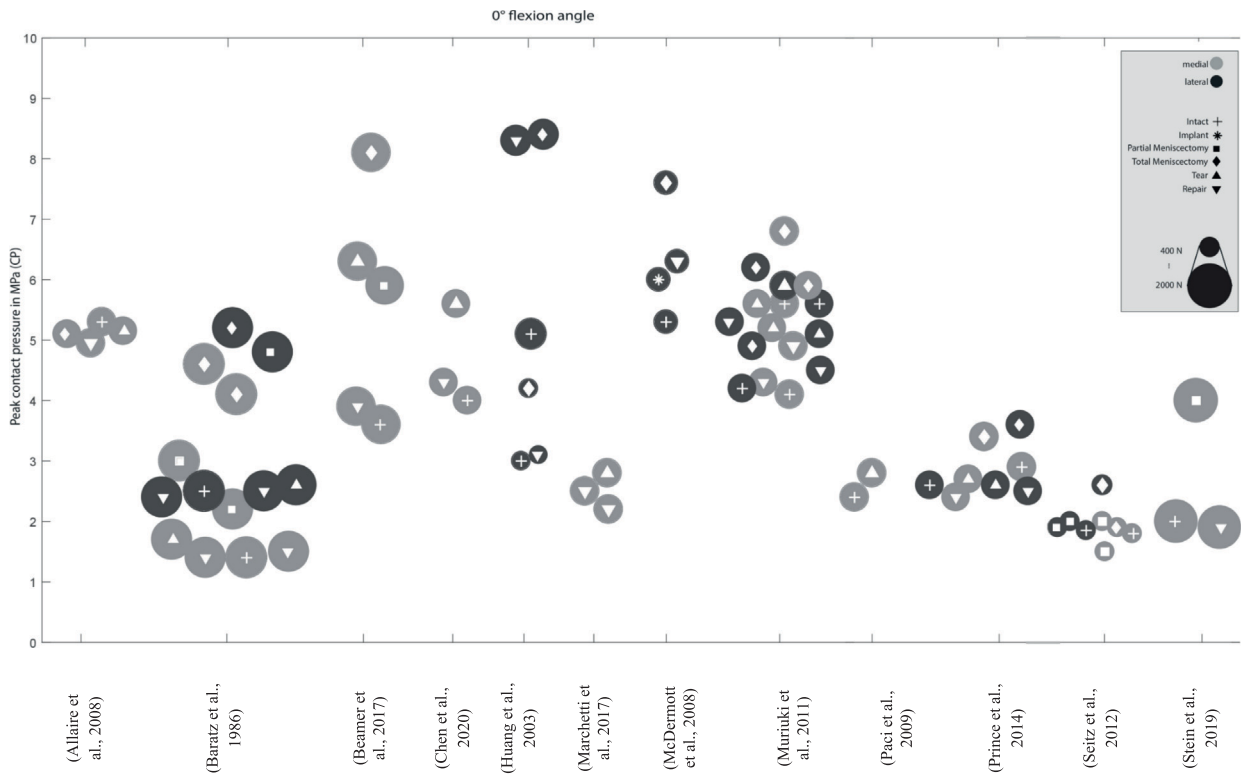

FIGURE 5 | Peak contact pressure at 0° knee joint flexion. Differentiation between lateral, medial menisci and meniscal states. Data point size represents the magnitude of the applied axial load ranging from 400 N to 2,000 N. (Data approximated from graphs).

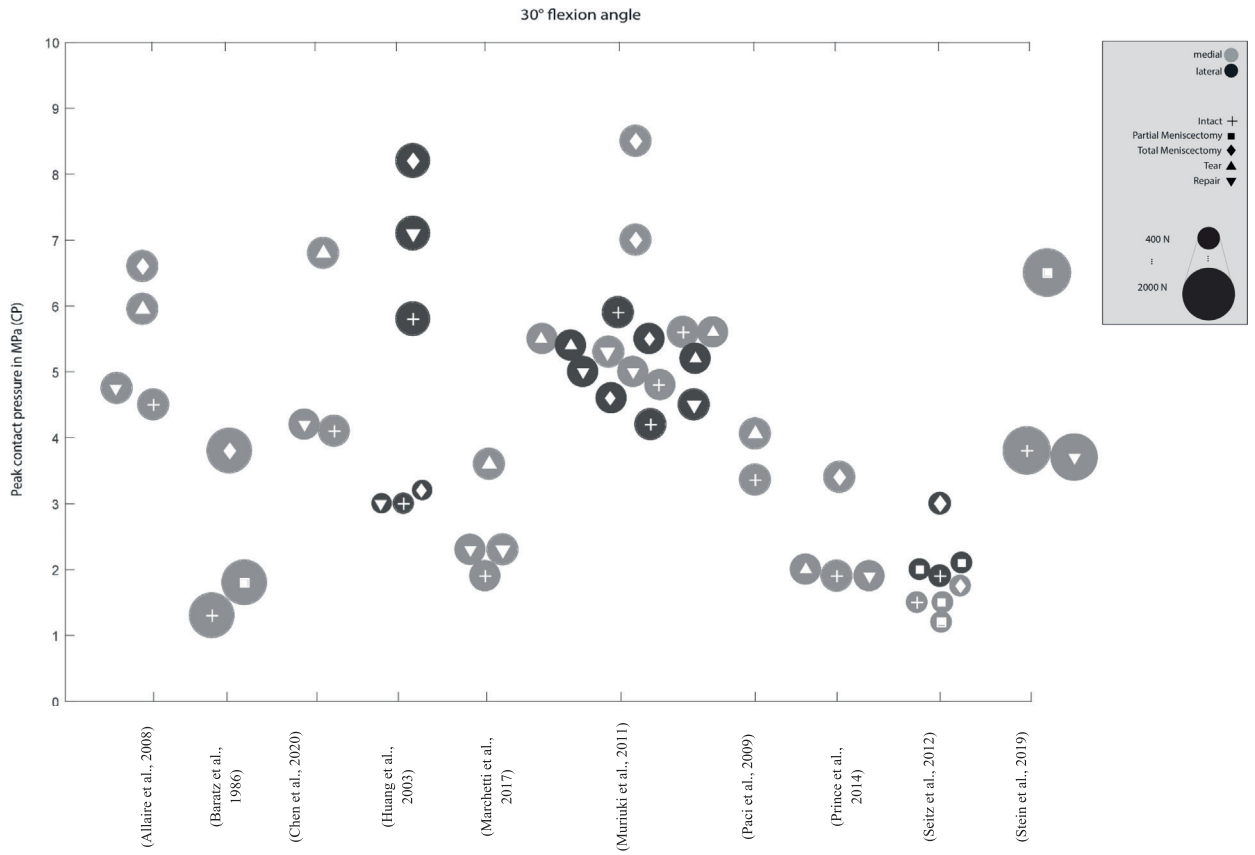

FIGURE 6 | Peak contact pressure at 30° knee joint flexion. Differentiation between lateral, medial menisci and meniscal states. Data point size represents the magnitude of the applied axial load ranging from 400 N to 2,000 N. (Data approximated from graphs).

technique, an inside-out repair and a partial meniscectomy on the peak CP (Zhang et al., 2015). Both, all-inside meniscal repair and the inside-out repair decreased the peak CP by approximately 40% compared to the partial meniscectomy state. In other studies, Bedi et al. (2012) and Padalecki et al. (2014) showed an increase in the medial compartment peak CP proportional to the width of the radial posterior horn tear of the medial meniscus. Lee et al. investigated the outcome on the peak CP after undergoing five consecutive medial meniscectomy conditions, beginning from intact over 50–75% to a segmental and finally total meniscectomy, finding that the medial compartment peak pressures continuously increased from approximately 4.5–9.27 MPa at 0° flexion angle, respectively (Lee et al., 2006). At a deflection angle of 30°, even an increase of 142% was determined. A similar study by Seitz et al. investigated the effect of partial meniscectomies of the medial posterion horn. Here, an increase in CP was reported, although only significantly in higher flexion angles (>30°) of the knee. Total meniscectomy, however, resulted in a significant increase in pressure in all knee flexion angles (Seitz et al., 2012).

Goyal et al. found only a minor increase in the peak CP from subsequent vertical tears in the periphery of the lateral meniscus compared to the intact meniscal state (Goyal et al., 2014). They argued that with the circumferential fibers being still intact in such a tear configuration, the torn meniscus is still able to provide a sufficient load transmission. Chen et al. also compared the medial peak CP of a repaired vertical longitudinal tear with that of the intact and injuried ones (Chen et al., 2020). They reported a significant improvement of tibiofemoral contact conditions after meniscus repair, although the peak CP and area after repair were not significantly different from those of the tear conditions. However, they found at high flexion of over 60°, new cutting effects appearing on the repaired meniscus, which might result in tear gapping and thereby causing new tears.

Partial and Total Meniscectomy

Various studies showed a significant 50–200% increase in the peak CP in medial meniscectomized versus intact knees (Fukubayashi and Kurosawa, 1980; Kurosawa et al., 1980; Baratz et al., 1986; Chen et al., 1996; McDermott et al., 2008; Muriuki et al., 2011; Prince et al., 2014). In their study, Brown et al. demonstrated, that after a horizontal medial meniscal tear, the resection of the horizontal inferior leaflet did not alter the peak CP compared to the intact state (Brown et al., 2016). They

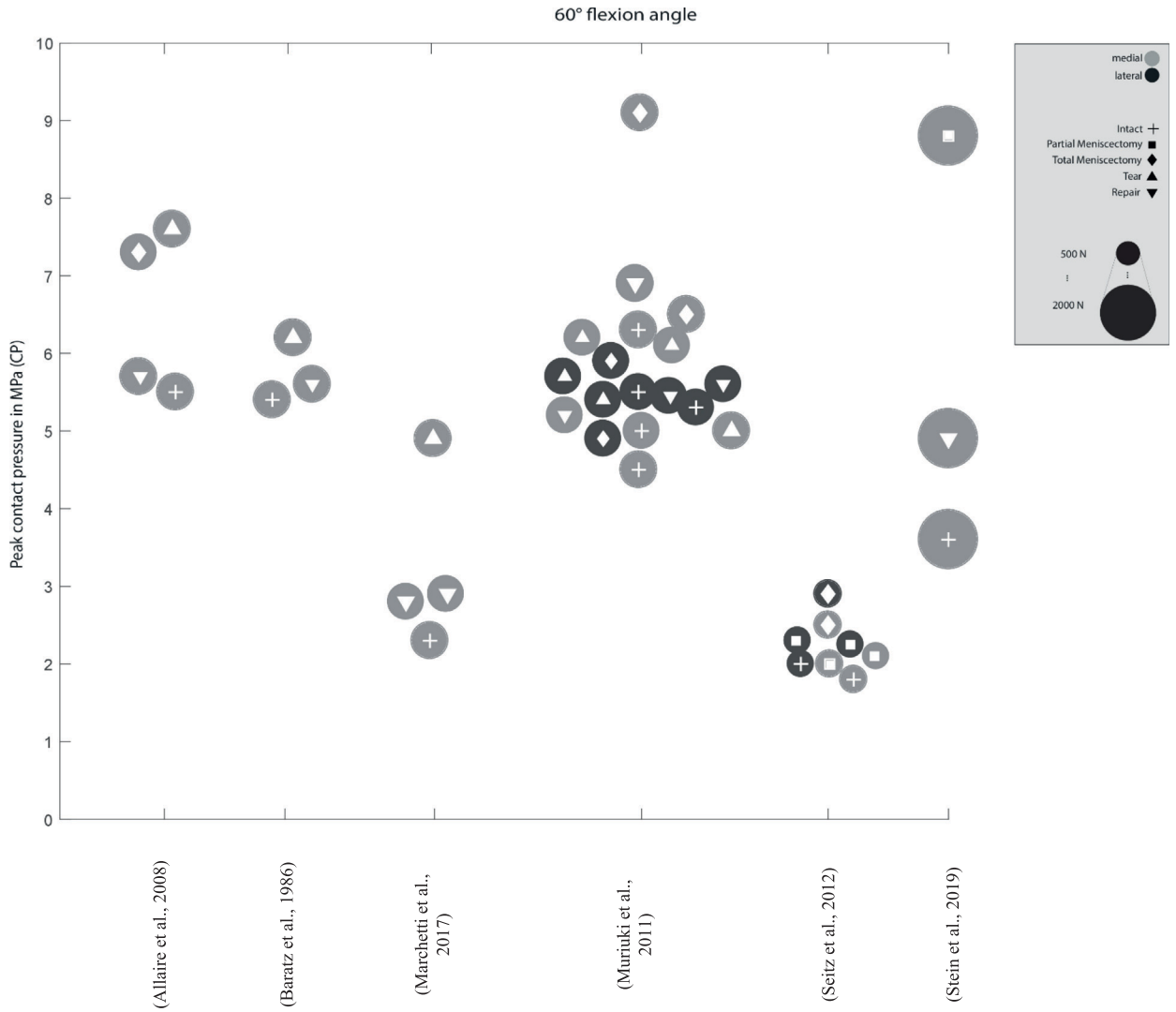

FIGURE 7 | Peak contact pressure at 60° knee joint flexion. Differentiation between lateral, medial menisci and meniscal states. Data point size represents the magnitude of the applied axial load ranging from 500 N to 2,000 N. (Data approximated from graphs).

explained, that in this tear configuration the continued dissipation of hoop stresses is still possible, thereby providing sufficient load transformation from axial loading into circumferential hoop stresses. However, the resection of both leaflets increased the peak CP in the medial compartment by approximately 35% in comparison to the intact state. They concluded that the resection of both leaflets had a biomechanically dramatic effect through contact area reduction on the articular surfaces. Therefore, axial loading forces can no longer be adequately dissipated from the cartilage surface (Yim et al., 2013), leading to an increased risk for OA (Brown et al., 2016). These findings are supported by the results of Beamer et al., who indicated a moderate 8% increased peak CP after a horizontal cleavage tear repair when compared to the intact meniscal state (Beamer et al., 2017). The post-injured peak CP increase was approximately 70% after a horizontal cleavage tear. Goyal et al. reported an increase in the peak CP after subtotal meniscectomy of the lateral meniscus of up to approximately 12% compared to the intact state, with more pronounced effects during deep knee flexion at 30 and 60° flexion (Goyal et al., 2014). Biomechanically, the meniscal rim is the structure that is most crucial for transferring axial loads into circumferential hoop stresses and retaining them. Therefore, the increase in the peak CP is dramtically higher when the meniscal rim is involved in a meniscal injury. Zhang et al. found a significant increase in the medial peak CP by simulating a radial tear at the posterior horn of the medial meniscus and a consecutive partial meniscectomy treatment compared to the intact state, indicating a peak CP increase of 67% after radial tear simulation and a 118% increase after partial meniscectomy compared to the intact state (Zhang et al., 2015). Therefore, whenever possible, meniscus tears should be repaired not only to

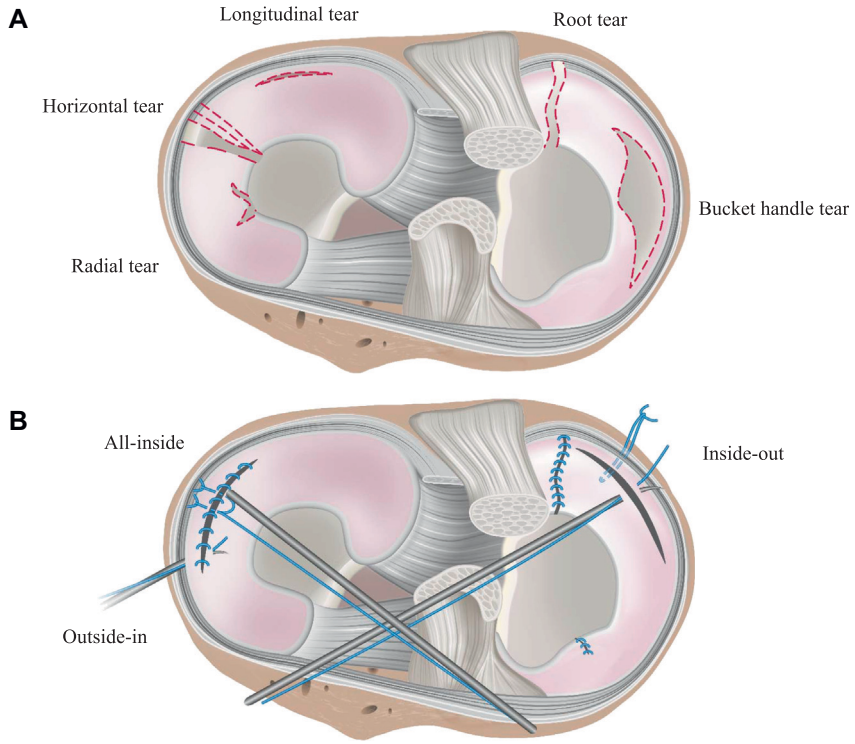

FIGURE 8 | Schematic illustration of the tibial plateau, representing **(A)** traumatic and damaged meniscal states and **(B)** repaired meniscal state. Meniscal tears shown in **(A)** are the most common tears, presented widely in the literature. Suture techniques for their treatment are shown in **(B)**.

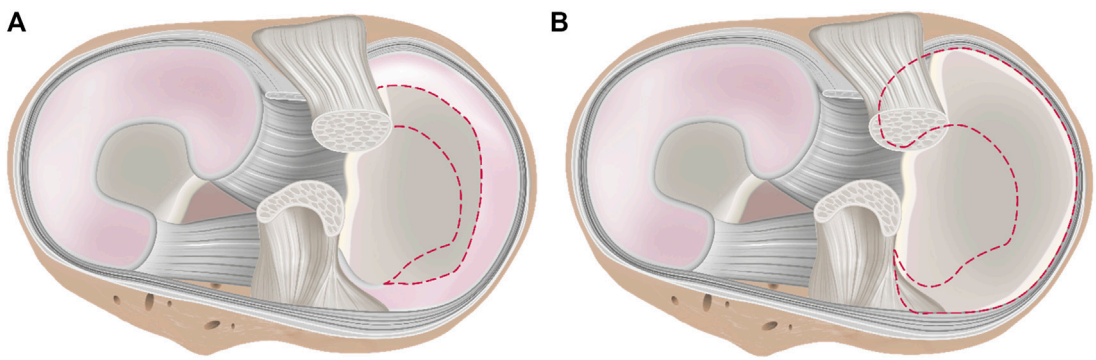

FIGURE 9 | Schematic illustration of the tibial plateau with **(A)** partial meniscectomy and **(B)** total meniscectomy. The dashed line indictes the removed meniscus tissue in each case.

avoid increased CP but also to prevent tear propagation (Goyal et al., 2014).

Implants, Partial and Total Meniscus Replacement

Becker et al. investigated the meniscofemoral peak CP in the medial and lateral compartments at full knee extension under an axial load of 1,400 N with five different biodegradable implants for meniscal repair after simulating a bucket-handle tear (Becker et al., 2005). They showed, that the repaired menisci led to a similar peak CP compared to intact knees. In the initial intact state, the medial peak CP was 3.12 MPa and the lateral pressure 2.3 MPa. In the medial compartment of the five implants, the peak CP ranged from 2.66 to 3.74 MPa. Laterally, pressure values between 2.84 and 3.73 MPa were identified.

Stein et al. investigated the use of a biocompatible silk fibroin meniscal replacement (Stein et al., 2019). A partial meniscectomy, leaving a 4 mm peripheral meniscal rim and both meniscal horns intact, was performed and replaced by the implant. Initially, a doubling of the peak CP was observed after partial meniscectomy

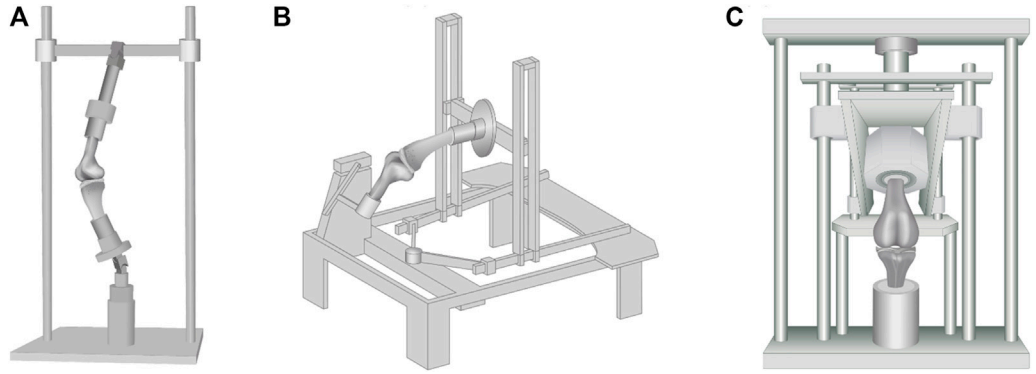

FIGURE 10 | Commonly used test setups found in literature: **(A)** Oxford-rig, **(B)** horizontal rig and **(C)** ("modified") material testing machines. They differ mainly in force application, knee alignment, and range of motion.

followed by a restoration of the peak CP to the intact situation after partial replacement. With a flexion angle of 60°, an increase of approximately 140% could be calculated. Subsequently, the initial intact peak CP could be achieved by using replacements (Wang et al., 2015; Stein et al., 2019). Huang et al. examined how different levels of compressive load (400 vs. 1,200 N) affect the CP outcomes after autograft procedures (Huang et al., 2003). The most important result was that an autograft can restore the initial intact peak CP at 400 N axial load. However, at 1,200 N, the restored peak CP were significantly higher than in initial intact state. They concluded that differences, therefore, cannot be scaled up from lower load scenarios to higher ones (Huang et al., 2003).

Test Setups

The different test setups clearly indicate that the used hardware and test strategies greatly influence the level and changes of CP values (**Figure 10**). A non-physiological alignment and embedding of knee specimens can lead to considerably changed and misleading values.

During natural movements, the knee joint offers six degrees of freedom (DOF) (Hirschmann and Muller, 2015). In the case of a limitation of these six DOF, the kinematics of the knee joint is altered, leading also to an altered CP. In addition, depending on the horizontal or vertical alignment of the knee joint during the experiments, the peak CP might also be altered. While the horizontal knee alignment is more likely to eliminate gravitational effects in the flexion-extension plane (Amis et al., 2006), because of its anatomically correct knee joint alignment, the vertical alignment reflects a more physiological load bearing situation. To obtain realistic kinematical parameters that are comparable to the *in vivo* situation, conventional or modified material testing machines, Oxford-rigs, horizontal rigs and wear simulators are used (**Supplementary Material**). Using conventional material testing machines (Agneskirchner et al., 2007; Marzo and Gurske-Deperio, 2009; Van Thiel et al., 2011; Forkel et al., 2014; Zhang et al., 2015; Brown et al., 2016), the application of an axial load on a vertically aligned knee joint can be readily implemented. Modified material testing machines with customized loading setups are normally able to provide all six DOF during *in vitro* experiments (Becker et al., 2005; Rodner et al., 2006; Schillhammer et al., 2012; Kim et al., 2013; Bryant et al., 2014; Goyal et al., 2014; Lee, 2014). The main components of custom-made vertical knee joint simulators, so-called Oxford-rig simulators (Mcculloch et al., 2016; Steinbruck et al., 2016), are ankle and hip assemblies that also enable an unconstrained movement of the knee joint in all six DOF (Zavatsky, 1997). In Oxford-rigs, a horizontal actuator normally simulates the flexion-extension movements without simulating an according axial or ground reaction force. Another type of the experimental setup is a horizontal rig (Stukenborg-Colsman et al., 2002; Ostermeier et al., 2006; Hofer et al., 2012), where the specimens are mounted with the femur or the tibia fixed horizontally and the patella facing up- or downwards (Stukenborg-Colsman et al., 2002). Movement of the tibia or femur is achieved either passively by an actuator or actively by means of active flexor and extensor muscle simulation, such as quadriceps or hamstring muscle. Additional muscle forces can be also simulated with dead weights. Lastly, CP can be investigated using a knee joint wear simulator (Bedi et al., 2010), which is normally used to examine different knee replacement designs. Such commercial simulators focus on long-term gait simulations, providing six DOF and flexion angles of up to 60°, while the flexion angle, axial force, anterior-posterior shear force or internal-external torque can be varied (Walker et al., 2000; van Houtem et al., 2006) accordingly.

Of course, the kinematical configuration of a test setup plays a crucial role when investigating the peak CP, where it is either possible to simulate dynamic (e.g., gait cycles, drop jump, etc.), static (e.g., fixed knee flexion angle) or so-called quasi-static (e.g., very slow simulation of predefined flexion-extension cycles) loading situations. Several groups used fixed knee flexion angles to simplify the testing apparatus (Marzo and Gurske-Deperio, 2009; Van Thiel et al., 2011; Forkel et al., 2014; Brown et al., 2016). The fixed angles and pre-defined axial loads allow groups to investigate research questions and their effects on knee kinematics without additional expense or new machine investment. Complex setups like Oxford-rigs, by contrast, offer greater dynamics and the simulation of muscle

forces and motion patterns (Bryant et al., 2014; Mcculloch et al., 2016; Steinbruck et al., 2016; Schall et al., 2019).

External Load Application

An adequate load application is essential when attempting to simulate *in vivo* knee joint loading conditions and, therefore, CP values at a realistic pathological or physiological level. Loads can be applied either directly *via* the bony structure (*isolated axial load*) by the loading apparatus, indirectly by *muscle force simulation*, or using a combination of both.

Axial Load

One of the most frequently applied loads is the (isolated) axial load, which can be applied either statically or dynamically. During pure axial loading situations, the knee flexion angle needs to be fixed at a previously defined position, otherwise the knee would not be loaded but rather flexed into a different position. Differences in applied isolated axial loads to the knee joints ranged from 0 up to 2,700 N (Lee et al., 2006; Bode et al., 2017; van Egmond et al., 2017).

Instead of isolated axial loads, extension moments or a combination of isolated axial load and external moments can be applied (Stukenborg-Colsman et al., 2002; Ostermeier et al., 2006; Bedi et al., 2010) to simulate gait cycles or isokinetic extension movements (Amadi et al., 2008; Bode et al., 2017). Additionally, a combination of isolated axial loads or external moments and muscle force simulations (Stukenborg-Colsman et al., 2002; Becker et al., 2005; Ostermeier et al., 2006; Hofer et al., 2012; Goyal et al., 2014; Lee, 2014; Mcculloch et al., 2016; Steinbruck et al., 2016), as well as variable muscles force simulations can be used (Bryant et al., 2014) to simulate different knee joint loading situations.

Peak CP measurements during joint weight-bearing is quite challenging (Rodner et al., 2006). In some studies, the applied forces were not able to achieve physiological loading conditions (Rodner et al., 2006; Schillhammer et al., 2012; Kim et al., 2013; Forkel et al., 2014; Mcculloch et al., 2016), resulting in a comparably lower peak CP and thus, being unable to simulate realistic load scenarios that occur during daily activities (Kim et al., 2013). Baratz et al. (1986), Paletta et al. (1997), Ode et al. (2012), and Dienst et al. (2007) measured CP after performing a total meniscectomy using material testing machines with different axial loads but with comparable test setups. Baratz et al. and Paletta et al. applied 1,800 N of axial load, whereas Ode et al. and Dienst et al. used an axial force of 800 and 1,000 N, respectively. Between healthy knee joints and total meniscectomized joints, Baratz et al. and Paletta et al. measured an increase in the peak CP of 100–235%. Ode et al. and Dienst et al. reported a more moderate increase in the peak CP of less than 50% after total meniscectomy. On the basis of only the differences in axial loads, it can be assumed that these differences are mainly attributed to the different axial loading conditions.

To investigate the influence of limb malalignments, Willinger et al. loaded their cadaveric knees axially with 750 N (Willinger et al., 2019) in neutral, varus and valgus alignments. They demonstrated that varus alignment significantly increased the medial peak CP compared to neutral or valgus alignment, with an intact medial meniscus. By contrast, valgus malalignment and a neutral axis resulted in a reduced medial CP. This findings were supported by Agneskirchner et al. (2007), Bruns et al. (1993) and Inaba et al. (1990). Summing up the results of these studies, all authors concluded that during varus malalignment, the medial compartment is loaded significantly more than the lateral compartment. Whereas in a valgus position, the ratios are consequently reverse.

Muscle Force Simulation

Muscle force simulation is important to achieve realistic and physiological loading conditions, particularly during dynamic *in vitro* knee joint simulations. The muscle forces stabilize the knee joint (Forkel et al., 2014) and are key for generating a dynamic compressive tibiofemoral force, for example, during knee flexion and extension (Bryant et al., 2014). Differences in muscle force simulation are due to the number of simulated muscles and the magnitude of the applied loads (Stukenborg-Colsman et al., 2002; Becker et al., 2005; Ostermeier et al., 2006; Hofer et al., 2012; Bryant et al., 2014; Goyal et al., 2014; Lee, 2014; Mcculloch et al., 2016; Steinbruck et al., 2016). Muscles can be simulated either *via* pneumatic or hydraulic actuators or simplified *via* dead weights. Simulation *via* actuators allows adjustment of the muscle forces over time or to be related to the knee flexion angle. However, due to the difficulty of a suitable control for the actuators (Maletsky and Hillberry, 2005; Muller et al., 2009) or challenges at the connection between muscle or tendon and the actuator itself, the simulated muscle forces are frequently lower than those encountered *in vivo* (Hofer et al., 2012). Abrupt increases in forces or dynamic gait scenarios frequently lead to tearing or slipping of fasteners or tissue grips. This finally leads to an underrepresentation of *in vivo* contact mechanics (Hofer et al., 2012; Bryant et al., 2014). A lack of variability of the muscle forces with varying knee flexion angle, particularly when using dead weights, and in different knee joint states might also lead to altered, mostly underestimated CP results (Li et al., 2002; Hofer et al., 2012). In principle, the muscle force simulation should be adapted to the *in vivo* muscle activation profile of the specific movement. These datasets can be acquired by inverse dynamic models that are based on kinematic and kinetic measurements in professional gait laboratories (Alimusaj et al., 2009) and even *via* open source database (e.g., OrthoLoad.com). Additionally, the simulation of agonist-antagonist interaction of the respective muscle groups needs to be considered when simulating dynamic recurring movements, for example, gait cycles. Otherwise, the knee joint is loaded insufficiently, leading to an underestimated CP. Ostermeier et al. found an increase in the peak CP of up to 15% of the initial peak CP with quadriceps muscle force and additional co-contraction of the hamstring muscles compared to single quadriceps muscle simulations (Ostermeier et al., 2006). The co-contraction of the simulated muscles thereby pulls the tibial compartment more strongly against the femoral condyle.

TABLE 2 | Recommendations for the determination of contact mechanics regarding the meniscus and meniscal injuries.

Test setup	Motion	Load	Muscle simulation
Modified material testing machine Oxford-rig Horizontal rig	Flexion-extension cycle with varying flexion rate	Axial load (body weight) External moments	Quadriceps Hamstring

DISCUSSION

The aim of this systematic review was to investigate the influence of menisci on tibiofemoral contact mechanics in human knees and to summarize the influence of various test setups, load applications and muscle force simulations on the determination of the tibiofemoral CP after simulated meniscal injuries and their surgical treatments, including sutures and meniscectomies. This study was also performed to describe the effects of CP-elevating events and thereby explain the increased risk for patients to develop PTOA and how this can be delayed or even prevented.

Meniscus Pathology

The results of our systematic literature review indicated, that an injured meniscus, for example, meniscal tears, leads to significantly increased CPs within the knee joint. The peak CP values increase up to 235% in total meniscectomized knees compared to their intact meniscal state (Baratz et al., 1986). The analysis of the published peak CPs showed a wide range from 0.1 MPa (van Egmond et al., 2017) to 12.06 MPa (Poh et al., 2012). Surgical treatments like sutures or meniscus replacements are able to restore the CP almost to the initial intact state. Degenerated or pathologically altered menisci lead to increased peak CPs and their repair is necessary to ideally restore the native CP distribution. This is essential because it is widely accepted that meniscal alteration, and thus an increased peak CP, is one crucial factor initiating the early onset of PTOA (Badlani et al., 2013; Thomas et al., 2017). Therefore, one primary treatment goal of a meniscus pathology is to restore the CP close to the intact state and ideally rebalance the load distribution between the lateral and medial compartments.

In summary, post-traumatic changes of the meniscus significantly increase the CP in the knee. Tears and partial or total meniscectomy treatments lead to increased CP in the knee joint, whereas repairing techniques, like meniscus sutures, are able to restore the CP almost similar to the intact meniscal state. The publications evaluated in this review widely coincide in their outcomes, particularly after a meniscal injury when the peak CP tendentially increases, whereas it can be restored by surgical treatment. Moreover, the published CP values showed clear trends after an injury or its treatment.

However, it is also clear from the present study that the absolute values of the reported CPs cannot be compared. The different approaches of the research groups make it difficult to determine the "truth" of the CP. Therefore, it more practical to compare the relative values, while real values (in MPa) are more likely to lead to non-comparable values, particularly because of the large number of different test setups and simulations. What has become clear, however, is the fact that untreated meniscal injuries inevitably lead to a significant increase in CP and in the long term are highly prone to progress to PTOA.

Testing Conditions

As indicated above, large differences were found in the application of loads and the alignment of the knee joint specimens in different test setups. It could be demonstrated that greater applied axial loads lead to a higher peak CP and muscle force simulation resulted in a more physiological knee joint loading condition with an accordingly higher peak CP. Muscle force simulation leads to a more realistic environment of the knee joint in *in vitro* testing. On the one hand, the knee is loaded multidimensionally, and on the other hand, the knee is held and guided more stably in the test environment. This results in a more physiological outcome compared to pure axial loads. The test setups and their respective load simulations in *in vitro* peak CP measurements indicated a remarkable axial loading range from 0 to 2,700 N. It appears clear that greater axial loads and applied muscle force simulations lead to higher CP, which makes it difficult for an objective comparison of the so gathered CP values. Values obtained through the different research approaches cannot be compared with each other. This can be seen, for example, in the comparison of the two studies with similar test setups by Agneskirchner et al. (isolated axial load 1,000 N) and Inaba et al. (isolated axial load 2,700 N), with peak CPs of 1.72 MPa (Agneskirchner et al., 2007) vs. 4.01 MPa (Inaba et al., 1990) shown in the intact knee state with normal alignment. Furthermore, Huang et al. demonstrated that pressure differences cannot be scaled up from lower load scenarios to higher ones (Huang et al., 2003). Rather, the trend of the peak CP outcome in each study needs to be evaluated, as well as its general research question. This can be used, for example, to determine the success of a treatment strategy, but not to investigate questions in which the magnitude of the peak CP is important. This could be the case, for example, when investigating the stability of load-critical replacements or implants.

In addition, lower limb varus malalignment leads to an increased medial CP, which is further considered as a promoter of premature OA (Inaba et al., 1990; Bruns et al., 1993; Agneskirchner et al., 2007; Willinger et al., 2020). The limb alignment must be considered in each test, because this elementary parameter can have a major effect on the result by increasing or decreasing CPs unintentionally. Therefore, care must be taken to ensure that the clamping is performed in a native manner without placing the knee unintentionally in a malalignment and thus influencing the peak CP.

Therefore, we propose recommendations for future *in vitro* testing of knee joint contact mechanics. This was done to obtain the most realistic *in vivo* data possible from testing in addition to the already gathered significant trends. This is also intended to make biomechanical studies more comparable, objective and consistent in approach and findings.

Recommendations for Future Biomechanical CP Studies

A biomechanically based recommendation regarding the experimental procedures for *in vitro* investigations on CP of the knee joint focusing on meniscus modifications is presented in **Table 2**, including the requirements for the test setup, static or dynamic testing methods, magnitude and direction of the applied loads and muscle force simulation. Here, the physiological vertical knee alignment is the key factor. The test setup should be extended by the knee-stabilizing quadriceps and hamstrings muscles and an axial load adapted to the specimen (*in vivo* weight simulation). For the kinematic examination, normal daily exercises with flexion and extension (e.g., gait cycle) should be selected (Huang et al., 2003).

Due to the time-dependent responses of meniscal tissue and its dynamic environment within the knee joint, motion of the knee joint may be better suited to investigate CP with meniscal tears or after meniscus resection (Goyal et al., 2014). The range of motion and the velocity of the motion should be as close as possible to the physiological movement of a human knee joint seen during activities of daily life. Ideally, the axial load should be either combined with a sufficient muscle force simulation or alternatively tibiofemoral contact forces should result from such an appropriate muscle force simulation. The major knee spanning muscles - quadriceps and the hamstrings - are particularly important for the stabilization of the knee joint and should be simulated. The preferred test setups are horizontal rigs, Oxford-rigs and modified material testing machines, in particular Oxford-rigs and material testing machines, because they may have advantages due to their upright knee joint position. The axial load should be related to the biometric data of the donor of the knee joint specimen to allow reasonable *in vivo*-like weight bearing simulation. Static knee joint loading should ideally be avoided, because the highly anisotropic and inhomogeneous viscoelastic menisci show a time- and localization-depending behavior. The latter is mainly determined by the interaction of the menisci with their surrounding soft tissues within the knee joint. Therefore, we recommend to rather simulate dynamic loading situations with varying knee joint flexion angles as seen during activities of daily life, like e.g. normal gait or stair climbing. However, dynamic testing is not possible in every research institution. If dynamic testing, as suggested by us, is not possible, static tests with different axial load profiles and different flexion angles should be performed. Additionally, the axial load and limb alignment should be adapted to the donor as a minimum requirement.

Considering this, it may lead to greater transparency and, therefore, an increased knowledge in the understanding of knee joint contact mechanics. When consistent test setups and test procedures are introduced and implemented by research institutions, different fields can thereby be investigated and a wide-ranging field of interest with a high level of knowledge exchange could be obtained.

At the very least, the description of the experimental procedure should be presented in a reproducible and thus fully transparent way. The description of the test setup, test procedure, load application, and muscle force simulation should be made very precisely to be able to reproduce tests and their results. Such a description should at least incorporate the following terms: Description of test setup and included modifications, DOF at all bearings, fixation of femur, and tibia, actuators, sensors, and the used control mode; for static testing all tested flexion angles should be mentioned; for motion cycles, both, the range and velocity of the motion should be indicated; direction and magnitude of the applied loads must be known. Information about muscle simulation should include the simulated muscle groups, simulation type with weights or actuators (control mode), magnitude and direction of the simulated muscles and a description of the change of magnitude over time or flexion angle.

DATA AVAILABILITY STATEMENT

The original contributions presented in the study are included in the article/**Supplementary Material**, further inquiries can be directed to the corresponding author.

AUTHOR CONTRIBUTIONS

MS is the first author and wrote the publication, conducted the review using the PRISMA guidelines, created the graphics and discussed the overall research question. FS and SH performed a initial rough literature search and contributed to conception and design of the study. LD, AI, and AS helped identify the topic, contributed with expertise in the topic, and edited the preliminary versions for subject matter accuracy. AS, AI, and LD contributed to the revision of the article and gave final approval to the submitted version.

FUNDING

This work was funded by the German Research Foundation (DFG SE3135/1-1).

ACKNOWLEDGMENTS

The authors would like to acknowledge Patrizia Horny from the Institute of Orthopaedic Research and Biomechanics Ulm for her design support.

SUPPLEMENTARY MATERIAL

The Supplementary Material for this article can be found online at: https://www.frontiersin.org/articles/10.3389/fbioe.2021.765596/full#supplementary-material

REFERENCES

Agneskirchner, J. D., Hurschler, C., Wrann, C. D., and Lobenhoffer, P. (2007). The Effects of Valgus Medial Opening Wedge High Tibial Osteotomy on Articular Cartilage Pressure of the Knee: a Biomechanical Study. *Arthrosc. J. Arthroscopic Relat. Surg.* 23, 852–861. doi:10.1016/j.arthro.2007.05.018

Alimusaj, M., Fradet, L., Braatz, F., Gerner, H. J., and Wolf, S. I. (2009). Kinematics and Kinetics with an Adaptive Ankle Foot System during Stair Ambulation of Transtibial Amputees. *Gait & Posture* 30, 356–363. doi:10.1016/j.gaitpost.2009.06.009

Allaire, R., Muriuki, M., Gilbertson, L., and Harner, C. D. (2008). Biomechanical Consequences of a Tear of the Posterior Root of the Medial Meniscus. *The J. Bone Jt. Surgery-American Volume* 90, 1922–1931. doi:10.2106/jbjs.g.00748

Amadi, H. O., Gupte, C. M., Lie, D. T. T., Mcdermott, I. D., Amis, A. A., and Bull, A. M. J. (2008). A Biomechanical Study of the Meniscofemoral Ligaments and Their Contribution to Contact Pressure Reduction in the Knee. *Knee Surg. Sports Traumatol. Arthr* 16, 1004–1008. doi:10.1007/s00167-008-0592-0

Amis, A. A., Senavongse, W., and Bull, A. M. J. (2006). Patellofemoral Kinematics during Knee Flexion-Extension: an *In Vitro* Study. *J. Orthop. Res.* 24, 2201–2211. doi:10.1002/jor.20268

Badlani, J. T., Borrero, C., Golla, S., Harner, C. D., and Irrgang, J. J. (2013). The Effects of Meniscus Injury on the Development of Knee Osteoarthritis. *Am. J. Sports Med.* 41, 1238–1244. doi:10.1177/0363546513490276

Baker, B. E., Peckham, A. C., Pupparo, F., and Sanborn, J. C. (1985). Review of Meniscal Injury and Associated Sports. *Am. J. Sports Med.* 13, 1–4. doi:10.1177/036354658501300101

Baratz, M. E., Fu, F. H., and Mengato, R. (1986). Meniscal Tears: The Effect of Meniscectomy and of Repair on Intraarticular Contact Areas and Stress in the Human Knee. *Am. J. Sports Med.* 14, 270–275. doi:10.1177/036354658601400405

Beamer, B. S., Walley, K. C., Okajima, S., Manoukian, O. S., Perez-Viloria, M., Deangelis, J. P., et al. (2017). Changes in Contact Area in Meniscus Horizontal Cleavage Tears Subjected to Repair and Resection. *Arthrosc. J. Arthroscopic Relat. Surg.* 33, 617–624. doi:10.1016/j.arthro.2016.09.004

Becker, R., Wirz, D., Wolf, C., Göpfert, B., Nebelung, W., and Friederich, N. (2005). Measurement of Meniscofemoral Contact Pressure after Repair of Bucket-Handle Tears with Biodegradable Implants. *Arch. Orthop. Trauma Surg.* 125, 254–260. doi:10.1007/s00402-004-0739-5

Bedi, A., Kelly, N., Baad, M., Fox, A. J. S., Ma, Y., Warren, R. F., et al. (2012). Dynamic Contact Mechanics of Radial Tears of the Lateral Meniscus: Implications for Treatment. *Arthrosc. J. Arthroscopic Relat. Surg.* 28, 372–381. doi:10.1016/j.arthro.2011.08.287

Bedi, A., Kelly, N. H., Baad, M., Fox, A. J., Brophy, R. H., Warren, R. F., et al. (2010). Dynamic Contact Mechanics of the Medial Meniscus as a Function of Radial Tear, Repair, and Partial Meniscectomy. *J. Bone Jt. Surgery-American Volume* 92, 1398–1408. doi:10.2106/jbjs.i.00539

Bode, G., Kloos, F., Feucht, M. J., Fleischer, B., Südkamp, N., Niemeyer, P., et al. (2017). Comparison of the Efficiency of an Extra-articular Absorber System and High Tibial Osteotomy for Unloading the Medial Knee Compartment: an *In Vitro* Study. *Knee Surg. Sports Traumatol. Arthrosc.* 25, 3695–3703. doi:10.1007/s00167-016-4358-9

Brown, M. J., Farrell, J. P., Kluczynski, M. A., and Marzo, J. M. (2016). Biomechanical Effects of a Horizontal Medial Meniscal Tear and Subsequent Leaflet Resection. *Am. J. Sports Med.* 44, 850–854. doi:10.1177/0363546515623782

Bruns, J., Volkmer, M., and Luessenhop, S. (1993). Pressure Distribution at the Knee Joint. *Arch. Orthop. Trauma Surg.* 113, 12–19. doi:10.1007/bf00440588

Bryant, B. J., Tilan, J. U., Mcgarry, M. H., Takenaka, N., Kim, W. C., and Lee, T. Q. (2014). The Biomechanical Effect of Increased Valgus on Total Knee Arthroplasty: a Cadaveric Study. *The J. Arthroplasty* 29, 722–726. doi:10.1016/j.arth.2013.09.003

Chen, M. I., Branch, T. P., and Hutton, W. C. (1996). Is it Important to Secure the Horns during Lateral Meniscal Transplantation? A Cadaveric Study. *Arthrosc. J. Arthroscopic Relat. Surg.* 12, 174–181. doi:10.1016/s0749-8063(96)90007-9

Chen, Z., Zhang, H., Luo, H., Yang, R., Zhang, Z., Jiang, C., et al. (2020). Contact Mechanics after Mattress Suture Repair of Medial Meniscus Vertical Longitudinal Tear: an *In Vitro* Study. *Arch. Orthop. Trauma Surg.* 140 (9), 1221–1230. doi:10.1007/s00402-020-03428-0

Cooper, C., Snow, S., Mcalindon, T. E., Kellingray, S., Stuart, B., Coggon, D., et al. (2000). Risk Factors for the Incidence and Progression of Radiographic Knee Osteoarthritis. *Arthritis Rheum.* 43, 995–1000. doi:10.1002/1529-0131(200005)43:5<995:aid-anr6>3.0.co;2-1

de Groot, J. (2010). *Actifit, Polyurethane Meniscus Implant*. Basic Science. Meniscus, 383–387. doi:10.1007/978-3-642-02450-4_48

Dienst, M., Greis, P. E., Ellis, B. J., Bachus, K. N., and Burks, R. T. (2007). Effect of Lateral Meniscal Allograft Sizing on Contact Mechanics of the Lateral Tibial Plateau. *Am. J. Sports Med.* 35, 34–42. doi:10.1177/0363546506291404

Dugas, J., Barrett, A., Beason, D., Plymale, M., and Fleisig, G. (2015). Tibiofemoral Contact Biomechanics Following Meniscocapsular Separation and Repair. *Int. J. Sports Med.* 36, 498–502. doi:10.1055/s-0034-1398656

Felson, D. T., Lawrence, R. C., Dieppe, P. A., Hirsch, R., Helmick, C. G., Jordan, J. M., et al. (2000). Osteoarthritis: New Insights. Part 1: the Disease and its Risk Factors. *Ann. Intern. Med.* 133, 635–646. doi:10.7326/0003-4819-133-8-200010170-00016

Felson, D. T., and Zhang, Y. (1998). An Update on the Epidemiology of Knee and Hip Osteoarthritis with a View to Prevention. *Arthritis Rheum.* 41, 1343–1355. doi:10.1002/1529-0131(199808)41:8<1343:aid-art3>3.0.co;2-9

Forkel, P., Herbort, M., Sprenker, F., Metzlaff, S., Raschke, M., and Petersen, W. (2014). The Biomechanical Effect of a Lateral Meniscus Posterior Root Tear with and without Damage to the Meniscofemoral Ligament: Efficacy of Different Repair Techniques. *Arthrosc. J. Arthroscopic Relat. Surg.* 30, 833–840. doi:10.1016/j.arthro.2014.02.040

Fukubayashi, T., and Kurosawa, H. (1980). The Contact Area and Pressure Distribution Pattern of the Knee:A Study of Normal and Osteoarthrotic Knee Joints. *Acta Orthopaedica Scand.* 51, 871–879. doi:10.3109/17453678008990887

Geeslin, A. G., Civitarese, D., Turnbull, T. L., Dornan, G. J., Fuso, F. A., and Laprade, R. F. (2016). Influence of Lateral Meniscal Posterior Root Avulsions and the Meniscofemoral Ligaments on Tibiofemoral Contact Mechanics. *Knee Surg. Sports Traumatol. Arthrosc.* 24, 1469–1477. doi:10.1007/s00167-015-3742-1

Goyal, K. S., Pan, T. J., Tran, D., Dumpe, S. C., Zhang, X., and Harner, C. D. (2014). Vertical Tears of the Lateral Meniscus: Effects on *In Vitro* Tibiofemoral Joint Mechanics. *Orthop. J. Sports Med.* 2, 2325967114541237. doi:10.1177/2325967114541237

Heckelsmiller, D. J., James Rudert, M., Baer, T. E., Pedersen, D. R., Fredericks, D. C., and Goetz, J. E. (2017). Changes in Joint Contact Mechanics in a Large Quadrupedal Animal Model after Partial Meniscectomy and a Focal Cartilage Injury. *J. Biomech. Eng.* 139. doi:10.1115/1.4036148

Hirschmann, M. T., and Müller, W. (2015). Complex Function of the Knee Joint: the Current Understanding of the Knee. *Knee Surg. Sports Traumatol. Arthrosc.* 23, 2780–2788. doi:10.1007/s00167-015-3619-3

Hofer, J. K., Gejo, R., Mcgarry, M. H., and Lee, T. Q. (2012). Effects of Kneeling on Tibiofemoral Contact Pressure and Area in Posterior Cruciate-Retaining and Posterior Cruciate-Sacrificing Total Knee Arthroplasty. *J. Arthroplasty* 27, 620–624. doi:10.1016/j.arth.2011.07.011

Huang, A., Hull, M. L., and Howell, S. M. (2003). The Level of Compressive Load Affects Conclusions from Statistical Analyses to Determine whether a Lateral Meniscal Autograft Restores Tibial Contact Pressure to normal: a Study in Human Cadaveric Knees. *J. Orthop. Res.* 21, 459–464. doi:10.1016/s0736-0266(02)00201-2

Inaba, H. I., Arai, M. A., and Watanabe, W. W. (1990). Influence of the Varus-Valgus Instability on the Contact of the Femoro-Tibial Joint. *Proc. Inst. Mech. Eng. H* 204, 61–64. doi:10.1243/pime_proc_1990_204_229_02

Kim, J. G., Lee, Y. S., Bae, T. S., Ha, J. K., Lee, D. H., Kim, Y. J., et al. (2013). Tibiofemoral Contact Mechanics Following Posterior Root of Medial Meniscus Tear, Repair, Meniscectomy, and Allograft Transplantation. *Knee Surg. Sports Traumatol. Arthrosc.* 21, 2121–2125. doi:10.1007/s00167-012-2182-4

Kurosawa, H., Fukubayashi, T., and Nakajima, H. (1980). Load-Bearing Mode of the Knee-Joint - Physical Behavior of the Knee-Joint with or without Menisci. *Clin. Orthopaedics Relat. Res.* 149, 283–290. doi:10.1097/00003086-198006000-00039

Laprade, C. M., Foad, A., Smith, S. D., Turnbull, T. L., Dornan, G. J., Engebretsen, L., et al. (2015). Biomechanical Consequences of a Nonanatomic Posterior

Medial Meniscal Root Repair. *Am. J. Sports Med.* 43, 912–920. doi:10.1177/0363546514566191

Lee, S. J., Aadalen, K. J., Malaviya, P., Lorenz, E. P., Hayden, J. K., Farr, J., et al. (2006). Tibiofemoral Contact Mechanics after Serial Medial Meniscectomies in the Human Cadaveric Knee. *Am. J. Sports Med.* 34, 1334–1344. doi:10.1177/0363546506286786

Lee, T. Q. (2014). Biomechanics of Hyperflexion and Kneeling before and after Total Knee Arthroplasty. *Clin. Orthop. Surg.* 6, 117–126. doi:10.4055/cios.2014.6.2.117

Li, G., Gill, T. J., Defrate, L. E., Zayontz, S., Glatt, V., and Zarins, B. (2002). Biomechanical Consequences of PCL Deficiency in the Knee under Simulated Muscle Loads-An *In Vitro* Experimental Study. *J. Orthop. Res.* 20, 887–892. doi:10.1016/s0736-0266(01)00184-x

Linke, R. D., Ulmer, M., and Imhoff, A. B. (2006). Der Meniskusersatz mit einem Kollagenimplantat (CMI). *Orthop. Traumatol.* 18, 453–462. doi:10.1007/s00064-006-1188-9

Makris, E. A., Hadidi, P., and Athanasiou, K. A. (2011). The Knee Meniscus: Structure-Function, Pathophysiology, Current Repair Techniques, and Prospects for Regeneration. *Biomaterials* 32, 7411–7431. doi:10.1016/j.biomaterials.2011.06.037

Maletsky, L. P., and Hillberry, B. M. (2005). Simulating Dynamic Activities Using a Five-axis Knee Simulator. *J. Biomechanical Engineering-Transactions Asme* 127, 123–133. doi:10.1115/1.1846070

Marchetti, D. C., Phelps, B. M., Dahl, K. D., Slette, E. L., Mikula, J. D., Dornan, G. J., et al. (2017). A Contact Pressure Analysis Comparing an All-Inside and Inside-Out Surgical Repair Technique for Bucket-Handle Medial Meniscus Tears. *Arthrosc. J. Arthroscopic Relat. Surg.* 33, 1840–1848. doi:10.1016/j.arthro.2017.04.013

Marzo, J. M., and Gurske-Deperio, J. (2009). Effects of Medial Meniscus Posterior Horn Avulsion and Repair on Tibiofemoral Contact Area and Peak Contact Pressure with Clinical Implications. *Am. J. Sports Med.* 37, 124–129. doi:10.1177/0363546508323254

Marzo, J. M., and Kumar, B. A. (2007). Primary Repair of Medial Meniscal Avulsions. *Am. J. Sports Med.* 35, 1380–1383. doi:10.1177/0363546506297907

Mcculloch, P. C., Dolce, D., Jones, H. L., Gale, A., Hogen, M. G., Alder, J., et al. (2016). Comparison of Kinematics and Tibiofemoral Contact Pressures for Native and Transplanted Lateral Menisci. *Orthop. J. Sports Med.* 4, 2325967116674441. doi:10.1177/2325967116674441

McDermott, I. D., Lie, D. T. T., Edwards, A., Bull, A. M. J., and Amis, A. A. (2008). The Effects of Lateral Meniscal Allograft Transplantation Techniques on Tibio-Femoral Contact Pressures. *Knee Surg. Sports Traumatol. Arthr* 16, 553–560. doi:10.1007/s00167-008-0503-4

Moher, D., Liberati, A., Tetzlaff, J., Altman, D. G., and Group, P. (2009). Preferred Reporting Items for Systematic Reviews and Meta-Analyses: the PRISMA Statement. *Open Med.* 3, e123–30. doi:10.1371/journal.pmed.1000097

Müller, O., Lo, J., Wünschel, M., Obloh, C., and Wülker, N. (2009). Simulation of force loaded knee movement in a newly developed *In Vitro* knee simulator/Simulation von belastungsabhängigen Kniebewegungen in einem neuartigen Knie-Simulator für In-vitro-Studien. *Biomedizinische Technik* 54, 142–149. doi:10.1515/bmt.2009.015

Muriuki, M. G., Tuason, D. A., Tucker, B. G., and Harner, C. D. (2011). Changes in Tibiofemoral Contact Mechanics Following Radial Split and Vertical Tears of the Medial Meniscus. *J. Bone Jt. Surg.* 93, 1089–1095. doi:10.2106/jbjs.i.01241

Nielsen, A. B., and Yde, J. (1991). Epidemiology of Acute Knee Injuries: a Prospective Hospital Investigation. *J. Trauma Inj. Infect. Crit. Care* 31, 1644–1648. doi:10.1097/00005373-199112000-00014

Ode, G. E., Van Thiel, G. S., Mcarthur, S. A., Dishkin-Paset, J., Leurgans, S. E., Shewman, E. F., et al. (2012). Effects of Serial Sectioning and Repair of Radial Tears in the Lateral Meniscus. *Am. J. Sports Med.* 40, 1863–1870. doi:10.1177/0363546512453291

Ostermeier, S., Schlomach, C., Hurschler, C., Windhagen, H., and Stukenborg-Colsman, C. (2006). Dynamic *In Vitro* Measurement of Posterior Cruciate Ligament Load and Tibiofemoral Stress after TKA in Dependence on Tibiofemoral Slope. *Clin. Biomech.* 21, 525–532. doi:10.1016/j.clinbiomech.2005.12.019

Paci, J. M., Scuderi, M. G., Werner, F. W., Sutton, L. G., Rosenbaum, P. F., and Cannizzaro, J. P. (2009). Knee Medial Compartment Contact Pressure Increases with Release of the Type I Anterior Intermeniscal Ligament. *Am. J. Sports Med.* 37, 1412–1416. doi:10.1177/0363546509331418

Padalecki, J. R., Jansson, K. S., Smith, S. D., Dornan, G. J., Pierce, C. M., Wijdicks, C. A., et al. (2014). Biomechanical Consequences of a Complete Radial Tear Adjacent to the Medial Meniscus Posterior Root Attachment Site. *Am. J. Sports Med.* 42, 699–707. doi:10.1177/0363546513499314

Paletta, G. A., Manning, T., Snell, E., Parker, R., and Bergfeld, J. (1997). The Effect of Allograft Meniscal Replacement on Intraarticular Contact Area and Pressures in the Human Knee. *Am. J. Sports Med.* 25, 692–698. doi:10.1177/036354659702500519

Perez-Blanca, A., Espejo-Baena, A., Amat Trujillo, D., Prado Nóvoa, M., Espejo-Reina, A., Quintero López, C., et al. (2016). Comparative Biomechanical Study on Contact Alterations after Lateral Meniscus Posterior Root Avulsion, Transosseous Reinsertion, and Total Meniscectomy. *Arthrosc. J. Arthroscopic Relat. Surg.* 32, 624–633. doi:10.1016/j.arthro.2015.08.040

Poh, S.-Y., Yew, K.-S. A., Wong, P.-L. K., Koh, S.-B. J., Chia, S.-L., Fook-Chong, S., et al. (2012). Role of the Anterior Intermeniscal Ligament in Tibiofemoral Contact Mechanics during Axial Joint Loading. *The Knee* 19, 135–139. doi:10.1016/j.knee.2010.12.008

Prince, M. R., Esquivel, A. O., Andre, A. M., and Goitz, H. T. (2014). Anterior Horn Lateral Meniscus Tear, Repair, and Meniscectomy. *J. Knee Surg.* 27, 229–234. doi:10.1055/s-0033-1360658

Rankin, C. C., Lintner, D. M., Noble, P. C., Paravic, V., and Greer, E. (2002). A Biomechanical Analysis of Meniscal Repair Techniques. *Am. J. Sports Med.* 30, 492–497. doi:10.1177/03635465020300040801

Rodner, C. M., Adams, D. J., Diaz-Doran, V., Tate, J. P., Santangelo, S. A., Mazzocca, A. D., et al. (2006). Medial Opening Wedge Tibial Osteotomy and the Sagittal Plane. *Am. J. Sports Med.* 34, 1431–1441. doi:10.1177/0363546506287297

Roos, E. M. (2005). Joint Injury Causes Knee Osteoarthritis in Young Adults. *Curr. Opin. Rheumatol.* 17, 195–200. doi:10.1097/01.bor.0000151406.64393.00

Schall, F., Seitz, A. M., Hacker, S., Van Drongelen, S., Wolf, S. I., Ignatius, A., et al. (2019). German Society of Biomechanics (DGfB) Young Investigator Award 2019: Proof-Of-Concept of a Novel Knee Joint Simulator Allowing Rapid Motions at Physiological Muscle and Ground Reaction Forces. *Front. Bioeng. Biotechnol.* 7, 244. doi:10.3389/fbioe.2019.00244

Schillhammer, C. K., Werner, F. W., Scuderi, M. G., and Cannizzaro, J. P. (2012). Repair of Lateral Meniscus Posterior Horn Detachment Lesions. *Am. J. Sports Med.* 40, 2604–2609. doi:10.1177/0363546512458574

Seitz, A. M., Lubomierski, A., Friemert, B., Ignatius, A., and Dürselen, L. (2012). Effect of Partial Meniscectomy at the Medial Posterior Horn on Tibiofemoral Contact Mechanics and Meniscal Hoop Strains in Human Knees. *J. Orthop. Res.* 30, 934–942. doi:10.1002/jor.22010

Seitz, A. M., Nelitz, M., Ignatius, A., and Dürselen, L. (2019). Release of the Medial Collateral Ligament Is Mandatory in Medial Open-Wedge High Tibial Osteotomy. *Knee Surg. Sports Traumatol. Arthrosc.* 27, 2917–2926. doi:10.1007/s00167-018-5167-0

Stein, S., Höse, S., Warnecke, D., Gentilini, C., Skaer, N., Walker, R., et al. (2019). Meniscal Replacement with a Silk Fibroin Scaffold Reduces Contact Stresses in the Human Knee. *J. Orthop. Res.* 37, 2583–2592. doi:10.1002/jor.24437

Steinbrück, A., Schröder, C., Woiczinski, M., Fottner, A., Pinskerova, V., Müller, P. E., et al. (2016). Femorotibial Kinematics and Load Patterns after Total Knee Arthroplasty: An *In Vitro* Comparison of Posterior-Stabilized versus Medial-Stabilized Design. *Clin. Biomech.* 33, 42–48. doi:10.1016/j.clinbiomech.2016.02.002

Stukenborg-Colsman, C., Ostermeier, S., Hurschler, C., and Wirth, C. J. (2002). Tibiofemoral Contact Stress after Total Knee Arthroplasty: Comparison of Fixed and mobile-bearing Inlay Designs. *Acta Orthopaedica Scand.* 73, 638–646. doi:10.1080/000164702321039598

Thomas, A. C., Hubbard-Turner, T., Wikstrom, E. A., and Palmieri-Smith, R. M. (2017). Epidemiology of Posttraumatic Osteoarthritis. *J. Athl Train.* 52, 491–496. doi:10.4085/1062-6050-51.5.08

van Egmond, N., Hannink, G., Janssen, D., Vrancken, A. C., Verdonschot, N., and Van Kampen, A. (2017). Relaxation of the MCL after an Open-Wedge High Tibial Osteotomy Results in Decreasing Contact Pressures of the Knee over Time. *Knee Surg. Sports Traumatol. Arthrosc.* 25, 800–807. doi:10.1007/s00167-017-4438-5

van Houtem, M., Clough, R., Khan, A., Harrison, M., and Blunn, G. W. (2006). Validation of the Soft Tissue Restraints in a Force-Controlled Knee Simulator. *Proc. Inst. Mech. Eng. H* 220, 449–456. doi:10.1243/09544119jeim57

Van Thiel, G. S., Frank, R. M., Gupta, A., Ghodadra, N., Shewman, E. F., Wang, V. M., et al. (2011). Biomechanical Evaluation of a High Tibial Osteotomy with a Meniscal Transplant. *J. Knee Surg.* 24, 45–53. doi:10.1055/s-0031-1275401

Verma, N. N., Kolb, E., Cole, B. J., Berkson, M. B., Garretson, R., Farr, J., et al. (2008). The Effects of Medial Meniscal Transplantation Techniques on Intra-articular Contact Pressures. *J. Knee Surg.* 21, 20–26. doi:10.1055/s-0030-1247787

Walker, P. S., Blunn, G. W., Perry, J. P., Bell, C. J., Sathasivam, S., Andriacchi, T. P., et al. (2000). Methodology for Long-Term Wear Testing of Total Knee Replacements. *Clin. Orthopaedics Relat. Res.* 372, 290–301. doi:10.1097/00003086-200003000-00032

Walker, P. S., and Erkiuan, M. J. (1975). The Role of the Menisci in Force Transmission across the Knee. *Clin. Orthopaedics Relat. Res.* 109, 184–192. doi:10.1097/00003086-197506000-00027

Wang, H., Chen, T., Gee, A. O., Hutchinson, I. D., Stoner, K., Warren, R. F., et al. (2015). Altered Regional Loading Patterns on Articular Cartilage Following Meniscectomy Are Not Fully Restored by Autograft Meniscal Transplantation. *Osteoarthritis and Cartilage* 23, 462–468. doi:10.1016/j.joca.2014.12.003

Wilder, F. V., Hall, B. J., Barrett, J. P., Jr., and Lemrow, N. B. (2002). History of Acute Knee Injury and Osteoarthritis of the Knee: a Prospective Epidemiological Assessment. *Osteoarthritis and Cartilage* 10, 611–616. doi:10.1053/joca.2002.0795

Willinger, L., Foehr, P., Achtnich, A., Forkel, P., Voss, A., Liska, F., et al. (2019). Effect of Lower Limb Alignment in Medial Meniscus-Deficient Knees on Tibiofemoral Contact Pressure. *Orthop. J. Sports Med.* 7, 2325967118824611. doi:10.1177/2325967118824611

Willinger, L., Lang, J. J., Berthold, D., Muench, L. N., Achtnich, A., Forkel, P., et al. (2020). Varus Alignment Aggravates Tibiofemoral Contact Pressure Rise after Sequential Medial Meniscus Resection. *Knee Surg. Sports Traumatol. Arthrosc.* 28, 1055–1063. doi:10.1007/s00167-019-05654-5

Yim, J.-H., Seon, J.-K., Song, E.-K., Choi, J.-I., Kim, M.-C., Lee, K.-B., et al. (2013). A Comparative Study of Meniscectomy and Nonoperative Treatment for Degenerative Horizontal Tears of the Medial Meniscus. *Am. J. Sports Med.* 41, 1565–1570. doi:10.1177/0363546513488518

Zavatsky, A. B. (1997). A Kinematic-freedom Analysis of a Flexed-Knee-Stance Testing Rig. *J. Biomech.* 30, 277–280. doi:10.1016/s0021-9290(96)00142-x

Zhang, A. L., Miller, S. L., Coughlin, D. G., Lotz, J. C., and Feeley, B. T. (2015). Tibiofemoral Contact Pressures in Radial Tears of the Meniscus Treated with All-Inside Repair, Inside-Out Repair and Partial Meniscectomy. *The Knee* 22, 400–404. doi:10.1016/j.knee.2015.05.008

Conflict of Interest: The authors declare that the research was conducted in the absence of any commercial or financial relationships that could be construed as a potential conflict of interest.

Publisher's Note: All claims expressed in this article are solely those of the authors and do not necessarily represent those of their affiliated organizations, or those of the publisher, the editors and the reviewers. Any product that may be evaluated in this article, or claim that may be made by its manufacturer, is not guaranteed or endorsed by the publisher.

frontiers in Bioengineering and Biotechnology

ORIGINAL RESEARCH
published: 10 December 2021
doi: 10.3389/fbioe.2021.779946

Meniscus Injury and its Surgical Treatment Does not Increase Initial Whole Knee Joint Friction

*Luisa de Roy[1†], Daniela Warnecke[1†], Steffen Paul Hacker[1], Ulrich Simon[2], Lutz Dürselen[1], Anita Ignatius[1] and Andreas Martin Seitz[1]**

[1]*Institute of Orthopedic Research and Biomechanics, Center for Trauma Research Ulm, Ulm University Medical Center, Ulm, Germany,* [2]*Scientific Computing Center Ulm (UZWR), Ulm University, Ulm, Germany*

OPEN ACCESS

Edited by:
Jin Nam,
University of California, Riverside, United States

Reviewed by:
Kristine Fischenich,
University of Colorado Anschutz Medical Campus, United States
Weifeng Lin,
Weizmann Institute of Science, Israel

***Correspondence:**
Andreas Martin Seitz
andreas.seitz@uni-ulm.de

[†]These authors have contributed equally to this work and share first authorship

Specialty section:
This article was submitted to Biomechanics, a section of the journal Frontiers in Bioengineering and Biotechnology

Received: *20 September 2021*
Accepted: *09 November 2021*
Published: *10 December 2021*

Citation:
de Roy L, Warnecke D, Hacker SP, Simon U, Dürselen L, Ignatius A and Seitz AM (2021) Meniscus Injury and its Surgical Treatment Does not Increase Initial Whole Knee Joint Friction. Front. Bioeng. Biotechnol. 9:779946. doi: 10.3389/fbioe.2021.779946

While it is generally accepted that traumatic meniscus pathologies lead to degenerative articular cartilage changes in the mid-to long-term and consecutively to post-traumatic osteoarthritis (PTOA), very little is known about how such injuries initiate tribological changes within the knee and their possible impact on PTOA acceleration. Therefore, the aim of this study was to investigate the influence of three different medial meniscus states (intact, posterior root tear, total meniscectomy) on the initial whole knee joint friction. Six ovine knee joints were tested in a passive pendulum friction testing device under an axial load of 250 N and an initial deflection of 12°, representing swing phase conditions, and under an axial load of 1000 N and an initial deflection of 5°, simulating stance phase conditions. To additionally consider the influence of the time-dependent viscoelastic nature of the knee joint soft tissues on whole joint friction, the tests were performed twice, directly following load application and after 20 min creep loading of either 250 N or 1000 N axial load. On the basis of a three-dimensional joint kinematic analysis, the energy loss during the passive joint motion was analyzed, which allowed considerations on frictional and damping processes within the joint. The so-called "whole knee joint" friction was evaluated using the boundary friction model from Stanton and a viscous friction model from Crisco et al., both analyzing the passive joint flexion-extension motion in the sagittal plane. Significantly lower friction coefficients were observed in the simulated swing phase after meniscectomy ($p < 0.05$) compared to the intact state. No initial whole joint friction differences between the three meniscus states ($p > 0.05$) were found under stance phase conditions. Soft tissue creeping significantly increased all the determined friction coefficients ($p < 0.05$) after resting under load for 20 min. The exponential decay function of the viscous friction model provided a better fit (R^2~0.99) to the decaying flexion-extension data than the linear decay function of the boundary friction model (R^2~0.60). In conclusion, this tribological *in vitro* study on ovine knee joints indicated that neither a simulated posterior medial meniscus root tear nor the removal of the medial meniscus resulted in an initially increased whole joint friction.

Keywords: meniscus, friction, pendulum, knee joint, meniscectomy, PTOA

INTRODUCTION

The menisci are two semi-lunar shaped fibrocartilages that are located between the tibia and femur inside the knee joint and play an essential role in sustaining knee joint health. Their wedge-shaped cross-section is of decisive importance for load transmission in the joint, because up to 50% of the compressive loads across the knee are transmitted via the lateral and medial menisci (Jones et al., 2006). They increase the contact area between the articulating surfaces of the femur and tibia, thus reducing the contact pressure on the articular cartilage (AC) while simultaneously serving as a passive joint stabilizer by compensating the incongruence of the curved articular surfaces. Further functions are shock absorption, proprioception and joint nutrition (Mow and Huiskes, 2005; Mcdermott and Amis, 2006). The menisci consist of a biphasic structure, defined by a fluid and a solid phase, leading to a time-dependent, viscoelastic material behavior (Mow et al., 1980; Mow and Huiskes, 2005). While the fluid phase mainly consists of water, the solid phase is comprised of an extracellular matrix with collagen and proteoglycans as major components (Mow and Huiskes, 2005). Joint motion is lubricated by the synovial fluid, which consists of hyaluronic acid, water, proteins, lipids and glucose (Bortel et al., 2015; Kosinska et al., 2015; Lin and Klein, 2021).

The menisci are rigidly anchored to the tibial plateau by ligamentous structures called meniscus root attachments, which evolve at the anterior and posterior horns of the menisci (Mcdermott and Amis, 2006; Masouros et al., 2008). Due to its firm connection to the medial collateral ligament, the medial meniscus is less mobile compared to the lateral meniscus (Jones et al., 2006). Meniscus aging and related degeneration, but also traumatic events, can cause meniscus injuries. Meniscus root injuries typically involve the posterior meniscal attachment, while the most impacted one is the posterior medial meniscus root (PMMR) (Jones et al., 2006; Petersen et al., 2014). On the one hand, for patients suffering from a severe traumatic meniscus injury, like a radial or complex tear, a meniscectomy can relieve symptoms for a short time (Pache et al., 2018). On the other hand, it is known, that such a total meniscectomy consequently leads to a decreased tibiofemoral contact area, which in turn results in an increased tibiofemoral pressure and altered knee kinematics (Allaire et al., 2008; Petersen et al., 2014; Pache et al., 2018). In particular, the increasing peak pressures result in a mechanical overloading of the AC, which in the long term causes premature degenerative knee joint changes. Therefore, it can be assumed, that both, a PMMR tear and meniscectomy precede and are thus clear risk factors for post traumatic osteoarthritis (PTOA) in the knee joint (Berthiaume et al., 2005; Jones et al., 2006; Marzo and Gurske-DePerio, 2008; Pache et al., 2018).

Clinically, because of fibrillation and softening of the articular joint surfaces and subsequent loss of cartilage tissue (Mccann et al., 2009), osteoarthritis (OA) is frequently referred to as joint wear. Technically, wear is defined as the abrasion of a material, caused by a relative movement of loaded surfaces, whereby the movement results in the generation of a frictional force (Neu et al., 2008). Transferring this technical definition to the clinical situation, it can be hypothesized that cartilage wear depends on the friction properties of the articulating surfaces in the knee joint. Numerous studies have investigated the friction properties of cartilage and meniscal tissue using different testing methods (Mccann et al., 2009; Akelman et al., 2013; Lakin et al., 2017; Warnecke et al., 2019). While pin-on-plate or pin-on-disc friction setups offer a simple method to analyze the *in vitro* tribological behavior of isolated tissue samples, pendulum testing devices are used to evaluate the tribology of whole synovial joints while maintaining joint conditions and interactions between tissues as seen during natural joint movements (Crisco et al., 2007; Drewniak et al., 2009; Elmorsy et al., 2014; Lakin et al., 2017). It was already stated that intraarticular ligaments and soft tissues have a significant effect on the viscous damping of a passive joint motion. For example, Bohinc et al. found in their study that the viscous damping of a human leg oscillation decreased the more tissue was resected (Bohinc et al., 2017). Therefore, joint friction does not only depend on the boundary friction between the tibia, femur and the meniscus surfaces, but also on the viscous damping of the surrounding soft tissues (Charnley, 1960; Akelman et al., 2013). The most applied setup for pendulum testing is the Stanton articular pendulum, in which the knee joint serves as the fulcrum of the pendulum during movement (Stanton, 1923). In this setup, one bone of the diarthrodial joint is attached to a physical pendulum, while the other is fixed (Stanton, 1923; Crisco et al., 2007). To initiate a passive joint motion, the pendulum is released from a defined starting deflection and the resulting decaying oscillation is tracked over time (Crisco et al., 2007; Drewniak et al., 2009; Elmorsy et al., 2014; Lakin et al., 2017). Energy loss by friction and viscous damping in the joint leads to a decay of the pendulum motion over time. In literature, this combination of frictional and viscous damping processes is referred to "whole joint friction" (Crisco et al., 2007). To evaluate whole joint friction, the decaying pendulum motion in the sagittal plane (flexion-extension joint movement) can be analyzed using the mathematical models of Stanton (Stanton, 1923) and Crisco et al. (Crisco et al., 2007). While the Stanton model accounts only for boundary friction, the exponential model of Crisco et al. also considers the viscous properties of the joint tissues.

Tribological studies proved that the menisci and AC in combination with the synovial fluid containing lubricative components play an essential role in sustaining low friction in synovial joints (Neu et al., 2008; Mccann et al., 2009; Majd et al., 2017; Warnecke et al., 2019). Moreover, it is well established that friction depends on the magnitude of the applied normal force and sliding velocity (Gleghorn and Bonassar, 2008; Warnecke et al., 2019). Consequently, the lubrication mechanisms between the articulating surfaces vary with changing loading conditions during walking (Neu et al., 2008; Murakami et al., 2017). The gait cycle is commonly divided into a stance and a swing phase. The stance phase accounts for approximately 60% of a single step and describes the period of gait in which the foot is in contact with the ground. Here, the tibiofemoral contact forces can reach up to 2–3 times body weight (BW) (ISO 14243-1:2009 (E), 2009; Bonnefoy-Mazure and Armand, 2015). During the swing phase, considerably lower loads are transmitted through the

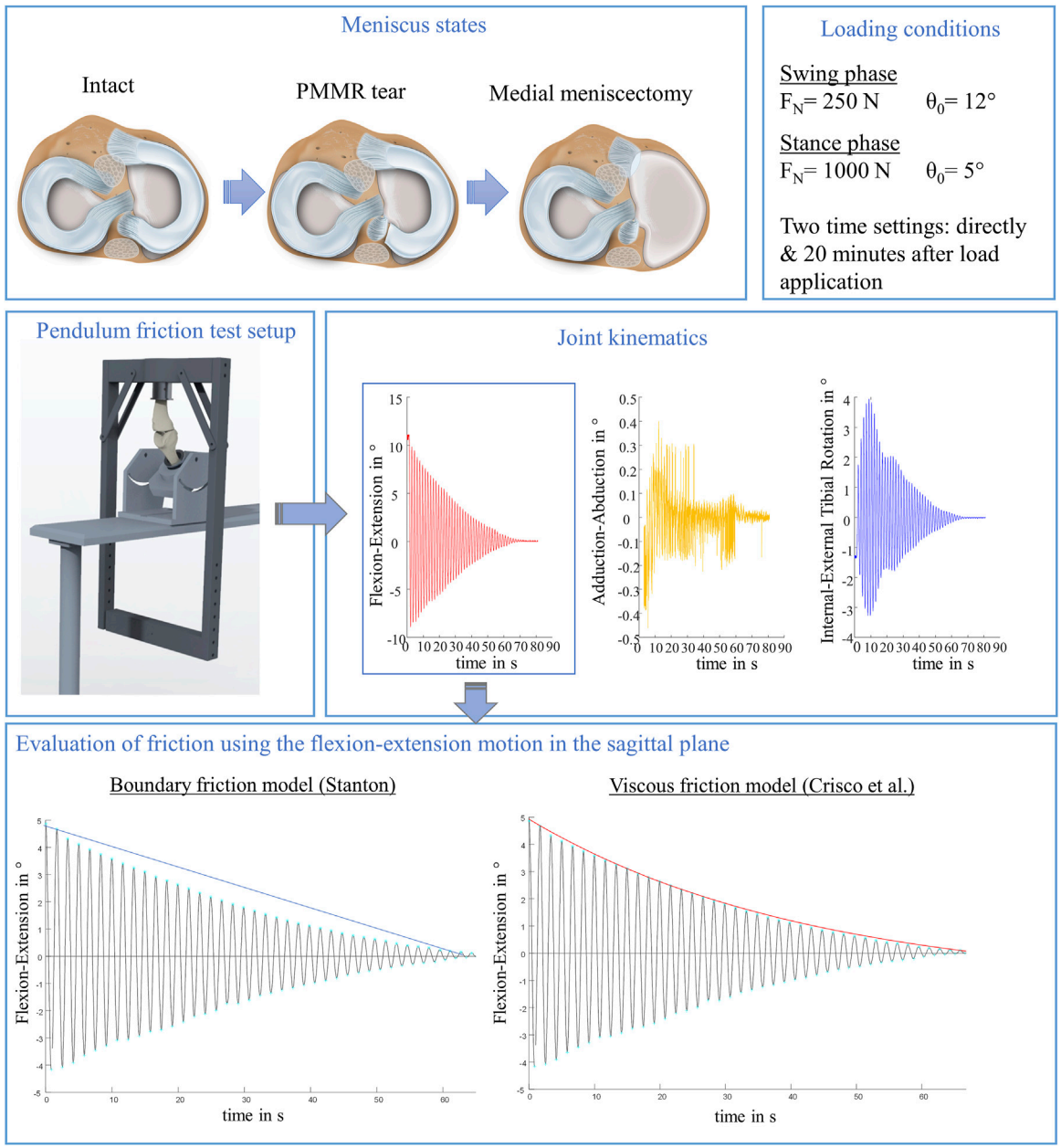

FIGURE 1 | Schematic overview of the study design. In total, three meniscus states were tested to examine the influence of the menisci on initial whole knee joint friction: intact, with posterior medial meniscus root tear (PMMR tear) and after medial meniscectomy. Each meniscus state was tested under simulated swing and stance phase conditions derived from an ovine gait cycle (Taylor et al., 2006; Taylor et al., 2011), each under two time settings: directly following loading the joints and after 20 min resting under the axial load using a passive pendulum friction testing device. Joint kinematics were recorded using a motion capturing system. The flexion-extension motion in the sagittal plane was used to calculate whole joint friction by applying a boundary friction model (Stanton, 1923) and a viscous friction model (Crisco et al., 2007).

knee joint because the foot has no contact with the ground (ISO 14243-1:2009 (E), 2009; Bonnefoy-Mazure and Armand, 2015). While the knee flexion angle varies between 0° and 15° during the stance phase, it rises up to 60° during the swing phase (ISO 14243-1:2009 (E), 2009; Bonnefoy-Mazure and Armand, 2015).

Because friction properties depend on the loading conditions, it is likely that knee joint friction changes both during the two phases of gait and if the load distribution on the joint surfaces is affected (Neu et al., 2008; Murakami et al., 2017). In this context, very limited research has been performed to examine the contribution of the menisci and meniscus injuries to the whole knee joint friction. McCann et al. studied the influence of a meniscectomy on friction in the medial compartment of bovine knee joints in an active pendulum friction device. The removal of

the meniscus resulted in greater contact pressure and higher friction coefficients compared to tests with an intact meniscus. Nevertheless, this study neither considered surrounding soft tissues nor the whole joint geometry (Mccann et al., 2009). It remains unknown how different meniscus states influence the energy dissipation (by friction and damping) when considering the whole knee joint geometry and the damping effect of surrounding knee joint soft tissues. Consequently, the question arises, whether deterioration of the meniscus immediately affects whole joint friction while maintaining more representative *in vivo* joint conditions or not. Based on the findings of McCann et al. and the development of PTOA after the loss of meniscus function, we hypothesized that a PMMR tear and subsequent medial total meniscectomy result in increased whole joint friction. Therefore, the aim of this study was to investigate the influence of the menisci on the initial whole knee joint friction using a passive pendulum test setup.

MATERIALS AND METHODS

Study Design

Ovine knee joints were tested in a passive pendulum friction test setup for large species, which allows for axial load application in a physiological range derived from the stance and swing phases of an ovine gait cycle (**Figure 1**). To investigate the influence of different medial meniscus states on joint friction, each knee joint was tested in three states: intact, after simulation of a PMMR tear and after total medial meniscectomy (MM). Kinematic measurements were performed by tracking two customized rigid body coordinate systems which were bicortically anchored at the tibia and femur and oriented according to Grood and Suntay (Grood and Suntay, 1983) using a motion capturing system (Optitrack, NaturalPoint, Corvallis, Oregon, United States). Flexion-extension motion in the sagittal plane was used to calculate whole knee joint friction using a boundary friction model (Stanton, 1923) and a viscous friction model (Crisco et al., 2007). To consider soft tissue creeping on knee joint friction, the tests were performed with two different time settings: first, directly after load application and second, after resting under a constant load of either 250 N or 1000 N for 20 min.

Sample Preparation

Six left ovine knee joints were obtained commercially from a local shepherd. Before testing, the skin was removed as well as the muscle tissue at the distal end of the tibia and the proximal end of the femur. The patellar ligament at the tibia, the collateral ligaments and fatty tissue surrounding the patella and the joint capsule were kept intact to maintain sufficient joint stability. The patella was not additionally stabilized by a dead weight. Two bone screws were drilled laterally into the femur and tibia to allow a rigid fixation of the coordinate systems with reflective markers for the kinematic measurements. The coordinate systems were aligned along the anatomic axes according to Grood and Suntay (Grood and Suntay, 1983). The distal end of the tibia and the proximal end of the femur were embedded in custom-made bone cylinders using polymethyl methacrylate (Technovit 3,040, Kulzer GmbH, Wehrheim, Germany) to allow for fixation of the joint in the pendulum setup. The knee joints were tested with three consecutive medial meniscus states: 1) intact, 2) PMMR tear and 3) MM. After testing the intact knee and after testing the PMMR tear, the joint was removed from the test setup to perform the subsequent meniscus intervention. The position of the femur in the mounting block and the position of the tibia in the pendulum arm was labelled before the first test run to enable a consistent joint orientation across all three test runs. Prior to opening the joint capsule at the medial tibia plateau using a scalpel, the synovial fluid was collected with a syringe to prevent a substantial loss of the lubricant during the meniscus preparation. The PMMR tear was simulated by transecting the posterior anchoring ligament using a scalpel. An additional incision at the anterior region allowed the detachment of the anterior root attachment. Other meniscotibial soft tissue connections were also detached, finally enabling a removal of the entire medial meniscus. Following PMMR tear and MM, the joint capsule was surgically sutured and the previously obtained synovial fluid was reinjected into the joint cavity. During the preparation and testing, the joints were kept moist with isotonic saline solution.

Testing Routine

The axial loads as well as the knee flexion angles were adopted to simulate conditions occurring during normal gait in sheep (Taylor et al., 2006; Taylor et al., 2011). All three meniscus states were tested under two loading conditions: First under an axial load of F_N = 250 N (25% BW) and an initial deflection angle of θ_0 = 12°, representing the swing phase conditions, and second under F_N = 1000 N (100% BW) and an initial deflection angle of θ_0 = 5° to simulate the higher loaded stance phase conditions. To account for the viscoelastic nature of the knee joint tissues, the influence of soft tissue creeping on joint friction (Forster and Fisher, 1996; Kazemi et al., 2011) was evaluated by testing each meniscus state and loading condition first directly after applying the respective load of 250 N or 1000 N (T_0) and secondly after resting under the respective axial load for 20 min (T_{20}) (**Figure 2**). In total, each knee underwent 12 test runs, resulting in a total testing time of approximately 160 min.

Pendulum Friction Test Setup

The initial whole joint friction was investigated using a custom-made passive pendulum friction testing device for large species (**Figure 3A**). The pendulum's center of rotation was described by the rotation axis of the knee joint in the sagittal plane, while the tibia was allowed to freely oscillate relative to the femur. To provide a physiological load transmission in the joint, the knee was mounted in approximately 140° flexion in the pendulum setup (α), representing the resting knee joint angle in sheep (Taylor et al., 2006; Diogo et al., 2020) (**Figure 3B**). The femur was firmly fixed upside-down in an inclined mounting block, which was assembled on a base plate. Subsequently, the pendulum arm was attached on the tibia. Physiological knee joint loading was achieved by the dead weight of the pendulum itself (250 N) for the simulation of the swing phase condition and by placing additional weights of 750 N (= 1000 N in total) on the lower pendulum beam to simulate the higher loaded stance phase

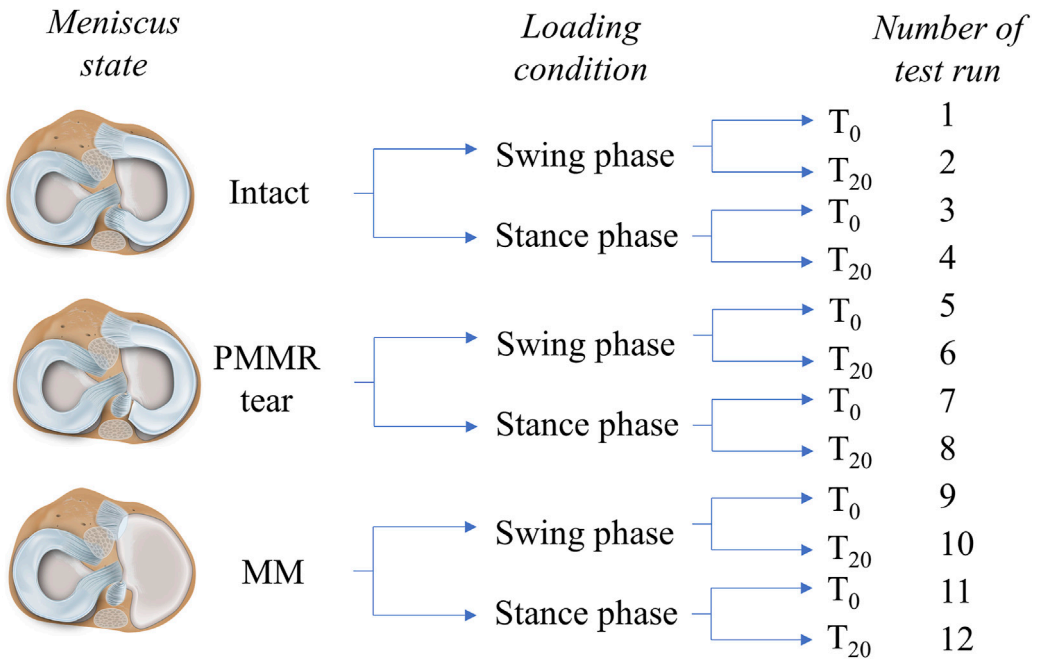

FIGURE 2 | Schematic overview of the testing routine. Three meniscus states were investigated in this study: intact, with a posterior medial meniscus root tear (PMMR tear) and after medial meniscectomy (MM). Two different loading conditions derived from an ovine gait cycle were applied to the joints: swing phase conditions (250 N axial loading and 12° initial deflection) and stance phase conditions (1000 N axial loading and 5° initial deflection) (Taylor et al., 2006; Taylor et al., 2011). Each meniscus state was first tested under swing phase conditions followed by tests under stance phase conditions. Both conditions were tested first directly after load application (T_0) and second after 20 min resting under the axial loading (T_{20}). In total, each knee underwent 12 test runs.

condition. The initial deflection angle (θ_0) was adjusted by deflecting the pendulum arm at the flexion-extension axis using a digital goniometer (DL134, Toolcraft, Conrad Electronic SE, Hirschau, Germany). To initiate a passive joint motion, the pendulum was released from this initial deflection. The oscillation frequency of the pendulum was approximately 1 Hz, which corresponds to the ovine normal gait frequency (Taylor et al., 2006).

Joint kinematics were recorded by tracking the movement of the tibial and femoral coordinate systems using a motion-capturing system (Optitrack, NaturalPoint). To ensure that all markers were continuously captured during the tests, nine cameras (Prime 13, NaturalPoint; mean error after calibration less than 0.3 mm, image acquisition rate: 240 fps) were semi-circularly positioned around the pendulum setup.

Data Analysis

A customized MATLAB script (MATLAB R2020a, The MathWorks Inc., Natick, United States) was used for data processing and analysis. The kinematic measurements were used to compute the joint rotation angles in flexion-extension, external-internal tibial rotation and adduction-abduction as defined by Grood and Suntay (Grood and Suntay, 1983). The energy loss resulting from friction and damping processes in the knee joint was evaluated with the boundary friction model (Stanton, 1923) and the viscous friction model (Crisco et al., 2007), both analyzing the decay of the flexion-extension motion in the sagittal plane. The equation of the boundary friction model (Equation 1) assumes that the damping of the pendulum movement is caused by surface friction. The decay of the flexion-extension in the sagittal plane is described by a linear function and the boundary friction coefficient (μ_{lin}) can be determined by the slope (Stanton, 1923) (**Figure 4A**):

$$\mu_{lin} = \frac{\Delta\theta L}{4r} \tag{1}$$

with $\Delta\theta$ = mean angular change in flexion-extension, r = radius of the femoral condyle, L = distance between the pendulum center of mass and the rotation axis (Stanton, 1923), which is located in the center of the femoral condyles. The boundary friction coefficient (μ_{lin}) was calculated by a linear fit of the decaying flexion-extension values (**Figure 4A**). The viscous friction model (Equation 2) (Crisco et al., 2007) additionally considers the viscoelastic response of biphasic materials by introducing a viscous damping coefficient (c), as well as a friction component (μ) in an exponential decay function (**Figure 4B**). The peak amplitude as a function over time is given by:

$$\theta_t = \theta_0 * \left[e^{-2\zeta t/T} - \frac{\mu mgrT^2}{4\pi^2 I\theta_0} * \frac{1 + e^{-\zeta}}{1 - e^{-\zeta}} * \left(1 - e^{-2\zeta t/T}\right) \right] \tag{2}$$

with,

$$\zeta = \frac{\frac{cT}{4L}}{\sqrt{1 - \left(\frac{cT}{4\pi L}\right)^2}}$$

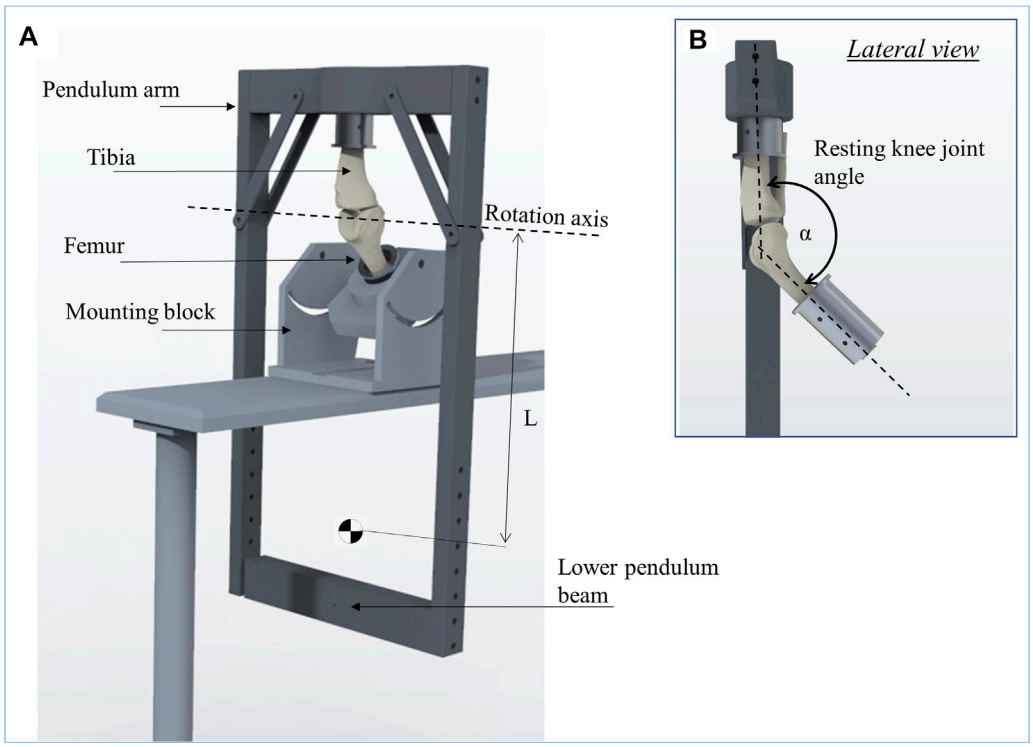

FIGURE 3 | Schematic representation of the passive pendulum friction testing device that was used **(A)**. The femur is fixed in an inclined mounting block and the pendulum arm is attached to the tibia, whereby the resting knee joint angle between the tibia and femur (α) was set to 140° to achieve a physiological joint loading **(B)**. The rotation axis of the pendulum motion is described by the rotation axis of the knee joint in flexion-extension. The length of the pendulum (L) is the distance from its center of mass to the rotation axis.

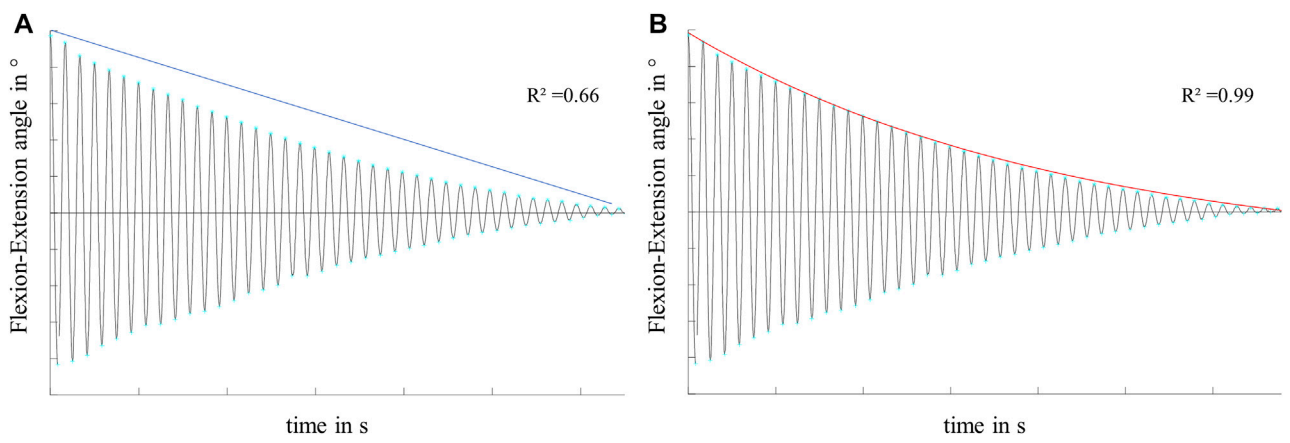

FIGURE 4 | Exemplary flexion-extension data in the sagittal plane of a knee joint motion, characterized by a non-linear decay over time. Illustration and exemplary values for the goodness of fit (R^2) of **(A)** the linear decay function of the boundary friction model (Stanton, 1923) and **(B)** the exponential decay function of the viscous friction model (Crisco et al., 2007) on the decaying motion.

and θ_0 = starting deflection, T = periodic time, I = moment of inertia about the joint rotation axis and m = mass of the pendulum (Crisco et al., 2007). Using standard MATLAB routines, the viscous damping coefficient (c) and the viscous friction coefficient (μ) can be determined by nonlinear curve-fitting of the exponential decay function by means of a least-square fitting method. R-Squared (R^2) values were determined to evaluate the goodness of fit of both models to the recorded flexion-extension data.

The radius of a medial ovine femoral condyle (r) was determined using a set of isotropic computer tomography scans, resulting in r = 15 mm. The distance between the pendulum center of mass and the rotation axis (L) was measured for each individual

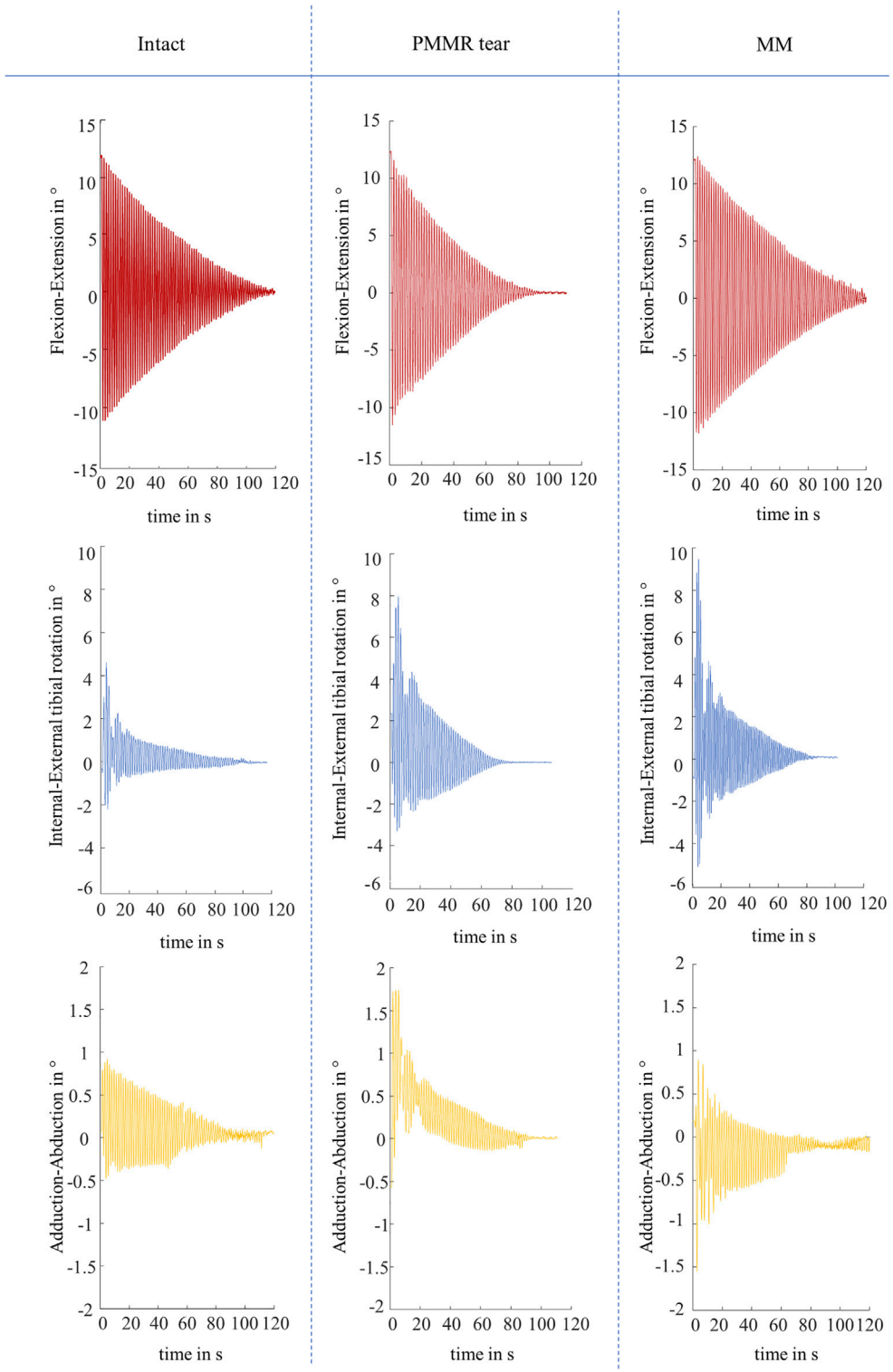

FIGURE 5 | Representative kinematic plots of one knee in flexion-extension in ° (red), internal-external tibial rotation in ° (blue) and adduction-abduction in ° (yellow) according to Grood and Suntay (Grood and Suntay, 1983) under swing phase conditions for the three meniscus states of intact, after simulation of a posterior medial meniscus root tear (PMMR tear) and after medial meniscectomy (MM).

TABLE 1 | Goodness of fit of the viscous (Crisco et al., 2007) and boundary (Stanton, 1923) friction model to the recorded flexion-extension data under swing and stance phase loading conditions and the meniscus states intact, after simulation of a posterior medial meniscus root tear (PMMR tear) and after medial meniscectomy (MM), represented by R-squared values (n = 6, mean ± standard deviation).

	Intact		PMMR tear		MM	
	Swing phase	Stance phase	Swing phase	Stance phase	Swing phase	Stance phase
Viscous friction model Crisco et al. (2007)	0.997 ± 0.002	0.990 ± 0.013	0.996 ± 0.003	0.990 ± 0.007	0.995 ± 0.002	0.940 ± 0.093
Boundary friction model Stanton (1923)	0.661 ± 0.103	0.642 ± 0.137	0.573 ± 0.125	0.571 ± 0.249	0.655 ± 0.107	0.517 ± 0.122

joint when mounted in the pendulum setup. Subsequently, the individual moment of inertia (I) was calculated using a CAD-analysis tool (PTC Creo Parametric 3.0 M030, Parametric Technology GmbH, Unterschleissheim, Germany).

To evaluate the energy loss in the joint regardless of any mathematical model or the shape of the decay, the total oscillation time of the pendulum motion represented by the damping time (t_D) was determined.

Statistics

Normal distribution was checked for the damping time (t_D), the friction coefficients (μ_{lin} and μ) and the damping coefficient (c) using a Shapiro-Wilk test, resulting in non-normally distributed data. The tests performed immediately after load application were referred to as T_0 tests, while those after 20 min under the axial loading were referred to as T_{20} tests. Differences in the damping time (t_D), μ_{lin}, μ and c between the three meniscus states (intact vs PMMR tear, PMMR tear vs MM, intact vs MM) were calculated using Friedman testing. This was performed for the simulated swing and stance phase conditions and for both, the T_0 and T_{20} tests. The influence of soft tissue creeping on knee joint friction was statistically analyzed by comparing the damping time (t_D), the friction coefficients (μ_{lin} and μ) and the viscous damping coefficient (c) of the T_0 tests with the respective parameters of the T_{20} tests using Wilcoxon testing. The statistical significance level was set to $p < 0.05$. All statistical analyses were performed using GraphPad Prism 7.03 software (GraphPad Software Inc., San Diego, United States).

RESULTS

Kinematics

Both, the boundary friction model (Stanton, 1923) and the viscous friction model (Crisco et al., 2007) were applied to the joint flexion-extension motion in the sagittal plane, which displayed a non-linear decay in all experiments (**Figure 5**). The internal-external tibial rotation and adduction-abduction were recorded to visualize the influence of the PMMR tear and MM on the passive joint kinematics. Under swing phase conditions, the recorded kinematics showed an increase in the internal-external tibial rotation angle and the adduction-abduction angle after the PMMR tear and after the MM (**Figure 5**). In the internal-external tibial rotation and adduction-abduction, the maximum rotation angle increased up to 100% from the intact to the MM state.

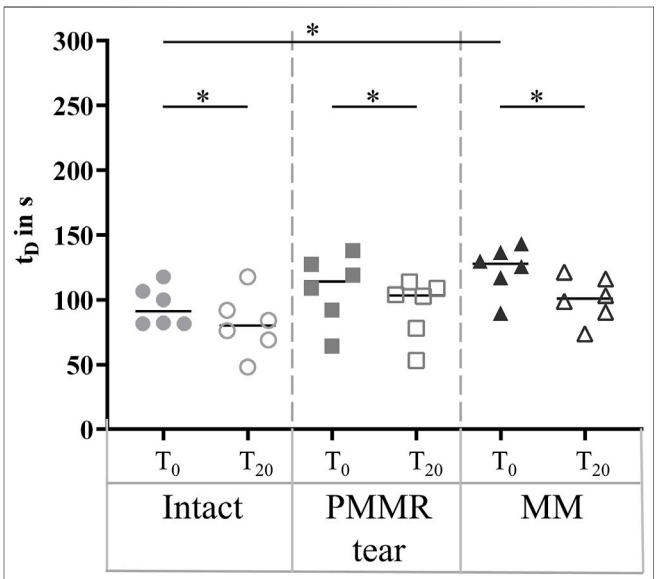

FIGURE 6 | Scatter plots (median with individual values) of the damping time (t_D) of the pendulum motion under swing phase conditions with the intact meniscus state (symbol shape: circles), with a posterior medial meniscus root tear (PMMR tear) (symbol shape: squares) and after medial meniscectomy (MM) (symbol shape: rectangles). The tests were performed directly after loading the joints with 250 N (T_0, filled symbols) and after resting under the axial load for 20 min (T_{20}, unfilled symbols). Non-parametric statistical analyses: n = 6; *$p < 0.05$.

The viscous friction model provided a better fit for the decaying flexion-extension data than the boundary friction model in all meniscus states and under both, the swing and stance phase loading conditions. The mean R^2 values ranged between 0.994 and 0.997 for the viscous friction model but only between 0.517 and 0.661 for the boundary friction model. A summary of the mean R^2 values is given in **Table 1**.

Swing Phase Conditions

In the T_0 tests, the damping time (t_D) increased from the intact to the MM state. Comparing the intact and the MM state a significantly longer damping time was found in the MM state (+39%; $p = 0.02$) (**Figure 6**). No differences were found in the damping time of the T_{20} tests. In both, the T_0 and T_{20} tests, the boundary friction coefficient (μ_{lin}) was by tendency lower in the simulated PMMR tear state compared to the intact state

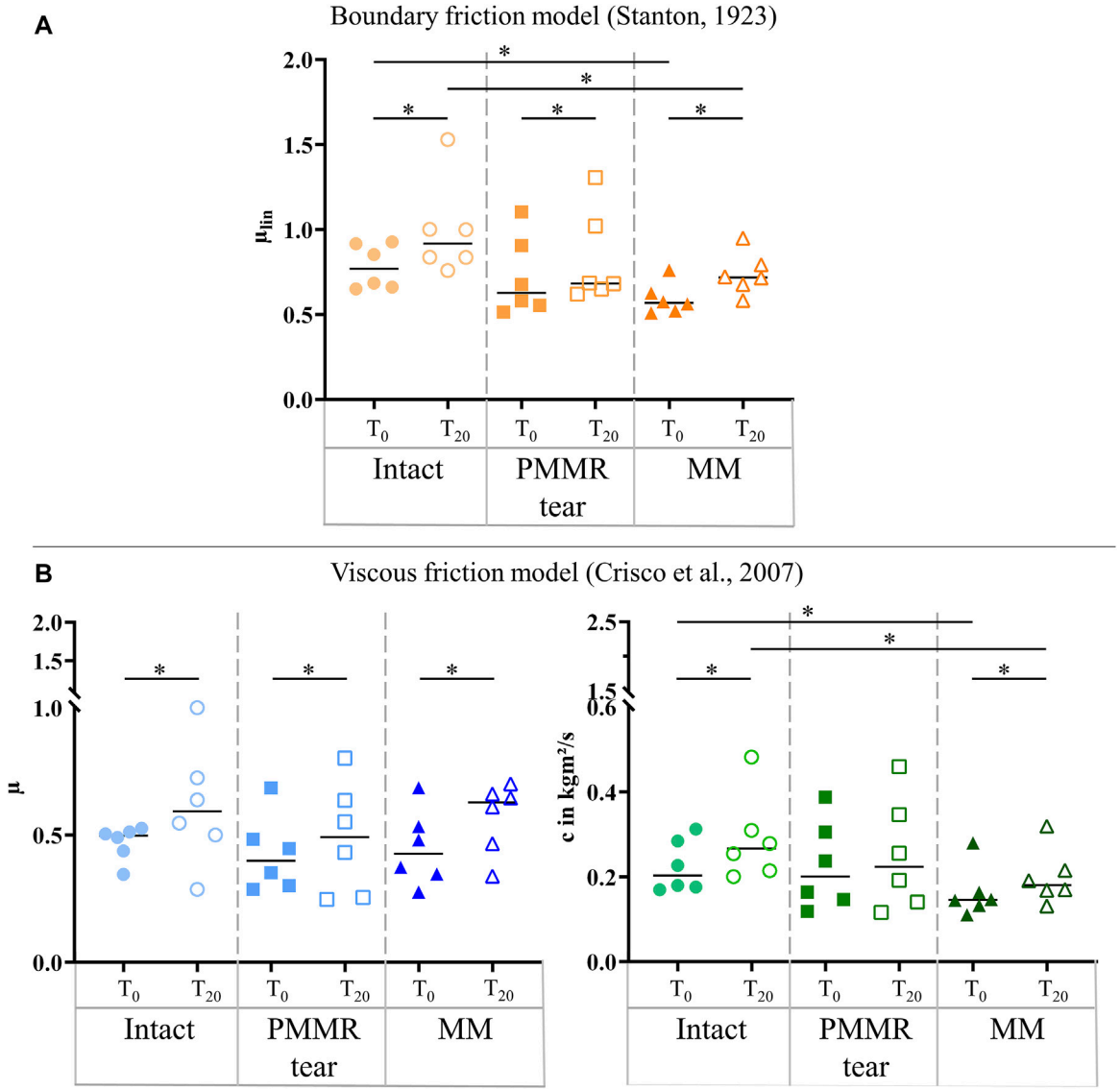

FIGURE 7 | (A) Scatter plots (median with individual values) of the boundary friction coefficient (μ_{lin}, symbol color: orange) under swing phase conditions. **(B)** Scatter plots (median with individual values) of the viscous friction coefficient (μ, symbol color: blue) and the viscous damping coefficient (c, symbol color: green) in kgm^2/s under swing phase conditions. Each joint was tested in three consecutive meniscus states: intact (symbol shape: circles), with a posterior medial meniscus root tear (PMMR tear) (symbol shape: squares) and medial meniscectomy (MM) (symbol shape: rectangles). The tests were performed directly after loading the joints with 250 N (T_0, filled symbols) and after resting under the axial load for 20 min (T_{20}, unfilled symbols). Non-parametric statistical analyses: n = 6; *$p < 0.05$.

(**Figure 7A**). μ_{lin} significantly decreased after meniscectomy when comparing to the intact state in the T_0 tests (−26%, Friedman test: $p = 0.03$) and the T_{20} tests (−22%, Friedman test: $p = 0.03$). No statistical differences were found for μ_{lin} when comparing the PMMR tear state and the MM state. In all three meniscus states, the boundary friction coefficient (μ_{lin}) was statistically higher in the T_{20} tests compared to the T_0 tests (Wilcoxon test: $p < 0.05$). Analyzing the decay of the flexion-extension motion in the sagittal plane with the viscous friction model (Crisco et al., 2007) (**Figure 7B**), no statistical differences between the three meniscus states were found for the viscous friction coefficient (μ), neither in the T_0 nor the T_{20} tests. The viscous friction coefficient (μ) was statistically higher in the T_{20} tests compared to the T_0 tests (Wilcoxon test: $p < 0.05$) in all three meniscus states. When comparing the viscous damping coefficient (c) of the intact state with the PMMR tear state, no differences were found. c did not indicate differences between the PMMR tear state and the MM state. Friedman testing revealed significantly lower values for the viscous damping coefficient (c) in the MM state compared to the intact state in the T_0 (−28%; $p = 0.03$) and T_{20} (−32%; $p = 0.01$) tests. When comparing the viscous damping coefficient (c) of the T_{20} tests with those of the T_0 tests, c was significantly higher in the T_{20} tests on the intact and MM states (Wilcoxon test: $p < 0.05$), but not in the PMMR tear state.

Comparing the boundary friction coefficient (μ_{lin}) with the viscous friction coefficient (μ), μ_{lin} indicated in general higher median values. In all meniscus states, a significant decrease was found when comparing the damping time (t_D) of the T_0 tests with that of the T_{20} tests (Wilcoxon test: $p < 0.05$) (**Figure 6**).

Stance Phase Conditions

The damping time (t_D) slightly increased from the intact to the MM state in the T_0 tests. No tendency was found when analyzing the damping time of the T_{20} test (**Figure 8**). For both, the T_0 and T_{20} tests, no statistical differences were observed for the boundary friction coefficient (μ_{lin}) when comparing all meniscus states (**Figure 9A**). The boundary friction coefficient (μ_{lin}) was significantly higher in the T_{20} tests compared to the T_0 tests (Wilcoxon test: $p < 0.05$) in all the meniscus states. Regarding the viscous friction coefficient (μ), neither the PMMR tear nor the MM resulted in statistical differences when comparing to the intact state, in both the T_0 and the T_{20} tests. When comparing the viscous friction coefficient (μ) of the T_0 and T_{20} tests, μ was significantly higher in the T_{20} tests, except in the PMMR tear state (**Figure 9B**). The viscous damping coefficient (c) tended to increase from the intact to the PMMR tear state, and also from the PMMR tear state to the MM state, but not significantly. This was found in the T_0 and the T_{20} tests (**Figure 8B**). In all meniscus states, c was statistically higher in the T_{20} tests compared to the T_0 tests (Wilcoxon test: $p < 0.05$). The damping time (t_D) of the T_{20} tests was significantly shorter compared to that of the T_0 tests in all meniscus states (Wilcoxon test: $p < 0.05$) (**Figure 8**).

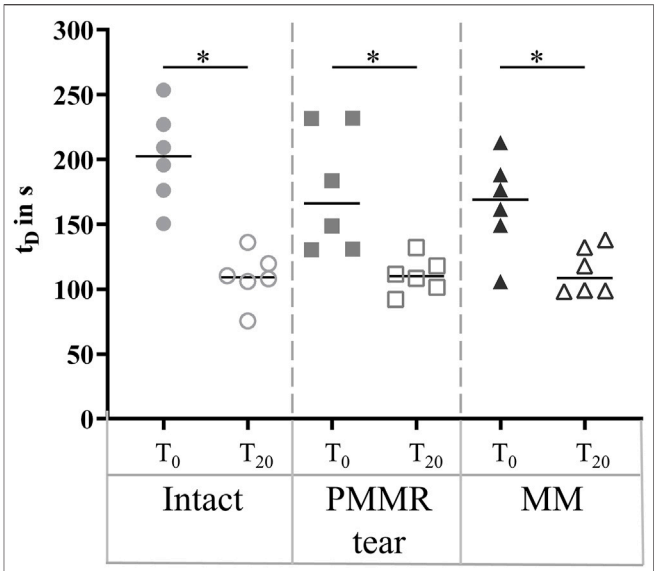

FIGURE 8 | Scatter plots (median with individual values) of the damping time (t_D) in seconds of the pendulum motion under stance phase conditions with the intact meniscus state (symbol shape: circles), with a posterior medial meniscus root tear (PMMR tear) (symbol shape: squares) and after medial meniscectomy (MM) (symbol shape: rectangles). The tests were performed directly after loading the joints with 1000 N (T_0, filled symbols) and after resting under the axial load for 20 min (T_{20}, unfilled symbols). Non-parametric statistical analyses: n = 6; *$p < 0.05$.

DISCUSSION

The aim of this study was to investigate the influence of a PMMR tear and a consecutive MM on the energy loss during passive motion of ovine knee joints using a passive pendulum friction test setup. The analysis of the energy loss over time enables considerations on friction and damping processes in the joint, which both contribute to a decay of the pendulum motion over time. A boundary friction model (Stanton, 1923) and a viscous friction model (Crisco et al., 2007) were applied to calculate the so called "whole joint friction" by analyzing the joint flexion-extension motion in the sagittal plane. Further, the damping time of the pendulum motion as a measure of energy loss in the knee was evaluated. Neither a simulated PMMR tear nor the MM resulted in a significantly decreased damping time or increased joint friction parameters, disproving our hypothesis.

Interestingly, the damping time (t_D) significantly increased from the intact to the MM state under swing phase conditions, indicating a decrease in energy dissipation processes through friction and damping. Analyzing relative differences of the determined coefficients, the boundary friction coefficient (μ_{lin}) was significantly reduced from the intact to the MM state under swing phase conditions. This was also found for the viscous damping coefficient (c). Our kinematic measurements indicated that in the intact state, the joint motion occurred predominantly in the sagittal plane. Following the PMMR tear and the MM, increased internal-external tibial rotation during the pendulum motion was confirmed under swing phase conditions. Allaire et al. showed that the meniscal state effects the tibial rotation as a function of the flexion angle in an *in vitro* biomechanical study (Allaire et al., 2008). They demonstrated that tibial rotation increases after PMMR tear and after MM in human cadaveric knee joints. Regarding our tests with the PMMR tear and MM, we assume that the increased motion content in the transversal and frontal planes affected the estimation of whole joint friction based on the analysis of the decaying flexion-extension motion in the sagittal plane. Because joint motion no longer occurred mainly in the sagittal plane, this may result in a reduced amount of damping and friction forces in this plane of motion. However, friction in the transversal and frontal planes were not considered (Stanton, 1923; Crisco et al., 2007). Furthermore, after removing the medial meniscus only the surfaces of the AC were in contact during motion, which could contribute to the significant decrease in the friction coefficients (μ_{lin}) when comparing the intact and the MM state. Therefore, a reduced contact area and the changed kinematic may explain the reduced whole joint friction under swing phase conditions. A model capable of analyzing the three-dimensional movement would be more appropriate for determining whole joint friction in the knee.

Though not statistically significant, the PMMR tear and the subsequent MM resulted in a decreased damping time. Hence, the

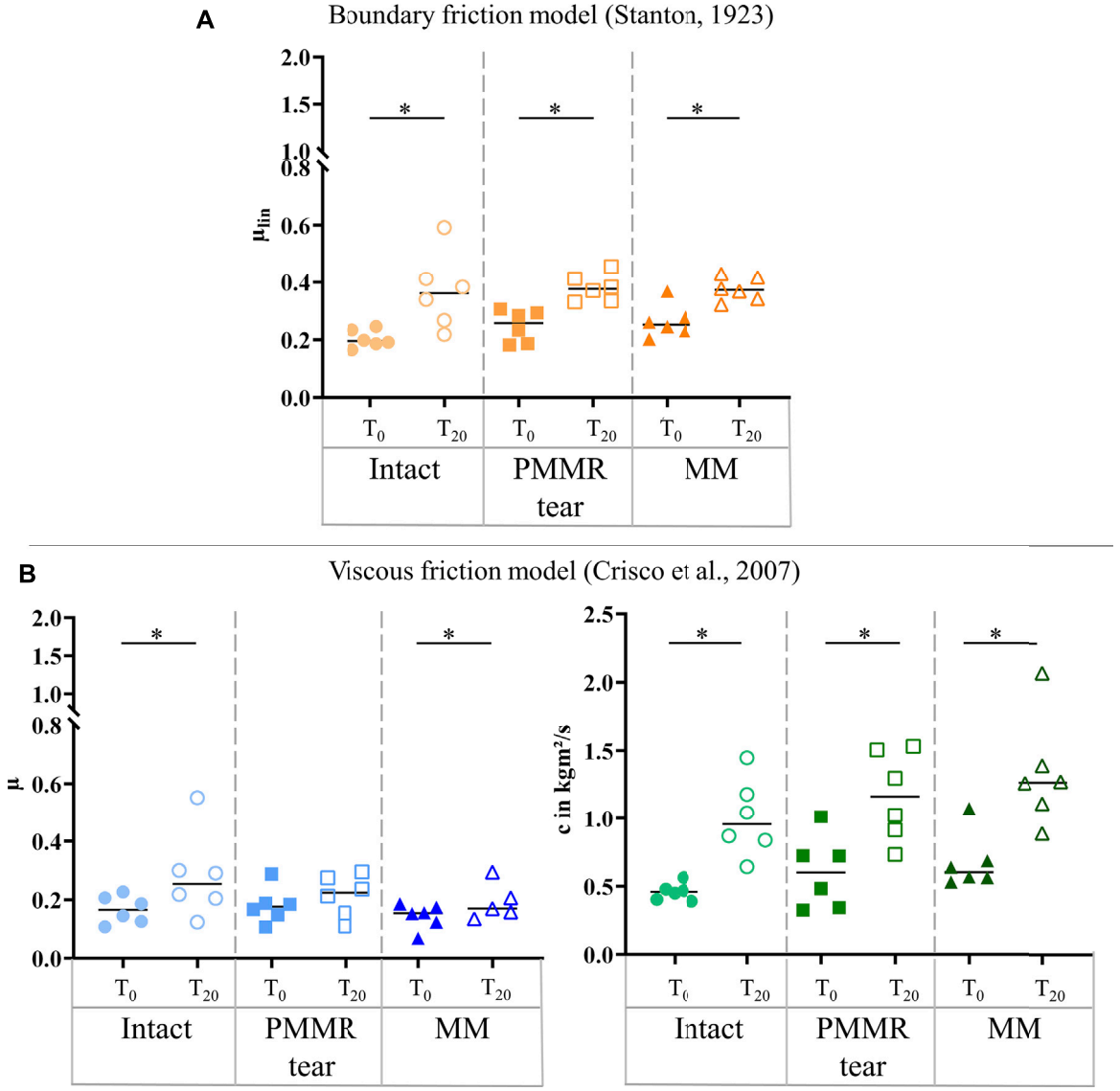

FIGURE 9 | (A) Scatter plots (median with individual values) of the boundary friction coefficient (μ_{lin}, symbol color: orange) under stance phase conditions. **(B)** Scatter plots (median with individual values) of the viscous friction coefficient (μ, symbol color: blue) and the viscous damping coefficient (c, symbol color: green) in kgm^2/s under stance phase conditions. Each joint was tested in three consecutive meniscus states: intact (symbol shape: circles), with a posterior medial meniscus root tear (PMMR tear) (symbol shape: squares) and medial meniscectomy (MM) (symbol shape: rectangles). The tests were performed directly after loading the joints with 1000 N (T_0, filled symbols) and after resting under the axial load for 20 min (T_{20}, unfilled symbols). Non-parametric statistical analyses: n = 6; *$p < 0.05$.

energy loss in the joint was slightly faster, which may indicate an increased friction and viscous damping. The mathematical models revealed by tendency an increased whole joint friction under stance phase conditions. In the PMMR tear and MM states the boundary friction coefficient (μ_{lin}) as well as the friction parameters of the viscous friction model (μ and c) were slightly higher compared to the intact state. We attribute this to the biphasic nature of AC. Krishan et al. proved the relationship between the friction coefficient of AC and the change in interstitial fluid load support (Krishnan et al., 2004). Under load, the interstitial fluid of cartilage tissue is pressurized and the joint forces are supported by both, the solid and fluid phases of this biphasic material. The interstitial fluid pressurization of AC is known to maintain low friction between cartilage surfaces (Krishnan et al., 2004; Caligaris and Ateshian, 2008; Ateshian, 2009). Over time, the fluid exudes out of the cartilage tissue and its volume reduces. As the fluid pressure within the tissue subsides, the contact force shifts to the tissue's solid matrix, which enhances boundary friction between the articulating surfaces. Consequently, higher friction coefficients are determined (Krishnan et al., 2004; Caligaris and Ateshian, 2008). In the context of the interstitial fluid load support also the magnitude of pressure on the AC seem to be relevant (Mccann et al., 2009). While the meniscus remains intact, the

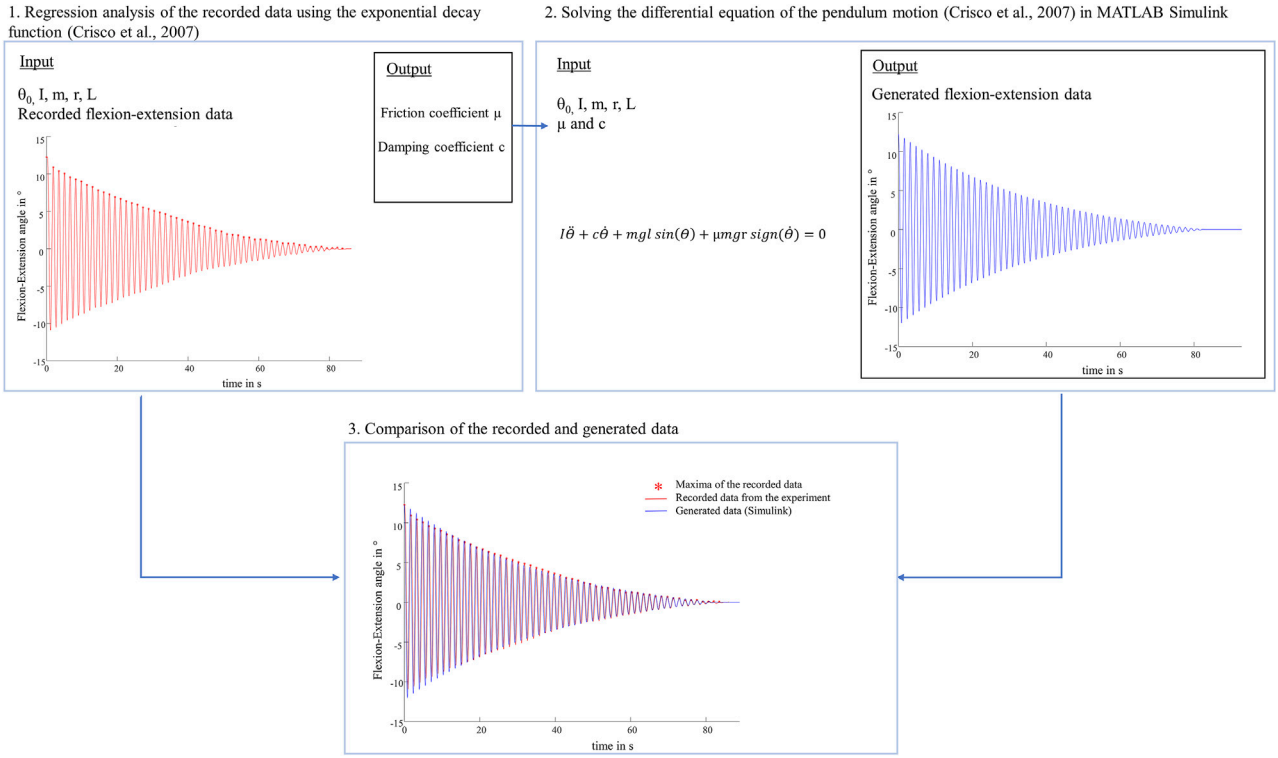

FIGURE 10 | Schematic representation of the performed identification procedure. 1. The viscous damping coefficient (c) and the viscous friction coefficient (μ) were determined by nonlinear curve-fitting of the exponential decay function (Crisco et al., 2007) as described in the materials and methods section. 2. Following, the differential equation of the physical pendulum motion (Crisco et al., 2007) was solved with the same input values (initial deflection (θ_0), moment of inertia (I), pendulum mass (m), radius of the femoral condyle (r), distance between the pendulum center of mass and the rotation axis (L)) and the determined values for the friction coefficient (μ) and damping coefficient (c) using MATLAB Simulink. 3. The comparison of the recorded flexion-extension motion (red) and the generated oscillation (blue) indicated very similar oscillation data over time.

contact pressure on the articulating surfaces is distributed evenly over a large contact area. A PMMR tear induces meniscal extrusion, which causes the tibial plateau to have more contact with the underlying cartilage of the femoral condyle (Berthiaume et al., 2005; Allaire et al., 2008). Unambiguous direct cartilage-cartilage contact between the convex medial tibial plateau and the convex medial femoral condyle occurs after MM (Mcdermott and Amis, 2006). In both cases, a reduced contact area leads to increasing peak contact forces on the adjacent cartilage (Berthiaume et al., 2005; Jones et al., 2006; Allaire et al., 2008). We expect that this was also the case in our experiments. Applying an axial load of 1000 N and reducing the tibiofemoral contact area by a PMMR tear and a MM probably caused severe local contact stresses on the AC. This in turn may resulted in an accelerated depletion of the interstitial fluid load support, which can explain the increasing tendency of the boundary friction coefficients (μ_{lin}) from the intact to the MM meniscus state under stance phase conditions. McCann et al. investigated the influence of a meniscectomy on the medial compartment in the bovine knee using an active pendulum testing device (Mccann et al., 2009). They also attributed the observed increase in friction after a MM to higher contact stresses on the AC causing a faster depletion of the interstitial fluid. The viscous damping coefficient (c) increased from the intact to the MM state under stance phase conditions, which can also be explained by the depletion of the interstitial fluid load support, because the viscoelastic properties of cartilage and meniscus are related to their biphasic structure (Mow and Huiskes, 2005). In summary, we attribute the increasing tendencies of the boundary friction coefficient (μ_{lin}) as well as the viscous damping coefficient (c) and friction coefficient (μ) to altered contact conditions after the PMMR tear and MM which in combination with the high axial loading of 1000 N may led to rapid deterioration of the friction reducing effect of the interstitial fluid pressurization. Moreover, the kinematics changed barely because the PMMR tear and the MM caused only slightly increased tibial rotation.

To our knowledge, we were the first to study knee joints of a large species under much higher loads and investigate different meniscus states using a passive pendulum setup. Literature values of whole knee joint friction coefficients of previous pendulum studies are in the range between 0.04 and 0.20 (Kawano et al., 2003; Drewniak et al., 2009; Teeple et al., 2011; Elmorsy et al., 2014). Compared with the results of the intact joints found in these studies, the friction coefficients of the present study were higher and seem to be overestimated (Kawano et al., 2003; Crisco et al., 2007; Teeple et al., 2011; Akelman et al., 2013). To verify the plausibility of the present friction coefficients, an identification procedure was performed (**Figure 10**). We solved the differential

equation of the pendulum motion (Crisco et al., 2007) with our input values (I, m, L, r, θ_0) and our results for the friction coefficient (μ) and damping coefficient (c) using MATLAB Simulink (Simulink R2020a, The MathWorks Inc., Natick, United States). Following, the generated oscillation and the recorded flexion-extension motion from the experiment were compared, indicating very similar oscillation data over time. From a tribological point of view, there is a distinct difference between cartilage to cartilage friction and whole joint friction. In passive pendulum setups, whole joint friction is determined by analysing the decay of the passive motion. This decay is caused by energy dissipation processes, induced by a combination of both, friction between AC and meniscus surfaces and damping forces created by the viscoelastic knee joint tissues. Thus, based on the here used method and the according results we can conclude that whole knee joint friction seems to be a black-box model. Although there are mathematical models quantifying whole joint friction coefficients, they are not able to distinguish between the different energy dissipation processes. As stated by Crisco et al., their "*lumped parameter model is not able to identify which tissues [. . .] are responsible for frictional damping and which are responsible for viscous damping, or even if they are separate tissues*" (Crisco et al., 2007). Their model further assumes that the joint moves without resistance from soft tissue constraints (Crisco et al., 2007) which is obviously not the case in physiological conditions. On the other hand, keeping ligaments and surrounding tissue intact, it can be assumed that they contribute significantly to the decay of the passive motion. Therefore, we hypothesize that in our study, the viscoelastic tissues significantly contributed to the energy loss, which may overlap the contribution of friction. However, we only manipulated the medial meniscus, which resulted in changes of energy dissipation processes in the knee as indicated by the damping time and also the determined whole knee joint friction coefficients. The absolute amount of viscoelastic tissues surrounding the ovine knee joints in the present study was relatively higher compared to previous studies testing mouse or guinea pig knee joints, where the soft tissues were more extensively resected (Drewniak et al., 2009; Elmorsy et al., 2014). Therefore, we expect that joint stiffness was not negligible in our tests, which may additionally contributed to the high values of the present study. In conclusion, friction pendulum setups should be used to determine relative differences between different knee joint states rather than to quantify whole joint friction coefficients. Quantitative comparisons of results determined in previous friction pendulum studies using smaller species and different axial loads are not suitable because of the mass dependency of the boundary and viscous friction coefficients found by Akelman et al. (Akelman et al., 2013). A mass dependency was also apparent in our study, because whole joint friction was higher under swing phase conditions than under stance phase conditions. This was already observed in several tribological studies of cartilage and meniscus tissue (Majd et al., 2017; Warnecke et al., 2019). Warnecke et al. investigated the tribological behavior of isolated tissue samples in a pin-on-plate test setup. They found higher friction coefficients in a test scenario adapted to swing phase conditions compared to stance phase conditions (Warnecke et al., 2019). Regarding pendulum test setups, Akelman et al. investigated how pendulum mass affects the measurement of whole joint friction in guinea pigs using the mathematical evaluations of Stanton and Crisco et al. (Akelman et al., 2013). To investigate the mass dependency on the initial joint friction in the present study, the experiments with an axial load of 250 N were additionally performed with the initial deflection of $\theta_0 = 5°$. When analyzing the intact state, a significant decrease of 61% in the boundary friction coefficient (μ_{lin}) and approximately 52% in the viscous friction coefficient (μ) were observed when the pendulum mass was increased from 250 to 1000 N (**Supplementary Material Figure 1**). These decreases are comparable to the findings of Akelman et al., where both, the boundary (μ_{lin}) and viscous (μ) friction coefficients declined proportionally as the mass increased (Akelman et al., 2013). In our study, the mass dependency was not only present in the friction coefficients (μ_{lin} and μ), but was also evident in the damping coefficients (c), which were highest under stance phase conditions. This was to be expected, because (c) reflects the velocity-dependent energy loss of the pendulum motion (Crisco et al., 2007; Akelman et al., 2013).

Friction in synovial joints is very complex. Wright and Dowson stated that in daily activities the lubrication performance of human joints is achieved by a combination of lubrication modes, which depend on loading conditions (Wright and Dowson, 1976). Furthermore, changing loading conditions during a gait cycle is believed to cause various lubrication mechanisms in the knee joint, including boundary, hydrodynamic, boosted and weeping lubrications (Neu et al., 2008; Murakami et al., 2017). Tribological studies using whole joint pendulum setups consider interactions between all joint structures, for example, cartilage, meniscus, synovial fluid, tendons and the joint capsule (Crisco et al., 2007). A pendulum study of Charnley et al. indicated that intraarticular ligaments and the synovial fluid contributed to viscous damping in a human cadaver ankle joint (Charnley, 1960). Viscous damping is associated with fluid film and hydrodynamic lubrication, which is indicated by a non-linear energy loss of a passive synovial joint motion (Crisco et al., 2007). In this context, the viscous friction model (Crisco et al., 2007) is more suitable to fit the non-linear decay of pendulum motion than the boundary friction model (Stanton, 1923), as was also observed in the present study. The goodness of fit of the viscous friction model revealed R^2 values of approximately 0.99, whereas the boundary friction model revealed lower values of approximately 0.60 (**Table 1**). This was also described by other authors (Crisco et al., 2007; Drewniak et al., 2009).

Moreover, the complex tribology in the knee joint itself (Neu et al., 2008) makes it challenging to determine specific lubrication mechanisms between the articulating surfaces during the pendulum motion. This limits more detailed considerations of the extent to which the meniscus state affects the boundary friction coefficient (μ_{lin}) or the viscous friction (μ) and the viscous damping coefficient (c). Another limitation is that a passive pendulum friction device cannot simulate active muscle forces or provide stabilization of the patella, which has an influence on the joint kinematics (Bull and Amis, 1998; Bohinc et al., 2017). When evaluating joint friction

based on kinematic data, this limits the comparability to the *in vivo* knee joint friction. The ovine model is considered a suitable experimental model for studying various conditions and treatments in OA research because their knee joint anatomy is very similar to that of humans (Nesbitt et al., 2014; Mccoy, 2015). However, in the present friction study, ovine knee joints without signs of PTOA were tested. It was not possible to perform long-term friction analysis, because the maximum damping time of the passive pendulum motion was approximately 100 s under the swing phase conditions and 200 s under the stance phase conditions. Therefore, this study only refers to changes in whole joint friction directly after a PMMR tear in knees without existing degeneration. Furthermore, the MM was also simulated directly after testing the PMMR tear, thus no long-term effects of the PMMR tear on cartilage degeneration were considered. However, insights into initial changes in whole joint friction after these pathologies may contribute to a better understanding of the onset of PTOA.

We demonstrated that constantly loading the joints 20 min prior to testing decreased the damping time of joint motion in all meniscus states, under stance and swing phase conditions, indicating increased energy dissipation processes. The influence of the time-dependent behavior of the knee joint soft tissues was particularly evident under 1000 N axial loading. Here, no tendency from the intact to the MM state was observed for the boundary friction coefficient (μ_{lin}) in the T_{20} tests. The higher boundary friction coefficients (μ_{lin}) and higher viscous friction (μ) and damping coefficients (c) in the T_{20} tests can again be explained by the depletion of the interstitial fluid pressurization (Krishnan et al., 2004; Ateshian, 2009). In daily activities, soft tissue creeping occurs during stationary standing (Murakami et al., 2017). When slowly moving after a long-resting period, boundary friction between the AC surfaces predominantly occurs. The surface asperity contact interactions can increase friction because of more solid-to-solid contact (Neu et al., 2008; Mccann et al., 2009). Our results indicated that this time-dependent viscoelastic behavior not only increases energy loss in the intact knee but even worsens the consequences of a PMMR tear and MM with regards to premature degeneration.

The results of our *in vitro* tribological investigation indicated that the simulation of a PMMR tear and a consecutive MM did not increase the energy dissipation processes in ovine knee joints, which implies that the initial friction and damping properties were not affected. McCann et al. investigated the influence of a meniscectomy on friction on the medial bovine compartment by using an active pendulum friction device. In contrast to our findings, the meniscectomized compartments revealed higher friction coefficients compared to intact specimens (Mccann et al., 2009). With our pendulum setup it was possible to investigate how the medial meniscus state affects the energy dissipation in the joint when considering the whole knee joint geometry and the damping effect of surrounding knee joint soft tissues. Because deterioration of the meniscus state did not result in significantly faster energy loss by friction and viscous damping, this might indicate that the knee joint is able to compensate a (partial) loss of function of the meniscus directly post injury or surgically treatment. However, it is known that a PMMR tear and a MM leads to a reduced tibio-femoral contact area and to a chronic overloading of the medial AC. This overloading can cause local fibrillation, which in turn has been shown to increase tissue-level friction (Mccann et al., 2009) and subsequently might affect whole joint friction.

Clinically, OA is frequently characterized by increased AC surface roughness and cartilage tissue loss. Neu et al. investigated the friction properties of human femoral cartilage samples with advanced OA (Neu et al., 2010). They found increased friction coefficients when comparing to non-degenerated samples. However, the tribology of degenerated human knee joints is not well understood and requires further research. *In vitro* friction studies on healthy and degenerated human specimens on the joint scale (whole joint friction) and the tissue scale (friction between isolated tissue samples) will provide comprehensive information on how joint friction is affected in the presence of naturally occurring OA. Assuming that fibrillation of the cartilage in PTOA in the knee is primarily caused by increased friction between the articulating surfaces in the joint, early treatment of a meniscus injury and restoration of the meniscus function may minimize progressive wear, even when no changes are initially apparent.

DATA AVAILABILITY STATEMENT

The raw data supporting the conclusions of this article will be made available by the authors, without undue reservation.

ETHICS STATEMENT

Ethical review and approval was not required for the animal study because the tested ovine knee joints were obtained commercially from a local shepherd.

AUTHOR CONTRIBUTIONS

LdR and DW drafted the manuscript and contributed to the study conception and design and performed the friction testing, data analysis and statistics. LD and DW conceived the idea of the study. SPH and US helped in the data analysis. AI and LD participated in the coordination of the study. AMS supported the drafting of the manuscript. All authors participated in the revision process of the article and gave final approval of the submitted version.

ACKNOWLEDGMENTS

We would like to thank Patrizia Horny from the Institute of Orthopedic Research and Biomechanics Ulm for her art design support.

SUPPLEMENTARY MATERIAL

The Supplementary Material for this article can be found online at: https://www.frontiersin.org/articles/10.3389/fbioe.2021.779946/full#supplementary-material

REFERENCES

Akelman, M. R., Teeple, E., Machan, J. T., Crisco, J. J., Jay, G. D., and Fleming, B. C. (2013). Pendulum Mass Affects the Measurement of Articular Friction Coefficient. *J. Biomech.* 46, 615–618. doi:10.1016/j.jbiomech.2012.09.034

Allaire, R., Muriuki, M., Gilbertson, L., and Harner, C. D. (2008). Biomechanical Consequences of a Tear of the Posterior Root of the Medial Meniscus. *The J. Bone Jt. Surgery Am.* 90, 1922–1931. doi:10.2106/jbjs.g.00748

Ateshian, G. A. (2009). The Role of Interstitial Fluid Pressurization in Articular Cartilage Lubrication. *J. Biomech.* 42, 1163–1176. doi:10.1016/j.jbiomech.2009.04.040

Berthiaume, M.-J., Raynauld, J. P., Martel-Pelletier, J., Labonté, F., Beaudoin, G., Bloch, D. A., et al. (2005). Meniscal Tear and Extrusion Are Strongly Associated with Progression of Symptomatic Knee Osteoarthritis as Assessed by Quantitative Magnetic Resonance Imaging. *Ann. Rheum. Dis.* 64, 556–563. doi:10.1136/ard.2004.023796

Bohinc, K., Vantur, N., Torkar, D., Lampe, T., Hribernik, M., and Jakovljević, M. (2017). Knee Stiffness and Viscosity: New Implementation and Perspectives in Prosthesis Development. *Bosn J. Basic Med. Sci.* 17, 164–171. doi:10.17305/bjbms.2017.1765

Bonnefoy-Mazure, A., and Armand, S. (2015). "Normal Gait," in *Orthopedic Management of Children With Cerebral Palsy: A Comprehensive Approach* (Hauppauge, NY: Nova Science Publishers Inc), 567. Available at: https://archive-ouverte.unige.ch/unige:81179.

Bortel, E., Charbonnier, B., and Heuberger, R. (2015). Development of a Synthetic Synovial Fluid for Tribological Testing. *Lubricants* 3, 664–686. doi:10.3390/lubricants3040664

Bull, A. M. J., and Amis, A. A. (1998). Knee Joint Motion: Description and Measurement. *Proc. Inst. Mech. Eng. H* 212, 357–372. doi:10.1243/0954411981534132

Caligaris, M., and Ateshian, G. A. (2008). Effects of Sustained Interstitial Fluid Pressurization under Migrating Contact Area, and Boundary Lubrication by Synovial Fluid, on Cartilage Friction. *Osteoarthr. Cartil.* 16, 1220–1227. doi:10.1016/j.joca.2008.02.020

Charnley, J. (1960). The Lubrication of Animal Joints in Relation to Surgical Reconstruction by Arthroplasty. *Ann. Rheum. Dis.* 19, 10–19. doi:10.1136/ard.19.1.10

Crisco, J. J., Blume, J., Teeple, E., Fleming, B. C., and Jay, G. D. (2007). Assuming Exponential Decay by Incorporating Viscous Damping Improves the Prediction of the Coeffcient of Friction in Pendulum Tests of Whole Articular Joints. *Proc. Inst. Mech. Eng. H* 221, 325–333. doi:10.1243/09544119jeim248

Diogo, C., Fonseca, B., Almeida, F., Costa, L., Pereira, J., Filipe, V., et al. (2020). *A Comparison of Two-Dimensional and Three-Dimensional Techniques for Determining the Kinematic Patterns for Hindlimb Obstacle Clearance during Sheep Locomotion*.

Drewniak, E. I., Jay, G. D., Fleming, B. C., and Crisco, J. J. (2009). Comparison of Two Methods for Calculating the Frictional Properties of Articular Cartilage Using a Simple Pendulum and Intact Mouse Knee Joints. *J. Biomech.* 42, 1996–1999. doi:10.1016/j.jbiomech.2009.05.024

Elmorsy, S., Funakoshi, T., Sasazawa, F., Todoh, M., Tadano, S., and Iwasaki, N. (2014). Chondroprotective Effects of High-Molecular-Weight Cross-Linked Hyaluronic Acid in a Rabbit Knee Osteoarthritis Model. *Osteoarthr. Cartil.* 22, 121–127. doi:10.1016/j.joca.2013.10.005

Forster, H., and Fisher, J. (1996). The Influence of Loading Time and Lubricant on the Friction of Articular Cartilage. *Proc. Inst. Mech. Eng. H* 210, 109–119. doi:10.1243/pime_proc_1996_210_399_02

Gleghorn, J. P., and Bonassar, L. J. (2008). Lubrication Mode Analysis of Articular Cartilage Using Stribeck Surfaces. *J. Biomech.* 41, 1910–1918. doi:10.1016/j.jbiomech.2008.03.043

Grood, E. S., and Suntay, W. J. (1983). A Joint Coordinate System for the Clinical Description of Three-Dimensional Motions: Application to the Knee. *J. Biomech. Eng.* 105, 136–144. doi:10.1115/1.3138397

ISO 14243-1:2009 (E) (2009). *Implants for Surgery–Wear of Total Knee Joint Prostheses– Part 1: Loading and Displacement Parameters for Wear-Testing Machines with Load Control and Corresponding Environmental Conditions for Test*. Switzerland.

Jones, A., Houang, M., Low, R., and Wood, D. (2006). Medial Meniscus Posterior Root Attachment Injury and Degeneration: MRI Findings. *Australas. Radiol.* 50, 306–313. doi:10.1111/j.1440-1673.2006.01586.x

Kawano, T., Miura, H., Mawatari, T., Moro-Oka, T., Nakanishi, Y., Higaki, H., et al. (2003). Mechanical Effects of the Intraarticular Administration of High Molecular Weight Hyaluronic Acid Plus Phospholipid on Synovial Joint Lubrication and Prevention of Articular Cartilage Degeneration in Experimental Osteoarthritis. *Arthritis Rheum.* 48, 1923–1929. doi:10.1002/art.11172

Kazemi, M., Li, L. P., Savard, P., and Buschmann, M. D. (2011). Creep Behavior of the Intact and Meniscectomy Knee Joints. *J. Mech. Behav. Biomed. Mater.* 4, 1351–1358. doi:10.1016/j.jmbbm.2011.05.004

Kosinska, M. K., Ludwig, T. E., Liebisch, G., Zhang, R., Siebert, H.-C., Wilhelm, J., et al. (2015). Articular Joint Lubricants during Osteoarthritis and Rheumatoid Arthritis Display Altered Levels and Molecular Species. *Plos One* 10, e0125192. doi:10.1371/journal.pone.0125192

Krishnan, R., Kopacz, M., and Ateshian, G. A. (2004). Experimental Verification of the Role of Interstitial Fluid Pressurization in Cartilage Lubrication. *J. Orthop. Res.* 22, 565–570. doi:10.1016/j.orthres.2003.07.002

Lakin, B. A., Snyder, B. D., and Grinstaff, M. W. (2017). Assessing Cartilage Biomechanical Properties: Techniques for Evaluating the Functional Performance of Cartilage in Health and Disease. *Annu. Rev. Biomed. Eng.* 19, 27–55. doi:10.1146/annurev-bioeng-071516-044525

Lin, W., and Klein, J. (2021). Recent Progress in Cartilage Lubrication. *Adv. Mater.* 33, 2005513. doi:10.1002/adma.202005513

Majd, S. E., Rizqy, A. I., Kaper, H. J., Schmidt, T. A., Kuijer, R., and Sharma, P. K. (2017). An *In Vitro* Study of Cartilage-Meniscus Tribology to Understand the Changes Caused by a Meniscus Implant. *Colloids Surf. B: Biointerfaces* 155, 294–303. doi:10.1016/j.colsurfb.2017.04.034

Marzo, J. M., and Gurske-Deperio, J. (2008). Effects of Medial Meniscus Posterior Horn Avulsion and Repair on Tibiofemoral Contact Area and Peak Contact Pressure with Clinical Implications. *Am. J. Sports Med.* 37, 124–129. doi:10.1177/0363546508323254

Masouros, S. D., Mcdermott, I. D., Amis, A. A., and Bull, A. M. J. (2008). Biomechanics of the Meniscus-Meniscal Ligament Construct of the Knee. *Knee Surg. Sports Traumatol. Arthr.* 16, 1121–1132. doi:10.1007/s00167-008-0616-9

Mccann, L., Ingham, E., Jin, Z., and Fisher, J. (2009). Influence of the Meniscus on Friction and Degradation of Cartilage in the Natural Knee Joint. *Osteoarthr. Cartil.* 17, 995–1000. doi:10.1016/j.joca.2009.02.012

Mccoy, A. M. (2015). Animal Models of Osteoarthritis. *Vet. Pathol.* 52, 803–818. doi:10.1177/0300985815588611

Mcdermott, I. D., and Amis, A. A. (2006). The Consequences of Meniscectomy. *J. Bone Jt. Surg. Br.* 88-B, 1549–1556. doi:10.1302/0301-620x.88b12.18140

Mow, V. C., and Huiskes, R. (2005). "Structure and Function of Articular Cartilage and Meniscus," in *Basic Orthopaedic Biomechanics & Mechano-Biology*. Editors V. C. Mow and R. Huiskes. Third Edition ed (Philadelphia: Lippincott Williams & Wilkins), 182–257.

Mow, V. C., Kuei, S. C., Lai, W. M., and Armstrong, C. G. (1980). Biphasic Creep and Stress Relaxation of Articular Cartilage in Compression: Theory and Experiments. *J. Biomech. Eng.* 102, 73–84. doi:10.1115/1.3138202

Murakami, T., Yarimitsu, S., Sakai, N., Nakashima, K., Yamaguchi, T., and Sawae, Y. (2017). Importance of Adaptive Multimode Lubrication Mechanism in Natural Synovial Joints. *Tribology Int.* 113, 306–315. doi:10.1016/j.triboint.2016.12.052

Nesbitt, R. J., Herfat, S. T., Boguszewski, D. V., Engel, A. J., Galloway, M. T., and Shearn, J. T. (2014). Primary and Secondary Restraints of Human and Ovine Knees for Simulated *In Vivo* Gait Kinematics. *J. Biomech.* 47, 2022–2027. doi:10.1016/j.jbiomech.2013.11.029

Neu, C. P., Komvopoulos, K., and Reddi, A. H. (2008). The Interface of Functional Biotribology and Regenerative Medicine in Synovial Joints. *Tissue Eng. B: Rev.* 14, 235–247. doi:10.1089/ten.teb.2008.0047

Neu, C. P., Reddi, A. H., Komvopoulos, K., Schmid, T. M., and Di Cesare, P. E. (2010). Increased Friction Coefficient and Superficial Zone Protein Expression in Patients with Advanced Osteoarthritis. *Arthritis Rheum.* 62, 2680–2687. doi:10.1002/art.27577

Pache, S., Aman, Z. S., Kennedy, M., Nakama, G. Y., Moatshe, G., Ziegler, C., et al. (2018). Meniscal Root Tears: Current Concepts Review. *Arch. Bone Jt. Surg.* 6, 250–259.

Petersen, W., Forkel, P., Feucht, M. J., Zantop, T., Imhoff, A. B., and Brucker, P. U. (2014). Posterior Root Tear of the Medial and Lateral Meniscus. *Arch. Orthop. Trauma Surg.* 134, 237–255. doi:10.1007/s00402-013-1873-8

Stanton, T. (1923). *Boundary Lubrication in Engineering Practice. The Engineer*.

Taylor, W. R., Ehrig, R. M., Heller, M. O., Schell, H., Seebeck, P., and Duda, G. N. (2006). Tibio-femoral Joint Contact Forces in Sheep. *J. Biomech.* 39, 791–798. doi:10.1016/j.jbiomech.2005.02.006

Taylor, W. R., Poepplau, B. M., König, C., Ehrig, R. M., Zachow, S., Duda, G. N., et al. (2011). The Medial-Lateral Force Distribution in the Ovine Stifle Joint during Walking. *J. Orthop. Res.* 29, 567–571. doi:10.1002/jor.21254

Teeple, E., Elsaid, K. A., Jay, G. D., Zhang, L., Badger, G. J., Akelman, M., et al. (2011). Effects of Supplemental Intra-articular Lubricin and Hyaluronic Acid on the Progression of Posttraumatic Arthritis in the Anterior Cruciate Ligament-Deficient Rat Knee. *Am. J. Sports Med.* 39, 164–172. doi:10.1177/0363546510378088

Warnecke, D., Messemer, M., De Roy, L., Stein, S., Gentilini, C., Walker, R., et al. (2019). Articular Cartilage and Meniscus Reveal Higher Friction in Swing Phase Than in Stance Phase under Dynamic Gait Conditions. *Sci. Rep.* 9, 5785. doi:10.1038/s41598-019-42254-2

Wright, V., and Dowson, D. (1976). Lubrication and Cartilage. *J. Anat.* 121, 107–118.

Conflict of Interest: The authors declare that the research was conducted in the absence of any commercial or financial relationships that could be construed as a potential conflict of interest.

frontiers in Bioengineering and Biotechnology

REVIEW
published: 22 December 2021
doi: 10.3389/fbioe.2021.787330

Post-Traumatic Osteoarthritis Assessment in Emerging and Advanced Pre-Clinical Meniscus Repair Strategies: A Review

*Jay Trivedi, Daniel Betensky, Salomi Desai and Chathuraka T. Jayasuriya**

Department of Orthopaedics, Alpert Medical School of Brown University/Rhode Island Hospital, Providence, RI, United States

Surgical repair of meniscus injury is intended to help alleviate pain, prevent further exacerbation of the injury, restore normal knee function, and inhibit the accelerated development of post-traumatic osteoarthritis (PTOA). Meniscus injuries that are treated poorly or left untreated are reported to significantly increase the risk of PTOA in patients. Current surgical approaches for the treatment of meniscus injuries do not eliminate the risk of accelerated PTOA development. Through recent efforts by scientists to develop innovative and more effective meniscus repair strategies, the use of biologics, allografts, and scaffolds have come into the forefront in pre-clinical investigations. However, gauging the extent to which these (and other) approaches inhibit the development of PTOA in the knee joint is often overlooked, yet an important consideration for determining the overall efficacy of potential treatments. In this review, we catalog recent advancements in pre-clinical therapies for meniscus injuries and discuss the assessment methodologies that are used for gauging the success of these treatments based on their effect on PTOA severity. Methodologies include histopathological evaluation of cartilage, radiographic evaluation of the knee, analysis of knee function, and quantification of OA predictive biomarkers. Lastly, we analyze the prevalence of these methodologies using a systemic PubMed® search for original scientific journal articles published in the last 3-years. We indexed 37 meniscus repair/replacement studies conducted in live animal models. Overall, our findings show that approximately 75% of these studies have performed at least one assessment for PTOA following meniscus injury repair. Out of this, 84% studies have reported an improvement in PTOA resulting from treatment.

Keywords: meniscus, repair, replacement, PTOA, osteoarthritis

OPEN ACCESS

Edited by:
Andreas Martin Seitz, Ulm University Medical Center, Germany

Reviewed by:
Muhammad Farooq Rai, Washington University School of Medicine in St. Louis, United States
Sonia Bansal, Hospital for Special Surgery, United States

****Correspondence:***
Chathuraka T. Jayasuriya Chathuraka_Jayasuriya@Brown.edu

Specialty section:
This article was submitted to Biomechanics, a section of the journal Frontiers in Bioengineering and Biotechnology

Received: *30 September 2021*
Accepted: *06 December 2021*
Published: *22 December 2021*

Citation:
Trivedi J, Betensky D, Desai S and Jayasuriya CT (2021) Post-Traumatic Osteoarthritis Assessment in Emerging and Advanced Pre-Clinical Meniscus Repair Strategies: A Review. Front. Bioeng. Biotechnol. 9:787330. doi: 10.3389/fbioe.2021.787330

INTRODUCTION

The meniscus in the knee joint is a fibrocartilaginous tissue positioned between the femoral condyle and the tibial plateau. The meniscus performs vital functions of shock absorption and provides mechanical stability to the knee joint. Unlike articular cartilage, which lines the tibial plateau and femoral condyle of the knee joint, the menisci are soft tissues that are kept in place by ligamentous attachments, and hence they can slide and contort during knee flexion/extension. The medial and lateral menisci are key structures in the knee joint that help to dissipate forces, provide stability, and

lubricate and protect the articular cartilage from injury (McDermott and Amis, 2006). With increases in physically active and aged populations, incidents of meniscus injury have spiked at a significant rate. For instance, in the United States alone, meniscus injuries are encountered by 6–8% of active young adults annually and this number is increased in the elderly population (Gee et al., 2020; Kennedy et al., 2020). Initially, the meniscus was considered to be vestigial tissue, which can simply be removed surgically upon major injury, as a means of alleviating pain and restoring function to the knee joint (Chivers and Howitt, 2009; McNulty and Guilak, 2015). However, it is now known that the absence of, or injury to, meniscal tissue significantly increases the risk of post-traumatic osteoarthritis (PTOA) (Badlani et al., 2013; Chang and Brophy, 2020; Rai et al., 2020; Adams et al., 2021; Bedrin et al., 2021). Indeed, according to a recent 2020 epidemiological study of young adults, approximately 13% of patients with meniscus injuries develop OA by 18 years post-injury, whereas only about 3% of patients with uninjured knees developed the disease (Snoeker et al., 2020). While there is a strong emphasis on improving meniscus healing in emerging biomedical research, it is equally important to assess how new strategies for treating these injuries affect the development of OA in the knee. Hence, the efficacy of treatment should not rely solely on the assessment of the extent of meniscus repair, but it should also include a comprehensive evaluation of secondary/indirect outcome measures of therapeutic efficacy, such as its ability to preserve cartilage health, prevent the expression of established PTOA serum and blood biomarkers, and restore knee joint mechanics/function as closely as possible to the pre-injury state. In this review, we have cataloged recent pre-clinical therapeutic strategies that are being developed to promote meniscus healing. We further discuss the methodologies used in these studies to evaluate their respective outcome measures and detail their findings.

BASIC MENISCUS STRUCTURE AND ANATOMY

Meniscus is divided into three zones from the outer peripheral region to the inner central thinnest region based on the degree of vascularization. The outermost region is thickest, and it is significantly vascularized. It is referred to as the red-red zone (Andrews et al., 2011; Bryceland et al., 2017). Due to the vascularization, the red-red zone is enriched in nutrients and cytokines, enabling the self-healing upon injury in this area. The inner (middle) region is referred as the red-white zone, which contains less vascularization than the red-red zone and has minimal self-healing capacity. The innermost (central) region of the meniscus is completely devoid of vasculature and lacks any ability to self-repair. This white-white zone is tapered in shape with an unattached free edge.

The lateral and medial menisci are smooth, lubricated crescent-shaped fibrocartilage tissues that partially cover and protect the articular cartilage surface from injury. In humans, the lateral and medial menisci vary greatly in their dimensions. The lateral meniscus is approximately 27–29 mm wide and 33–35 mm in length, whereas the medial meniscus ranges from 27–28 mm in width and 41–45 mm in length (Shaffer et al., 2000; McDermott et al., 2004). The lateral meniscus occupies almost one-third of the tibial plateau with the superior concave surface pivoting the femoral condyles, while the ventral surface articulates the tibial condyle (Erdemir, 2016; Zhang et al., 2020). The lateral meniscus has a constant width that occupies a large portion of the total articular surface. The medial meniscus articulates inferiorly with the medial condyle of the tibia and superiorly with the medial condyle of the femur bone. The medial meniscus occupies more than half of the contact portion of the medial compartment. The anterior horn of the medial meniscus attaches near the ACL on the tibia, whereas the posterior horn attaches above the PCL. The medial meniscus is more crescent-shaped and covers a smaller surface of the tibial plateau compared to the lateral meniscus (Makris et al., 2011; Fox et al., 2015). Reduction of meniscal tissue due to surgical resection performed as a treatment for severe meniscus tears can result in increased forces on the articular cartilage during knee loading. Veritably, the amount of meniscus tissue resected is reported to have a positive relationship with detrimental shear stress on the cartilage surfaces that can lead to OA (Vadher et al., 2006).

CLINICAL SURGICAL INTERVENTIONS FOR MENISCUS INJURIES

Meniscal injury is one of the most common sports-related knee injuries in the United States (Majewski et al., 2006; Korpershoek et al., 2017). The combined hypovascularity and hypocellularity within the white-white zone of the meniscus significantly hinders its ability to adequately heal (Athanasiou, 2009). A meniscal injury, especially one in a hard-of-healing area such as the white-white zone, becomes a strong predictor for the accelerated development of osteoarthritis (OA). This can be attributed to the undeniable importance of meniscus in maintaining knee joint health as well as the shortcomings of traditional arthroscopic meniscus repair strategies.

Deciding the best clinical course of action for surgically treating a meniscal tear not only depends on the location, nature of the injury, and tear type, but it also relies on the age of the patient and potential co-morbidities (i.e., obesity, concomitant chondral/ligamentous damage that is presented with the meniscus injury). Treatment strategies can range from minor non-surgical means such as physical therapy and the use of non-steroidal anti-inflammatory medications, to surgical means such as meniscus suturing or partial meniscectomy/resection (surgical removal of a portion of the meniscus) (Terry Canale S, 2012; Wells et al., 2021).

Suturing and Resection

Suturing is the most conservative of the surgical approaches for meniscus repair; however, this treatment strategy has the most long-term success rate for repairing isolated tears in younger patients (Hagmeijer et al., 2019). Meniscus tears are commonly sutured according to suture placement orientation, relative to the

tear: all inside (Darabos et al., 2012), outside-in (Rodeo, 2000), and inside-out (Steenbrugge et al., 2004) techniques. For more complex tears that present with tissue loss, meniscal resection is used to remove the damaged and unrepairable areas of fibrocartilage in order to reshape the meniscus to its natural semilunar shape, but this removal of tissue has been shown to alter the contact pressures within the joint (Terry Canale S, 2012). Several long-term follow-up studies in athletes and youths who have undergone either partial or complete meniscectomy suggest an increased risk of PTOA (Allen et al., 1984; Jørgensen et al., 1987; Faunø and Nielsen, 1992; Hede et al., 1992; Benedetto and Rangger, 1993; Rangger et al., 1997; Papalia et al., 2011; Longo et al., 2019).

Meniscus Allograft Transplantation

Additionally, meniscal allograft transplantation (MAT) is implemented in cases of severe meniscal injuries which cannot be rectified using suturing or partial resection. MAT has become more frequently used as a state-of-the-art technique utilized in the pursuit of preserving/restoring the function and mechanics of the knee in severe or irreparable meniscus injuries. MAT was first described by Milachowski et al. (Milachowski et al., 1989) in 1989; since then, this strategy has been the subject of refinement in the pre-clinical and clinical settings to restore meniscus (and ultimately joint) function while preventing the development of degenerative changes in the knee (Rodeo, 2001; Lee et al., 2012). While the refined implementation of MAT has shown promising results in patients and athletes (Pereira et al., 2019; Searle et al., 2020), it still has several limitations including extrusion and shrinkage of the graft (Lee et al., 2012). The success rate for the two major scaffolds (i.e., collagen scaffolds, polyurethane scaffolds) varies from 38% to as low as 0% after 4 years of follow-up (Houck et al., 2018). The long-term results of scaffolds and allografts can be unpredictable, and it is documented that some may become non-functional due to shrinkage, extrusion, and fragmentation (Trentacosta et al., 2016; Houck et al., 2018). Taken together, these findings highlight the importance of long-term follow-up studies to inspect not only the health of the meniscus but also the entire knee in order to adequately determine the success of any treatment.

GAUGING THE SUCCESS OF EMERGING MENISCUS REPAIR STRATEGIES IN THE PRE-CLINICAL STAGE

Clinical assessment of long-term outcomes following meniscus repair/replacement primarily involves looking at reoperation rates for each respective surgical procedure. Other individual assessments include radiographic imaging, surveying the degree of knee pain (as reported by the patient), joint function (i.e., during walking, single hop test), and range of motion (ROM) of the knee in patients using scales such as the Knee injury and Osteoarthritis Outcome Score (KOOS) system, Lysholm, and the Tegner activity scale, to name a few. Some of these outcome measures are understandably difficult if not impractical to implement in animal models that are used in pre-clinical investigations, depending on the species that is used. For this reason, there is a set of assessments that are commonly used in pre-clinical animal studies to gain similar insight into the short and long-term efficacy of treatments.

Developing new and more effective strategies to stimulate meniscus healing is an active area of biomedical research. A number of strategies that are still in the pre-clinical stages of development focus on the use of biologics and biomimetic natural/synthetic materials, which encompass utilizing cells, bioactive factors (both chemical and biological), and injectable/implantable scaffolds, to accelerate meniscus healing (Shimomura et al., 2018). Current primary outcome measures for the success of advanced, pre-clinical meniscal repair treatments include macroscopic and microscopic (histology) assessment of meniscal fibrocartilage using routine/special/immunostaining analysis or magnetic resonance imaging (MRI) of the meniscus, and biomechanical testing of meniscal tissue. Other avenues of assessment include functional analysis of knee kinematics, quantification of secreted inflammation/catabolism associated biomarkers, and macro- and microscopic assessment of the articular surfaces and synovium for PTOA changes.

Histological Assessment of Meniscus Repair Efficacy

Post-mortem histological assessment of meniscal fibrocartilage is currently the gold standard of evaluating the success with which a treatment stimulates healing, especially in pre-clinical animal models. Routine stains such as hematoxylin and eosin (H&E) are useful for the qualitative evaluation of newly formed tissue and its cellularity. Other stains such as Safranin O/Fast Green and Toluidine blue are used primarily to determine molecules of interest that constitute said tissue (i.e., glycosaminoglycans). Further special stains like Picrosirius red allow for the visualization of collagen matrices when imaged under polarized light, providing not only information about the collagen makeup of tissues but also enabling the detection of continuous collagen fiber bundles, which bridge newly formed tissue and pre-existing meniscus tissue at the periphery of the injury site. Furthermore, these stains allow investigators to determine how the orientation of fibers may be changed.

Immunohistochemistry involves the staining of tissue with specific antibodies to detect and visualize matrix molecules (and sometimes even soluble proteins). This technique is used to determine the presence of specific proteins or cells in a given tissue. For instance, López-Franco et al. employed COMP and Ki67 immunohistochemistry to evaluate the differences between healthy human menisci and osteoarthritic human menisci (López-Franco et al., 2016). The use of immunostaining to detect several endogenous markers such as Human Nucleus Antigen (HNA) and cell surface markers CD44 and CD99 have been employed to visualize the endogenous cell localization to the meniscal injury site (Tarafder et al., 2018). Additionally, immunostaining for CD34 and CD146 has been used to distinguish progenitor cell populations in the meniscus, which are proposed to be useful for meniscus repair applications (Osawa et al., 2013).

Longitudinal MRI Imaging to Assess Meniscus Healing Over Time

While histology is arguably the gold standard for evaluating meniscus healing/pathology, it first requires a terminal experimental endpoint where tissue must be extracted for analysis. The benefit of the development and refinement of accurate *in vivo* imaging techniques for the assessment of meniscus healing is that it allows for longitudinal evaluation in the same subject over time. It has been established that longitudinal Magnetic Resonance Imaging (MRI) using T2 mapping is an informative means of post-injury/repair assessment (Berton et al., 2020; Yamasaki et al., 2020). Additional techniques such as T2Rho and T2* mapping are being adapted and applied to improve the sensitivity of meniscal evaluation (Koff et al., 2013; Zellner et al., 2013; Nakagawa et al., 2016). These techniques have been used to predict tissue degeneration through their ability to detect changes in fiber orientation and tissue biochemistry, including altered water, collagen, and proteoglycan content. For instance, Kondo et al. implanted synovial MSCs (syMSCs) in aged cynomolgus primates and used T1rho MRI mapping to show that this inhibited meniscal degeneration (Kondo et al., 2017). Additionally, Hatsushika et al. reported that repeated intra-articular syMSCs injections were able to stimulate healing of meniscal defects in a porcine *in vivo* model and used T2 MRI mapping to evaluate their results (Hatsushika et al., 2014). Similarly, Lucidi et al. evaluated the long-term results of medial collagen meniscal implants in human patients approximately 20 years after surgery by performing MRI scans on their knees and analyzing the results using the Yulish scoring system, which takes into account the detection of cartilage and subchondral bone elements (Lucidi et al., 2021). They found that four of the eight patients who underwent surgery developed mild OA symptoms. These studies highlight the importance of long-term longitudinal radiographic evaluation of the knee over the years in patients to evaluate the possible onset and progression of OA.

Assessment of Meniscal Mechanical Properties Following Repair

The measurement of meniscal strength and the characterization of its mechanical compressive properties are used as a means of assessing tissue integrity. Tensile loading (to failure) is a commonly utilized method for testing tensile repair strength (Zellner et al., 2013; Nakagawa et al., 2015; Peloquin et al., 2016; Newberry et al., 2020); indentation testing is used to determine changes in tissue compression (Shen et al., 2013) (Pan et al., 2017), and pushout testing is used to evaluate the extent of shear strength due to integrative repair (Hennerbichler et al., 2007; Wilusz et al., 2008; Newberry et al., 2020). Additionally, detection of changes in the contact forces on tibial femoral articular cartilage can be used as an outcome measure of meniscal injury repair/treatment success. The most common methodologies for achieving this end include the use of MRI and CT mapping (Flanigan et al., 2010). Direct pressure mapping technologies are also commonly used to evaluate the effects of changes in knee forces following non-surgical or surgical treatment to the meniscus (Hennerbichler et al., 2007; Flanigan et al., 2010). In addition, these approaches are crucial to evaluate the effect on the cartilage surface followed by treatment when suturing or partial meniscectomy is performed.

Assessment of Biomarkers

The quantification of protein biomarkers, as a means of detecting specific types of meniscal injuries, has more recently become an area of active investigation with the popularization of sophisticated multiplexing technologies such as Luminex, which allow nanoscale detection of robust sets of soluble protein markers. A meniscus injury is linked to the development of PTOA (Kennedy et al., 2020; Sherman et al., 2020; Tarafder et al., 2020; Adams et al., 2021). As such, the events that occur after traumatic injury or degenerative changes in the meniscus that govern the progression of OA are regulated at the molecular level. For instance, following joint injury, several inflammatory proteins (such as interleukins, TNF-alpha, Prostaglandin E2), collagenases/aggrecanases (such as matrix metalloproteinases, ADAMTS family members), and reactive oxygen species are produced (Roberts et al., 2015; Lepetsos and Papavassiliou, 2016; Roller et al., 2016; Liu et al., 2017; Clair et al., 2019). Collagenases are involved in the metabolism of cartilage and subchondral bones, and they are considered candidate biomarkers for pathological tissue remodeling upon meniscus injury or osteoarthritis (Karsdal et al., 2011; Karsdal et al., 2013). Clair et al., observed a significant upregulation of IL-6, MCP-1, MIP-1β, and MMP-13 in the synovial fluid of the patients with meniscal injury (Clair et al., 2019). These studies reveal that a range of biomarkers is modulated in the synovial fluid as well as in the serum upon injury to the meniscus. A recent study by Brophy et al., has also demonstrated that gene expression analysis of meniscal tissue obtained during arthroscopic meniscal debridement procedures may be used to predict degenerative changes in the cartilage (Brophy et al., 2017). This study reported a differential expression of the adipokines, adiponectin and resistin in meniscal tissue from knees with degenerative changes, suggesting a potential causal relationship. This study highlights the importance of biological signaling in the meniscus for maintaining articular cartilage health.

Overall, the quantification of PTOA biomarkers in the blood and synovial fluid provide a fundamental advantage over more invasive approaches, such as histopathology analysis, while also providing an additional advantage of enabling frequent analysis at multiple time points in the same subject. Analyzing synovial fluid (SF) biomarker profiles can also have advantages since SF is drawn directly from the injury micro-environment. Additionally, due to the small volume of synovial fluid, biomarkers are less diluted as compared to those dispersed into the peripheral blood.

Functional Assessment of the Knee

Lastly, the implication on meniscus repair/replacement on longitudinal knee function is used to gauge overall efficacy in pre-clinical animal models, including both small animals such as

TABLE 1 | Summary of our literature analysis on recent pre-clinical live animal studies.

Treatment	Animal model	Major techniques used to evaluate tissue outcomes							Meniscus (primary) outcomes	Knee health/ function (secondary) outcome	Ref.
		Meniscus examination	Cartilage examination	Synovium	Sub-chondral bone	Knee function	Biomarker analysis	Radiographic evaluation			
Cells	Mouse	Histology (Saf-O), Immunofluorescence (IF)	Histology (Saf-O), Von Frey assay for OA, Mankin Score	NA	NA	NA	Ihh, Dhh, Ptch1, Gli1, Gli2, Gli3, Hhip, Smo	microCT	Collagen fibers mediated increased bridging of broken meniscus	Reduced cartilage degradation and delayed OA progression	Wei et al. (2021)
Cells	Rabbit	Macroscopic evaluation, Histology (Toluidine Blue), Cell tracking by Dil labelling	NA	NA	NA	NA	NA	MRI	Larger area and transverse diameter of regenerated tissue; greater histological scores in ADSC group than controls	NA	Takata et al. (2020)
Cells	Pigs	Histology (Saf-O, Picrosirius Red, and H&E), Immunohistochemistry (IHC)	NA	NA	NA	NA	NA	MRI	Increased Proteoglycan content; improved histological score, T2 values comparable with control menisci	NA	Ozeki et al. (2021)
Cells	Mouse	Histology (Saf-O), IHC	Histology (Saf-O), IHC	NA	NA	NA	NA	NA	Reduced inflammation; increase chondrogenesis in MSCs; increased proteoglycan content	Reduced cartilage degradation; reduced OARSI scoring	Ding, (2021)
Cells	Rabbit	Macroscopic evaluation, Histology (DMMB stain), IHC	NA	NA	NA	NA	NA	NA	Significantly enhanced regeneration of the meniscus in time dependent manner	NA	Koch et al. (2019)
Scaffold	Rabbit	Macroscopic evaluation	Histology (H&E)	NA	NA	NA	NA	NA	Scaffolds maintained integrity with no degradation of the native tissue	No degradation of cartilage surface as compared to other controls	Fan et al. (2021)
Scaffold	Sheep	Macroscopic observation, Histology (H&E) and Biomechanical	Macroscopic observation using India ink stain, Histology (Saf-O) and Biomechanical, Semi-quantitative analysis (Mankin), Indentation testing	Histology (H&E)	NA	NA	NA	NA	Most implants at the defects resembled native tissue without any signs of inflammation; increased equilibrium modules of scaffolds after 6 months	Visible softening and fibrillation of articular cartilage	Stein et al. (2019)
Scaffold	Mini Pig	Histology (Saf-O), Pauli Score, Ishida Score, MRI	Histology (Saf-O), Mankin Score	NA	NA	NA	NA	MRI	Ultimate tensile stress was similar to native tissue and scaffolds were covered with native tissue; increased cell infiltration	No cartilage degradation, fluid accumulation or Inflammation	Otsuki et al. (2019)
Scaffold	Rabbit	Macroscopic evaluation, Histology (H&E, Saf-O, Fast Green)	NA	NA	NA	NA	NA	NA	Wounds healed completely, at a faster rate and formed native tissue structure in the treatment group as compared to other controls	NA	Liu et al. (2019)

(Continued on following page)

TABLE 1 | (*Continued*) Summary of our literature analysis on recent pre-clinical live animal studies.

Treatment	Animal model	Major techniques used to evaluate tissue outcomes							Meniscus (primary) outcomes	Knee health/ function (secondary) outcome	Ref.
		Meniscus examination	Cartilage examination	Synovium	Sub-chondral bone	Knee function	Biomarker analysis	Radiographic evaluation			
Scaffold	Sheep	Macroscopic evaluation, Histology (Saf-O, Alcian Blue, IHC)	NA	NA	NA	NA	NA	NA	Meniscal tissue repair 6-months post-implant	NA	Cojocaru et al. (2020)
Scaffold	Rabbit	Histology (H&E, Saf-O), IHC	Histology (H&E)	NA	Histology (H&E)	NA	NA	NA	Increased tissue regenerationand enhanced tissue quality	No degeneration observed on cartilage or subchondral bone	Kim et al. (2021)
Scaffold	Rabbit	Histology (H&E, Masson trichrome), IHC	Macroscopic observation using India Ink, Histology (H&E, Saf-O, Masson's Trichrome, Alcian Blue), Modified Mankin score	NA	NA	NA	NA	NA	Enhanced cytocompatibility of the collagen coated scaffold; increased cell infiltration and ECM deposition; higher expression of COL1 in composite sponge and no significant changes in COL 2 and aggrecan	Significantly reduced cartilage degradation and considerably better gross scores and Mankin scores	Yan et al. (2019)
Scaffold	Rabbit	Histology (H&E, Sirus Red, Alcian Blue), MRI	Macroscopic evaluation, OARSI scoring, MRI	NA	NA	NA	Type I collagen and Type II collagen, Aggrecan	MRI	Increased inflammatory signals in total meniscectomy as compared to scaffold group; meniscus like tissue formation with better tensile strength	Significantly slower progression of cartilage degradation and better OARSI scoring however the scaffold group also degenerated progressively with time.	Li et al. (2020a)
Scaffold	Sheep	Histology (H&E), Macroscopic observation, IF	Histology (Saf-O, Fast Green)	NA	NA	NA	NA	NA	Scaffold retained original thickness; no anatomic variation between scaffold and native tissue, vascularization in scaffold, with increasing collagen content	No articular cartilage surface degradation	Ghodbane et al. (2019)
Scaffold	Rabbit	Histology (H&E), (H&E, Toluidine Blue), IHC, Ishida score	Histology (H&E)	NA	NA	NA	NA	X-Ray (K-L grading), MRI (WORMS assessment)	Meniscal regeneration with similar histological, biochemical and biomechanical properties as compared to native tissue	No articular cartilage surface degradation	Chen et al. (2019)
Scaffold	Rabbit	Histology (H&E), Rodeo scoring, Hayes scores, Indentation test	Macroscopic evaluation using India Ink, Indentation testing	NA	NA	NA	NA	NA	No inflammation or infection; significantly higher surface area, higher mechanical properties and higher Hayes score in scaffold group as compared to other controls	No significant difference between groups	Demirkıran et al. (2019)
Scaffold	Rabbit	Histology (H&E, Masson staining)	Macroscopic evaluation using India Ink, Histology (H&E), Mankin Score	NA	NA	NA	Col 1, Aggrecan	X-ray	Sustained release of TGF-B1 over 1-week with increased cell infiltration	Reduced cartilage surface degradation at 3 months	Wu et al. (2019)

(Continued on following page)

TABLE 1 | (*Continued*) Summary of our literature analysis on recent pre-clinical live animal studies.

Treatment	Animal model	Major techniques used to evaluate tissue outcomes							Meniscus (primary) outcomes	Knee health/ function (secondary) outcome	Ref.
		Meniscus examination	Cartilage examination	Synovium	Sub-chondral bone	Knee function	Biomarker analysis	Radiographic evaluation			
Scaffold	Rat	Histology (H&E, Sirius Red, Saf-O), IHC (MMP-13)	Histology (H&E, Sirius Red, Saf-O), IHC (MMP-13), OARSI scoring	NA	NA	NA	IL-6, IL-8, and MMP-3	NA	Significantly reduced expression of inflammatory cytokines	Significant reduction in the cartilage surface degradation and reduced OARSI scoring	Li et al. (2021)
Scaffold	Rabbit	Macroscopic analysis and Histology (H&E, Masson's trichrome), Quantitative modified meniscus scoring.	NA	NA	NA	NA	NA	NA	Significant regeneration of damaged meniscal tissue	NA	Abpeikar et al. (2021)
Scaffold	Sheep	Gross inspection, Histology (H&E, Saf-O) and MRI	Gross inspection, Histology (H&E, Saf-O), OARSI scoring and MRI	OARSI histopathologic synovial scoring	NA	NA	NA	MRI	No significant difference in the groups in terms of meniscal regeneration	All groups exhibited cartilage degradation, signs of synovitis, meniscal extrusion was observed in most animals	Nakagawa et al. (2019)
Scaffold	Rabbit	Histology (Toluidine Blue, Picrosirius Red, and H&E)	Histology (H&E, Saf-O), Mankin score, ICRS cartilage lesion score	NA	NA	NA	ACAN, R\FRZB, Sox9, HAPLN1, CHA Type I collagen, Type II collagen	NA	Recapitulation of healthy meniscal tissue	Reduced cartilage degradation	Sun et al. (2021)
Scaffold	Rat, Rabbit and Sheep	Histology (Toluidine Blue, Saf-O)	Histology (Toluidine Blue, Saf-O), IHC, Mankin score	NA	NA	NA	NA	microCT, X-ray	Regeneration of meniscal tissue	Improved Mankin score, Reduced cartilage degradation	Guo et al. (2021)
Scaffold	Rabbit	Histology (H&E, Saf-O, Picrosirius red), Macroscopic evaluation, IHC	Histology (H&E), OARSI scoring, Macroscopic evaluation	Histology (H&E), semi-quantitative synovitis scoring	NA	NA	Type I collagen, Type II collagen	NA	Increased reparative tissue in defects	No degradation on cartilage surface and subchondral bone	Okuno et al. (2021)
Scaffold	Rabbit	Histology (H&E, Toluidine Blue, Saf-O, Picrosirius red), IHC	Histology (Toluidine Blue, Saf-O) ICRS cartilage lesion classification Scanning Electron Microscopy	ELISA for IL-1 and TNF-alpha	NA	NA	IL-1 and TNF-alpha	NA	Meniscus structural and biomechanical properties of the scaffold group was comparable to that of native meniscus group	No degradation of cartilage surface	Li et al. (2020b)
Cell based scaffold	Rabbit	Histology (Saf-O), Ishida scoring system, IHC	NA	NA	NA	NA	NA	NA	Defect filling with fibrocartilaginous tissue	NA	Chen et al. (2020)
Cell based scaffold	Dog	Histology (H&E, Toluidine Blue, Picrosirius red), IHC	Histology (H&E, Saf-O, Fast Green), IHC	NA	NA	Lysholm score	NA	NA	Hormone (PTH) + Cells + Scaffold formed more neo-cartilage tissue compared to the cells + scaffold group with more ECM deposition	Less degenerative changes in the cartilage in treatment group	Zhao et al. (2020)
Cell based scaffold	Rat	Histology (H&E, Saf-O Toluidine Blue), IHC	microCT	NA	microCT	NA	NA	microCT	Regeneration of the meniscal tissue, reduced osteophyte formation, reduction of joint spance narrowing	Reduced cartilage degradation and delayed OA progression	Zhong et al. (2020)

(Continued on following page)

TABLE 1 | (*Continued*) Summary of our literature analysis on recent pre-clinical live animal studies.

Treatment	Animal model	Major techniques used to evaluate tissue outcomes							Meniscus (primary) outcomes	Knee health/ function (secondary) outcome	Ref.
		Meniscus examination	Cartilage examination	Synovium	Sub-chondral bone	Knee function	Biomarker analysis	Radiographic evaluation			
Cell based scaffold	Rabbit	Histology (H&E, Saf-O)	Histology (H&E, Saf-O), IHC	NA	NA	NA	NA	NA	Prevention of meniscal extrusion; filling of meniscal defects	No cartilage degradation	Shimomura et al. (2019)
Allograft	Dog	Histology (H&E, Toluidine Blue)	Histology (H&E, Toluidine Blue)	Histology (H&E)	Histology (H&E, Toluidine Blue)	Comfortable knee range of motion (CROM), clinical lameness and limb kinetics, knee pain, knee effusion, visual analogue scale	NA	MRI	Pain, CROM, histological scores and cell viability were superior in fresh menisco-tibial group as compared to other techniques	restoring joint healt Fresh, MOPS preserved and meniscal osteochondral allograft are safe and effective to restore knee joint function	Schreiner et al. (2021)
Allograft	Sheep	Histology (H&E, Saf-O, Masson's Trichrome, Fast Green), IHC, Ishida score, Rodeo score	Histology (Saf-O), Histopathology scoreing	NA	NA	NA	NA	NA	Three early euthanized animals showed moderate Rodeo score and low Ishida score; full-term animals showed improved Rodeo scoring, improved Ishida scoring and Improved healing	Three animals were euthanized early due to resulting knee health. Three animals (euthanized 90 days post-surgery) showed less cartilage degradation and improved histopathology scoring	Strauss et al. (2019)
Circular unidentified RNA (PDE4B)	Mouse	Histology (Saf-O)	Histology (Saf-O),OARSI Scoring	NA	microCT	Hot plate test, knee extension test and electric shock stimulated treadmill test	Aggrecan, COL2A1, SOX9, MMP13, MMP3, ADAMTS4	microCT	Increased proteoglycan content	Reduced cartilage degradation, reduced proteoglycan content, reduced OARSI scoring, and reduced discomfort and pain	Shen et al. (2021)
Extracellular vesicles	Mouse	Histology (Saf-O, Fast Green)	Histology (Saf-O),OARSI Scoring	NA	NA	NA	Aggrecan, COL2A1, ADAMTS5	NA	Increased proteoglycan content; increased proliferation and migration of chondrocyte	Reduced cartilage degradation and reduced OARSI scoring	Duan et al. (2021)
Erythropoietin	Mouse	Histology (Alcian Blue, Orange G)	Histology (Alcian Blue, Orange G)	NA	NA	NA	Type I collagen, Type II collagen, MMP13		Increased regeneration of damaged meniscal tissue; increased production of ECM; increased cell proliferation and reduced MMP-13 expression	Reduced MMP-13 expression and reduced OA severity	Fu et al. (2020)
N/A	Rabbit	Histology (H&E, Fast Green), Indentation relaxation testing	micro-CT	NA	micro-CT	NA	NA	microCT	Severe degradation in both lateral and medial menisci	Minimal changes in bone quality and morphometry, Increased osteophyte formation	Narez et al. (2021)
SDF-1	Rat	Histology (H&E, Toluidine Blue, Saf-O)	NA	NA	NA	NA	NA	NA	Enhanced migration of macrophages at the injury site, Defect repair	NA	Nishida et al. (2020)

(Continued on following page)

TABLE 1 | (*Continued*) Summary of our literature analysis on recent pre-clinical live animal studies.

Treatment	Animal model	Major techniques used to evaluate tissue outcomes							Meniscus (primary) outcomes	Knee health/ function (secondary) outcome	Ref.
		Meniscus examination	Cartilage examination	Synovium	Sub-chondral bone	Knee function	Biomarker analysis	Radiographic evaluation			
Platelet Rich Plasma and Platelet Rich Fibrin Matrix	Rabbit	Histology (H&E)	NA	NA	NA	NA	NA	NA	No obvious benefits of PRP and PRFM on meniscus healing and matrix formation	NA	Kurnaz et al. (2020)
Local administration of Magnesium	Rabbit	Histology (H&E, Toluidine Blue), IHC	Histology (H&E, Toluidine Blue), ICRS cartilage lesion classification, Mankin score	Colony forming cells analysis	NA	NA	IL-1, TNF-alpha	NA	Enhanced adhesion, migration and fibrochondrogenesis of SMSCs in meniscus lesions	Less degradation of cartilage surface than control group, retained mechanical strength	Zhang et al. (2019)

These studies were indexed by searching PubMed for original scientific articles employing live animal models that were published between 1/1/2019 and 9/26/2021, using the following search terms in the title and abstract fields: meniscus repair, meniscus replacement, meniscus regeneration, meniscus scaffold. *Studies are organized based on the category of therapeutic strategy tested.*

rodents and guinea pigs and large animal models like pigs, dogs, and horses. Accurate assessment of knee function is also crucial to make informed treatment decisions, as well as to monitor debilitating effects associated with traumatic joint injury (Ericsson et al., 2006; Bremander et al., 2007; Katz et al., 2013). Gait analysis is one of most commonly used methods to evaluate knee function in the patients with meniscus injury (Bulgheroni et al., 2007; Hyodo et al., 2020; Liu et al., 2020). Similarly, unilateral and bilateral gait analysis is a mainstay in pre-clinical studies investigating the functional implication of meniscus/ACL injury and repair (Jacobs et al., 2014; Karamchedu et al., 2021). Asymmetric gait patterns are typically indicative of potential functional impairment due to the change in the normal range of motion.

Assessment of Knee Histopathology for Signs of OA

Pre-clinical meniscus repair/replacement studies have used knee histopathology as a secondary outcome measure of success (**Table 1**). However, the effect of meniscus repair/replacement on the pathology of the entire knee is a crucial metric and should arguably be considered a primary outcome measure when assessing the success of treatments. Assessment of the degree of articular cartilage degradation, synovial hyperplasia, mast cell infiltration, and changes in subchondral bone are all features that can be qualitatively and/or semi-quantitatively detected by histopathology analysis of tissue sections using the same staining techniques described previously (i.e., routine/special/immunostaining) for assessing meniscus histopathology.

EMERGING PRE-CLINICAL MENISCAL REPAIR/REPLACEMENT STRATEGIES AND THEIR IMPACT ON KNEE FUNCTION AND PATHOLOGY

Partial meniscal resection can be an effective short-term treatment for symptomatic complex meniscus tears; however, sizeable evidence shows that this approach leads to the accelerated development of OA. Similarly, MAT has its own set of challenges which were discussed above. Therefore, novel therapeutic approaches are being developed in the pre-clinical models to find effective alternative therapies. These approaches largely include the use of synthetic/biological scaffolds and/or autologous/allogeneic cells. In order to conduct a comprehensive evaluation of the efficacy of such emerging treatments, it is necessary to assess not only the repaired/replaced meniscus itself but also other important metrics that have been discussed in this article that ultimately help to assess knee functionality and/or pathology as fundamental indirect/secondary criteria. These secondary measures can help define the level of success achieved by said treatments.

In 2015, Nakagawa et al. (Nakagawa et al., 2015) performed a study in a porcine model in which they combined suture repair with allogenic MSCs enriched from synovial fluid. The study

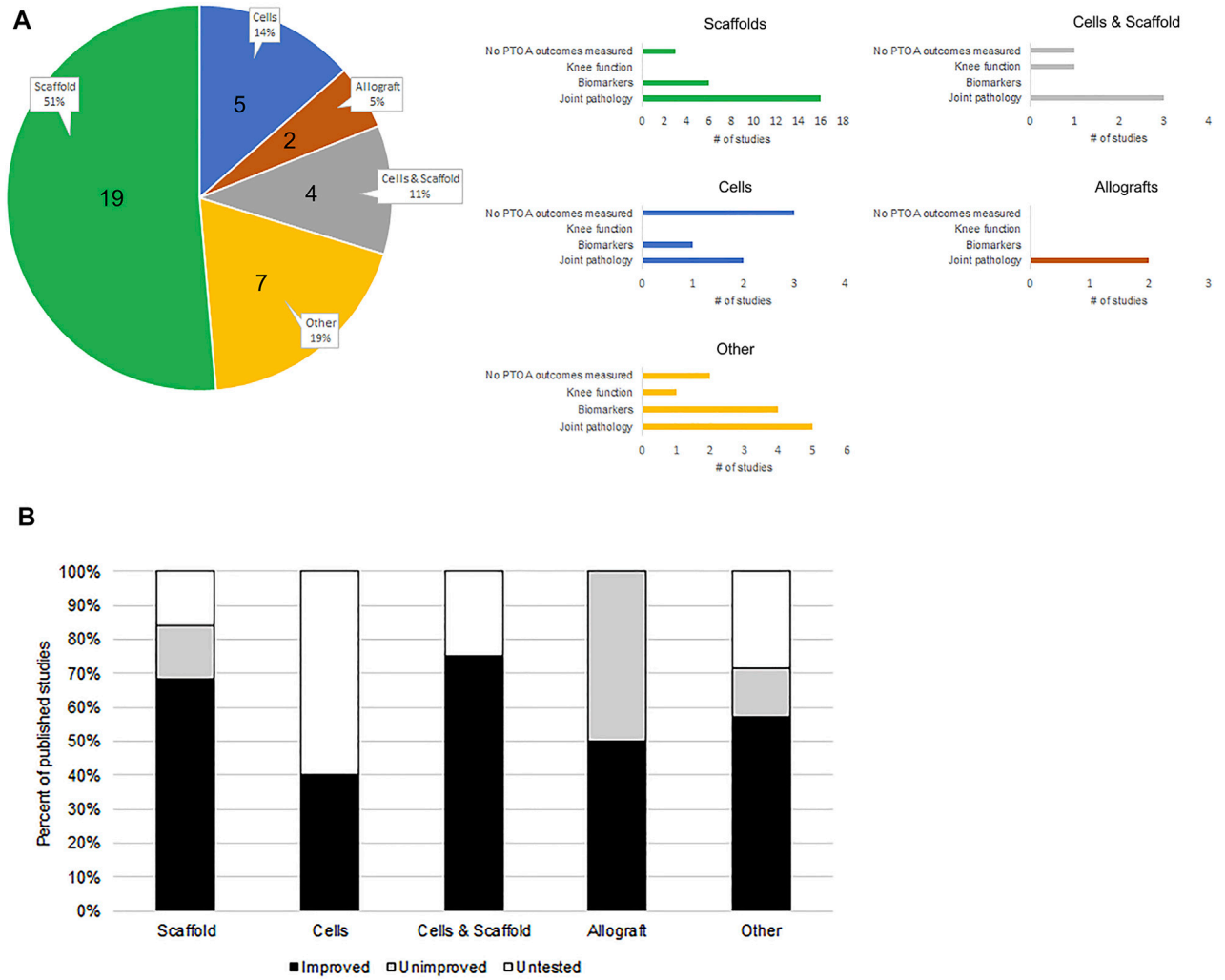

FIGURE 1 | Recent pre-clinical meniscus treatment studies in animal models and their PTOA attenuation success rate. **(A)** The 37 studies indexed in **Table 1** were used to extrapolate the distribution of published investigations that utilize different strategies for meniscus injury treatment. Studies have been categorized based on their use of cells, scaffolds, cell and scaffold combination, allografts, or altogether different (other) strategies, by a percentage of all indexed studies. The number of studies is indicated in the pie chart. These categories are further broken down (see respective bar graphs) based on secondary outcome measures used to evaluate therapeutic success, including knee function, mRNA/protein biomarker analysis, and joint pathology detection. Note that some studies have performed more than one type of analysis. **(B)** Therapy categories were further broken down based on percent distribution of studies in each that reported knee PTOA outcomes.

reported positive outcomes in meniscal histology, collagen deposition and tensile strength in the animal groups that received the combination treatment as compared to those that received only suture repairs (Nakagawa et al., 2015). Hatsushika et al. (Hatsushika et al., 2014), performed similar studies with larger meniscus tears and involved multiple injections of the synovium-derived MSCs. Their results supported the previous finding by noting that multiple injections is advantageous compared to a single injection (Hatsushika et al., 2014). Both studies involved acute injections immediately after the injury. Further studies in which the animals were treated after 3–4 weeks of injury demonstrated that the animal groups that are acutely treated show significantly better repair compared to those that are treated 3–4 weeks post-injury (Ruiz-Ibán et al., 2011). These studies suggest that both the chronology of the injury and the treatment is vital for meniscus injury repair. Inspection of cartilage health and/or knee function would have been most informative regarding the efficacy of this cell-based biologic treatment approach.

There are, however, many recent studies conducted in multiple animal models that have evaluated outcome measures of PTOA as important parameters of success (**Table 1**). For instance, Wei et al. (Wei et al., 2021) identified a novel progenitor cell population located in the horns of the meniscus that not only helps meniscus repair but also prevents cartilage degradation. The study identified Hedgehog (Hh) signaling as a crucial player in progenitor cell migration to the injury site and the inhibition of cartilage degradation. Further, they used microCT analysis to reveal that the use of Hh agonist does not induce calcification. In another study, Ding et al. (Ding, 2021) demonstrated that the

intra-articular injection of BM-MSCs pretreated with c-Jun N-terminal kinase (JNK) inhibitor SP600125 in C57BL/6 mice significantly induced meniscus repair and inhibited cartilage degradation in comparison to the animals that received BM-MSCs without SP600125 pretreatment. Immunohistochemical analysis revealed that the pretreatment of SP600125 inhibits the inflammation on the articular cartilage surface suggesting SP600125 as a potential therapeutic candidate to inhibit the cartilage degradation and OA progression (Ding, 2021). Ozeki et al. (Ozeki et al., 2021) developed a meniscus injury model in micro minipigs and investigated the reparative effects of synovial MSCs on meniscus injury repair. They used cartilage surface degradation as an outcome measure. Histological evaluation and MRI analysis indicated that synovial MSCs improved meniscus healing and also protected the articular cartilage surface from degradation as compared to the controls (Ozeki et al., 2021).

Further, in a recent study by Shimomura et al. (Shimomura et al., 2019), the investigators used an MSC monolayer sheet wrapped around an electrospun nanofiber scaffold to treat a radial meniscal injury in rabbits. In addition to evaluating the meniscus, they conducted a histological evaluation of the articular cartilage and showed that there was significantly less degradation in the cell scaffold treated animals, compared to the control animals. Zhong et al. (Zhong et al., 2020) utilized a rat model of meniscus injury-induced osteoarthritis to investigate the efficacy of an injectable extracellular matrix (ECM) hydrogel on meniscus repair and OA development. Radiographic evaluation using micro-CT scans revealed that the ECM hampers osteophyte formation, prevents narrowing of the joint space, and inhibits OA development. **Table 1** is a comprehensive list of meniscus repair/replacement studies in live animal models that were published and referenced on PubMed in the past 3-years. **Table 1** summarizes the outcomes and assessment techniques used to evaluate the meniscus itself, knee function, and knee health. **Figure 1** illustrates the distribution of these recent studies based on the implemented therapeutic techniques and their efficacy in the assessment of PTOA outcomes.

Besides cell/scaffold-based pre-clinical investigations of meniscus injury treatment, other less common approaches have also been explored. Some studies that use these approaches also include the additional evaluation of outcome measures that do not directly address the health of the meniscus, but rather the health of the surrounding tissue. For example, Shen et al., recently identified a circulating RNA, circPDE4B, as a potential target for the prevention of cartilage degradation and OA progression upon meniscus injury in mice. Histological evaluation of the mouse knee suggested that adeno-associated virus mediated delivery of circPDE4B inhibits the cartilage matrix breakdown, which was otherwise observed in the control mice knees. Fu et al. (Fu et al., 2020) investigated the actions of Erythropoietin (EPO) in meniscus organ culture and reported the mechanistic details of its effects on meniscus regeneration. Their histological analysis using Alcian Blue and Orange G staining revealed that the EPO treatment significantly reduced the degradation of the cartilage surface and ultimately attenuated OA development. Another recent study by Duan et al. (Duan et al., 2021) underscored the crucial role of extracellular vesicles (EVs) in OA progression upon meniscus injury. Through extensive *in vitro* and *in vivo* characterization, the authors revealed that EVs secreted by lipopolysaccharide enriched synovial MSCs inhibit aggrecan and collagen 2 reduction and attenuate the upregulation of IL-1β responsive ADAMTS5. They used histological analysis to reveal that the EVs significantly prevented joint degeneration in a mouse model of OA.

CONCLUSION

The detection of PTOA development in response to meniscus injury can be achieved using metrics designed to evaluate knee function, its inflammatory microenvironment (through biomarker detection), and the histopathology of tissues in the joint. Our analysis of recent scientific literature shows that 84% of studies involving the use of meniscus scaffolds and 100% of studies using allografts for meniscus injury treatment have examined at least a single outcome measure that reveals the effect on overall knee function/health to help gauge treatment success. On the other hand, only 40% of studies that use cells, and 71% of studies involving non-conventional (other) treatment approaches, have done the same. Altogether, we have found that 75% of all recent studies catalogued in our search have examined at least a single outcome assessment that is relevant to PTOA, as part of the analysis. Approximately 84% of these studies have reported an improved outcome due to treatment.

AUTHOR CONTRIBUTIONS

JT: Composed most of the manuscript, assembled table and figures, reviewed and revised manuscript. DB: Composed components of the manuscript, reviewed and revised manuscript. SD: Composed components of the manuscript, reviewed and revised manuscript. CJ: Conceptualized review, composed components of the manuscript, reviewed and revised manuscript.

REFERENCES

Abpeikar, Z., Javdani, M., Mirzaei, S. A., Alizadeh, A., Moradi, L., Soleimannejad, M., et al. (2021). Macroporous Scaffold Surface Modified with Biological Macromolecules and Piroxicam-Loaded Gelatin Nanofibers toward Meniscus Cartilage Repair. *Int. J. Biol. Macromolecules* 183, 1327–1345. doi:10.1016/j.ijbiomac.2021.04.151

Adams, B. G., Houston, M. N., and Cameron, K. L. (2021). The Epidemiology of Meniscus Injury. *Sports Med. Arthrosc. Rev.* 29 (3), e24–e33. doi:10.1097/jsa.0000000000000329

Allen, P., Denham, R., and Swan, A. (1984). Late Degenerative Changes after Meniscectomy. Factors Affecting the Knee after Operation. *The J. Bone Jt. Surg. Br. volume* 66-B (5), 666–671. doi:10.1302/0301-620x.66b5.6548755

Andrews, S., Shrive, N., and Ronsky, J. (2011). The Shocking Truth about Meniscus. *J. Biomech.* 44 (16), 2737–2740. doi:10.1016/j.jbiomech.2011.08.026

Athanasiou, K. A., and Sanchez-Adams, J. (2009). Engineering The Knee Meniscus. *Synthesis Lectures Tissue Eng* 1, 1–97. doi:10.2200/S00186ED1V01Y200903TIS001

Badlani, J. T., Borrero, C., Golla, S., Harner, C. D., and Irrgang, J. J. (2013). The Effects of Meniscus Injury on the Development of Knee Osteoarthritis. *Am. J. Sports Med.* 41 (6), 1238–1244. doi:10.1177/0363546513490276

Bedrin, M. D., Kartalias, K., Yow, B. G., and Dickens, J. F. (2021). Degenerative Joint Disease after Meniscectomy. *Sports Med. Arthrosc. Rev.* 29 (3), e44–e50. doi:10.1097/jsa.0000000000000301

Benedetto, K. P., and Rangger, C. (1993). Arthroscopic Partial Meniscectomy: 5-year Follow-Up. *Knee Surg. Sports Traumatol. Arthrosc.* 1 (3-4), 235–238. doi:10.1007/BF01560216

Berton, A., Longo, U. G., Candela, V., Greco, F., Martina, F. M., Quattrocchi, C. C., et al. (2020). Quantitative Evaluation of Meniscal Healing Process of Degenerative Meniscus Lesions Treated with Hyaluronic Acid: A Clinical and MRI Study. *J. Clin. Med.* 9 (7). doi:10.3390/jcm9072280

Bremander, A. B., Dahl, L. L., and Roos, E. M. (2007). Validity and Reliability of Functional Performance Tests in Meniscectomized Patients with or without Knee Osteoarthritis. *Scand. J. Med. Sci. Sports* 17 (2), 120–127. doi:10.1111/j.1600-0838.2006.00544.x

Brophy, R. H., Sandell, L. J., Cheverud, J. M., and Rai, M. F. (2017). Gene Expression in Human Meniscal Tears Has Limited Association with Early Degenerative Changes in Knee Articular Cartilage. *Connect. Tissue Res.* 58 (3-4), 295–304. doi:10.1080/03008207.2016.1211114

Bryceland, J. K., Powell, A. J., and Nunn, T. (2017). Knee Menisci. *Cartilage* 8 (2), 99–104. doi:10.1177/1947603516654945

Bulgheroni, P., Bulgheroni, M. V., Ronga, M., and Manelli, A. (2007). Gait Analysis of Pre- and post-meniscectomy Knee: a Prospective Study. *The Knee* 14 (6), 472–477. doi:10.1016/j.knee.2007.08.003

Chang, P. S., and Brophy, R. H. (2020). As Goes the Meniscus Goes the Knee. *Clin. Sports Med.* 39 (1), 29–36. doi:10.1016/j.csm.2019.08.001

Chen, C., Song, J., Qiu, J., and Zhao, J. (2020). Repair of a Meniscal Defect in a Rabbit Model through Use of a Thermosensitive, Injectable, *In Situ* Crosslinked Hydrogel with Encapsulated Bone Mesenchymal Stromal Cells and Transforming Growth Factor β1. *Am. J. Sports Med.* 48 (4), 884–894. doi:10.1177/0363546519898519

Chen, M., Feng, Z., Guo, W., Yang, D., Gao, S., Li, Y., et al. (2019). PCL-MECM-Based Hydrogel Hybrid Scaffolds and Meniscal Fibrochondrocytes Promote Whole Meniscus Regeneration in a Rabbit Meniscectomy Model. *ACS Appl. Mater. Inter.* 11 (44), 41626–41639. doi:10.1021/acsami.9b13611

Chivers, M. D., and Howitt, S. D. (2009). Anatomy and Physical Examination of the Knee Menisci: a Narrative Review of the Orthopedic Literature. *J. Can. Chiropr Assoc.* 53 (4), 319–333.

Clair, A. J., Kingery, M. T., Anil, U., Kenny, L., Kirsch, T., and Strauss, E. J. (2019). Alterations in Synovial Fluid Biomarker Levels in Knees with Meniscal Injury as Compared with Asymptomatic Contralateral Knees. *Am. J. Sports Med.* 47 (4), 847–856. doi:10.1177/0363546519825498

Cojocaru, D. G., Hondke, S., Krüger, J. P., Bosch, C., Croicu, C., Florescu, S., et al. (2020). Meniscus-shaped Cell-free Polyglycolic Acid Scaffold for Meniscal Repair in a Sheep Model. *J. Biomed. Mater. Res.* 108 (3), 809–818. doi:10.1002/jbm.b.34435

Darabos, N., Dovzak-Bajs, I., Bilić, V., Darabos, A., Popović, I., and Cengić, T. (2012). All-inside Arthroscopic Suturing Technique for Meniscal Ruptures. *Acta Clin. Croat.* 51 (1), 51–54.

Demirkıran, N. D., Havıtçıoğlu, H., Ziylan, A., Cankurt, Ü., and Hüsemoğlu, B. (2019). Novel Multilayer Meniscal Scaffold Provides Biomechanical and Histological Results Comparable to Polyurethane Scaffolds: An 8 Week Rabbit Study. *Acta Orthop. Traumatol. Turc* 53 (2), 120–128. doi:10.1016/j.aott.2019.02.004

Ding, N. (2021). SP600125 Restored Tumor Necrosis Factor-α-Induced Impaired Chondrogenesis in Bone Mesenchymal Stem Cells and its Anti-osteoarthritis Effect in Mice. *Stem Cell Dev* 30, 1028–1036. doi:10.1089/scd.2021.0146

Duan, A., Shen, K., Li, B., Li, C., Zhou, H., Kong, R., et al. (2021). Extracellular Vesicles Derived from LPS-Preconditioned Human Synovial Mesenchymal Stem Cells Inhibit Extracellular Matrix Degradation and Prevent Osteoarthritis of the Knee in a Mouse Model. *Stem Cel Res Ther* 12 (1), 427. doi:10.1186/s13287-021-02507-2

Erdemir, A. (2016). Open Knee: Open Source Modeling and Simulation in Knee Biomechanics. *J. Knee Surg.* 29 (2), 107–116. doi:10.1055/s-0035-1564600

Ericsson, Y. B., Roos, E. M., and Dahlberg, L. (2006). Muscle Strength, Functional Performance, and Self-Reported Outcomes Four Years after Arthroscopic Partial Meniscectomy in Middle-Aged Patients. *Arthritis Rheum.* 55 (6), 946–952. doi:10.1002/art.22346

Fan, C., Xu, Z., Wu, T., Cui, C., Liu, Y., Liu, B., et al. (2021). 3D Printing of Lubricative Stiff Supramolecular Polymer Hydrogels for Meniscus Replacement. *Biomater. Sci.* 9 (15), 5116–5126. doi:10.1039/d1bm00836f

Faunø, P., and Nielsen, A. B. (1992). Arthroscopic Partial Meniscectomy: a Long-Term Follow-Up. *Arthroscopy* 8 (3), 345–349.

Flanigan, D. C., Lin, F., Koh, J. L., and Zhang, L. Q. (2010). Articular Contact Pressures of Meniscal Repair Techniques at Various Knee Flexion Angles. *Orthopedics* 33 (7), 475. doi:10.3928/01477447-20100526-04

Fox, A. J. S., Wanivenhaus, F., Burge, A. J., Warren, R. F., and Rodeo, S. A. (2015). The Human Meniscus: a Review of Anatomy, Function, Injury, and Advances in Treatment. *Clin. Anat.* 28 (2), 269–287. doi:10.1002/ca.22456

Fu, X. N., Li, H. W., Du, N., Liang, X., He, S. H., Guo, K. J., et al. (2020). Erythropoietin Enhances Meniscal Regeneration and Prevents Osteoarthritis Formation in Mice. *Am. J. Transl Res.* 12 (10), 6464–6477.

Gee, S. M., Tennent, D. J., Cameron, K. L., and Posner, M. A. (2020). The Burden of Meniscus Injury in Young and Physically Active Populations. *Clin. Sports Med.* 39 (1), 13–27. doi:10.1016/j.csm.2019.08.008

Ghodbane, S. A., Brzezinski, A., Patel, J. M., Plaff, W. H., Marzano, K. N., Gatt, C. J., et al. (2019). Partial Meniscus Replacement with a Collagen-Hyaluronan Infused Three-Dimensional Printed Polymeric Scaffold. *Tissue Eng. Part. A.* 25 (5-6), 379–389. doi:10.1089/ten.TEA.2018.0160

Guo, W., Chen, M., Wang, Z., Tian, Y., Zheng, J., Gao, S., et al. (2021). 3D-printed Cell-free PCL-MECM Scaffold with Biomimetic Micro-structure and Micro-environment to Enhance *In Situ* Meniscus Regeneration. *Bioactive Mater.* 6 (10), 3620–3633. doi:10.1016/j.bioactmat.2021.02.019

Hagmeijer, M. H., Kennedy, N. I., Tagliero, A. J., Levy, B. A., Stuart, M. J., Saris, D. B. F., et al. (2019). Long-term Results after Repair of Isolated Meniscal Tears Among Patients Aged 18 Years and Younger: An 18-Year Follow-Up Study. *Am. J. Sports Med.* 47 (4), 799–806. doi:10.1177/0363546519826088

Hatsushika, D., Muneta, T., Nakamura, T., Horie, M., Koga, H., Nakagawa, Y., et al. (2014). Repetitive Allogeneic Intraarticular Injections of Synovial Mesenchymal Stem Cells Promote Meniscus Regeneration in a Porcine Massive Meniscus Defect Model. *Osteoarthritis and Cartilage* 22 (7), 941–950. doi:10.1016/j.joca.2014.04.028

Hede, A., Larsen, E., and Sandberg, H. (1992). The Long Term Outcome of Open Total and Partial Meniscectomy Related to the Quantity and Site of the Meniscus Removed. *Int. Orthopaedics* 16 (2), 122–125. doi:10.1007/bf00180200

Hennerbichler, A., Moutos, F. T., Hennerbichler, D., Weinberg, J. B., and Guilak, F. (2007). Interleukin-1 and Tumor Necrosis Factor Alpha Inhibit Repair of the Porcine Meniscus *In Vitro*. *Osteoarthritis and Cartilage* 15 (9), 1053–1060. doi:10.1016/j.joca.2007.03.003

Houck, D. A., Kraeutler, M. J., Belk, J. W., McCarty, E. C., and Bravman, J. T. (2018). Similar Clinical Outcomes Following Collagen or Polyurethane Meniscal Scaffold Implantation: a Systematic Review. *Knee Surg. Sports Traumatol. Arthrosc.* 26 (8), 2259–2269. doi:10.1007/s00167-018-4838-1

Hyodo, K., Kanamori, A., Kadone, H., Takahashi, T., Kajiwara, M., and Yamazaki, M. (2020). Gait Analysis Comparing Kinematic, Kinetic, and Muscle Activation Data of Modern and Conventional Total Knee Arthroplasty. *Arthroplasty Today* 6 (3), 338–342. doi:10.1016/j.artd.2020.03.011

Jacobs, B. Y., Kloefkorn, H. E., and Allen, K. D. (2014). Gait Analysis Methods for Rodent Models of Osteoarthritis. *Curr. Pain Headache Rep.* 18 (10), 456. doi:10.1007/s11916-014-0456-x

Jørgensen, U., Sonne-Holm, S., Lauridsen, F., and Rosenklint, A. (1987). Long-term Follow-Up of Meniscectomy in Athletes. A Prospective Longitudinal Study. *J. Bone Jt. Surg Br* 69 (1), 80–83. doi:10.1302/0301-620X.69B1.3818740

Karamchedu, N. P., Murray, M. M., Sieker, J. T., Proffen, B. L., Portilla, G., Costa, M. Q., et al. (2021). Bridge-Enhanced Anterior Cruciate Ligament Repair Leads to Greater Limb Asymmetry and Less Cartilage Damage Than Untreated ACL Transection or ACL Reconstruction in the Porcine Model. *Am. J. Sports Med.* 49 (3), 667–674. doi:10.1177/0363546521989265

Karsdal, M. A., Nielsen, M. J., Sand, J. M., Henriksen, K., Genovese, F., Bay-Jensen, A.-C., et al. (2013). Extracellular Matrix Remodeling: The Common Denominator in Connective Tissue DiseasesPossibilities for Evaluation and Current Understanding of the Matrix as More Than a Passive Architecture, but a Key Player in Tissue Failure. *ASSAY Drug Development Tech.* 11 (2), 70–92. doi:10.1089/adt.2012.474

Karsdal, M. A., Woodworth, T., Henriksen, K., Maksymowych, W. P., Genant, H., Vergnaud, P., et al. (2011). Biochemical Markers of Ongoing Joint Damage in Rheumatoid Arthritis - Current and Future Applications, Limitations and Opportunities. *Arthritis Res. Ther.* 13 (2), 215. doi:10.1186/ar3280

Katz, J. N., Brophy, R. H., Chaisson, C. E., de Chaves, L., Cole, B. J., Dahm, D. L., et al. (2013). Surgery versus Physical Therapy for a Meniscal Tear and Osteoarthritis. *N. Engl. J. Med.* 368 (18), 1675–1684. doi:10.1056/NEJMoa1301408

Kennedy, M. I., Strauss, M., and LaPrade, R. F. (2020). Injury of the Meniscus Root. *Clin. Sports Med.* 39 (1), 57–68. doi:10.1016/j.csm.2019.08.009

Kim, J.-A., An, Y.-H., Yim, H.-G., Han, W.-J., Park, Y.-B., Park, H. J., et al. (2021). Injectable Fibrin/Polyethylene Oxide Semi-IPN Hydrogel for a Segmental Meniscal Defect Regeneration. *Am. J. Sports Med.* 49 (6), 1538–1550. doi:10.1177/0363546521998021

Koch, M., Hammer, S., Fuellerer, J., Lang, S., Pfeifer, C. G., Pattappa, G., et al. (2019). Bone Marrow Aspirate Concentrate for the Treatment of Avascular Meniscus Tears in a One-step Procedure-Evaluation of an *In Vivo* Model. *Int. J. Mol. Sci.* 20 (5). doi:10.3390/ijms20051120

Koff, M. F., Shah, P., Pownder, S., Romero, B., Williams, R., Gilbert, S., et al. (2013). Correlation of Meniscal T2* with Multiphoton Microscopy, and Change of Articular Cartilage T2 in an Ovine Model of Meniscal Repair. *Osteoarthritis and Cartilage* 21 (8), 1083–1091. doi:10.1016/j.joca.2013.04.020

Kondo, S., Muneta, T., Nakagawa, Y., Koga, H., Watanabe, T., Tsuji, K., et al. (2017). Transplantation of Autologous Synovial Mesenchymal Stem Cells Promotes Meniscus Regeneration in Aged Primates. *J. Orthop. Res.* 35 (6), 1274–1282. doi:10.1002/jor.23211

Korpershoek, J. V., de Windt, T. S., Hagmeijer, M. H., Vonk, L. A., and Saris, D. B. (2017). Cell-Based Meniscus Repair and Regeneration: At the Brink of Clinical Translation?: A Systematic Review of Preclinical Studies. *Orthop. J. Sports Med.* 5 (2), 2325967117690131. doi:10.1177/2325967117690131

Kurnaz, R., Balta, O., and Balta, O. (2020). Effect of Platelet-Rich Plasma and Platelet-Rich Fibrin Matrix on Healing of Vertical Meniscal Tears in a Rabbit Model. *Aott* 54 (2), 186–195. doi:10.5152/j.aott.2020.02.20

Lee, S. R., Kim, J. G., and Nam, S. W. (2012). The Tips and Pitfalls of Meniscus Allograft Transplantation. *Knee Surg. Relat. Res.* 24 (3), 137–145. doi:10.5792/ksrr.2012.24.3.137

Lepetsos, P., and Papavassiliou, A. G. (2016). ROS/oxidative Stress Signaling in Osteoarthritis. *Biochim. Biophys. Acta (Bba) - Mol. Basis Dis.* 1862 (4), 576–591. doi:10.1016/j.bbadis.2016.01.003

Li, Y., Chen, M., Yan, J., Zhou, W., Gao, S., Liu, S., et al. (2021). Tannic acid/Sr2+-Coated Silk/graphene Oxide-Based Meniscus Scaffold with Anti-inflammatory and Anti-ROS Functions for Cartilage protection and Delaying Osteoarthritis. *Acta Biomater.* 126, 119–131. doi:10.1016/j.actbio.2021.02.046

Li, Y., Chen, M., Zhou, W., Gao, S., Luo, X., Peng, L., et al. (2020). Cell-free 3D Wet-Electrospun PCL/silk fibroin/Sr2+ Scaffold Promotes Successful Total Meniscus Regeneration in a Rabbit Model. *Acta Biomater.* 113, 196–209. doi:10.1016/j.actbio.2020.06.017

Li, Z., Wu, N., Cheng, J., Sun, M., Yang, P., Zhao, F., et al. (2020). Biomechanically, Structurally and Functionally Meticulously Tailored Polycaprolactone/silk Fibroin Scaffold for Meniscus Regeneration. *Theranostics* 10 (11), 5090–5106. doi:10.7150/thno.44270

Liu, B., Goode, A. P., Carter, T. E., Utturkar, G. M., Huebner, J. L., Taylor, D. C., et al. (2017). Matrix Metalloproteinase Activity and Prostaglandin E2 Are Elevated in the Synovial Fluid of Meniscus Tear Patients. *Connect. Tissue Res.* 58 (3-4), 305–316. doi:10.1080/03008207.2016.1256391

Liu, F., Xu, H., and Huang, H. (2019). A Novel Kartogenin-Platelet-Rich Plasma Gel Enhances Chondrogenesis of Bone Marrow Mesenchymal Stem Cells *In Vitro* and Promotes Wounded Meniscus Healing *In Vivo*. *Stem Cel Res Ther* 10 (1), 201. doi:10.1186/s13287-019-1314-x

Liu, X., Huang, H., Ren, S., Rong, Q., and Ao, Y. (2020). Use of the Normalcy index for the Assessment of Abnormal Gait in the Anterior Cruciate Ligament Deficiency Combined with Meniscus Injury. *Computer Methods Biomech. Biomed. Eng.* 23 (14), 1102–1108. doi:10.1080/10255842.2020.1789119

Longo, U. G., Ciuffreda, M., Candela, V., Rizzello, G., D'Andrea, V., Mannering, N., et al. (2019). Knee Osteoarthritis after Arthroscopic Partial Meniscectomy: Prevalence and Progression of Radiographic Changes after 5 to 12 Years Compared with Contralateral Knee. *J. Knee Surg.* 32 (5), 407–413. doi:10.1055/s-0038-1646926

López-Franco, M., López-Franco, O., Murciano-Antón, M. A., Cañamero-Vaquero, M., Fernández-Aceñero, M. J., Herrero-Beaumont, G., et al. (2016). Meniscal Degeneration in Human Knee Osteoarthritis: *In Situ* Hybridization and Immunohistochemistry Study. *Arch. Orthopaedic Trauma Surg.* 136 (2), 175–183. doi:10.1007/s00402-015-2378-4

Lucidi, G. A., Grassi, A., Al-Zu'bi, B. B. H., Macchiarola, L., Agostinone, P., Marcacci, M., et al. (2021). Satisfactory Clinical Results and Low Failure Rate of Medial Collagen Meniscus Implant (CMI) at a Minimum 20 Years of Follow-Up. *Knee Surg. Sports Traumatol. Arthrosc.* 29 (12), 4270–4277. doi:10.1007/s00167-021-06556-1

Majewski, M., Susanne, H., and Klaus, S. (2006). Epidemiology of Athletic Knee Injuries: A 10-year Study. *The Knee* 13 (3), 184–188. doi:10.1016/j.knee.2006.01.005

Makris, E. A., Hadidi, P., and Athanasiou, K. A. (2011). The Knee Meniscus: Structure-Function, Pathophysiology, Current Repair Techniques, and Prospects for Regeneration. *Biomaterials* 32 (30), 7411–7431. doi:10.1016/j.biomaterials.2011.06.037

McDermott, I. D., and Amis, A. A. (2006). The Consequences of Meniscectomy. *J. Bone Jt. Surg. Br. volume* 88-B (12), 1549–1556. doi:10.1302/0301-620x.88b12.18140

McDermott, I. D., Sharifi, F., Bull, A. M. J., Gupte, C. M., Thomas, R. W., and Amis, A. A. (2004). An Anatomical Study of Meniscal Allograft Sizing. *Knee Surg. Sports Traumatol. Arthrosc.* 12 (2), 130–135. doi:10.1007/s00167-003-0366-7

McNulty, A. L., and Guilak, F. (2015). Mechanobiology of the Meniscus. *J. Biomech.* 48 (8), 1469–1478. doi:10.1016/j.jbiomech.2015.02.008

Milachowski, K. A., Weismeier, K., and Wirth, C. J. (1989). Homologous Meniscus Transplantation. Experimental and Clinical Results. *Int. Orthop.* 13 (1), 1–11. doi:10.1007/BF00266715

Nakagawa, Y., Fortier, L. A., Mao, J. J., Lee, C. H., Goodale, M. B., Koff, M. F., et al. (2019). Long-term Evaluation of Meniscal Tissue Formation in 3-Dimensional-Printed Scaffolds with Sequential Release of Connective Tissue Growth Factor and TGF-B3 in an Ovine Model. *Am. J. Sports Med.* 47 (11), 2596–2607. doi:10.1177/0363546519865513

Nakagawa, Y., Muneta, T., Kondo, S., Mizuno, M., Takakuda, K., Ichinose, S., et al. (2015). Synovial Mesenchymal Stem Cells Promote Healing after Meniscal Repair in Microminipigs. *Osteoarthritis and Cartilage* 23 (6), 1007–1017. doi:10.1016/j.joca.2015.02.008

Nakagawa, Y., Sekiya, I., Kondo, S., Tabuchi, T., Ichinose, S., Koga, H., et al. (2016). Relationship between MRIT1rho Value and Histological Findings of Intact and Radially Incised Menisci in Microminipigs. *J. Magn. Reson. Imaging* 43 (2), 434–445. doi:10.1002/jmri.24988

Narez, G. E., Brown, G., Herrick, A., Ek, R. J., Dejardin, L., Wei, F., et al. (2021). Assessment of Changes in the Meniscus and Subchondral Bone in a Novel Closed-Joint Impact and Surgical Reconstruction Lapine Model. *J. Biomech.* 126, 110630. doi:10.1016/j.jbiomech.2021.110630

Newberry, J., Desai, S., Adler, C., Li, N., Karamchedu, N. P., Fleming, B. C., et al. (2020). SDF-1 Preconditioned HPC Scaffolds Mobilize Cartilage-Derived Progenitors and Stimulate Meniscal Fibrocartilage Repair in Human Explant Tissue Culture. *Connect. Tissue Res.* 61 (3-4), 338–348. doi:10.1080/03008207.2019.1689966

Nishida, Y., Hashimoto, Y., Orita, K., Nishino, K., Kinoshita, T., and Nakamura, H. (2020). Intra-Articular Injection of Stromal Cell-Derived Factor 1α Promotes Meniscal Healing via Macrophage and Mesenchymal Stem Cell Accumulation in a Rat Meniscal Defect Model. *Int. J. Mol. Sci.* 21 (15). doi:10.3390/ijms21155454

Okuno, N., Otsuki, S., Aoyama, J., Nakagawa, K., Murakami, T., Ikeda, K., et al. (2021). Feasibility of a Self-assembling Peptide Hydrogel Scaffold for Meniscal Defect: An *In Vivo* Study in a Rabbit Model. *J. Orthop. Res.* 39 (1), 165–176. doi:10.1002/jor.24841

Osawa, A., Harner, C. D., Gharaibeh, B., Matsumoto, T., Mifune, Y., Kopf, S., et al. (2013). The Use of Blood Vessel-Derived Stem Cells for Meniscal Regeneration

and Repair. *Med. Sci. Sports Exerc.* 45 (5), 813–823. doi:10.1249/mss.0b013e31827d1e06

Otsuki, S., Nakagawa, K., Murakami, T., Sezaki, S., Sato, H., Suzuki, M., et al. (2019). Evaluation of Meniscal Regeneration in a Mini Pig Model Treated with a Novel Polyglycolic Acid Meniscal Scaffold. *Am. J. Sports Med.* 47 (8), 1804–1815. doi:10.1177/0363546519850578

Ozeki, N., Kohno, Y., Kushida, Y., Watanabe, N., Mizuno, M., Katano, H., et al. (2021). Synovial Mesenchymal Stem Cells Promote the Meniscus Repair in a Novel Pig Meniscus Injury Model. *J. Orthop. Res.* 39 (1), 177–183. doi:10.1002/jor.24846

Pan, Z., Wu, Y., Zhang, X., Fu, Q., Li, J., Yang, Y., et al. (2017). Delivery of Epidermal Growth Factor Receptor Inhibitor via a Customized Collagen Scaffold Promotes Meniscal Defect Regeneration in a Rabbit Model. *Acta Biomater.* 62, 210–221. doi:10.1016/j.actbio.2017.07.008

Papalia, R., Del Buono, A., Osti, L., Denaro, V., and Maffulli, N. (2011). Meniscectomy as a Risk Factor for Knee Osteoarthritis: a Systematic Review. *Br. Med. Bull.* 99, 89–106. doi:10.1093/bmb/ldq043

Peloquin, J. M., Santare, M. H., and Elliott, D. M. (2016). Advances in Quantification of Meniscus Tensile Mechanics Including Nonlinearity, Yield, and Failure. *J. Biomech. Eng.* 138 (2), 021002. doi:10.1115/1.4032354

Pereira, H., Fatih Cengiz, I., Gomes, S., Espregueira-Mendes, J., Ripoll, P. L., Monllau, J. C., et al. (2019). Meniscal Allograft Transplants and New Scaffolding Techniques. *EFORT Open Rev.* 4 (6), 279–295. doi:10.1302/2058-5241.4.180103

Rai, M. F., Brophy, R. H., and Rosen, V. (2020). Molecular Biology of Meniscus Pathology: Lessons Learned from Translational Studies and Mouse Models. *J. Orthop. Res.* 38 (9), 1895–1904. doi:10.1002/jor.24630

Rangger, C., Kathrein, A., Klestil, T., and Glötzer, W. (1997). Partial Meniscectomy and Osteoarthritis. *Sports Med.* 23 (1), 61–68. doi:10.2165/00007256-199723010-00006

Roberts, S., Evans, H., Wright, K., van Niekerk, L., Caterson, B., Richardson, J. B., et al. (2015). ADAMTS-4 Activity in Synovial Fluid as a Biomarker of Inflammation and Effusion. *Osteoarthritis and Cartilage* 23 (9), 1622–1626. doi:10.1016/j.joca.2015.05.006

Rodeo, S. A. (2000). Arthroscopic Meniscal Repair with Use of the Outside-In Technique. *Instr. Course Lect* 49, 195–206.

Rodeo, S. A. (2001). Meniscal Allografts-Where Do We Stand? *Am. J. Sports Med.* 29 (2), 246–261. doi:10.1177/03635465010290022401

Roller, B. L., Monibi, F., Stoker, A. M., Bal, B. S., and Cook, J. L. (2016). Identification of Novel Synovial Fluid Biomarkers Associated with Meniscal Pathology. *J. Knee Surg.* 29 (1), 47–62. doi:10.1055/s-0034-1394165

Ruiz-Ibán, M. Á., Díaz-Heredia, J., García-Gómez, I., Gonzalez-Lizán, F., Elías-Martín, E., Abraira, V., et al. (2011). The Effect of the Addition of Adipose-Derived Mesenchymal Stem Cells to a Meniscal Repair in the Avascular Zone: an Experimental Study in Rabbits. *Arthroscopy* 27 (12), 1688–1696. doi:10.1016/j.arthro.2011.06.041

Schreiner, A. J., Stannard, J. P., Cook, C. R., Bozynski, C. C., Kuroki, K., Stoker, A. M., et al. (2021). Comparison of Meniscal Allograft Transplantation Techniques Using a Preclinical Canine Model. *J. Orthop. Res.* 39 (1), 154–164. doi:10.1002/jor.24668

Searle, H., Asopa, V., Coleman, S., and McDermott, I. (2020). The Results of Meniscal Allograft Transplantation Surgery: what Is success? *BMC Musculoskelet. Disord.* 21 (1), 159. doi:10.1186/s12891-020-3165-0

Shaffer, B., Kennedy, S., Klimkiewicz, J., and Yao, L. (2000). Preoperative Sizing of Meniscal Allografts in Meniscus Transplantation. *Am. J. Sports Med.* 28 (4), 524–533. doi:10.1177/03635465000280041301

Shen, S., Yang, Y., Shen, P., Ma, J., Fang, B., Wang, Q., et al. (2021). circPDE4B Prevents Articular Cartilage Degeneration and Promotes Repair by Acting as a Scaffold for RIC8A and MID1. *Ann. Rheum. Dis.* 80 (9), 1209–1219. doi:10.1136/annrheumdis-2021-219969

Shen, W., Chen, J., Zhu, T., Yin, Z., Chen, X., Chen, L., et al. (2013). Osteoarthritis Prevention through Meniscal Regeneration Induced by Intra-articular Injection of Meniscus Stem Cells. *Stem Cell Development* 22 (14), 2071–2082. doi:10.1089/scd.2012.0563

Sherman, S. L., DiPaolo, Z. J., Ray, T. E., Sachs, B. M., and Oladeji, L. O. (2020). Meniscus Injuries. *Clin. Sports Med.* 39 (1), 165–183. doi:10.1016/j.csm.2019.08.004

Shimomura, K., Hamamoto, S., Hart, D. A., Yoshikawa, H., and Nakamura, N. (2018). Meniscal Repair and Regeneration: Current Strategies and Future Perspectives. *J. Clin. Orthopaedics Trauma* 9 (3), 247–253. doi:10.1016/j.jcot.2018.07.008

Shimomura, K., Rothrauff, B. B., Hart, D. A., Hamamoto, S., Kobayashi, M., Yoshikawa, H., et al. (2019). Enhanced Repair of Meniscal Hoop Structure Injuries Using an Aligned Electrospun Nanofibrous Scaffold Combined with a Mesenchymal Stem Cell-Derived Tissue Engineered Construct. *Biomaterials* 192, 346–354. doi:10.1016/j.biomaterials.2018.11.009

Snoeker, B., Turkiewicz, A., Magnusson, K., Frobell, R., Yu, D., Peat, G., et al. (2020). Risk of Knee Osteoarthritis after Different Types of Knee Injuries in Young Adults: a Population-Based Cohort Study. *Br. J. Sports Med.* 54 (12), 725–730. doi:10.1136/bjsports-2019-100959

Steenbrugge, F., Verdonk, R., Hrel, C., and Verstraete, K. (2004). Arthroscopic Meniscus Repair: Inside-Out Technique vs. Biofix Meniscus Arrow. *Knee Surg. Sports Traumatol. Arthrosc.* 12 (1), 43–49. doi:10.1007/s00167-003-0446-8

Stein, S. E. C., von Luebken, F., Warnecke, D., Gentilini, C., Skaer, N., Walker, R., et al. (2019). The challenge of Implant Integration in Partial Meniscal Replacement: an Experimental Study on a Silk Fibroin Scaffold in Sheep. *Knee Surg. Sports Traumatol. Arthrosc.* 27 (2), 369–380. doi:10.1007/s00167-018-5160-7

Strauss, E., Caborn, D. N. M., Nyland, J., Horng, S., Chagnon, M., and Wilke, D. (2019). Tissue Healing Following Segmental Meniscal Allograft Transplantation: a Pilot Study. *Knee Surg. Sports Traumatol. Arthrosc.* 27 (6), 1931–1938. doi:10.1007/s00167-019-05355-z

Sun, Y., Zhang, Y., Wu, Q., Gao, F., Wei, Y., Ma, Y., et al. (2021). 3D-bioprinting Ready-To-Implant Anisotropic Menisci Recapitulate Healthy Meniscus Phenotype and Prevent Secondary Joint Degeneration. *Theranostics* 11 (11), 5160–5173. doi:10.7150/thno.54864

Takata, Y., Nakase, J., Shimozaki, K., Asai, K., and Tsuchiya, H. (2020). Autologous Adipose-Derived Stem Cell Sheet Has Meniscus Regeneration-Promoting Effects in a Rabbit Model. *Arthrosc. J. Arthroscopic Relat. Surg.* 36 (10), 2698–2707. doi:10.1016/j.arthro.2020.06.004

Tarafder, S., Park, G., and Lee, C. H. (2020). Explant Models for Meniscus Metabolism, Injury, Repair, and Healing. *Connect. Tissue Res.* 61 (3-4), 292–303. doi:10.1080/03008207.2019.1702031

Tarafder, S., Gulko, J., Sim, K. H., Yang, J., Cook, J. L., and Lee, C. H. (2018). Engineered Healing of Avascular Meniscus Tears by Stem Cell Recruitment. *Sci. Rep.* 8 (1), 8150. doi:10.1038/s41598-018-26545-8

Terry Canale S, B. J. (2012). *Campbell's Operative Orthopaedics*, Vol. 12. St. Louis, MO: Elsevier.

Trentacosta, N., Graham, W. C., and Gersoff, W. K. (2016). Meniscal Allograft Transplantation: State of the Art. *Sports Med. Arthrosc. Rev.* 24 (2), e23–e33. doi:10.1097/jsa.0000000000000107

Vadher, S. P., Nayeb-Hashemi, H., Canavan, P. K., and Warner, G. M. (2006). Finite Element Modeling Following Partial Meniscectomy: Effect of Various Size of Resection. *Conf. Proc. IEEE Eng. Med. Biol. Soc.* 2006, 2098–2101. doi:10.1109/IEMBS.2006.259378

Wei, Y., Sun, H., Gui, Y., Yao, L., Han, L., Yu, W., et al. (2021). The Critical Role of Hedgehog-Responsive Mesenchymal Progenitors in Meniscus Development and Injury Repair. *Elife* 10. doi:10.7554/elife.62917

Wells, M. E., Scanaliato, J. P., Dunn, J. C., and Garcia, E. S. J. (2021). Meniscal Injuries: Mechanism and Classification. *Sports Med. Arthrosc. Rev.* 29 (3), 154–157. doi:10.1097/jsa.0000000000000311

Wilusz, R. E., Weinberg, J. B., Guilak, F., and McNulty, A. L. (2008). Inhibition of Integrative Repair of the Meniscus Following Acute Exposure to Interleukin-1 *In Vitro*. *J. Orthop. Res.* 26 (4), 504–512. doi:10.1002/jor.20538

Wu, Y., Hong, J., Jiang, G., Li, S., Chen, S., Chen, W., et al. (2019). Platelet-rich Gel-Incorporated Silk Scaffold Promotes Meniscus Regeneration in a Rabbit Total Meniscectomy Model. *Regenerative Med.* 14 (8), 753–768. doi:10.2217/rme-2018-0087

Yamasaki, S., Hashimoto, Y., Nishida, Y., Teraoka, T., Terai, S., Takigami, J., et al. (2020). Assessment of Meniscal Healing Status by Magnetic Resonance Imaging T2 Mapping after Meniscal Repair. *Am. J. Sports Med.* 48 (4), 853–860. doi:10.1177/0363546520904680

Yan, R., Chen, Y., Gu, Y., Tang, C., Huang, J., Hu, Y., et al. (2019). A Collagen-Coated Sponge Silk Scaffold for Functional Meniscus Regeneration. *J. Tissue Eng. Regen. Med.* 13 (2), 156–173. doi:10.1002/term.2777

Zellner, J., Hierl, K., Mueller, M., Pfeifer, C., Berner, A., Dienstknecht, T., et al. (2013). Stem Cell-Based Tissue-Engineering for Treatment of Meniscal Tears in the Avascular Zone. *J. Biomed. Mater. Res.* 101 (7), 1133–1142. doi:10.1002/jbm.b.32922

Zhang, L., Liu, G., Han, B., Wang, Z., Yan, Y., Ma, J., et al. (2020). Knee Joint Biomechanics in Physiological Conditions and How Pathologies Can Affect it: A Systematic Review. *Appl. Bionics Biomech.* 2020, 7451683. doi:10.1155/2020/7451683

Zhang, Z.-Z., Zhou, Y.-F., Li, W.-P., Jiang, C., Chen, Z., Luo, H., et al. (2019). Local Administration of Magnesium Promotes Meniscal Healing through Homing of Endogenous Stem Cells: A Proof-Of-Concept Study. *Am. J. Sports Med.* 47 (4), 954–967. doi:10.1177/0363546518820076

Zhao, W., Zou, T., Cui, H., Lv, Y., Gao, D., Ruan, C., et al. (2020). Parathyroid Hormone (1-34) Promotes the Effects of 3D Printed Scaffold-Seeded Bone Marrow Mesenchymal Stem Cells on Meniscus Regeneration. *Stem Cel Res Ther* 11 (1), 328. doi:10.1186/s13287-020-01845-x

Zhong, G., Yao, J., Huang, X., Luo, Y., Wang, M., Han, J., et al. (2020). Injectable ECM Hydrogel for Delivery of BMSCs Enabled Full-Thickness Meniscus Repair in an Orthotopic Rat Model. *Bioactive Mater.* 5 (4), 871–879. doi:10.1016/j.bioactmat.2020.06.008

Conflict of Interest: The authors declare that the research was conducted in the absence of any commercial or financial relationships that could be construed as a potential conflict of interest.

frontiers in Bioengineering and Biotechnology

ORIGINAL RESEARCH
published: 02 February 2022
doi: 10.3389/fbioe.2022.810705

Pneumatospinning Biomimetic Scaffolds for Meniscus Tissue Engineering

Erik W. Dorthé[1], *Austin B. Williams*[2], *Shawn P. Grogan*[1] *and Darryl D. D'Lima*[1]*

[1]Department of Orthopaedics, Shiley Center for Orthopaedic Research and Education, Scripps Health, San Diego, CA, United States, [2]Intitute for Biomedical Sciences, San Diego, CA, United States

Nanofibrous scaffolds fabricated via electrospinning have been proposed for meniscus tissue regeneration. However, the electrospinning process is slow, and can only generate scaffolds of limited thickness with densely packed fibers, which limits cell distribution within the scaffold. In this study, we explored whether pneumatospinning could produce thicker collagen type I fibrous scaffolds with higher porosity, that can support cell infiltration and neo-fibrocartilage tissue formation for meniscus tissue engineering. We pneumatospun scaffolds with solutions of collagen type I with thicknesses of approximately 1 mm in 2 h. Scanning electron microscopy revealed a mix of fiber sizes with diameters ranging from 1 to 30 µm. The collagen scaffold porosity was approximately 48% with pores ranging from 7.4 to 100.7 µm. The elastic modulus of glutaraldehyde crosslinked collagen scaffolds was approximately 45 MPa, when dry, which reduced after hydration to 0.1 MPa. Mesenchymal stem cells obtained from the infrapatellar fat pad were seeded in the scaffold with high viability (>70%). Scaffolds seeded with adipose-derived stem cells and cultured for 3 weeks exhibited a fibrocartilage meniscus-like phenotype (expressing COL1A1, COL2A1 and COMP). *Ex vivo* implantation in healthy bovine and arthritic human meniscal explants resulted in the development of fibrocartilage-like neotissues that integrated with the host tissue with deposition of glycosaminoglycans and collagens type I and II. Our proof-of-concept study indicates that pneumatospinning is a promising approach to produce thicker biomimetic scaffolds more efficiently that electrospinning, and with a porosity that supports cell growth and neo-tissue formation using a clinically relevant cell source.

Keywords: pneumatospinning, solution blow spinning, electrospinning, fibrous scaffolds, infra patella fat pad, meniscal tears, meniscal repair

OPEN ACCESS

Edited by:
Jay Patel,
Emory University, United States

Reviewed by:
Amy McNulty,
Duke University, United States
Axel Moore,
University of Delaware, United States

***Correspondence:**
Darryl D. D'Lima
ddlima@scripps.edu

Specialty section:
This article was submitted to Biomechanics, a section of the journal Frontiers in Bioengineering and Biotechnology

Received: *07 November 2021*
Accepted: *10 January 2022*
Published: *02 February 2022*

Citation:
Dorthé EW, Williams AB, Grogan SP and D'Lima DD (2022) Pneumatospinning Biomimetic Scaffolds for Meniscus Tissue Engineering. Front. Bioeng. Biotechnol. 10:810705. doi: 10.3389/fbioe.2022.810705

INTRODUCTION

Menisci are an essential tissue in knee joints that contribute to load distribution, knee stability, and protect articular cartilage during normal activity. Injuries to menisci are common, with an estimated incidence between 600,000 and 850,000 in the United States alone, 90% of which require surgical intervention (Milachowski et al., 1989; DeHaven, 1999; Turman and Diduch, 2008). Tears occurring in the vascular zone have a higher rate of repair *via* surgery (Makris et al., 2011). Very few tears in the avascular zone heal, and around a third of repairs fail. Smaller tears are frequently repaired using sutures, screws, arrows or darts (Fillingham et al., 2017; Ardizzone et al., 2020). However, many tears are too complex or extensive to repair and thus most surgeries involve partial, subtotal or total

meniscectomy (Ford et al., 2005; Fetzer et al., 2009). Loss of meniscal tissue alters joint loading dynamics, leading to joint destabilization and finally a progression to osteoarthritis (OA) (Englund et al., 2001; Lohmander et al., 2007; Rai et al., 2020; Rodeo et al., 2020). To address large tears or for the replacement of menisci, meniscal substitutions have been proposed for partial and total meniscus replacement (Winkler et al., 2020).

Efforts towards engineering meniscus tissues typically combine cells (Angele et al., 2021) with a variety of diverse natural and synthetic scaffolds (Kwon et al., 2019; Li et al., 2021). However, a central feature that underlies the load bearing role of meniscus is the unique organization of collagen fibers, which is an essential requirement for a functional engineered meniscus. To this end, we, and other groups, have applied electrospinning (ES) to create nanofibrous scaffolds that emulate the meniscus collagen fibrillar matrix using natural and synthetic polymer (Grogan et al., 2020; Wang et al., 2021).

Examples of ES scaffolds explored for meniscus regeneration include synthetic polymers such as polylactic acid (PLA) (Baek et al., 2015), polycaprolactone (PCL) (Baker and Mauck, 2007; Ionescu et al., 2012; Gopinathan et al., 2015), natural polymers such as collagen (Baek et al., 2016, Baek et al., 2018), or combinations such as PCL and silk fibroin (Li et al., 2020), poly(lactic-co-glycolic) acid (PLGA) and gelatin (Li et al., 2016), or PLA and collagen (Baek et al., 2019). These electrospun scaffolds were biocompatible, supported attachment of a variety of cell types including meniscus fibroblasts (Kang et al., 2006; Martinek et al., 2006; Puetzer et al., 2015; Baek et al., 2020), various sources of MSC (Pak et al., 2014; Oda et al., 2015; Chew et al., 2017; Baek et al., 2018; Sasaki et al., 2018; Rothrauff et al., 2019) and synovial cells (Horie et al., 2009; Kondo et al., 2019; Sekiya et al., 2019), and lead to neo-tissue formation and repair of *ex vivo* meniscal tears (Baek et al., 2016; Baek et al., 2019). Electrospun scaffolds show promise in terms of cytocompatibility and neotissue formation, however, electrospinning often requires days to generate a scaffold of even a few millimeters in thickness (Dos Santos et al., 2020). Layering of ES scaffolds (Baek et al., 2015; Fisher et al., 2015) or incorporating ES collagen micro/nanofibers within a macroporous PLA/PLGA foam have been described (Bahcecioglu et al., 2014) to generate thicker constructs. However, the issue of delamination under loading remains a concern. Moreover, the highly dense nature of the fibers comprising the scaffold hinder efficient cell seeding and migration throughout the scaffold. To overcome this issue, strategies have been adopted to increase scaffold porosity by including water soluble sacrificial fibers (Baker et al., 2012; Shimomura et al., 2015), or by incorporating growth factors or chemoattractants within the scaffold to facilitate cell migration, support proliferation and tissue formation (Qu et al., 2017; Qu et al., 2019; Baek et al., 2019).

Solution blow spinning or pneumatospinning is an alternate method of generating fibrous scaffolds. Pressurized gas driven through an outer nozzle generates a stream of polymer solution fed through the inner nozzle of a coaxial system (Dos Santos et al., 2020). Pneumatospinning relies on gas pressure instead of an electric charge, which facilitates the fabrication of thicker constructs without the insulating effect that limits the thickness of electrospun constructs. Pneumatospinning is reportedly simpler, safer, more efficient, and can be achieved with less expensive and commercially available tools and therefore has the potential to overcome some of the limitations of electrospinning for meniscal repair (Behrens et al., 2014; Daristotle et al., 2016; Polk et al., 2018; Molde et al., 2020).

A wide range of materials have been pneumatospun to create nano- and microfibrous scaffolds. While pneumatospinning of synthetic polymers such as polyurethane (PU), polymethylmethacrylate, polyvinyl alcohol, PLA, and PCL is most commonly reported (Medeiros et al., 2009; Oliveira et al., 2011; Srinivasan et al., 2011; Behrens et al., 2014; Santos et al., 2016; Tomecka et al., 2017; Akentjew et al., 2019; Kopec et al., 2020); natural polymers such as silk fibroin and collagen have also been successfully pneumatospun (Magaz et al., 2018; Polk et al., 2018).

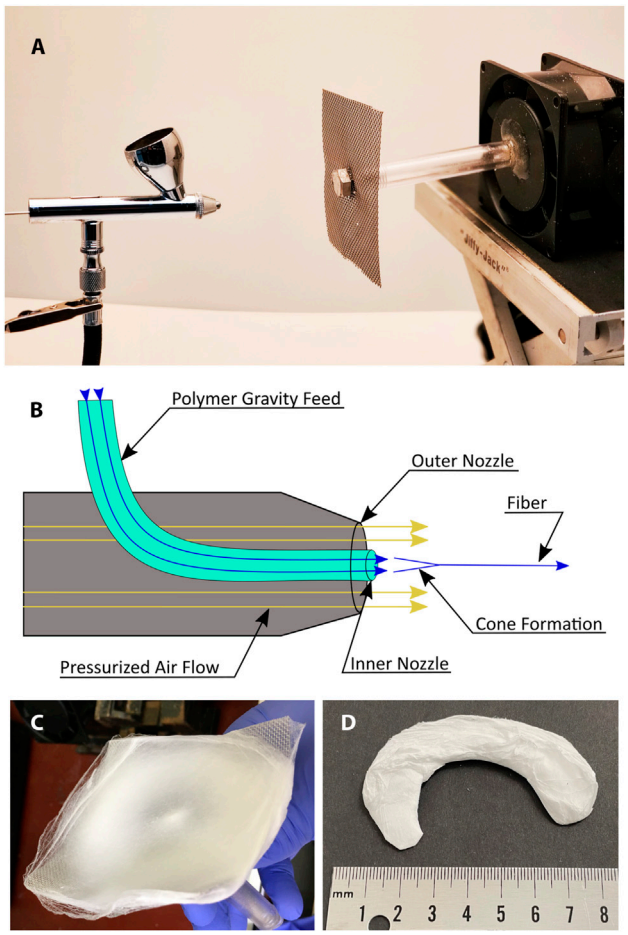

FIGURE 1 | Pneumatospinning setup **(A)** Photograph of airbrush and mesh collector. **(B)** Diagram of polymer jet generated by air flow. **(C)** Photograph of scaffold spun on mesh collector. **(D)** Scaffold cut to the shape of a human meniscus.

We therefore explored the potential of pneumatospinning for rapid generation of microfibrous collagen scaffolds seeded with human infrapatellar fat pad progenitors (IPFP-MSC) to facilitate meniscogenesis. We characterized scaffold microstructure, mechanical properties, and cytocompatibility. We analyzed cell migration and distribution, neotissue formation, and assessed proof of concept in the repair of meniscal tears in *ex vivo* bovine and human osteoarthritic menisci.

MATERIALS AND METHODS

Pneumatospinning System

Collagen type I (Semed S, generously supplied by DSM Biomedical, Exton, PA) was dissolved in hexafluoroisopropanol (HFIP) at concentrations between 5 and 10% wt/vol to establish the optimal concentration for spinning. The collagen solution was loaded into a customized gravity feed airbrush with a 350 µm nozzle (Anest Iwata, Yokohama) modified to run continuously. The airbrush consisted of an inner feed line, fed by gravity, leading to a nozzle and an outer air line, ending in a cap to form a coaxial outlet with the nozzle (**Figure 1**). The low pressure created by the escaping air drew solution from the inner nozzle. Air pressure on the air brush was set to 30 psi.

The target was a square section of flat stainless-steel mesh with a .03 cm wire diameter (TWP Inc., Berkeley) mounted on an electric motor and rotated at 650 RPM with the axis of rotation co-linear with the axis of the airbrush nozzle. The distance between the nozzle and target was set to 12 cm (**Figure 1**). The shape of the target mesh was varied by introducing 3-dimensional curvatures to assess potential for spinning a net meniscal shape (**Supplementary Figure S1**).

For comparison with electrospinning, scaffolds were fabricated as previously reported (Baek et al., 2016). Briefly, a collagen solution of 20% wt/vol was extruded toward a rotating drum with a potential difference of 18 kV.

Glutaraldehyde Crosslinking of Collagen Scaffolds

Collagen scaffolds were subjected to glutaraldehyde (GA, 25%, Thermo Fisher Scientific, Waltham, MA) vapor to induce crosslinking. We had previously used glutaraldehyde (GA) for electrospun collagen and found this to be an effective means of crosslinking collagen scaffolds (Baek et al., 2016; Baek et al., 2018). Collagen scaffolds on the collector mesh were suspended over an open beaker containing 30 ml GA solution and enclosed in a glass container for 48 h to contain the GA fumes in a chemical fume cabinet at 40°C. After GA crosslinking, scaffolds were cut to size and washed in PBS four to five times and stored in PBS at 4°C.

Mechanical Properties

Specimens were tested for tensile strength and tensile modulus using an Instron 8511 servohydraulic testing machine (Instron, Norwood, MA). Briefly, rectangular sections of 8 mm by 26 mm ($n = 5$) were cut from dry pneumatospun mats with the long axis tangent to the rotation of the collector (circumferentially oriented) or the long axis radial to the rotation of the collector (radially oriented, **Figure 2**). To test the effect of hydration, specimens were hydrated in 1x PBS for 1 h before mechanical testing ($n = 6$). The thickness and width of each specimen was measured with a digital caliper immediately prior to mechanical testing. Gauge length was measured for each specimen after mounting in the tensile grips. Specimens were mounted with a set of Instron grips and loaded to failure under tension at 4.2 mm/s. Load and displacement were recorded throughout the loading process.

Scanning Electron Microscopy (SEM)

For SEM, scaffolds were coated with 3.7 nm of Iridium and imaged on a Hitachi S-4800 SEM at 3 kV and 8 mm WD. SEM images were assessed for porosity and fiber morphology using ImageJ software (NIH, Bethesda, MD). Porosity was measured using ASTM F1854-15 (ASTM, 2015). Briefly, images were segmented to separate foreground fibers from background. Four lines were drawn horizontally across the image and values were measured along the corresponding profile. The percentage of pore space along these profiles was averaged to arrive at a value for the image. Pore size was measured across the longest axis of the pores to calculate average pore size in the transverse plane.

Cell Harvesting and Culture

Infrapatellar fat pad (IPFP) tissue was obtained from patients (74 year old female and 75 year old male) undergoing total knee replacement (approved by Scripps Institutional Review Board). Mesenchymal stem cells (IPFP-MSC) were isolated using a previously described method (Grogan et al., 2020). Briefly, IPFP tissues were minced using a scalpel to create fragments (~5 mm^3), which were placed into 6-well plate wells precoated with human collagen type I (Cell Adhere, StemCell Technologies, Vancouver, Canada). For the first 12 h, the tissue fragments were maintained in a CO_2 incubator at 37°C in only .5 ml MSC-medium (LONZA, Walkersville, MD) supplemented with Fibroblast Growth Factor 2 (FGF-2) (10 ng/ml; PeproTech, RockyHill, NJ). After 12 h, 1.5 ml of medium was added and the tissue fragments were cultured for 1–2 weeks until emergence of cells from the tissue. The remaining tissue fragments were discarded, and the emerging cells were detached using Accutase (Innovative Cell Technologies, Inc. San Diego, CA) and reseeded into collagen coated flasks at a density of 350,000 cells per cm^2.

Scaffold Cell Seeding and Culture Conditions

Pneumatospun and GA cross-linked collagen scaffolds were cut into rectangular specimens (approx. 1 cm by .5 cm) and washed in PBS extensively (at least 5 times in 5 ml PBS over 24 h). These scaffolds were seeded with IPFP-MSC ($.5 \times 10^6$ cells per scaffold specimen), cultured in MSC medium, and placed upon an orbital shaker at 100 RPM (Ohaus Parsippany, NJ) in a CO_2 incubator at 37°C. The seeded scaffolds were maintained in MSC medium for

3–4 days for initial cell proliferation before changing to differentiation medium that consisted of Dulbecco's Modified Eagle Medium (DMEM) (Mediatech Inc., Manassas, VA), 1x ITS+1 supplement (Sigma-Aldrich, St. Louis, MO), 100 nM Dexamethasone (Sigma), 1.25 mg/ml human serum albumin (Bayer, Leverkusen, Germany), 100 μM ascorbic acid 2-phospahate (Sigma), 1% penicillin/streptomycin/gentamycin (PSG, Gibco, Carlsbad, CA) and supplemented with 10 ng/ml TGFβ3 (PeproTech, Rocky Hill, NJ). Scaffolds were cultured for 3 weeks (with medium changes every 3–4 days) to assess cell attachment, viability, and gene expression.

Cell Viability Assessments

A total of 11 seeded scaffolds were used to assess viability using two different donors after 21 days in culture. Cell viability and distribution after 24 h or following 3 weeks in culture was measured with the Live/Dead kit (Invitrogen, Waltham, MA). The staining buffer consisted of Ethidium Homodimer-1 (8 mM) and Calcein-AM (1.6 mM) suspended in PBS. The cell seeded collagen scaffolds were incubated for 30–40 min before visualization with either a fluorescence microscope (Axiovert 200M, Zeiss, Jena, Germany) or via a confocal laser microscope (LSM-810; Zeiss). Image processing by thresholding and segmentation was used to remove the background scaffold stain (**Supplementary Figure S2**). The percentage of live and dead cells was calculated using ImageJ/Fiji (Rueden et al., 2017).

Ex vivo Meniscus Repair Models

Bovine explants: Whole bovine knees with the knee capsule intact were obtained from Animal Technologies, Inc. (Tyler, TX). Meniscal tissue explants of approximately 1 cm wide and x 3 cm deep were cut under sterile conditions. Explants were cultured in DMEM with 10% CS and 1% PSG until ready to use.

Human explants: Menisci were obtained from four patients (69.3 ± 10.1 years, three female, one male) following total knee arthroplasty (approved by Scripps Institutional Review Board). The menisci were cut into tissue explants of around 1 cm × 1 cm and each cultured in DMEM with 10% CS and 1% PSG until ready for scaffold implantation (within 2 days).

Collagen scaffolds (approx. 1 cm long, .5 cm wide, and .2 cm thick) were seeded with IPFP-MSC ($.5 \times 10^6$ per scaffold) and cultured for 3 days in MSC-medium, followed by 7 days in differentiation medium. Scaffolds (n = 29) were implanted to repair surgically created longitudinal or transverse defects in human (n = 4 human donors, n = 17 explants) and bovine explants (n = 2 knees, n = 12 explants). The longitudinal defects were created in the red-white region and the transverse defects spanned the red-white regions. The implanted scaffolds and explant tissue was cultured for 3 weeks in the differentiation medium, with changes every 3–4 days. At the end of culture, the explants were fixed and processed for paraffin embedding and subsequent histological analyses.

Histology and Immunohistochemistry

Paraffin embedded sections (4 μm thick) were mounted on glass slides for staining with Safranin O-fast green or immunohistochemistry for collagen types I and II as previously described (van Schaik et al., 2021). Briefly, paraffin cut sections were deparaffinized and treated with pepsin for 9 min at 37°C in a humidified chamber (Digest-All 3, Thermo Fisher Scientific). Rabbit anti-human collagen type I antibody (1 μg/ml; Ab 34,710, Abcam, Cambridge, MA) and mouse anti-human collagen type II (2 μg/ml; II-II6B3, Hybridoma Bank, University of Iowa) was used as the primary antibodies, which were incubated at 4°C for 12–16 h in a humid chamber. The ImmPRESS secondary DAB (Brown) or AP (red) kits were used for color development (Vector Laboratories, Burlingame, CA). Non-specific staining was evaluated using species-matched isotype controls at the same concentration as the specific primary antibodies.

Gene Expression

Following the manufacturer's instructions (Qiagen, Valencia, CA), scaffolds were minced by scalpel in RLT buffer and then subjected to homogenization using the Qiashredder. Total RNA was extracted using the RNeasy kit (Qiagen) and cDNA was made using the High Capacity cDNA Reverse Transcription Kit (Applied Biosystems, Foster City, California). Verified primer/probe assays were purchased from Applied Biosystems to monitor the expression levels of COL1A1, COL2A1, COMP, ACAN, and THY1 relative to the GAPDH (housekeeping gene). The gene expression levels of IPFP-MSC in monolayer culture were used to calculate relative changes in expression level following culture on the pneumatospun collagen scaffolds. Gene expression was normalized to GAPDH and we used the ΔCt method as previously reported (Martin et al., 2001).

Statistical Analysis

Difference in gene expression between IPFP-MSC cultured on pneumatospun scaffolds and cells in monolayer cultures were tested for significance at $p < .05$, using the online BootstRatio application (http://regstattools.net/br) (Cleries et al., 2012).

RESULTS

Efficient Fabrication of Microfibrous Collagen Scaffolds

Pneumatospinning involves a gravity-fed airbrush which generated undesirable turbulence at traditional collector targets used in electrospinning such as flat plates or solid drums. We therefore selected meshed collectors that permit air flow through the target, reduce turbulence, and result in more consistent accumulation of spun fibers. To further reduce turbulence at the target, we mounted a fan behind a stationary collector to direct air through the target and mounted the target to the spinning fan to induce circumferential alignment of fibers.

We tested a range of collagen solution concentrations between 5 and 10% wt/vol to identify the optimal solution that could be reliably dispensed. Solutions below 6% formed insufficient fibers, while those above 9% tended to clog the nozzle of the airbrush. A 9% solution was chosen for all following experiments. 60 ml of collagen solution generated a 1 mm thick scaffold of collagen

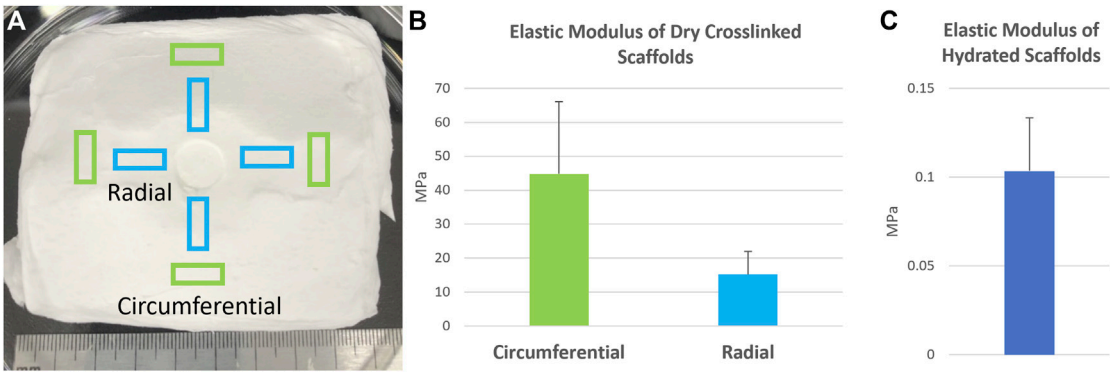

FIGURE 2 | Mechanical properties of pneumatospun collagen scaffolds deposited upon a spinning mesh collector. **(A)** Scaffold specimens were harvested from the mesh collector in either in the circumferential or radial directions in relation to the rotation of the scaffold. **(B)** Elastic modulus of dry collagen scaffolds after glutaraldehyde crosslinking and **(C)** following hydration in medium. Error bars represent standard deviations.

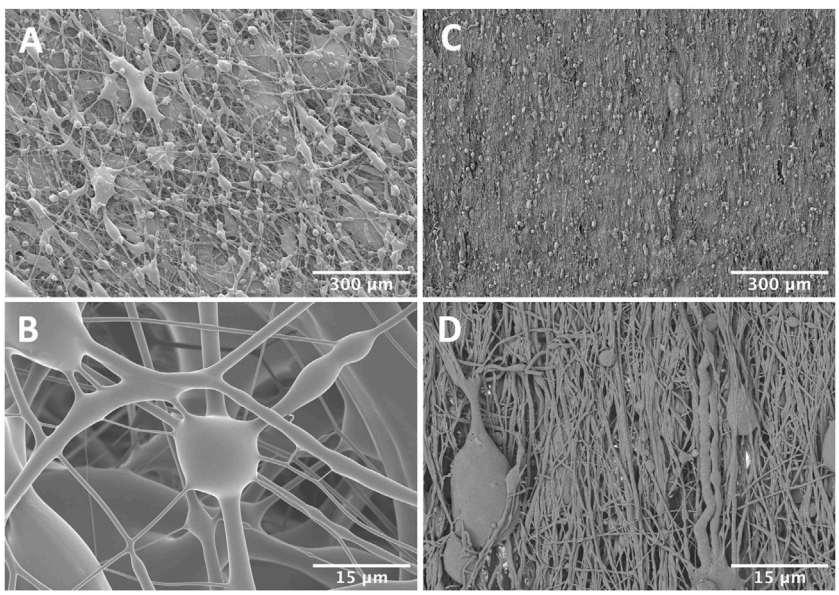

FIGURE 3 | Scanning electron micrographs of pneumatospun **(A,B)** or electrospun **(C,D)** collagen scaffolds after glutaraldehyde crosslinking. Note the larger interconnected porosities in the pneumatospun scaffolds.

fibers in less than 2 h. This was significantly faster than our electrospinning experiments which required over 24 h to generate 250 µm thick scaffolds.

We also demonstrated the potential to create scaffolds of varying shapes, using curved targets with radial ripples (**Supplementary Figure S1**). Glutaraldehyde crosslinked mats spun onto these targets retained the curvature of the targets after removal, but showed no appreciable variation in thickness. For subsequent experiments in this study, we used flat square mesh collectors.

Scaffold Properties

Before crosslinking, spun collagen mats were fragile, fragmented upon removed from the target substrate, and dissolved in culture. After glutaraldehyde crosslinking, collagen mats could be easily removed intact from the target. By 3 weeks, cultured scaffolds swelled and softened, but retained their net spun shape and could be easily manipulated with forceps for loading into mechanical testing fixtures or for surgical implantation in *ex vivo* tissue samples.

Dry collagen GA crosslinked scaffolds exhibited an elastic modulus of around 45 MPa, which was reduced significantly after hydration to .1 ± .03 MPa (**Figure 2**). Dry scaffolds failed consistently within the gauge length of the test setup, while hydrated scaffolds tended to fail near the tissue grips. SEM imaging of the GA crosslinked pneumatospun scaffolds revealed a heterogenous distribution of fiber sizes and large, interconnected porosities (**Figure 3**). This contrasted with aligned, electrospun

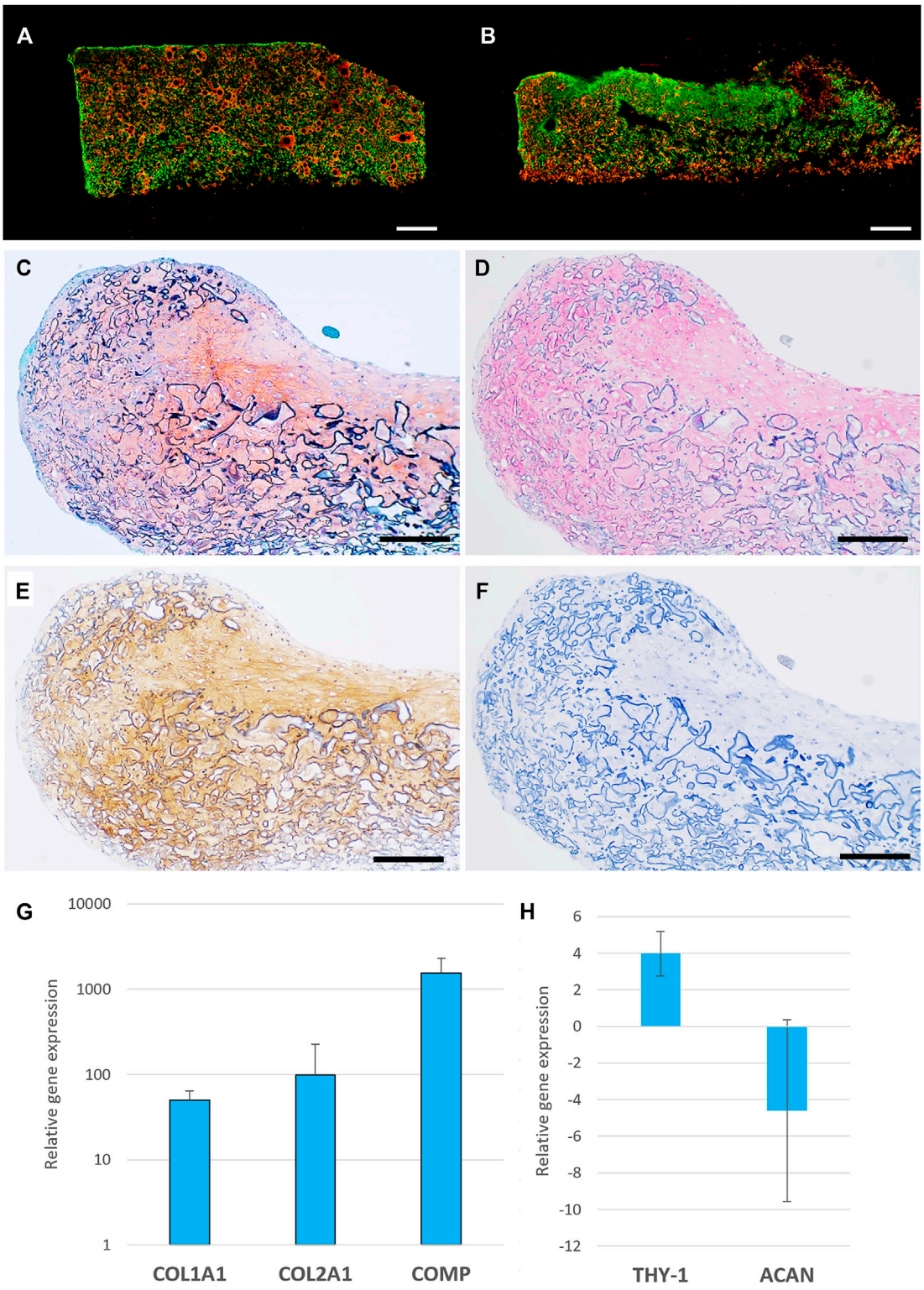

FIGURE 4 | Cell viability, histology and gene expression of IPFP-MSC seeded pneumatospun collagen scaffolds. **(A,B)** Cell viability of IPFP-MSC seeded collagen scaffolds (live cells = green), dead cells = red, bar = 1000 μm) **(C)** Safranin O stain of neotissue formed on collagen scaffold. **(D)** Collagen type I immunostaining (AP red). **(E)** Collagen type II immunostaining (DAB brown). **(F)** Isotype control immunostaining. (Bar = 200 μm) **(G,H)**. Gene expression levels of IPFP-MSC seeded on collagen scaffolds after 3 weeks in serum free medium relative to monolayer undifferentiated cultured IPFP-MSC (n = 6).

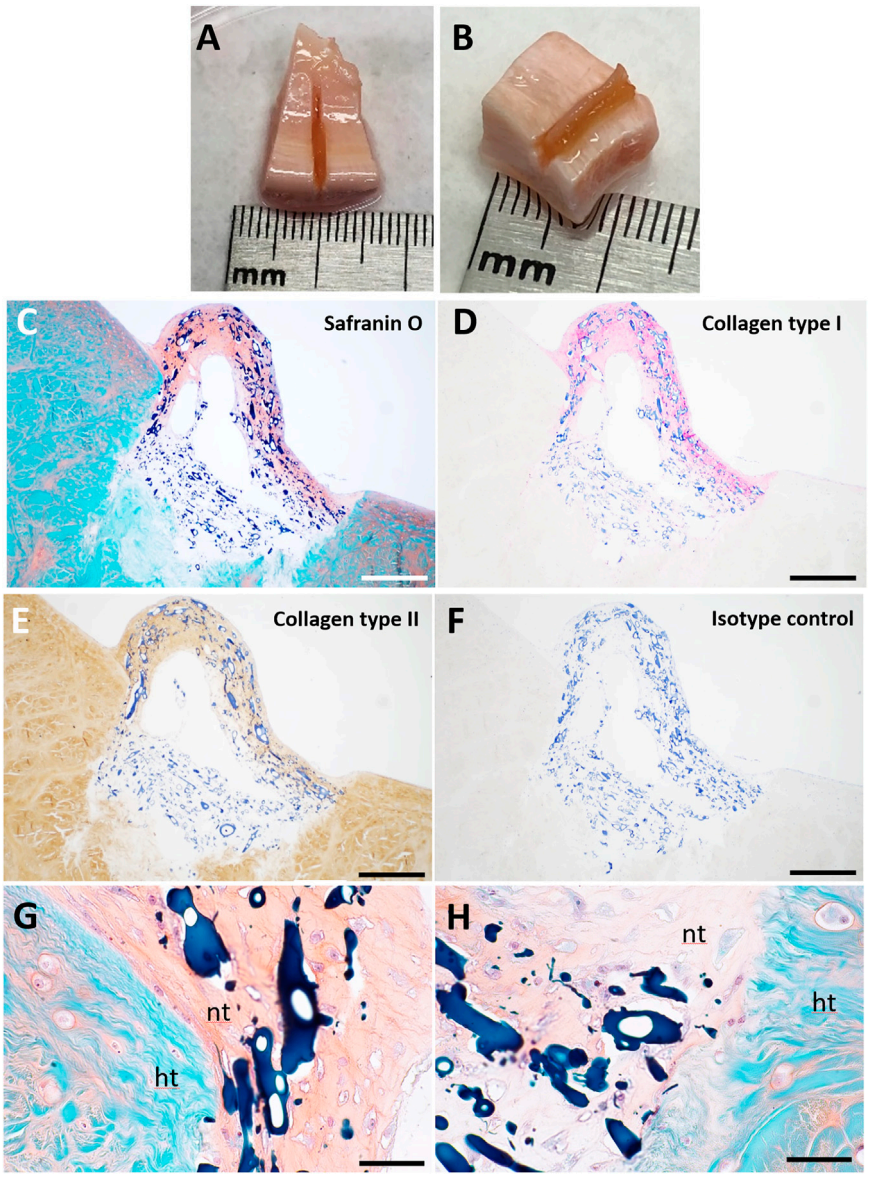

FIGURE 5 | Pneumatospun collagen scaffolds seeded with human IPFP cells and implanted into *ex vivo* bovine meniscus and culture for 3 weeks. **(A,B)** Photographs of implanted collagen scaffolds. **(C)** Safranin O staining. **(D)** Collagen type I immunostaining. **(E)** Collagen type II immunostaining. **(F)** Isotype control. **(G,H)** Higher magnification of Safranin O stained image showing integration of neotissue (nt) with host tissue (ht). The collagen scaffold is stained dark blue. (C-F Bar = 200 μm; G-H Bar = 50 μm).

scaffolds which have low porosity and more uniform, nanoscale fibers (**Figure 3**). Pneumatospun fibers appeared irregular with diameters ranging from 1 to 30 μm. The overall porosity of the collagen scaffold in the transverse plane was approximately 48% with pore sizes ranging from 7.4 to 100.7 μm with a median of 23.8 μm and a mean of 25.7 μm. We also observed bead formation which is related to the surface tension of the solution and can be reduced by optimizing solution and spinning parameters.

Neotissue Formation

Glutaraldehyde crosslinked pneumatospun collagen scaffolds were seeded with IPFP-MSC, cultured in 6-well plates in MSC medium and placed on an orbital shaker overnight in the incubator. This approach enhanced cell attachment and infiltration into the scaffold (**Supplementary Figure S3**). After 3 weeks of culture in serum-free differentiation medium, IPFP-MSC were observed throughout the pneumatospun collagen scaffolds with 70.2 ± 7.5% viability (**Figures 4A,B**).

On histological analysis, IPFP-MSC seeded into the scaffolds generated a fibrocartilage-like neotissue with extracellular matrix containing glycosaminoglycans (Safranin O positive; **Figure 4C**), collagen types I and II (**Figures 4D–F**). This histology was generally consistent with the gene expression profile of

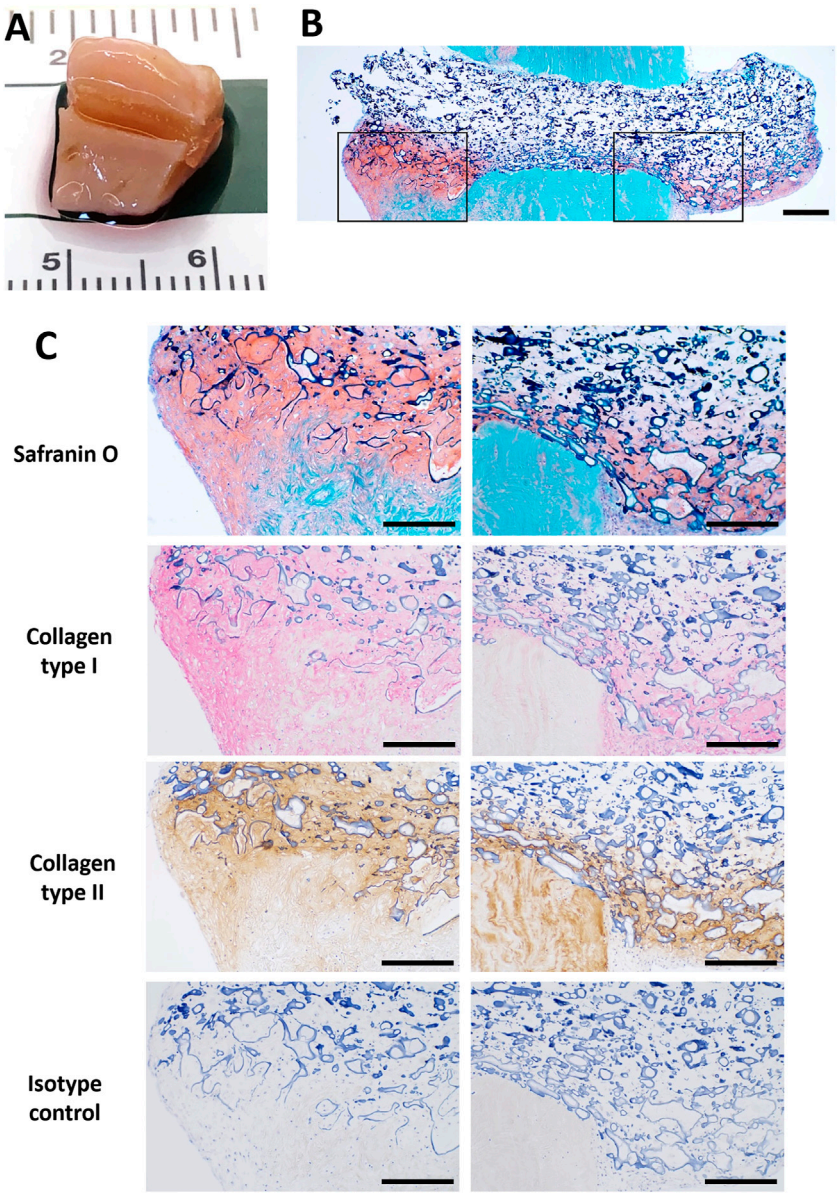

FIGURE 6 | Pneumatospun collagen scaffolds seeded with human IPFP cells and implanted into human OA meniscus explant (72 year-old female) and cultured for 3 weeks. **(A)** Photograph of implanted scaffold. **(B)** Overview of section stained with Safranin O showing neotissue development in meniscus defect (bar = 500 μm). **(C)** Histologic images of sections stained with Safranin O and immunostained with collagen type I (AP red), collagen type II (DAB brown), and isotype control regions of inset regions outlined in **(B)** (bar = 300 μm).

increased COL1A1, COL2A1 and COMP, THY-1 (CD90) and reduced ACAN expression compared to IPFP-MSC in monolayer culture (**Figures 4G,H**).

Repair of Ex Vivo Meniscus Tears

We assessed potential for repair of meniscus tears by implanting scaffolds seeded with IPFP-MSC into surgically created defects in normal healthy bovine meniscus (**Figures 5A,B**) or in osteoarthritic human meniscus resected from patients that had undergone TKA (**Figure 6A**). After 3 weeks of culture in differentiation medium, neo-fibrocartilaginous tissue developed in the bovine meniscus that integrated with the host tissue (**Figure 5**). More GAG deposition was noted in the superficial region corresponding spatially with the GAG seen in the host tissue (**Figure 5C**). The mix of collagen types I and II indicated a fibrocartilage-like composition. Cell-seeded collagen scaffolds implanted into osteoarthritic human menisci (**Figure 6A**) also resulted in similar fibrocartilage-like neotissue which integrated with host tissue with a positive Safranin O and a collagen type I and II staining profile (**Figures 6B,C**).

DISCUSSION

We explored pneumatospinning to fabricate microfibrous collagen scaffolds as a more efficient approach to electrospinning (ES) for meniscal tissue engineering, with potential for greater porosity to facilitate cell seeding and migration, generation of meniscus-like tissue, and to repair meniscal tears. We demonstrated that pneumatospinning can rapidly produce scaffolds with a spectrum of micron-sized fibers and appropriate porosity. Pneumatospun collagen scaffolds were biocompatible, and permitted rapid IPFP-MSC attachment and colonization, and formation of neo-fibrocartilage meniscus-like tissue, especially when implanted into healthy bovine or osteoarthritic human meniscus explants.

Several synthetic polymers (polymethylmethacrylate, polylactic acid, and polystyrene) have been pneumatospun to produce micro- and nano-fibers up to 100x faster than electrospinning) (Medeiros et al., 2009). The authors found that electrospinning typically dispensed solutions between 4 and 10 µl/min while pneumatospinning dispensing rates can be increased up to 200 µl/min without altering fiber diameter (Medeiros et al., 2009). Most other studies did not report on the final thickness of the deposited scaffold or the accumulation rate over a given time. However, pneumatospun fiber mats are reported to take a few seconds to minutes to build a mat of significant thickness with deposition rates of .1 ml/min or more (Medeiros et al., 2009; Oliveira et al., 2011; Behrens et al., 2016). Others have reported pneumatospun mat thickness ranging from 130 µm to 1 mm (Behrens et al., 2016; Kopec et al., 2020; Molde et al., 2020). Polk et al. (2018) rapidly pneumatospun 200 µm thick collagen type I scaffolds in 5 min, which was 32x faster than electrospun scaffolds. To our knowledge, this is the first study reporting on pneumatospinning for fabricating scaffolds for meniscus regeneration. We generated scaffolds at approximately .5 mm in thickness/hr, which was significantly more efficient than our previous reports on electrospinning which required over 24 h to produce a .25 mm thick electrospun scaffold (Baek et al., 2016); equivalent to a 50x increase in fiber deposition rate.

Pneumatospinning can generate fibers with diameters ranging from 70 nm to as large as 100 µm (Sinha-Ray et al., 2015; Daristotle et al., 2016; Dos Santos et al., 2020) by tuning process variables such as the polymer injection rate and concentration, temperature, air/gas pressure and nozzle geometry (Sinha-Ray et al., 2015; Medeiros et al., 2016; Dos Santos et al., 2020). We pneumatospun collagen fibers ranging from 1 to 30 µm, which were larger than our previous studies with ES collagen fiber (250–860 nm) (Baek et al., 2016). Our pneumatospun collagen fiber diameters were also larger than the average fiber diameter of 224 nm reported for pneumatospun type I atelocollagen scaffolds (Polk et al., 2018). This difference in fiber diameters could be attributed to differences in collagen (atelocollagen vs. soluble collagen), collagen concentration (40 vs. 9%), solvent (acetic acid vs. HFIP), air pressure (60 psi vs. 30 psi), and collector properties.

Electrospinning typically generates densely packed nanofibrous mats with low porosity which can inhibit cell migration into the scaffolds (Baker et al., 2008). Modifications such as sacrificial fibers or microparticles of polyethylene oxide are required to increase porosity and enhance cell infiltration (Baker et al., 2008; Wang et al., 2013). One advantage of our pneumatospun scaffolds was the inherent increased porosity which enhances potential for cell migration. We noted a porosity of nearly 50% in our scaffolds (with pore sizes averaging 26 µm) which supported cell migration. Others have reported varying pore sizes with pneumatospun materials, ranging from 3 to 6 µm for PU (Kopec et al., 2020); 10–50 µm with E1001 (1 k), a tyrosine-derived polycarbonate (Molde et al., 2020); and 25 µm to over 100 µm for scaffolds of PLA and dimethyl carbonate (Medeiros et al., 2016).

Fiber alignment replicating the microstructure of meniscal tissue is important to engineer tissue with biomimetic properties. We used a rotating mesh collector to direct circumferential fiber alignment. Although, SEM did not reveal differences in alignment of fibers, crosslinked collagen scaffold samples in the circumferential direction were three times stiffer in comparison to samples in the radial direction (15 KPa) from the same scaffold. Increasing the speed of collector rotation or modifying collector shape may enhance fiber alignment (Baek et al., 2015; Baek et al., 2016; Baek et al., 2018). For example, a funnel between the nozzle and the collector has been effective in channeling airflow and aligning in-flight fibers (Magaz et al., 2018); and a cylindrical tube with internal spokes collected aligned pneumatospun fibers (Polk et al., 2018).

The meniscus is composed of a fibrocartilaginous tissue that displays variations in the distribution of ECM molecules particularly collagens type I and II, and GAGs (Makris et al., 2011; Murphy et al., 2019). In our study, seeding IPFP-MSC upon pneumatospun collagen scaffolds increased expression of COL1A1, COL2A1, COMP and THY-1 (CD90). COMP plays a critical role in mediating various ECM component interactions such as fibronectin, many collagens (types I, II IX, XII, and XIV) and proteoglycans such as aggrecan, chondroitin sulfates, and heparan sulfate (Chen et al., 2007; Acharya et al., 2014). The increased gene expression of THY-1 also corresponds with a fibrocartilaginous phenotype (Grogan et al., 2017; Grogan et al., 2018). These increases in meniscogenic gene expression were reflected in development of fibrocartilaginous-like neotissue with distinct collagen type I and II protein deposition in a matrix containing GAGs.

Ex vivo meniscus tissue cultures are increasingly being utilized as models to assess *in vitro* repair and regeneration (Cucchiarini et al., 2009; Cucchiarini et al., 2015; Marrella et al., 2018; Resmi et al., 2020). We previously characterized an *ex vivo* meniscus explant model of longitudinal tears repaired with collagen ES scaffolds seeded with human meniscus cells (Baek et al., 2016; Baek et al., 2019) and documented composition of neotissue and integration with host explant. In the present study, implantation of thicker pneumatospun scaffolds seeded with IPFP-MSC into meniscal defects resulted in fibrocartilaginous tissues composed of GAGs and collagen types I and II. The scaffolds used in this study may therefore be more suitable for supporting the development of avascular meniscus-like tissues, that typically

contain higher concentrations of collagen type II and GAGs than the vascular meniscus regions.

Despite the promising results with pneumatospun collagen scaffolds, there are limitations to overcome. Hydration of glutaraldehyde crosslinked collagen scaffolds in culture significantly decreased mechanical properties, reducing its potential for broader clinical applications such as meniscus replacement. Incorporation of artificial polymers, such as PLA, may increase the mechanical properties as we and others have previously demonstrated with coaxial electrospun fibers (Tong et al., 2015; Singh et al., 2018; Baek et al., 2019; Baek et al., 2020). Our nozzle to collector arrangement did generate encouraging differences in mechanical properties based on sample orientation but did not result in visible fiber alignment; and alternate approaches need to be explored. Our *in vitro* and *ex vivo* systems provided proof of concept of cytocompatibility, cell distributions neo-tissue formation. However, *in vivo* experiments are needed to validate suitability of translation of tissue engineered scaffolds for meniscus repair.

CONCLUSION

Pneumatospinning is a promising approach to rapidly generate collagen fibers for meniscus tissue engineering with significantly greater efficiency of scaffold fabrication than electrospinning. The increased porosity effectively supported IPFP-derived cell colonization and differentiation. The resultant neo-fibrocartilage tissue integrated into normal bovine and arthritic human menisci defects. For translation to clinical applications, enhanced mechanical properties and validation in clinically relevant meniscal repair and regeneration models are required.

DATA AVAILABILITY STATEMENT

The original contributions presented in the study are included in the article/**Supplementary Material**, further inquiries can be directed to the corresponding author.

ETHICS STATEMENT

The studies involving human participants were reviewed and approved by Scripps Institutional Review Board. The patients/participants provided their written informed consent to participate in this study.

AUTHOR CONTRIBUTIONS

ED, AW, SG, and DD'D were responsible for the overall experimental design. ED, SG, and DD'D wrote the manuscript in close collaboration with the other authors. ED and AW designed and conducted the pneumatospinning and electrospinning. SG coordinated cell culture studies, RT-PCR and histology. ED, AW, and DD'D designed and performed mechanical tests. All authors discussed the results and approved the final version of the article.

FUNDING

This project was supported by the Shaffer Family Foundation and by Donald and Darlene Shiley.

ACKNOWLEDGMENTS

We thank April Damon and Nick Glembotski for technical assistance (RT-PCR, histology and immunostainings). We thank Scott Henderson, Kimberly Vanderpool, and Theresa Fassel of The Core Microscopy Facility at The Scripps Research Institute for imaging support. Collagen type I was generously provided by DSM Biomedical, Exton, PA.

SUPPLEMENTARY MATERIAL

The Supplementary Material for this article can be found online at: https://www.frontiersin.org/articles/10.3389/fbioe.2022.810705/full#supplementary-material

Supplementary Figure S1 | Photographs of different collector shapes. **(A)** Flat mesh **(B)** Curved mesh **(C,D)** 3D curved shapes.

Supplementary Figure S2 | Cell viability of IPFP-MSC seeded pneumatospun collagen scaffolds after overnight incubation on orbital shaker. **(A)** Live cells (green) and **(B)** dead cells (red) (Magnification 10x).

Supplementary Figure S3 | ImageJ was used for image processing to remove background staining and extract green (live/cytoplasm) and dead (red /nuclei) cells for viability assessments. **(A)** Confocal microscopy image; **(B)** Live cells labeled green (cell count = 13,773); **(C)** Dead cells labeled red (cell count = 1201): cell viability = 92% (bar = 1000 μm).

Supplementary Figure S4 | Immunohistochemistry for collagen types I and II. Left column: Negative isotype controls; Right column: positive stains. **(A,B)** Type I collagen stain for bovine meniscus; **(C,D)** Type I collagen stain for human meniscus; **(E,F)** Type II collagen stain for human articular cartilage.

REFERENCES

Acharya, C., Yik, J. H. N., Kishore, A., Van Dinh, V., Di Cesare, P. E., and Haudenschild, D. R. (2014). Cartilage Oligomeric Matrix Protein and its Binding Partners in the Cartilage Extracellular Matrix: Interaction, Regulation and Role in Chondrogenesis. *Matrix Biol.* 37, 102–111. doi:10.1016/j.matbio.2014.06.001

Akentjew, T. L., Terraza, C., Suazo, C., Maksimcuka, J., Wilkens, C. A., Vargas, F., et al. (2019). Rapid Fabrication of Reinforced and Cell-Laden Vascular Grafts Structurally Inspired by Human Coronary Arteries. *Nat. Commun.* 10 (1), 3098. doi:10.1038/s41467-019-11090-3

Angele, P., Docheva, D., Pattappa, G., and Zellner, J. (2021). Cell-based Treatment Options Facilitate Regeneration of Cartilage, Ligaments and Meniscus in Demanding Conditions of the Knee by a Whole Joint Approach. *Knee Surg. Sports Traumatol. Arthrosc.* doi:10.1007/s00167-021-06497-9

Ardizzone, C. A., Houck, D. A., McCartney, D. W., Vidal, A. F., and Frank, R. M. (2020). All-Inside Repair of Bucket-Handle Meniscal Tears: Clinical Outcomes and Prognostic Factors. *Am. J. Sports Med.* 48 (13), 3386–3393. doi:10.1177/0363546520906141

ASTM (2015). *Standard Test Method for Stereological Evaluation of Porous Coatings on Medical Implants*. West Conshohocken, PA: ASTM International. Vol. ASTM F1854-15.

Baek, J., Chen, X., Sovani, S., Jin, S., Grogan, S. P., and D'Lima, D. D. (2015). Meniscus Tissue Engineering Using a Novel Combination of Electrospun Scaffolds and Human Meniscus Cells Embedded within an Extracellular Matrix Hydrogel. *J. Orthop. Res.* 33 (4), 572–583. doi:10.1002/jor.22802

Baek, J., Lee, E., Lotz, M. K., and D'Lima, D. D. (2020). Bioactive Proteins Delivery through Core-Shell Nanofibers for Meniscal Tissue Regeneration. *Nanomedicine: Nanotechnology, Biol. Med.* 23, 102090. doi:10.1016/j.nano.2019.102090

Baek, J., Lotz, M. K., and D'Lima, D. D. (2019). Core-Shell Nanofibrous Scaffolds for Repair of Meniscus Tears. *Tissue Eng. A* 25 (23-24), 1577–1590. doi:10.1089/ten.TEA.2018.0319

Baek, J., Sovani, S., Choi, W., Jin, S., Grogan, S. P., and D'Lima, D. D. (2018). Meniscal Tissue Engineering Using Aligned Collagen Fibrous Scaffolds: Comparison of Different Human Cell Sources. *Tissue Eng. Part A* 24 (1-2), 81–93. doi:10.1089/ten.TEA.2016.0205

Baek, J., Sovani, S., Glembotski, N. E., Du, J., Jin, S., Grogan, S. P., et al. (2016). Repair of Avascular Meniscus Tears with Electrospun Collagen Scaffolds Seeded with Human Cells. *Tissue Eng. Part A* 22 (5-6), 436–448. doi:10.1089/ten.TEA.2015.0284

Bahcecioglu, G., Buyuksungur, A., Kiziltay, A., Hasirci, N., and Hasirci, V. (2014). Construction and *In Vitro* Testing of a Multilayered, Tissue-Engineered Meniscus. *J. Bioactive Compatible Polym.* 29 (3), 235–253. doi:10.1177/0883911514529688

Baker, B. M., Gee, A. O., Metter, R. B., Nathan, A. S., Marklein, R. A., Burdick, J. A., et al. (2008). The Potential to Improve Cell Infiltration in Composite Fiber-Aligned Electrospun Scaffolds by the Selective Removal of Sacrificial Fibers. *Biomaterials* 29 (15), 2348–2358. doi:10.1016/j.biomaterials.2008.01.032

Baker, B. M., and Mauck, R. L. (2007). The Effect of Nanofiber Alignment on the Maturation of Engineered Meniscus Constructs. *Biomaterials* 28 (11), 1967–1977. doi:10.1016/j.biomaterials.2007.01.004

Baker, B. M., Shah, R. P., Silverstein, A. M., Esterhai, J. L., Burdick, J. A., and Mauck, R. L. (2012). Sacrificial Nanofibrous Composites Provide Instruction without Impediment and Enable Functional Tissue Formation. *Proc. Natl. Acad. Sci.* 109 (35), 14176–14181. doi:10.1073/pnas.1206962109

Behrens, A. M., Casey, B. J., Sikorski, M. J., Wu, K. L., Tutak, W., Sandler, A. D., et al. (2014). *In Situ* Deposition of PLGA Nanofibers via Solution Blow Spinning. *ACS Macro Lett.* 3 (3), 249–254. doi:10.1021/mz500049x

Behrens, A. M., Kim, J., Hotaling, N., Seppala, J. E., Kofinas, P., and Tutak, W. (2016). Rapid Fabrication of poly(DL-Lactide) Nanofiber Scaffolds with Tunable Degradation for Tissue Engineering Applications by Air-Brushing. *Biomed. Mater.* 11 (3), 035001. doi:10.1088/1748-6041/11/3/035001

Chen, F. H., Herndon, M. E., Patel, N., Hecht, J. T., Tuan, R. S., and Lawler, J. (2007). Interaction of Cartilage Oligomeric Matrix Protein/thrombospondin 5 with Aggrecan. *J. Biol. Chem.* 282 (34), 24591–24598. doi:10.1074/jbc.M611390200

Chew, E., Prakash, R., and Khan, W. (2017). Mesenchymal Stem Cells in Human Meniscal Regeneration: A Systematic Review. *Ann. Med. Surg.* 24, 3–7. doi:10.1016/j.amsu.2017.09.018

Clèries, R., Galvez, J., Espino, M., Ribes, J., Nunes, V., and de Heredia, M. L. (2012). BootstRatio: A Web-Based Statistical Analysis of Fold-Change in qPCR and RT-qPCR Data Using Resampling Methods. *Comput. Biol. Med.* 42 (4), 438–445. doi:10.1016/j.compbiomed.2011.12.012

Cucchiarini, M., Schetting, S., Terwilliger, E. F., Kohn, D., and Madry, H. (2009). rAAV-mediated Overexpression of FGF-2 Promotes Cell Proliferation, Survival, and α-SMA Expression in Human Meniscal Lesions. *Gene Ther.* 16 (11), 1363–1372. doi:10.1038/gt.2009.91

Cucchiarini, M., Schmidt, K., Frisch, J., Kohn, D., and Madry, H. (2015). Overexpression of TGF-β via rAAV-Mediated Gene Transfer Promotes the Healing of Human Meniscal Lesions *Ex Vivo* on Explanted Menisci. *Am. J. Sports Med.* 43 (5), 1197–1205. doi:10.1177/0363546514567063

Daristotle, J. L., Behrens, A. M., Sandler, A. D., and Kofinas, P. (2016). A Review of the Fundamental Principles and Applications of Solution Blow Spinning. *ACS Appl. Mater. Inter.* 8 (51), 34951–34963. doi:10.1021/acsami.6b12994

DeHaven, K. E. (1999). Meniscus Repair. *Am. J. Sports Med.* 27 (2), 242–250. doi:10.1177/03635465990270022301

Dos Santos, D. M., Correa, D. S., Medeiros, E. S., Oliveira, J. E., and Mattoso, L. H. C. (2020). Advances in Functional Polymer Nanofibers: From Spinning Fabrication Techniques to Recent Biomedical Applications. *ACS Appl. Mater. Inter.* 12 (41), 45673–45701. doi:10.1021/acsami.0c12410

Englund, M., Roos, E. M., Roos, H. P., and Lohmander, L. S. (2001). Patient-relevant Outcomes Fourteen Years after Meniscectomy: Influence of Type of Meniscal Tear and Size of Resection. *Rheumatology (Oxford)* 40 (6), 631–639. doi:10.1093/rheumatology/40.6.631

Fetzer, G., Spindler, K., Amendola, A., Andrish, J., Bergfeld, J., Dunn, W., et al. (2009). Potential Market for New Meniscus Repair Strategies -Evaluation of the MOON Cohort. *J. Knee Surg.* 22 (3), 180–186. doi:10.1055/s-0030-1247746

Fillingham, Y. A., Riboh, J. C., Erickson, B. J., Bach, B. R., Jr., and Yanke, A. B. (2017). Inside-Out versus All-Inside Repair of Isolated Meniscal Tears: An Updated Systematic Review. *Am. J. Sports Med.* 45 (1), 234–242. doi:10.1177/0363546516632504

Fisher, M. B., Henning, E. A., Söegaard, N., Bostrom, M., Esterhai, J. L., and Mauck, R. L. (2015). Engineering Meniscus Structure and Function via Multi-Layered Mesenchymal Stem Cell-Seeded Nanofibrous Scaffolds. *J. Biomech.* 48 (8), 1412–1419. doi:10.1016/j.jbiomech.2015.02.036

Ford, G. M., Hegmann, K. T., White, G. L., Jr., and Holmes, E. B. (2005). Associations of Body Mass index with Meniscal Tears. *Am. J. Prev. Med.* 28 (4), 364–368. doi:10.1016/j.amepre.2005.01.013

Gopinathan, J., Mano, S., Elakkiya, V., Pillai, M. M., Sahanand, K. S., Rai, B. K. D., et al. (2015). Biomolecule Incorporated Poly-ε-Caprolactone Nanofibrous Scaffolds for Enhanced Human Meniscal Cell Attachment and Proliferation. *RSC Adv.* 5 (90), 73552–73561. doi:10.1039/c5ra14315b

Grogan, S. P., Baek, J., and D'Lima, D. D. (2020). Meniscal Tissue Repair with Nanofibers: Future Perspectives. *Nanomedicine* 15 (25), 2517–2538. doi:10.2217/nnm-2020-0183

Grogan, S. P., Duffy, S. F., Pauli, C., Lotz, M. K., and D'Lima, D. D. (2018). Gene Expression Profiles of the Meniscus Avascular Phenotype: A Guide for Meniscus Tissue Engineering. *J. Orthop. Res.* 36 (7), 1947–1958. doi:10.1002/jor.23864

Grogan, S. P., Pauli, C., Lotz, M. K., and D'Lima, D. D. (2017). Relevance of Meniscal Cell Regional Phenotype to Tissue Engineering. *Connect. Tissue Res.* 58 (3-4), 259–270. doi:10.1080/03008207.2016.1268604

Horie, M., Sekiya, I., Muneta, T., Ichinose, S., Matsumoto, K., Saito, H., et al. (2009). Intra-articular Injected Synovial Stem Cells Differentiate into Meniscal Cells Directly and Promote Meniscal Regeneration without Mobilization to Distant Organs in Rat Massive Meniscal Defect. *Stem Cells* 27 (4), 878–887. doi:10.1634/stemcells.2008-0616

Ionescu, L. C., Lee, G. C., Huang, K. L., and Mauck, R. L. (2012). Growth Factor Supplementation Improves Native and Engineered Meniscus Repair *In Vitro*. *Acta Biomater.* 8 (10), 3687–3694. doi:10.1016/j.actbio.2012.06.005

Kang, S.-W., Sun-Mi, S., Jae-Sun, L., Eung-Seok, L., Kwon-Yong, L., Sang-Guk, P., et al. (2006). Regeneration of Whole Meniscus Using Meniscal Cells and Polymer Scaffolds in a Rabbit Total Meniscectomy Model. *J. Biomed. Mater. Res.* 77A (4), 659–671. doi:10.1002/jbm.a.30579

Kondo, S., Nakagawa, Y., Mizuno, M., Katagiri, K., Tsuji, K., Kiuchi, S., et al. (2019). Transplantation of Aggregates of Autologous Synovial Mesenchymal Stem Cells for Treatment of Cartilage Defects in the Femoral Condyle and the Femoral Groove in Microminipigs. *Am. J. Sports Med.* 47 (10), 2338–2347. doi:10.1177/0363546519859855

Kopeć, K., Wojasiński, M., and Ciach, T. (2020). Superhydrophilic Polyurethane/Polydopamine Nanofibrous Materials Enhancing Cell Adhesion for Application in Tissue Engineering. *Ijms* 21 (18), 6798. doi:10.3390/ijms21186798

Kwon, H., Brown, W. E., Lee, C. A., Wang, D., Paschos, N., Hu, J. C., et al. (2019). Surgical and Tissue Engineering Strategies for Articular Cartilage and Meniscus Repair. *Nat. Rev. Rheumatol.* 15 (9), 550–570. doi:10.1038/s41584-019-0255-1

Li, H., Li, P., Yang, Z., Gao, C., Fu, L., Liao, Z., et al. (2021). Meniscal Regenerative Scaffolds Based on Biopolymers and Polymers: Recent Status and Applications. *Front. Cel Dev. Biol.* 9, 661802. doi:10.3389/fcell.2021.661802

Li, P., Zhang, W., Yu, H., Zheng, L., Yang, L., Liu, G., et al. (2016). Applying Electrospun Gelatin/Poly(lactic Acid-Co-Glycolic Acid) Bilayered Nanofibers to Fabrication of Meniscal Tissue Engineering Scaffold. *J. Nanosci Nanotechnol* 16 (5), 4718–4726. doi:10.1166/jnn.2016.12412

Li, Y., Chen, M., Zhou, W., Gao, S., Luo, X., Peng, L., et al. (2020). Cell-free 3D Wet-Electrospun PCL/silk fibroin/Sr2+ Scaffold Promotes Successful Total Meniscus Regeneration in a Rabbit Model. *Acta Biomater.* 113, 196–209. doi:10.1016/j.actbio.2020.06.017

Lohmander, L. S., Englund, P. M., Dahl, L. L., and Roos, E. M. (2007). The Long-Term Consequence of Anterior Cruciate Ligament and Meniscus Injuries. *Am. J. Sports Med.* 35 (10), 1756–1769. doi:10.1177/0363546507307396

Magaz, A., Roberts, A. D., Faraji, S., Nascimento, T. R. L., Medeiros, E. S., Zhang, W., et al. (2018). Porous, Aligned, and Biomimetic Fibers of Regenerated Silk Fibroin Produced by Solution Blow Spinning. *Biomacromolecules* 19 (12), 4542–4553. doi:10.1021/acs.biomac.8b01233

Makris, E. A., Hadidi, P., and Athanasiou, K. A. (2011). The Knee Meniscus: Structure-Function, Pathophysiology, Current Repair Techniques, and Prospects for Regeneration. *Biomaterials* 32 (30), 7411–7431. doi:10.1016/j.biomaterials.2011.06.037

Marrella, A., Lagazzo, A., Dellacasa, E., Pasquini, C., Finocchio, E., Barberis, F., et al. (2018). 3D Porous Gelatin/PVA Hydrogel as Meniscus Substitute Using Alginate Micro-particles as Porogens. *Polymers* 10 (4), 380. doi:10.3390/polym10040380

Martin, I., Jakob, M., Schäfer, D., Dick, W., Spagnoli, G., and Heberer, M. (2001). Quantitative Analysis of Gene Expression in Human Articular Cartilage from normal and Osteoarthritic Joints. *Osteoarthritis and Cartilage* 9 (2), 112–118. doi:10.1053/joca.2000.0366

Martinek, V., Ueblacker, P., Bräun, K., Nitschke, S., Mannhardt, R., Specht, K., et al. (2006). Second Generation of Meniscus Transplantation: *In-Vivo* Study with Tissue Engineered Meniscus Replacement. *Arch. Orthop. Trauma Surg.* 126 (4), 228–234. doi:10.1007/s00402-005-0025-1

Medeiros, E. L. G., Braz, A. L., Porto, I. J., Menner, A., Bismarck, A., Boccaccini, A. R., et al. (2016). Porous Bioactive Nanofibers via Cryogenic Solution Blow Spinning and Their Formation into 3D Macroporous Scaffolds. *ACS Biomater. Sci. Eng.* 2 (9), 1442–1449. doi:10.1021/acsbiomaterials.6b00072

Medeiros, E. S., Glenn, G. M., Klamczynski, A. P., Orts, W. J., and Mattoso, L. H. C. (2009). Solution Blow Spinning: A New Method to Produce Micro- and Nanofibers from Polymer Solutions. *J. Appl. Polym. Sci.* 113 (4), 2322–2330. doi:10.1002/app.30275

Milachowski, K. A., Weismeier, K., and Wirth, C. J. (1989). Homologous Meniscus Transplantation. *Int. Orthopaedics* 13 (1), 1–11. doi:10.1007/BF00266715

Molde, J., Steele, J. A. M., Pastino, A. K., Mahat, A., Murthy, N. S., and Kohn, J. (2020). A Step toward Engineering Thick Tissues: Distributing Microfibers within 3D Printed Frames. *J. Biomed. Mater. Res.* 108 (3), 581–591. doi:10.1002/jbm.a.36838

Murphy, C. A., Garg, A. K., Silva-Correia, J., Reis, R. L., Oliveira, J. M., and Collins, M. N. (2019). The Meniscus in Normal and Osteoarthritic Tissues: Facing the Structure Property Challenges and Current Treatment Trends. *Annu. Rev. Biomed. Eng.* 21, 495–521. doi:10.1146/annurev-bioeng-060418-052547

Oda, S., Otsuki, S., Kurokawa, Y., Hoshiyama, Y., Nakajima, M., and Neo, M. (2015). A New Method for Meniscus Repair Using Type I Collagen Scaffold and Infrapatellar Fat Pad. *J. Biomater. Appl.* 29 (10), 1439–1448. doi:10.1177/0885328215568984

Oliveira, J. E., Moraes, E. A., Costa, R. G. F., Afonso, A. S., Mattoso, L. H. C., Orts, W. J., et al. (2011). Nano and Submicrometric Fibers of poly(D,L-lactide) Obtained by Solution Blow Spinning: Process and Solution Variables. *J. Appl. Polym. Sci.* 122 (5), 3396–3405. doi:10.1002/app.34410

Pak, J., Lee, J. H., and Lee, S. H. (2014). Regenerative Repair of Damaged Meniscus with Autologous Adipose Tissue-Derived Stem Cells. *Biomed. Res. Int.* 2014, 1–10. doi:10.1155/2014/436029

Polk, S., Sori, N., Thayer, N., Kemper, N., Maghdouri-White, Y., Bulysheva, A. A., et al. (2018). Pneumatospinning of Collagen Microfibers from Benign Solvents. *Biofabrication* 10 (4), 045004. doi:10.1088/1758-5090/aad7d0

Puetzer, J. L., Koo, E., and Bonassar, L. J. (2015). Induction of Fiber Alignment and Mechanical Anisotropy in Tissue Engineered Menisci with Mechanical Anchoring. *J. Biomech.* 48 (8), 1436–1443. doi:10.1016/j.jbiomech.2015.02.033

Qu, D., Zhu, J. P., Childs, H. R., and Lu, H. H. (2019). Nanofiber-based Transforming Growth Factor-B3 Release Induces Fibrochondrogenic Differentiation of Stem Cells. *Acta Biomater.* 93, 111–122. doi:10.1016/j.actbio.2019.03.019

Qu, F., Holloway, J. L., Esterhai, J. L., Burdick, J. A., and Mauck, R. L. (2017). Programmed Biomolecule Delivery to Enable and Direct Cell Migration for Connective Tissue Repair. *Nat. Commun.* 8 (1), 1780. doi:10.1038/s41467-017-01955-w

Rai, M. F., Brophy, R. H., and Rosen, V. (2020). Molecular Biology of Meniscus Pathology: Lessons Learned from Translational Studies and Mouse Models. *J. Orthop. Res.* 38 (9), 1895–1904. doi:10.1002/jor.24630

Resmi, R., Parvathy, J., John, A., and Joseph, R. (2020). Injectable Self-Crosslinking Hydrogels for Meniscal Repair: A Study with Oxidized Alginate and Gelatin. *Carbohydr. Polym.* 234, 115902. doi:10.1016/j.carbpol.2020.115902

Rodeo, S. A., Monibi, F., Dehghani, B., and Maher, S. (2020). Biological and Mechanical Predictors of Meniscus Function: Basic Science to Clinical Translation. *J. Orthop. Res.* 38 (5), 937–945. doi:10.1002/jor.24552

Rothrauff, B. B., Sasaki, H., Kihara, S., Overholt, K. J., Gottardi, R., Lin, H., et al. (2019). Point-of-Care Procedure for Enhancement of Meniscal Healing in a Goat Model Utilizing Infrapatellar Fat Pad-Derived Stromal Vascular Fraction Cells Seeded in Photocrosslinkable Hydrogel. *Am. J. Sports Med.* 47 (14), 3396–3405. doi:10.1177/0363546519880468

Rueden, C. T., Schindelin, J., Hiner, M. C., DeZonia, B. E., Walter, A. E., Arena, E. T., et al. (2017). ImageJ2: ImageJ for the Next Generation of Scientific Image Data. *BMC Bioinformatics* 18 (1), 529. doi:10.1186/s12859-017-1934-z

Santos, A. M. C., Medeiros, E. L. G., Blaker, J. J., and Medeiros, E. S. (2016). Aqueous Solution Blow Spinning of Poly(vinyl Alcohol) Micro- and Nanofibers. *Mater. Lett.* 176, 122–126. doi:10.1016/j.matlet.2016.04.101

Sasaki, H., Rothrauff, B. B., Alexander, P. G., Lin, H., Gottardi, R., Fu, F. H., et al. (2018). *In Vitro* Repair of Meniscal Radial Tear with Hydrogels Seeded with Adipose Stem Cells and TGF-B3. *Am. J. Sports Med.* 46 (10), 2402–2413. doi:10.1177/0363546518782973

Sekiya, I., Koga, H., Otabe, K., Nakagawa, Y., Katano, H., Ozeki, N., et al. (2019). Additional Use of Synovial Mesenchymal Stem Cell Transplantation Following Surgical Repair of a Complex Degenerative Tear of the Medial Meniscus of the Knee: A Case Report. *Cel Transpl.* 28 (11), 1445–1454. doi:10.1177/0963689719863793

Shimomura, K., Bean, A. C., Lin, H., Nakamura, N., and Tuan, R. S. (2015). *In Vitro* Repair of Meniscal Radial Tear Using Aligned Electrospun Nanofibrous Scaffold. *Tissue Eng. Part A* 21 (13-14), 2066–2075. doi:10.1089/ten.TEA.2014.0549

Singh, R., Ahmed, F., Polley, P., and Giri, J. (2018). Fabrication and Characterization of Core-Shell Nanofibers Using a Next-Generation Airbrush for Biomedical Applications. *ACS Appl. Mater. Inter.* 10 (49), 41924–41934. doi:10.1021/acsami.8b13809

Sinha-Ray, S., Sinha-Ray, S., Yarin, A. L., and Pourdeyhimi, B. (2015). Theoretical and Experimental Investigation of Physical Mechanisms Responsible for Polymer Nanofiber Formation in Solution Blowing. *Polymer* 56, 452–463. doi:10.1016/j.polymer.2014.11.019

Srinivasan, S., Chhatre, S. S., Mabry, J. M., Cohen, R. E., and McKinley, G. H. (2011). Solution Spraying of Poly(methyl Methacrylate) Blends to Fabricate Microtextured, Superoleophobic Surfaces. *Polymer* 52 (14), 3209–3218. doi:10.1016/j.polymer.2011.05.008

Tomecka, E., Wojasinski, M., Jastrzebska, E., Chudy, M., Ciach, T., and Brzozka, Z. (2017). Poly(L -lactic Acid) and Polyurethane Nanofibers Fabricated by Solution Blow Spinning as Potential Substrates for Cardiac Cell Culture. *Mater. Sci. Eng. C* 75, 305–316. doi:10.1016/j.msec.2017.02.055

Tong, J., Xu, X., Wang, H., Zhuang, X., and Zhang, F. (2015). Solution-blown Core-Shell Hydrogel Nanofibers for Bovine Serum Albumin Affinity Adsorption. *RSC Adv.* 5 (101), 83232–83238. doi:10.1039/c5ra19420b

Turman, K., and Diduch, D. (2008). Meniscal Repair - Indications and Techniques. *J. Knee Surg.* 21 (2), 154–162. doi:10.1055/s-0030-1247812

van Schaik, T. J. A., Gaul, F., Dorthé, E. W., Lee, E. E., Grogan, S. P., and D'Lima, D. D. (2021). Development of an *Ex Vivo* Murine Osteochondral Repair Model. *Cartilage* 12 (1), 112–120. doi:10.1177/1947603518809402

Wang, K., Xu, M., Zhu, M., Su, H., Wang, H., Kong, D., et al. (2013). Creation of Macropores in Electrospun Silk Fibroin Scaffolds Using Sacrificial PEO-Microparticles to Enhance Cellular Infiltration. *J. Biomed. Mater. Res.* 101 (12), 3474–3481. doi:10.1002/jbm.a.34656

Wang, X., Ding, Y., Li, H., Mo, X., and Wu, J. (2021). Advances in Electrospun Scaffolds for Meniscus Tissue Engineering and Regeneration. *J. Biomed. Mater. Res.* doi:10.1002/jbm.b.34952

Winkler, P. W., Rothrauff, B. B., Buerba, R. A., Shah, N., Zaffagnini, S., Alexander, P., et al. (2020). Meniscal Substitution, a Developing and Long-Awaited Demand. *J. Exp. Ortop* 7 (1), 55. doi:10.1186/s40634-020-00270-6

Conflict of Interest: The authors declare that the research was conducted in the absence of any commercial or financial relationships that could be construed as a potential conflict of interest.

Publisher's Note: All claims expressed in this article are solely those of the authors and do not necessarily represent those of their affiliated organizations, or those of the publisher, the editors and the reviewers. Any product that may be evaluated in this article, or claim that may be made by its manufacturer, is not guaranteed or endorsed by the publisher.

frontiers in Bioengineering and Biotechnology

OPINION
published: 01 March 2022
doi: 10.3389/fbioe.2022.843166

Impediments to Meniscal Repair: Factors at Play Beyond Vascularity

Jay M. Patel[1,2]*

[1]Department of Orthopaedics, Emory University School of Medicine, Atlanta, GA, United States, [2]Atlanta VA Medical Center, Department of Veterans Affairs, Decatur, GA, United States

Keywords: meniscus, meniscus repair, mechanobiolgy, tissue engineering, vascularity

INTRODUCTION

The menisci are semi-lunar wedge-shaped discs that are vital to load distribution, stability, and lubrication of the knee (Fox et al., 2012). Due to the variety of stresses placed on these tissues, they are often injured, both through trauma and degeneration. Due to the relative avascularity in the tissue (Henning et al., 1987), it mostly lacks the capacity to self-heal, necessitating surgical intervention, with nearly 500,000 arthroscopic meniscal procedures annually in the US alone (Kim et al., 2011). Meniscectomy, or removal of the torn tissue, remains a leading treatment modality (Abrams et al., 2013; DeFroda et al., 2020), as it provides symptomatic relief from catching and locking; however, it predisposes the joint to long-term degeneration due to increased stresses placed on the articular surfaces (McDermott and Amis, 2006; Wang et al., 2015). Meniscus replacement options, such as allografts and scaffolds (Rodeo, 2001; Steadman and Rodkey, 2005; Efe et al., 2012; Lee et al., 2012), certainly exist, but they are currently limited in their long-term efficacy due to lacking formation and/or maintenance of functional meniscus tissue. For this reason, meniscal suture repair to preserve the native tissue has become increasingly popular (Beaufils and Pujol, 2017; Momaya, 2019), yet these procedures are only performed at a fraction of the rate (10–15%) of meniscectomy.

The decision to perform meniscectomy versus suture repair is often predicated on the region, geometry, and severity of the tear (**Figure 1A**). Furthermore, there are often many patient-level and joint-level factors that influence a clinician's decision-making process. For example, degraded meniscal tissue in older patients may be treated more conservatively to provide symptomatic relief as opposed to a younger patient with more acute tears, where the goal would be to preserve the meniscus and its function. Other factors such as comorbidities (e.g., cartilage wear, ligament status, alignment) may also factor into this decision. Even in a relatively healthy patient, there are many complex and challenging tear types, such as posterior root tears, that cannot simply be repaired. Here, we focus on acute tears within the body of the meniscus, where a surgeon often decides between meniscectomy and suture repair. In this subset, tears in the outer half of the meniscus, which is relatively more vascular (Henning et al., 1987), are mostly repaired, since the vascular supply is thought to provide enough nutrients to naturally bridge the tissue gap following suturing. However, since tears in the inner half (almost devoid of vascularity) lack access to this blood supply, the torn tissue is typically removed to alleviate symptoms (Henning et al., 1987; Mordecai, 2014), since suturing the torn edges may not result in eventual tissue bridging. This inner vs. outer dogma of meniscus repair has long governed mode of injury management; however, findings from the musculoskeletal research field may challenge this philosophy as the sole player. The purpose of this opinion article is to extend the impediments of meniscal repair beyond the traditional inner vs. outer paradigm, suggesting the role of other factors: disruption of the circumferential network, dense matrix as an obstruction to tissue joining, and other joint pathologies that may influence repair quality.

OPEN ACCESS

Edited by:
Mustafa Zakkar, University of Leicester, United Kingdom

Reviewed by:
Eran Linder-Ganz, Active Implants, United States
Francesco Travascio, University of Miami, United States

***Correspondence:**
Jay M. Patel
jay.milan.patel@emory.edu

Specialty section:
This article was submitted to Biomechanics, a section of the journal Frontiers in Bioengineering and Biotechnology

Received: *24 December 2021*
Accepted: *04 February 2022*
Published: *01 March 2022*

Citation:
Patel JM (2022) Impediments to Meniscal Repair: Factors at Play Beyond Vascularity. Front. Bioeng. Biotechnol. 10:843166. doi: 10.3389/fbioe.2022.843166

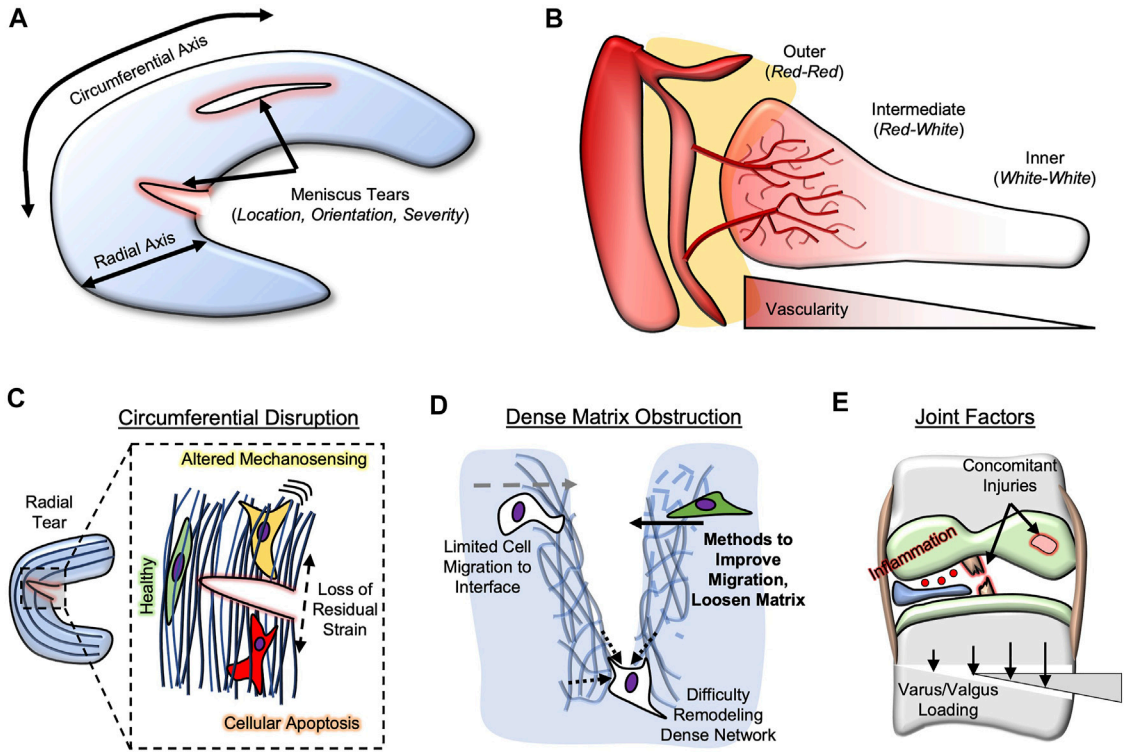

FIGURE 1 | Meniscus Repair Impediments. **(A)** Meniscus tears are often classified based on location, orientation, and severity. Location is usually classified by radial axis (inner, intermediate, outer) and circumferential axis (anterior, body, posterior). **(B)** Meniscus vascularity penetrates only partially into the meniscal body. **(C)** Circumferential network disruption (radial tears) lead to loss of residual strain, resulting in altered mechano-sensing and potentially cellular apoptosis. **(D)** Dense extracellular matrix can obstruct repair by limiting cell migration and matrix remodeling. Methods (e.g., growth factors) can improve migration and loosen matrix. **(E)** Joint factors that influence meniscal repair include concomitant injuries (e.g., ACI, cartilage), inflammation, and varus/valgus loading.

THE INNER VERSUS OUTER PARADIGM

The meniscus is often divided into zones along the radial axis, perpendicular to the circumferential network (**Figure 1B**). Often, the outer meniscus is deemed the red zone, as it contains vascular structures that penetrate, from the meniscosynovial junction, into the tissue. These vessels terminate in the middle third of the meniscus, deemed the red-white zone, leaving the inner third to half of the meniscus devoid of blood supply (termed the white zone). Studies comparing inner to outer meniscus healing rates are few in number (Cinque et al., 2019), perhaps since inner meniscus tears have not historically been repaired. Thus, the recent push to "save the meniscus" is complicated by the majority of tears occurring in either the red-white or white zones (Terzidis et al., 2006), limiting repair potential with suturing. Further exacerbating this issue is that the posterior horn of the meniscus appears to be most injured (Mansori et al., 2018; Jackson et al., 2019), yet exhibits the lowest vascular penetration (Crawford et al., 2020).

The role of vascularity in outer meniscal healing seems to rely on a wound healing response from blood supply, as well as the availability of stimulating growth factors, such as hypoxia inducible factor-1 (HIF-1a) and vascular endothelial growth factor (VEGF) (Lu et al., 2017). For this reason, a plethora of basic science researchers have attempted to augment inner meniscal repair using these vascular-derived factors. Meniscal "perforations", or surgical holes punctured from the inner-zone meniscus tear outwards towards the periphery, have been attempted preclinically and clinically (Zhongnan et al., 1988; Cook and Fox, 2007), albeit with inconsistent improvement in outcomes. Platelet-rich plasma and bone marrow aspirate have both been widely utilized in conjunction with avascular meniscal tears (Griffin et al., 2015; Muckenhirn et al., 2017; Kaminski et al., 2018), further highlighting the propensity towards "recreating vascularity" to enhance healing of inner meniscal tears. Certainly, vascularity is a player in meniscal healing, but is it the only one? Findings from the musculoskeletal field suggest that there may be others involved, and these may need to be considered to advance the meniscal repair field.

DISRUPTION OF CIRCUMFERENTIAL COLLAGEN NETWORK

As mentioned previously, the menisci are semi-lunar fibrocartilage tissues, and perhaps most important to their function is their array of circumferentially-aligned collagen fibers (Bullough et al., 1970; Fithian et al., 1990). This organization enables the tissue to distribute loads in the knee by generating circumferential hoop stresses (Lee et al., 2006).

Meniscus tears occur in a variety of orientations relative to this network; vertical and horizontal tears are parallel to the circumferential arrangement, while radial tears are perpendicular. Thus, radial tears disrupt the aligned collagen network; disruption of similar networks in other aligned tissues, such as tendon and annulus fibrosus, have been shown to be especially problematic. For example, annulus fibrosus cells exhibit aberrant behavior, including fibrotic phenotypic changes (alpha-smooth muscle actin expression) and even apoptosis, following removal of residual strains (Bonnevie et al., 2019). Similarly, transection of tendons (e.g., rotator cuff (Osti et al., 2017)) perpendicular to the aligned axis leads to similar fibrotic and apoptotic behavior (Egerbacher et al., 2008; Maeda et al., 2011; Lundgreen et al., 2013; T. et al., 2020). Thus, it is expected that radial meniscus tears may cause similar cellular changes (**Figure 1C**), especially near the lesion site, altering their capacity for healing. Of interest is that there seems to be a trend towards more radial tears in the lateral meniscus (Terzidis et al., 2006), which also exhibits a greater number of white-zone tears than the medial meniscus, potentially implicating circumferential network disruption, and not avascularity alone, as a player in lower healing capacity of the inner meniscus. Differences in the medial vs. lateral meniscus could also be influential in a surgeon's management; the lateral meniscus displaces more during loading (Bylski-Austrow et al., 1994) and less force is typically transmitted through the lateral compartment (Zhao et al., 2007), meaning that circumferential disruption could present a greater issue in the medial meniscus. Clinical systematic reviews, and perhaps preclinical animal studies (Bansal et al., 2020), that investigate the healing rates of inner vs. outer zone radial tears, and inner vertical vs. inner radial tears, would help to test this hypothesis.

DENSE EXTRACELLULAR MATRIX AS AN OBSTRUCTOR TO HEALING

One of the greatest obstacles in the field of musculoskeletal repair is the re-integration of wound edges. Frequently thought of in the context of tissue engineering [scaffold-to-tissue integration; (Moffat et al., 2009)], healing of meniscal tears requires two edges of the meniscus to join back together. Suturing holds these edges together initially, but long-term bridging of this gap will require a combination of tissue deposition and remodeling along the interface. A plethora of researchers have attempted to improve meniscal repair healing with scaffolds [e.g., fibrin, collagen, electrospun polymers (Scotti et al., 2009; González-Fernández et al., 2016; Baek et al., 2019)] that are often supplemented with cells (meniscal fibrochondrocytes, marrow stromal cells) and factors (transforming growth factor-beta 3, connective tissue growth factor) (He et al., 2011; Cucchiarini et al., 2015; Sasaki et al., 2018), yet the overall shear strengths of this repair interface are typically orders of magnitude lower than the native meniscus, leaving it susceptible to re-tear. A potential obstructor in this repair interface is the dense nature of native meniscal tissue; the dense matrix limits cell migration to, and eventual healing at, the tear site, and it may lack the capacity to undergo active remodeling to integrate the two edges (**Figure 1D**).

Many techniques have been employed to improve meniscus cell migration to improve integrative repair. This is especially important in older patients, as both cell motility and proliferation decrease with age (Bartling et al., 2009; Qu et al., 2019), affecting repair potential and efficacy. For example, resident meniscus cells can be "activated" with electrical stimulation (Gunja et al., 2012; Yuan et al., 2014), growth factor delivery (e.g., platelet derived growth factor; (Qu et al., 2017)), or perhaps the addition of exogenous cells/biologics [e.g., endothelial cells (Yuan et al., 2015), platelets (Wong et al., 2017), hyaluronic acid (Murakami et al., 2019)]. A portion of the field is also studying a subpopulation of meniscal progenitor cells that further aid in the process of regeneration (Muhammad et al., 2014; Seol et al., 2017); thus, their migration and recruitment to the site of injury using these techniques would be greatly beneficial. Since the stiffest part of these cells is their nucleus, nuclear softening is also a promising approach to improve migration through the dense connective networks of the meniscus (Heo et al., 2020). Rather than improving cell recruitment by altering the cells, the matrix around the cell could also be loosened *via* local digestion (Qu et al., 2013, 2015). Similar techniques have been employed in cartilage repair (van de Breevaart Bravenboer et al., 2004; Seol et al., 2014; Liebesny et al., 2019), showing that loosening the network can not only enhance migration, but also improve the ability of the two torn edges to merge back together. This latter concept may be most important, as the dense meniscal network experiences little to no remodeling (Våben et al., 2020), whereas slightly degraded matrix can be remodeled more readily to integrate the two edges.

OTHER JOINT FACTORS THAT INFLUENCE HEALING

Perhaps the most obvious environmental factor that has been implicated in meniscal healing potential is inflammation. The release of pro-inflammatory cytokines (e.g., interleukin-1, tumor necrosis factor-alpha) following soft tissue injury in the joint is well-documented (Irie et al., 2003; Haslauer et al., 2014; Ogura et al., 2016), both by the synovial/synovium cells and the injured tissue itself. In the meniscus specifically, integrative repair of the meniscus, both *in vitro* and *in vivo*, is reduced under inflamed environments (Hennerbichler et al., 2007; Riera et al., 2011), perhaps due to reduced proliferation and migration, and reduced capacity for meniscus specific matrix deposition and remodeling. Thus, intra-articular augmentation with, and perhaps even localized delivery of, anti-inflammatory agents may present promising improvements in repair success. Novel methods to deliver these drugs include capsules, carriers, spheres, both at the micro-scale and nano-scale to enhance retention, duration, and activity of both anti-inflammatory and pro-regenerative cues (Patel et al., 2019). Since both inflammation post-injury and the reparative process occur on the order of weeks to months, these prolonging attributes are especially helpful. Delaying

meniscal repair procedures after injury, similar to what is done with anterior cruciate ligament reconstruction (Inoue et al., 2016), may help to delay repair until inflammation has subsided, improving the integrative nature, and thus long-term stability, of the repair.

Beyond the biological milieu within the joint, there are a variety of biomechanical joint factors at play. First and foremost, concomitant injuries, especially anterior cruciate ligament injuries and reconstruction, place a large mechanical burden on the meniscus (Dargel et al., 2007; Chen et al., 2017), and restoration of these tissues and their function are paramount to meniscal function and its ability to be repaired. This may also include an open-wedge osteotomy to correct varus or valgus malalignment (Jing et al., 2019; Rocha de Faria et al., 2021), to alleviate loads that are placed on one compartment of the knee. Furthermore, along the same lines, the rehabilitation timeline needs to be precisely controlled (Cavanaugh and Killian, 2012; Spang Iii et al., 2018); early overloading may cause re-tear before adequate tissue has been deposited to bridge the tear. Alternatively, since mechanical loading is beneficial to meniscal cell activity and matrix deposition (McNulty et al., 2010; Puetzer et al., 2012), a protocol that is too conservative can prohibit the increased regenerative capacity provided by loading. Timing prior to the procedure is also an important biomechanical consideration. While waiting can calm inflammation to enhance repair potential, it must be balanced with the increased risk of other injuries that can occur in this timeframe (Fok and Yau, 2013; Kolin et al., 2021; Prodromidis et al., 2021).

CONCLUSION

The meniscal repair field has long cited the location along the radial axis, indicative of vascular content, as the sole determinant of treatment modality. I believe that other factors (circumferential disruption, dense matrix obstruction, and joint factors) may be just as influential to repair potential. Thus, the field would greatly benefit from additional clinical studies and reviews to better track outcomes with regards to these variables, which is fully possible with the increasing performance of inner zone repairs. Additional preclinical work, both *in vitro* and *in vivo*, will help to elucidate the healing potential of various tear configurations, especially as they relate to the alignment of collagen bundles, the relative density of the matrix, and the environmental inflammatory state. The recent shift to "save the meniscus" with repair techniques would greatly benefit from consideration of these alternative impediments to healing.

AUTHOR CONTRIBUTIONS

The author confirms being the sole contributor of this work and has approved it for publication.

REFERENCES

Abrams, G. D., Frank, R. M., Gupta, A. K., Harris, J. D., McCormick, F. M., and Cole, B. J. (2013). Trends in Meniscus Repair and Meniscectomy in the United States, 2005-2011. *Am. J. Sports Med.* 41, 2333–2339. doi:10.1177/0363546513495641

Baek, J., Lotz, M. K., and D'Lima, D. D. (2019). Core-Shell Nanofibrous Scaffolds for Repair of Meniscus Tears. *Tissue Eng. A* 25, 1577–1590. doi:10.1089/ten.tea.2018.0319

Bansal, S., Miller, L. M., Patel, J. M., Meadows, K. D., Eby, M. R., Saleh, K. S., et al. (2020). Transection of the Medial Meniscus Anterior Horn Results in Cartilage Degeneration and Meniscus Remodeling in a Large Animal Model. *J. Orthop. Res.* 38, 2696–2708. doi:10.1002/jor.24694

Bartling, B., Desole, M., Rohrbach, S., Silber, R. E., and Simm, A. (2009). Age-associated Changes of Extracellular Matrix Collagen Impair Lung Cancer Cell Migration. *FASEB J.* 23, 1510–1520. doi:10.1096/fj.08-122648

Beaufils, P., and Pujol, N. (2017). Management of Traumatic Meniscal Tear and Degenerative Meniscal Lesions. Save the Meniscus. *Orthopaedics Traumatol. Surg. Res.* 103, S237–S244. doi:10.1016/j.otsr.2017.08.003

Bonnevie, E. D., Gullbrand, S. E., Ashinsky, B. G., Tsinman, T. K., Elliott, D. M., Chao, P., et al. (2019). Aberrant Mechanosensing in Injured Intervertebral Discs as a Result of Boundary-Constraint Disruption and Residual-Strain Loss. *Nat. Biomed. Eng.* 3, 998–1008. doi:10.1038/s41551-019-0458-4

Bullough, P. G., Munuera, L., Murphy, J., and Weinstein, A. M. (1970). The Strength of the Menisci of the Knee as it Relates to Their fine Structure. *The J. Bone Jt. Surg. Br. volume* 52-B, 564–570. doi:10.1302/0301-620x.52b3.564

Bylski-Austrow, D. I., Ciarelli, M. J., Kayner, D. C., Matthews, L. S., and Goldstein, S. A. (1994). Displacements of the Menisci under Joint Load: An *In Vitro* Study in Human Knees. *J. Biomech.* 27, 421–431. doi:10.1016/0021-9290(94)90018-3

Cavanaugh, J. T., and Killian, S. E. (2012). Rehabilitation Following Meniscal Repair. *Curr. Rev. Musculoskelet. Med.* 5, 46–58. doi:10.1007/s12178-011-9110-y

Chen, T., Wang, H., Warren, R., and Maher, S. (2017). Loss of ACL Function Leads to Alterations in Tibial Plateau Common Dynamic Contact Stress Profiles. *J. Biomech.* 61, 275–279. doi:10.1016/j.jbiomech.2017.07.024

Cinque, M. E., DePhillipo, N. N., Moatshe, G., Chahla, J., Kennedy, M. I., Dornan, G. J., et al. (2019). Clinical Outcomes of Inside-Out Meniscal Repair According to Anatomic Zone of the Meniscal Tear. *Orthop. J. Sport Med.* 7 (7), 2325967119860806. doi:10.1177/2325967119860806

Cook, J. L., and Fox, D. B. (2007). A Novel Bioabsorbable Conduit Augments Healing of Avascular Meniscal Tears in a Dog Model. *Am. J. Sports Med.* 35 (11), 1877–1887. doi:10.1177/0363546507304330

Crawford, M. D., Hellwinkel, J. E., Aman, Z., Akamefula, R., Singleton, J. T., Bahney, C., et al. (2020). Microvascular Anatomy and Intrinsic Gene Expression of Menisci from Young Adults. *Am. J. Sports Med.* 48, 3147–3153. doi:10.1177/0363546520961555

Cucchiarini, M., Schmidt, K., Frisch, J., Kohn, D., and Madry, H. (2015). Overexpression of TGF-β via rAAV-Mediated Gene Transfer Promotes the Healing of Human Meniscal Lesions *Ex Vivo* on Explanted Menisci. *Am. J. Sports Med.* 43 (5), 1197–1205. doi:10.1177/0363546514567063

DeFroda, S. F., Yang, D. S., Donnelly, J. C., Bokshan, S. L., Owens, B. D., and Daniels, A. H. (2020). Trends in the Surgical Treatment of Meniscal Tears in Patients with and without Concurrent Anterior Cruciate Ligament Tears. *Phys. Sportsmed* 48 (2), 229–235. doi:10.1080/00913847.2019.1685363

Efe, T., Getgood, A., Schofer, M. D., Fuchs-Winkelmann, S., Mann, D., Paletta, J. R. J., et al. (2012). The Safety and Short-Term Efficacy of a Novel Polyurethane Meniscal Scaffold for the Treatment of Segmental Medial Meniscus Deficiency. *Knee Surg. Sports Traumatol. Arthrosc.* 20, 1822–1830. doi:10.1007/s00167-011-1779-3

Egerbacher, M., Arnoczky, S. P., Caballero, O., Lavagnino, M., and Gardner, K. L. (2008). Loss of Homeostatic Tension Induces Apoptosis in Tendon Cells: an *In Vitro* Study. *Clin. Orthop. Relat. Res.* 466, 1562–1568. doi:10.1007/s11999-008-0274-8

Fithian, D. C., Kelly, M. A., and Mow, V. C. (1990). Material Properties and Structure-Function Relationships in the Menisci. *Clin. Orthopaedics Relat. Res.* 252, 19–31. doi:10.1097/00003086-199003000-00004

Fok, A. W. M., and Yau, W. P. (2013). Delay in ACL Reconstruction Is Associated with More Severe and Painful Meniscal and Chondral Injuries. *Knee Surg. Sports Traumatol. Arthrosc.* 21, 928–933. doi:10.1007/s00167-012-2027-1

Fox, A. J. S., Bedi, A., and Rodeo, S. A. (2012). The Basic Science of Human Knee Menisci. *Sports Health* 4, 340–351. doi:10.1177/1941738111429419

González-Fernández, M. L., Pérez-Castrillo, S., Sánchez-Lázaro, J. A., Prieto-Fernández, J. G., López-González, M. E., Lobato-Pérez, S., et al. (2016). Assessment of Regeneration in Meniscal Lesions by Use of Mesenchymal Stem Cells Derived from Equine Bone Marrow and Adipose Tissue. *Am. J. Vet. Res.* 77 (7), 779–788. doi:10.2460/ajvr.77.7.779

Griffin, J. W., Hadeed, M. M., Werner, B. C., Diduch, D. R., Carson, E. W., and Miller, M. D. (2015). Platelet-rich Plasma in Meniscal Repair: Does Augmentation Improve Surgical Outcomes? *Clin. Orthop. Relat. Res.* 473 (5), 1665–1672. doi:10.1007/s11999-015-4170-8

Gunja, N. J., Dujari, D., Chen, A., Luengo, A., Fong, J. V., and Hung, C. T. (2012). Migration Responses of Outer and Inner Meniscus Cells to Applied Direct Current Electric fields. *J. Orthop. Res.* 30, 103–111. doi:10.1002/jor.21489

Haslauer, C. M., Proffen, B. L., Johnson, V. M., Hill, A., and Murray, M. M. (2014). Gene Expression of Catabolic Inflammatory Cytokines Peak before Anabolic Inflammatory Cytokines after ACL Injury in a Preclinical Model. *J. Inflamm.* 11, 34. doi:10.1186/s12950-014-0034-3

He, W., Liu, Y. J., Wang, Z. G., Guo, Z. K., Wang, M. X., and Wang, N. (2011). Enhancement of Meniscal Repair in the Avascular Zone Using Connective Tissue Growth Factor in a Rabbit Model. *Chin. Med. J. (Engl)* 124, 3968–3975. doi:10.3760/cma.j.issn.2011.23.023

Hennerbichler, A., Moutos, F. T., Hennerbichler, D., Weinberg, J. B., and Guilak, F. (2007). Interleukin-1 and Tumor Necrosis Factor Alpha Inhibit Repair of the Porcine Meniscus *In Vitro*. *Osteoarthritis and Cartilage* 15, 1053–1060. doi:10.1016/j.joca.2007.03.003

Henning, C. E., Lynch, M. A., and Clark, J. R. (1987). Vascularity for Healing of Meniscus Repairs. *Arthrosc. J. Arthroscopic Relat. Surg.* 3, 13–18. doi:10.1016/S0749-8063(87)80004-X

Heo, S.-J., Song, K. H., Thakur, S., Miller, L. M., Cao, X., Peredo, A. P., et al. (2020). Nuclear Softening Expedites Interstitial Cell Migration in Fibrous Networks and Dense Connective Tissues. *Sci. Adv.* 6 (25), eaax5083. doi:10.1126/sciadv.aax5083

Inoue, M., Muneta, T., Ojima, M., Nakamura, K., Koga, H., Sekiya, I., et al. (2016). Inflammatory Cytokine Levels in Synovial Fluid 3, 4 Days Postoperatively and its Correlation with Early-phase Functional Recovery after Anterior Cruciate Ligament Reconstruction: a Cohort Study. *J. Exp. Ortop* 3, 30. doi:10.1186/s40634-016-0067-z

Irie, K., Uchiyama, E., and Iwaso, H. (2003). Intraarticular Inflammatory Cytokines in Acute Anterior Cruciate Ligament Injured Knee. *The Knee* 10, 93–96. doi:10.1016/S0968-0160(02)00083-2

Jackson, T., Fabricant, P. D., Beck, N., Storey, E., Patel, N. M., and Ganley, T. J. (2019). Epidemiology, Injury Patterns, and Treatment of Meniscal Tears in Pediatric Patients: A 16-Year Experience of a Single Center. *Orthop. J. Sport Med.* 7 (12), 2325967119890325. doi:10.1177/2325967119890325

Jing, L., Liu, K., Wang, X., Wang, X., Li, Z., Zhang, X., et al. (2019). Second-look Arthroscopic Findings after Medial Open-Wedge High Tibial Osteotomy Combined with All-Inside Repair of Medial Meniscus Posterior Root Tears. *J. Orthop. Surg. (Hong Kong)* 28, 230949901988883. doi:10.1177/2309499019888836

Kaminski, R., Kulinski, K., Kozar-Kaminska, K., Wielgus, M., Langner, M., Wasko, M. K., et al. (2018). A Prospective, Randomized, Double-Blind, Parallel-Group, Placebo-Controlled Study Evaluating Meniscal Healing, Clinical Outcomes, and Safety in Patients Undergoing Meniscal Repair of Unstable, Complete Vertical Meniscal Tears (Bucket Handle) Augmented Wit. *Biomed. Res. Int.* 2018, 9315815. doi:10.1155/2018/9315815

Kim, S., Bosque, J., Meehan, J. P., Jamali, A., and Marder, R. (2011). Increase in Outpatient Knee Arthroscopy in the United States: A Comparison of National Surveys of Ambulatory Surgery, 1996 and 2006. *J. Bone Jt. Surg Am* 93 (11), 994–1000. Available at:doi:10.2106/JBJS.I.01618https://journals.lww.com/jbjsjournal/Fulltext/2011/06010/Increase_in_Outpatient_Knee_Arthroscopy_in_the.2.aspx

Kolin, D. A., Dawkins, B., Park, J., Fabricant, P. D., Gilmore, A., Seeley, M., et al. (2021). ACL Reconstruction Delay in Pediatric and Adolescent Patients Is Associated with a Progressive Increased Risk of Medial Meniscal Tears. *J. Bone Jt. Surg Am.* 103 (15), 1368–1373. Available at:doi:10.2106/jbjs.20.01459https://journals.lww.com/jbjsjournal/Fulltext/2021/08040/ACL_Reconstruction_Delay_in_Pediatric_and.2.aspx

Lee, S. J., Aadalen, K. J., Malaviya, P., Lorenz, E. P., Hayden, J. K., Farr, J., et al. (2006). Tibiofemoral Contact Mechanics after Serial Medial Meniscectomies in the Human Cadaveric Knee. *Am. J. Sports Med.* 34, 1334–1344. doi:10.1177/0363546506286786

Lee, S. R., Kim, J. G., and Nam, S. W. (2012). The Tips and Pitfalls of Meniscus Allograft Transplantation. *Knee Surg. Relat. Res.* 24, 137–145. doi:10.5792/ksrr.2012.24.3.137

Liebesny, P. H., Mroszczyk, K., Zlotnick, H., Hung, H.-H., Frank, E., Kurz, B., et al. (2019). Enzyme Pretreatment Plus Locally Delivered HB-IGF-1 Stimulate Integrative Cartilage Repair *In Vitro*. *Tissue Eng. Part A* 25, 1191–1201. doi:10.1089/ten.tea.2019.0013

Lu, Z., Furumatsu, T., Fujii, M., Maehara, A., and Ozaki, T. (2017). The Distribution of Vascular Endothelial Growth Factor in Human Meniscus and a Meniscal Injury Model. *J. Orthopaedic Sci.* 22, 715–721. doi:10.1016/j.jos.2017.02.006

Lundgreen, K., Lian, Ø., Scott, A., and Engebretsen, L. (2013). Increased Levels of Apoptosis and P53 in Partial-Thickness Supraspinatus Tendon Tears. *Br. J. Sports Med.* 47, 46. e2 LP-e2. doi:10.1136/bjsports-2013-092459.50

Mader, K., Pennig, D., Dargel, J., Gotter, M., Koebke, J., and Schmidt-Wiethoff, R. (2007). Biomechanics of the Anterior Cruciate Ligament and Implications for Surgical Reconstruction. *Strateg. Trauma Limb Reconstr.* 2, 1–12. doi:10.1007/s11751-007-0016-6

Maeda, T., Sakabe, T., Sunaga, A., Sakai, K., Rivera, A. L., Keene, D. R., et al. (2011). Conversion of Mechanical Force into TGF-β-Mediated Biochemical Signals. *Curr. Biol.* 21, 933–941. doi:10.1016/j.cub.2011.04.007

Mansori, A. E., Lording, T., Schneider, A., Dumas, R., Servien, E., and Lustig, S. (2018). Incidence and Patterns of Meniscal Tears Accompanying the Anterior Cruciate Ligament Injury: Possible Local and Generalized Risk Factors. *Int. Orthop.* 42 (9), 2113–2121. doi:10.1007/s00264-018-3992-x

McDermott, I. D., and Amis, A. A. (2006). The Consequences of Meniscectomy. *J. Bone Jt. Surg. Br. volume* 88-B, 1549–1556. doi:10.1302/0301-620X.88B12.18140

McNulty, A. L., Estes, B. T., Wilusz, R. E., Weinberg, J. B., and Guilak, F. (2010). Dynamic Loading Enhances Integrative Meniscal Repair in the Presence of Interleukin-1. *Osteoarthritis and Cartilage* 18, 830–838. doi:10.1016/j.joca.2010.02.009

Moffat, K. L., Wang, I.-N. E., Rodeo, S. A., and Rodeo, H. H. (2009). Orthopedic Interface Tissue Engineering for the Biological Fixation of Soft Tissue Grafts. *Clin. Sports Med.* 28, 157–176. doi:10.1016/j.csm.2008.08.006

Momaya, A. (2019). Editorial Commentary: Save the Meniscus? Show Me the Money! *Arthrosc. J. Arthroscopic Relat. Surg.* 35, 3287–3288. doi:10.1016/j.arthro.2019.08.008

Mordecai, S. C. (2014). Treatment of Meniscal Tears: An Evidence Based Approach. *Wjo* 5, 233. doi:10.5312/wjo.v5.i3.233

Muckenhirn, K. J., Kruckeberg, B. M., Cinque, M. E., Chahla, J., DePhillipo, N. N., Godin, J. A., et al. (2017). Arthroscopic Inside-Out Repair of a Meniscus Bucket-Handle Tear Augmented with Bone Marrow Aspirate Concentrate. *Arthrosc. Tech.* 6 (4), e1221–e1227. doi:10.1016/j.eats.2017.04.014

Muhammad, H., Schminke, B., Bode, C., Roth, M., Albert, J., von der Heyde, S., et al. (2014). Human Migratory Meniscus Progenitor Cells Are Controlled via the TGF-β Pathway. *Stem Cel. Rep.* 3, 789–803. doi:10.1016/j.stemcr.2014.08.010

Murakami, T., Otsuki, S., Okamoto, Y., Nakagawa, K., Wakama, H., Okuno, N., et al. (2019). Hyaluronic Acid Promotes Proliferation and Migration of Human Meniscus Cells via a CD44-dependent Mechanism. *Connect. Tissue Res.* 60, 117–127. doi:10.1080/03008207.2018.1465053

Ogura, T., Suzuki, M., Sakuma, Y., Yamauchi, K., Orita, S., Miyagi, M., et al. (2016). Differences in Levels of Inflammatory Mediators in Meniscal and Synovial Tissue of Patients with Meniscal Lesions. *J. Exp. Ortop* 3, 7. doi:10.1186/s40634-016-0041-9

Osti, L., Buda, M., Del Buono, A., Osti, R., Massari, L., and Maffulli, N. (2017). Apoptosis and Rotator Cuff Tears: Scientific Evidence from Basic Science to Clinical Findings. *Br. Med. Bull.* 122, 123–133. doi:10.1093/bmb/ldx008

Patel, J. M., Saleh, K. S., Burdick, J. A., and Mauck, R. L. (2019). Bioactive Factors for Cartilage Repair and Regeneration: Improving Delivery, Retention, and Activity. *Acta Biomater.* 93, 222–238. doi:10.1016/j.actbio.2019.01.061

Prodromidis, A. D., Drosatou, C., Mourikis, A., Sutton, P. M., and Charalambous, C. P. (2021). Relationship between Timing of Anterior Cruciate Ligament Reconstruction and Chondral Injuries: A Systematic Review and Meta-Analysis. *Am. J. Sports Med.*, 036354652110361. doi:10.1177/03635465211036141

Puetzer, J. L., Ballyns, J. J., and Bonassar, L. J. (2012). The Effect of the Duration of Mechanical Stimulation and Post-Stimulation Culture on the Structure and Properties of Dynamically Compressed Tissue-Engineered Menisci. *Tissue Eng. Part A* 18, 1365–1375. doi:10.1089/ten.tea.2011.0589

Qu, F., Guilak, F., and Mauck, R. L. (2019). Cell Migration: Implications for Repair and Regeneration in Joint Disease. *Nat. Rev. Rheumatol.* 15, 167–179. doi:10.1038/s41584-018-0151-0

Qu, F., Holloway, J. L., Esterhai, J. L., Burdick, J. A., and Mauck, R. L. (2017). Programmed Biomolecule Delivery to Enable and Direct Cell Migration for Connective Tissue Repair. *Nat. Commun.* 8, 1780. doi:10.1038/s41467-017-01955-w

Qu, F., Lin, J.-M. G., Esterhai, J. L., Fisher, M. B., and Mauck, R. L. (2013). Biomaterial-mediated Delivery of Degradative Enzymes to Improve Meniscus Integration and Repair. *Acta Biomater.* 9, 6393–6402. doi:10.1016/j.actbio.2013.01.016

Qu, F., Pintauro, M. P., Haughan, J. E., Henning, E. A., Esterhai, J. L., Schaer, T. P., et al. (2015). Repair of Dense Connective Tissues via Biomaterial-Mediated Matrix Reprogramming of the Wound Interface. *Biomaterials* 39, 85–94. doi:10.1016/j.biomaterials.2014.10.067

Riera, K. M., Rothfusz, N. E., Wilusz, R. E., Weinberg, J. B., Guilak, F., and McNulty, A. L. (2011). Interleukin-1, Tumor Necrosis Factor-Alpha, and Transforming Growth Factor-Beta 1 and Integrative Meniscal Repair: Influences on Meniscal Cell Proliferation and Migration. *Arthritis Res. Ther.*. 13(6):R187. doi:10.1186/ar3515

Rocha de Faria, J. L., Pavão, D. M., Moreirão, M. d. C., Titonelli, V. E., de Sousa, E. B., Minamoto, S. T. N., et al. (2021). Posterior Root Repair of Medial Meniscus Combined with Valgus Opening Wedge Tibial Osteotomy. *Arthrosc. Tech.* 10, e1373–e1382. doi:10.1016/j.eats.2021.01.042

Rodeo, S. A. (2001). Meniscal Allografts-Where Do We Stand? *Am. J. Sports Med.* 29, 246–261. doi:10.1177/03635465010290022401

Sasaki, H., Rothrauff, B. B., Alexander, P. G., Lin, H., Gottardi, R., Fu, F. H., et al. (2018). *In Vitro* Repair of Meniscal Radial Tear with Hydrogels Seeded with Adipose Stem Cells and TGF-B3. *Am. J. Sports Med.* 46 (10), 2402–2413. doi:10.1177/0363546518782973

Scotti, C., Pozzi, A., Mangiavini, L., Vitari, F., Boschetti, F., Domeneghini, C., et al. (2009). Healing of Meniscal Tissue by Cellular Fibrin Glue: An *In Vivo* Study. *Knee Surgery, Sport Traumatol. Arthrosc.* 17 (6), 645–651. doi:10.1007/s00167-009-0745-9

Seol, D., Yu, Y., Choe, H., Jang, K., Brouillette, M. J., Zheng, H., et al. (2014). Effect of Short-Term Enzymatic Treatment on Cell Migration and Cartilage Regeneration: *In Vitro* Organ Culture of Bovine Articular Cartilage. *Tissue Eng. Part A* 20, 1807–1814. doi:10.1089/ten.tea.2013.0444

Seol, D., Zhou, C., Brouillette, M. J., Song, I., Yu, Y., Choe, H. H., et al. (2017). Characteristics of Meniscus Progenitor Cells Migrated from Injured Meniscus. *J. Orthop. Res.* 35, 1966–1972. doi:10.1002/jor.23472

Spang Iii, R. C., Mohamadi, A., DeAngelis, J. P., Nazarian, A., Ramappa, A. J., and Ramappa, A. J. (2018). Rehabilitation Following Meniscal Repair: a Systematic Review. *BMJ Open Sport Exerc. Med.* 4, e000212. doi:10.1136/bmjsem-2016-000212

Steadman, J. R., and Rodkey, W. G. (2005). Tissue-engineered Collagen Meniscus Implants: 5- to 6-year Feasibility Study Results. *Arthrosc. J. Arthroscopic Relat. Surg.* 21, 515–525. doi:10.1016/j.arthro.2005.01.006

Terzidis, I. P., Christodoulou, A., Ploumis, A., Givissis, P., Natsis, K., and Koimtzis, M. (2006). Meniscal Tear Characteristics in Young Athletes with a Stable Knee: Arthroscopic Evaluation. *Am. J. Sports Med.* 34 (7), 1170–1175. doi:10.1177/0363546506287939

Våben, C., Heinemeier, K. M., Schjerling, P., Olsen, J., Petersen, M. M., Kjaer, M., et al. (2020). No Detectable Remodelling in Adult Human Menisci: an Analysis Based on the C14 Bomb Pulse. *Br. J. Sports Med.* 54, 1433–1437. doi:10.1136/bjsports-2019-101360

van de Breevaart Bravenboer, J., In der Maur, C. D., Bos, P. K., Feenstra, L., Verhaar, J. A., Weinans, H., et al. (2004). Improved Cartilage Integration and Interfacial Strength after Enzymatic Treatment in a Cartilage Transplantation Model. *Arthritis Res. Ther.* 6, R469. doi:10.1186/ar1216

Wang, H., Chen, T., Gee, A. O., Hutchinson, I. D., Stoner, K., Warren, R. F., et al. (2015). Altered Regional Loading Patterns on Articular Cartilage Following Meniscectomy Are Not Fully Restored by Autograft Meniscal Transplantation. *Osteoarthritis and Cartilage* 23, 462–468. doi:10.1016/j.joca.2014.12.003

Wong, C. C., Kuo, T. F., Yang, T. L., Tsuang, Y. H., Lin, M. F., Chang, C. H., et al. (2017). Platelet-rich Fibrin Facilitates Rabbit Meniscal Repair by Promoting Meniscocytes Proliferation, Migration, and Extracellular Matrix Synthesis. *Int. J. Mol. Sci.* 18 (8), 1722. doi:10.3390/ijms18081722

Yuan, X., Arkonac, D. E., Chao, P.-h. G., and Vunjak-Novakovic, G. (2014). Electrical Stimulation Enhances Cell Migration and Integrative Repair in the Meniscus. *Sci. Rep.* 4, 3674. doi:10.1038/srep03674

Yuan, X., Eng, G. M., Arkonac, D. E., Chao, P. H. G., and Vunjak-Novakovic, G. (2015). Endothelial Cells Enhance the Migration of Bovine Meniscus Cells. *Arthritis Rheumatol.* 67 (1), 182–192. doi:10.1002/art.38889

Zhao, D., Banks, S. A., D'Lima, D. D., Colwell, C. W., Jr., and Fregly, B. J. (2007). *In Vivo* medial and Lateral Tibial Loads during Dynamic and High Flexion Activities. *J. Orthop. Res.* 25, 593–602. doi:10.1002/jor.20362

Zhongnan, Z., Kaiyuan, T., Yinkan, X., Wenming, Z., Zhentian, L., and Shihuan, O. (1988). Treatment of Longitudinal Injuries in Avascular Area of Meniscus in Dogs by Trephination. *Arthrosc. J. Arthroscopic Relat. Surg.* 4, 151–159. doi:10.1016/S0749-8063(88)80019-7

Conflict of Interest: The author declares that the research was conducted in the absence of any commercial or financial relationships that could be construed as a potential conflict of interest.

Publisher's Note: All claims expressed in this article are solely those of the authors and do not necessarily represent those of their affiliated organizations, or those of the publisher, the editors and the reviewers. Any product that may be evaluated in this article, or claim that may be made by its manufacturer, is not guaranteed or endorsed by the publisher.

frontiers in Bioengineering and Biotechnology

ORIGINAL RESEARCH
published: 01 March 2022
doi: 10.3389/fbioe.2022.837619

A Tale of Two Loads: Modulation of IL-1 Induced Inflammatory Responses of Meniscal Cells in Two Models of Dynamic Physiologic Loading

Benjamin D. Andress[1†], *Rebecca M. Irwin*[2†], *Ishaan Puranam*[3], *Brenton D. Hoffman*[3,4] *and Amy L. McNulty*[1,2*]

[1]Department of Pathology, Duke University, Durham, NC, United States, [2]Department of Orthopaedic Surgery, Duke University School of Medicine, Durham, NC, United States, [3]Department of Biomedical Engineering, Duke University, Durham, NC, United States, [4]Department of Cell Biology, Duke University, Durham, NC, United States

OPEN ACCESS

Edited by:
Jay Patel,
Emory University, United States

Reviewed by:
Feini Qu,
Washington University in St. Louis, United States
Diane Wagner,
Indiana University, Purdue University Indianapolis, United States
Nathaniel Dyment,
University of Pennsylvania, United States

***Correspondence:**
Amy L. McNulty
alr@duke.edu

[†]These authors have contributed equally to this work and share first authorship

Specialty section:
This article was submitted to Biomechanics, a section of the journal Frontiers in Bioengineering and Biotechnology

Received: 16 December 2021
Accepted: 24 January 2022
Published: 01 March 2022

Citation:
Andress BD, Irwin RM, Puranam I, Hoffman BD and McNulty AL (2022) A Tale of Two Loads: Modulation of IL-1 Induced Inflammatory Responses of Meniscal Cells in Two Models of Dynamic Physiologic Loading. Front. Bioeng. Biotechnol. 10:837619. doi: 10.3389/fbioe.2022.837619

Meniscus injuries are highly prevalent, and both meniscus injury and subsequent surgery are linked to the development of post-traumatic osteoarthritis (PTOA). Although the pathogenesis of PTOA remains poorly understood, the inflammatory cytokine IL-1 is elevated in synovial fluid following acute knee injuries and causes degradation of meniscus tissue and inhibits meniscus repair. Dynamic mechanical compression of meniscus tissue improves integrative meniscus repair in the presence of IL-1 and dynamic tensile strain modulates the response of meniscus cells to IL-1. Despite the promising observed effects of physiologic mechanical loading on suppressing inflammatory responses of meniscus cells, there is a lack of knowledge on the global effects of loading on meniscus transcriptomic profiles. In this study, we compared two established models of physiologic mechanical stimulation, dynamic compression of tissue explants and cyclic tensile stretch of isolated meniscus cells, to identify conserved responses to mechanical loading. RNA sequencing was performed on loaded and unloaded meniscus tissue or isolated cells from inner and outer zones, with and without IL-1. Overall, results from both models showed significant modulation of inflammation-related pathways with mechanical stimulation. Anti-inflammatory effects of loading were well-conserved between the tissue compression and cell stretch models for inner zone; however, the cell stretch model resulted in a larger number of differentially regulated genes. Our findings on the global transcriptomic profiles of two models of mechanical stimulation lay the groundwork for future mechanistic studies of meniscus mechanotransduction, which may lead to the discovery of novel therapeutic targets for the treatment of meniscus injuries.

Keywords: inflammation, gene expression, NFATc2, Nos2, CXCL10, STAT, IRF1, cartilage

1 INTRODUCTION

Meniscus injuries are highly prevalent, affecting people of all ages and stages of life (Nielsen and Yde, 1991). Meniscus injury and subsequent surgery are linked to the development of post-traumatic osteoarthritis (PTOA), with 50% of partial meniscectomy patients developing radiographic osteoarthritis (OA) within 10–20 years following surgery (Lohmander et al., 2007). Therefore, more recent clinical treatments have focused on repair surgeries to preserve meniscal function as

much as possible. Notably, the avascular inner zone of the meniscus heals poorly due to the lack of blood supply (Rath and Richmond, 2000), therefore repair of inner zone meniscal tears is still only recommended in limited cases (Gallacher et al., 2010; Ghazi Zadeh et al., 2018). Although the pathogenesis of PTOA following meniscus injury remains poorly understood, the involvement of inflammation-mediated tissue degradation is increasingly appreciated as a major contributing factor in disease progression. Indeed, it has been found that inflammatory cytokines, including IL-1, IL-6, IL-8, TNF-α, and PGE2 are elevated following acute knee injuries (Bigoni et al., 2013; Liu et al., 2017; Clair et al., 2019), chronic knee injuries (Larsson et al., 2015; Bigoni et al., 2017), and in OA knees (van den Berg et al., 1999). Even very low concentrations of IL-1 have been shown to cause degradation of meniscus tissue (McNulty et al., 2013) and inhibit repair in an explant model of meniscus injury (McNulty et al., 2007; Wilusz et al., 2008; McNulty et al., 2009).

There are no approved disease modifying drugs for OA or PTOA, so novel therapeutic targets to stimulate meniscus healing and break the injury, inflammation, and tissue damage cycle are greatly needed. One promising area of investigation for novel therapeutic targets are mechanosensors and mechanotransduction pathways (McNulty and Guilak, 2015). Dynamic mechanical compression of meniscus tissue has been shown to improve integrative repair in the presence of IL-1 in an explant model of meniscus injury (McNulty et al., 2010). Dynamic tensile strain has also been shown to modulate the response of meniscus cells to an inflammatory stimulus (Deschner et al., 2006; Ferretti et al., 2006; Madhavan et al., 2007), and studies have linked mechanical stimulation of meniscal cells to increased synthesis of extracellular matrix (ECM) (Fermor et al., 2004; Puetzer et al., 2012). In contrast, joint immobilization leads to meniscus atrophy and OA (Videman et al., 1979). Therefore, mechanotransduction pathways could represent novel therapeutic targets to modulate inflammation to limit degradation of meniscus tissue and stimulate regenerative healing of the meniscus. Further understanding of meniscal mechanobiology in both non-inflammatory and inflammatory conditions may provide insight into mechanisms to improve tissue repair after injury.

Despite the promising effects of physiologic loading on meniscus cells, there remains a dearth of knowledge on global effects of loading on meniscus cell phenotype and transcriptomic profiles. This may be due in large part to the lack of well-characterized models to study the effects of mechanical stimulation on meniscus cells. Indeed, the complex geometry and anisotropic nature of the meniscus makes it difficult to model the mechanical environment of meniscus cells. Meniscus cells *in vivo* are subjected to a variety of dynamic mechanical forces, including compression and stretch due to deformation of the tissue, and hydrostatic pressure and fluid flow as the highly hydrated tissue is compressed and water is extruded. Since it is challenging to replicate all of these forces simultaneously in a single *in vitro* model system, previous studies of meniscus mechanotransduction have employed a wide variety of methods to model individual aspects of physiologic load.

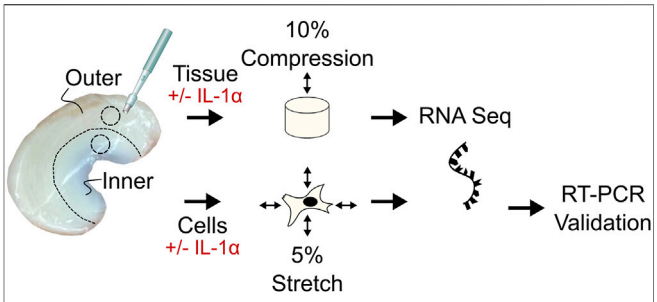

FIGURE 1 | Study methods. Tissue explants and cells were harvested from the inner and outer zone of porcine menisci and subjected to dynamic cyclic loading (tissue: 10% axial compression, cells: 5% biaxial stretch) with or without IL-1α stimulation (0.1 ng/ml). RNA sequencing was performed on both tissue explants and cells to identify pathways and gene targets differentially expressed with load and IL-1α stimulation in inner and outer zones. For the cell stretch samples, RT-qPCR was performed to validate gene targets identified from RNA sequencing analysis.

These model systems include dynamic compression of tissue explants (Shin et al., 2003; Upton et al., 2003; McHenry et al., 2006; McNulty et al., 2010; Han et al., 2014), dynamic compression of cells embedded in engineered constructs (Ballyns and Bonassar, 2011), cyclic tensile strain of isolated meniscus cells grown on a flexible substrate (Fermor et al., 2004; Deschner et al., 2006; Ferretti et al., 2006; Furumatsu et al., 2012; Kanazawa et al., 2012), fluid flow stimulation of isolated cells (Eifler et al., 2006), and hydrostatic pressure on isolated cells in monolayer (Zhang et al., 2019) or engineered constructs (Gunja and Athanasiou, 2010). Overall these studies have shown that dynamic loads at strain levels thought to correspond to physiologic loading promote anabolism (Eifler et al., 2006; Ballyns and Bonassar, 2011; Furumatsu et al., 2012; Kanazawa et al., 2012; Puetzer et al., 2012) and reduce expression of pro-inflammatory mediators (Deschner et al., 2006; Ferretti et al., 2006; Madhavan et al., 2007), while hyperphysiologic strain magnitudes (McHenry et al., 2006) or static loading (Upton et al., 2003) induce expression of inflammatory mediators and catabolic enzymes that lead to breakdown of the ECM. Notably, only a few studies have compared the responses of inner and outer zone cells to mechanical stimulation (Furumatsu et al., 2012; Kanazawa et al., 2012). The meniscus inner and outer zones vary in regard to cellular phenotype (Upton et al., 2006a; Son and Levenston, 2012; Grogan et al., 2017; Andress et al., 2021), ECM composition, and mechanical properties (Cheung, 1987; Scott et al., 1997; Sanchez-Adams et al., 2011), and experience different forces *in vivo* (Upton et al., 2006b; Freutel et al., 2014). Therefore, the inner and outer zone cells may exhibit differences in mechanoresponsiveness.

In this study, we sought to compare two established models of dynamic physiologic loading of meniscus cells to identify conserved responses to mechanical loading. We utilized an unbiased approach by performing RNA sequencing (RNA-seq) on loaded and unloaded meniscus tissue explants or isolated cells from inner and outer zones, with and without IL-1 (**Figure 1**). The two *in vitro* models of dynamic loading employed in this study were cell stretch of isolated meniscus cells and a tissue explant

compression model (McNulty et al., 2010). The *ex vivo* tissue compression model retains the native ECM microenvironment and ECM-cell interactions. This model may recapitulate more features of *in vivo* loading, as macro-scale tissue strain is transmitted to cells through the ECM and pericellular matrix, which may have either strain amplifying or attenuating properties (Upton et al., 2008; Han et al., 2013). Tissue explants from inner and outer zones of porcine medial menisci were stimulated with 10% dynamic compression, which is within the range of physiologic loading of the meniscus based on finite element modeling (Zielinska and Haut Donahue, 2005) and experimental data (Freutel et al., 2014). The cell stretch model may not recapitulate as many features of *in vivo* load, but allows for better control of experimental parameters, including intra-individual variability through pooling of cells from multiple subjects, and is not subject to variation due to irregularities in explants and individual menisci. Meniscus cells from inner and outer zones of porcine medial menisci were subjected to 5% dynamic equibiaxial stretch, which is within the range of strains predicted to be experienced at the cellular level for both inner and outer zone meniscus cells *in vivo* (Upton et al., 2006b). Both models were performed in the presence and absence of IL-1α at 0.1 ng/ml, which is a concentration observed in synovial fluid of moderate OA porcine knees (McNulty et al., 2013), has been shown to induce degradation of meniscus tissue *in vitro* (McNulty et al., 2013), and inhibits repair in an explant model of meniscus injury (McNulty et al., 2007; Wilusz et al., 2008; McNulty et al., 2010). The goals of this study were: 1) to identify IL-1 induced inflammatory responses modulated by load and 2) to determine conserved cellular responses to mechanical load in the presence and absence of IL-1 between two established models of mechanical stimulation in both the inner and outer zones of the meniscus.

2 MATERIALS AND METHODS

2.1 Cell Stretch Experiments

2.1.1 Meniscus Cell Isolation

Cells were isolated from the inner third and outer two-thirds of porcine medial menisci from skeletally mature female pigs obtained from a local abattoir, as previously described (Riera et al., 2011; McNulty et al., 2013; Andress et al., 2021). Briefly, menisci were separated into inner and outer regions and minced. Tissue was then digested by sequential 0.5% pronase (SKU 53702; EMD Millipore Corp., Temecula, CA) in Dulbecco's Modified Eagle Medium, high glucose (DMEM-HG; Catalog # 11995073; Gibco, Carlsbad, CA) with 10X antibiotic/antimycotic (Catalog # 15240062; Gibco) for 1 h and then 0.2% collagenase type I (Catalog # LS004197; Worthington Biochemical Corp., Lakewood, NJ) in DMEM-HG with 10% fetal bovine serum (Catalog # SH30396.03; HyClone, Logan, UT) for approximately 16 h. Cells were isolated with a 70 μm cell strainer and frozen for later use.

2.1.2 Cell Stretch

For each experiment, cells from at least three separate menisci were pooled and expanded for one passage in culture media containing DMEM-HG, 10% fetal bovine serum, 1× non-essential amino acids (Catalog # 11140050; Gibco), 1× antibiotic/antimycotic, 10 mM HEPES (Cat # 15630080; Gibco), and 40 μg/ml L-proline (SKU #H54409; Sigma-Aldrich, St. Louis, MO), and 50 μg/ml ascorbic acid (SKU # A8960; Sigma-Aldrich) added at time of use. Cells were then seeded onto Collagen type I coated Bioflex® 6-well plates (Catalog # BF-3001C; Flexcell® International Corporation, Burlington, NC) at a density of 250,000 cells/well (n = 3/group). Approximately 40 h after seeding, cells received fresh culture media, with or without recombinant porcine IL-1α (Catalog # 680-PI-010; R&D Systems, Minneapolis, MN) at a concentration of 0.1 ng/ml. Cells were then stimulated for a single bout of loading on a Flexcell® FX-6000T™ with 5% equibiaxial dynamic strain in a sine wave pattern at 0.5 Hz for 4 h at 37°C (Agarwal et al., 2004; Furumatsu et al., 2012; Kanazawa et al., 2012). Unloaded cells (0%) with or without 0.1 ng/ml IL-1 were cultured in parallel on Bioflex plates in the same incubator.

2.1.3 RNA Extraction

Immediately after loading, cells were lysed and total RNA was extracted and column purified according to the Norgen RNA extraction kit protocol (Catalog # 48300; Norgen Biotek Corp., Thorold, Canada).

2.2 Dynamic Compression Experiments

2.2.1 Tissue Explant Harvest and Compression

Cylindrical explants from the inner and outer regions of six separate porcine medial menisci were obtained using a 5 mm biopsy punch (Catalog # 33-35; Integra, York, PA) and trimmed to a uniform 2 mm thickness retaining the femoral surface, using a custom cutting jig. Explants were distributed among treatment groups (loaded/unloaded, +/−IL-1), such that no group contained two explants from the same meniscus. Samples were washed for 1 h in DMEM-HG with 10X antibiotic/antimycotic, then transferred to culture media. The next day, fresh culture media with or without 0.1 ng/ml IL-1α was added and explants were subjected to 10% dynamic compression in a sine wave pattern at 1 Hz, using a custom bioreactor (McNulty et al., 2010), for 4 h at 37°C. Unloaded explants (0%) with or without 0.1 ng/ml IL-1 were cultured in parallel in the same incubator. Loading was repeated every 24 h for a total of three loading sessions. Immediately following the final loading session, explants were rinsed in phosphate buffered saline (PBS; catalog # 10010-023; Gibco), flash frozen in liquid nitrogen, and stored at −80°C until RNA extraction was performed.

2.2.2 RNA Extraction

Explants were pulverized in TRIzol (Catalog # 15596026; Life Technologies, Carlsbad, CA) under liquid nitrogen using a freezer mill (Model 6875; SPEX SamplePrep, Metuchen, NJ) for three cycles of 2 min each at maximum frequency with 2 min precooling between cycles. RNA was extracted by TRIzol/chloroform separation, according to the manufacturer's protocol. RNA was then resuspended in lysis buffer and column purified, according to the Norgen RNA extraction kit protocol (Catalog # 48300; Norgen Biotek Corp).

2.3 RNA-Sequencing (RNA-seq)

Stranded mRNA-sequencing was performed by the Duke Center for Genomic and Computational Biology (Durham, NC). All samples used for RNA-seq had an RNA integrity number (RIN) > 6.5. Tissue compression and cell stretch experiments were sequenced and analyzed separately. For each experiment, reads that were 20 nt or longer after trimming were mapped to the Sscrofa11.1v91 version of the pig genome and transcriptome (Kersey et al., 2012), using the STAR RNA-seq alignment tool (Dobin et al., 2013), and kept for subsequent analysis only if mapped to a single genomic location. Gene counts were compiled using the HTSeq tool, and genes that had at least 10 reads in any given library were used in subsequent analyses. Normalization and differential expression was performed using the DESeq2 (Love et al., 2014) Bioconductor (Huber et al., 2015) package within the R statistical programming environment. The false discovery rate (FDR) was calculated to control for multiple hypothesis testing. Genes with a base-2 log fold-change (LogFC) > 1 and FDR adjusted p-value <0.05 were considered significant. Gene set enrichment analysis (GSEA) (Mootha et al., 2003; Subramanian et al., 2005) was performed using the Hallmark pathways geneset database (Liberzon et al., 2015) comparing loaded/unloaded and IL-1 treated/untreated samples for each condition. Genesets with an FDR q-value < 0.25 were compared between the two loading models to identify genesets/pathways showing co-regulation (e.g., upregulated by loading in both models) or opposite regulation (e.g., upregulated by cell stretch, downregulated by tissue compression).

2.4 Reverse Transcriptase Quantitative PCR (RT-qPCR)

Genes selected from the RNA-sequencing results based on fold-change and potential biologic relevance were validated by RT-qPCR. Two hundred nanograms of total RNA per reaction was used to synthesize cDNA using the SuperScript VILO cDNA Synthesis Kit (Catalog # 11754050; Life Technologies). Then qPCR was performed using PowerUP SYBR Green master mix (Catalog # A25776; Thermo Fisher Scientific Baltics UAB, Vilnius, Lithuania) with gene specific primers (**Supplementary Table 1**) and the StepOne Plus real-time PCR system (Model 4376374; Applied Biosystems, Foster City, CA). Relative fold-change was determined by the $2^{-\Delta\Delta Ct}$ method (Livak and Schmittgen, 2001), using 18S as a reference gene. Results are presented as the base-2 log fold-change relative to the inner zone unloaded control group. Two-way ANOVAs were performed for each zone (inner and outer) separately where factors were load (0% and 5%) and IL-1 stimulation (+/−). A Tukey multiple comparison post hoc analysis was performed with targets that had a significant interaction term. For the targets that did not have a significant interaction term, factor level significance is depicted on the graph. ANOVA results for the *RRAD* target for outer zone samples are reported but failed the Shapiro-Wilk test for normality of residuals ($p = 0.027$, see **Supplementary Figure 1** for QQ plot of residuals). ANOVA assumptions of homogeneity and normality were met for all other targets.

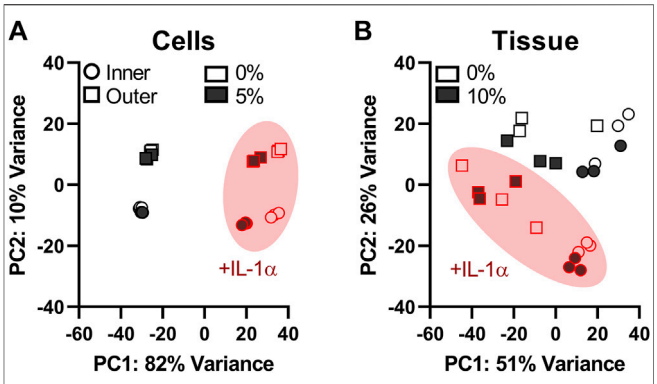

FIGURE 2 | Effects of IL-1 treatment, zone, and dynamic load on global gene expression are more consistent in the cell stretch model than tissue compression. Principal component analysis (PCA) plots of the cell stretch experiment **(A)** show distinct clustering of samples by zone (inner and outer) and treatment (+/−IL-1, +/−dynamic loading). Samples from the tissue compression experiment **(B)** display considerable overlap between experimental groups. Shape corresponds to zone (circle: inner, square: outer), shape fill denotes load (unfilled: 0%, filled: loaded), and samples stimulated with IL-1α are outlined and circled in red. The *x*-axis (PC1) is the first principal direction along which samples from the RNA-seq experiment show the largest variation. The *y*-axis (PC2) is the second principal axis and the direction along which samples show the second largest variation. The total variability accounted for by each principal component is indicated in the axis labels.

3 RESULTS

In a principal component analysis (PCA) of the cell stretch model, experimental groups cluster distinctly by region (inner/outer) and treatment (+/−IL-1, +/−load) (**Figure 2A**). Principal component 1 (PC1), accounting for 82% of variance, appears to be dominated by the effect of IL-1 treatment, while PC2, accounting for 10% of variance, separates inner and outer zone cells. PCA of the tissue compression dataset shows much more overlap between samples in different experimental groups, indicating that there is considerable heterogeneity in gene expression within the experimental groups in this model (**Figure 2B**).

IL-1 treatment induced significant changes in expression for many genes in both monolayer cells and tissue explants. IL-1 treatment of inner zone cells resulted in significant downregulation ($p < 0.05$, LogFC < −1) of 976 genes and upregulation ($p < 0.05$, LogFC > 1) of 1,129 genes (**Figure 3A**). Treatment of inner zone tissue explants with IL-1 resulted in downregulation of 1,241 genes and upregulation of 526 genes (**Figure 3B**). Outer zone cells displayed similar numbers of differentially regulated genes upon treatment with IL-1, with 925 downregulated and 1,129 upregulated transcripts (**Figure 3C**). Outer zone tissue explants were slightly less responsive to IL-1 treatment, with 413 genes displaying downregulation and 169 showing upregulation (**Figure 3D**). IL-1 treatment induced upregulation of genes known to contribute to OA development, including inflammatory cytokines *IL6* and *LIF* (Kapoor et al., 2011), and degradative enzymes *MMP3* (Burrage et al., 2006) and *ADAMTS5* (Santamaria, 2020), in tissue and monolayer cells from inner

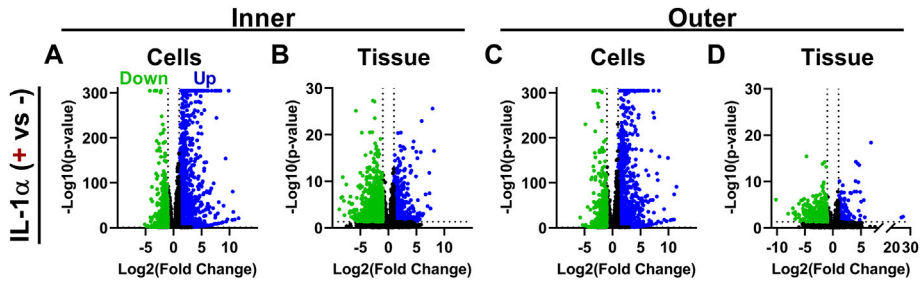

FIGURE 3 | IL-1 treatment induces significant changes in gene expression. Volcano plots showing genes significantly up and downregulated by IL-1α (0.1 ng/ml) treatment in **(A)** inner zone cells in monolayer **(B)** inner zone tissue explants **(C)** outer zone cells in monolayer, and **(D)** outer zone tissue explants. Each data point is an individual gene; *y*-axis capped at 300 (adjusted *p*-value < 10^{-300}). Color denotes if the gene was significantly upregulated (blue), downregulated (green), or not significant (black). Dashed lines indicate cutoffs for significant genes (FDR adjusted *p*-value < 0.05 and a base-2 log fold-change > |1|).

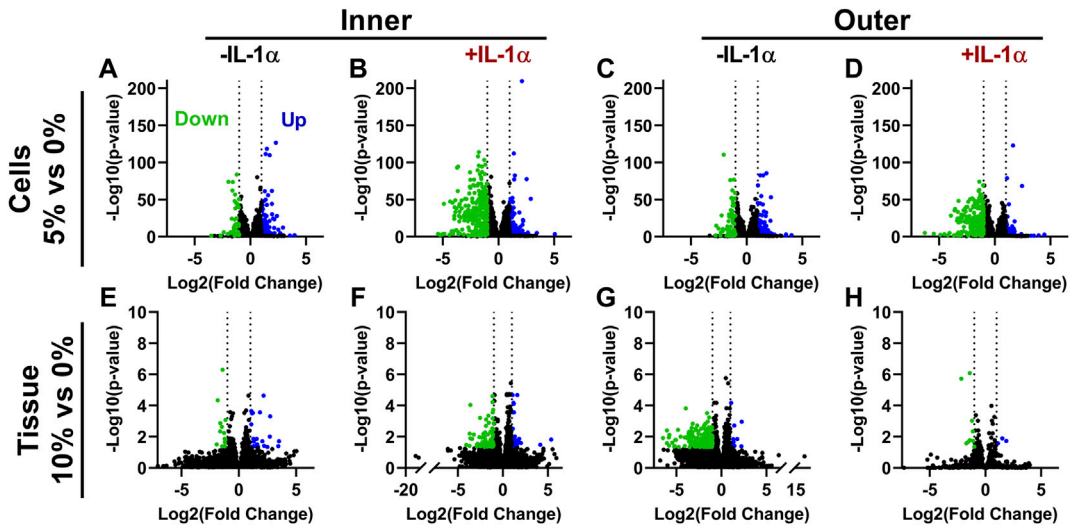

FIGURE 4 | Dynamic loading downregulates gene expression in the presence of IL-1α. Volcano plots showing genes significantly up and downregulated by dynamic cell stretch of **(A)** inner zone cells **(B)** inner zone cells in the presence of IL-1α **(C)** outer zone cells, and **(D)** outer zone cells in the presence of IL-1α, or dynamic compression of **(E)** inner zone tissue **(F)** inner zone tissue in the presence IL-1α **(G)** outer zone tissue, and **(H)** outer zone tissue in the presence of IL-1α. Each data point is an individual gene. Color denotes if the gene was significantly up-regulated (blue), down-regulated (green), or not significant (black).

and outer zones. **Supplementary Data Sheets 1–4** provide lists of genes significantly differentially expressed with IL-1 treatment.

The effect of loading alone on global gene expression was modest in both models. There were only 158 transcripts showing significant differential expression with cell stretch and 35 with tissue compression (**Figures 4A,F**; LogFC>|1| and $p < 0.05$). Both models of dynamic loading (inner zone cell stretch and tissue compression) resulted in a larger number of downregulated transcripts in the presence of IL-1 (**Figures 4B,F**; LogFC < −1 and $p < 0.05$; 299 genes for cell stretch and 85 for tissue compression). Similarly, outer zone cells subjected to 5% stretch in the presence of IL-1 displayed a larger number of downregulated transcripts (**Figure 4D**; 242 genes with LogFC < −1 and $p < 0.05$) than outer zone cells subjected to loading in the absence of IL-1 (**Figure 4C**; 65 genes with LogFC < −1 and $p < 0.05$). However, compression of outer zone tissue induced a large number of downregulated genes in the absence of IL-1 (**Figure 4G**; 187 genes with LogFC < −1 and $p < 0.05$) but relatively little effect on overall gene expression in the presence of IL-1 (**Figure 4H**; 13 genes with LogFC > |1| and $p < 0.05$). **Supplementary Data Sheets 5–12** provide lists of genes significantly differentially expressed with load.

In order to identify IL-1 regulated transcripts modulated by cell stretch or compression, genes with a significant interaction term between IL-1 treatment and dynamic load were identified from each dataset ($p < 0.05$, no LogFC cutoff). For cells subjected to 5% stretch, over 2,500 genes were identified with a significant interactive effect between load and IL-1 for inner zone (**Figure 5A**) and over 1,500 genes for outer zone (**Figure 5C**). For explants subjected to tissue compression, only 15 genes with a significant interactive effect were identified for inner zone (**Figure 5B**), and only one gene (VEGFA) displayed a

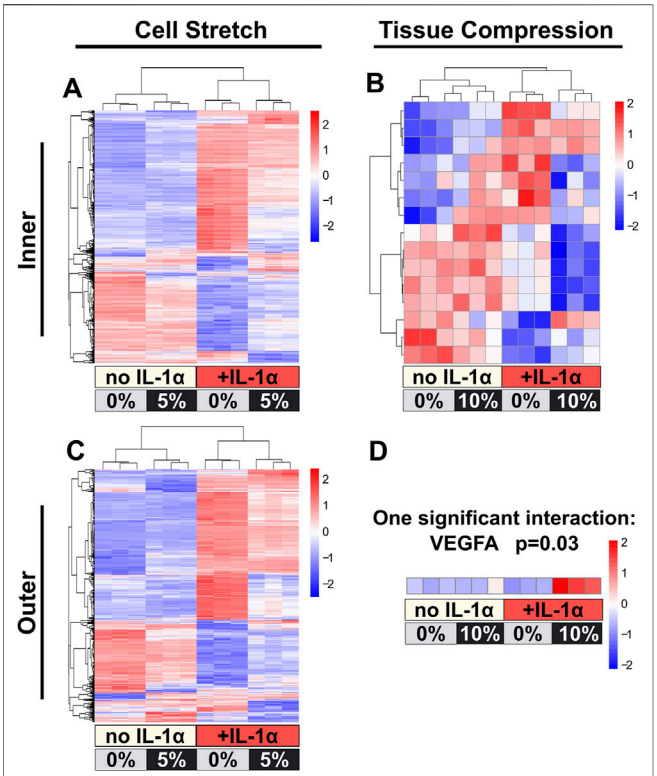

FIGURE 5 | Dynamic cell stretch resulted in a larger number of differentially regulated genes with significant load and IL-1α interaction than dynamic tissue compression. Z-score heat maps for genes that had a significant interaction term between IL-1α and load are shown for cell stretch inner **(A)** and outer **(C)** zones, and tissue compression inner **(B)** and outer **(D)** zones. Cell stretch had a larger number of differentially regulated genes than tissue compression for both zones. Each column is an individual replicate. Hierarchical clustering grouped samples within their corresponding treatment (+/–IL-1α and +/–load).

significant interaction term for the outer zone (**Figure 5D**). **Supplementary Data Sheets 13–15** provide lists of genes with a significant interaction between load and IL-1 treatment for each model and zone.

GSEA similarly revealed interesting differences in hallmark pathways differentially regulated by dynamic loading between zones and with or without IL-1. For the inner zone, 9 pathways were upregulated and 2 pathways were downregulated in common between the two loading modalities, while 7 pathways showed opposite regulation and were upregulated by tissue compression but downregulated by cell stretch (**Figures 6A,E**). However, in the presence of IL-1, there was strong agreement between the two models: 12 pathways were downregulated by loading in both models, and there were no pathways displaying opposite regulation (**Figures 6B,F**). Outer zone results were much less congruent between models, with only 3 pathways showing similar regulation and 11 pathways showing opposite regulation in response to loading alone (**Figures 6C,G**). Upon loading in the presence of IL-1, there were 6 pathways showing similar regulation and 5 pathways showing opposite regulation in the outer zone (**Figures 6D,H**). Notably, only a few pathways were significantly differentially regulated by both dynamic compression and cell stretch across both inner and outer zones. MYC Targets v2 was upregulated by both tissue compression and cell stretch across zones. Interferon-γ Response, TNF-α Signaling *via* NF-κB, and Interferon-α Response pathways were all downregulated by cell stretch but upregulated by tissue compression for both inner and outer zones (**Figures 6E,G**). In the presence of IL-1, Bile Acid Metabolism and Fatty Acid Metabolism pathways were downregulated by loading across models and zones (**Figures 6F,H**). However, no other GSEA pathway responses were conserved between inner and outer zones across both models of loading.

Further evidence of the inflammation modulating effects of mechanical loading is seen by the effect of dynamic load on genesets significantly differentially regulated by IL-1 treatment. A total of 18 of the 19 genesets upregulated by IL-1 treatment of inner zone cells were downregulated by cell stretch in the presence of IL-1, and 7 of these pathways are downregulated by tissue compression (**Figure 7A**). Stretched cells from the outer zone display similar results, with 16 out of 20 pathways upregulated by IL-1 treatment showing downregulation by cell stretch in the presence of IL-1 (**Figure 7B**). However, only four of these pathways were downregulated by compression of outer zone tissue in the presence of IL-1, while three were further upregulated by tissue compression in the presence of IL-1 (**Figure 7B**).

Individual genes identified by RNA-seq as significantly differentially regulated by dynamic cell stretch in the presence of IL-1 and with known functions related to inflammation and PTOA development were chosen for further validation by RT-qPCR, which confirmed the patterns of gene expression seen in the RNA-seq data. *NFATC2* expression was downregulated by IL-1 treatment (**Figure 8A**, $p < 0.0001$), and was significantly upregulated by loading both in the presence and absence of IL-1 ($p < 0.005$). *RRAD* expression was also significantly upregulated by load for both inner and outer zone (**Figure 8B**, $p < 0.0001$) and expression was upregulated by IL-1 in inner zone cells ($p < 0.005$). There was a significant effect of load in both the inner and outer zone cells on *CASP7* expression (**Figure 8C**, $p < 0.05$) and expression was significantly downregulated by load in the presence of IL-1 for inner zone cells ($p < 0.05$). Expression of *CXCL10* was increased with IL-1 treatment (**Figure 8D**, $p < 0.0001$) and decreased both by loading in the absence of IL-1 ($p < 0.01$) and by loading of IL-1 treated inner and outer zone cells ($p < 0.0001$). There was a main effect of load ($p < 0.0001$) causing downregulation of *IRF1* (**Figure 8E**), *NOS2* (**Figure 8F**, inner zone cells only), *STAT1* (**Figure 8G**), and *STAT2* (**Figure 8H**). In both zones for each of these genes, IL-1 caused an upregulation of expression ($p < 0.001$) and there was an interactive effect of load and IL-1, which resulted in downregulation of gene expression compared to IL-1 alone ($p < 0.05$).

4 DISCUSSION

Together the findings from this study support the idea that diverse types of dynamic load can modulate the IL-1 response

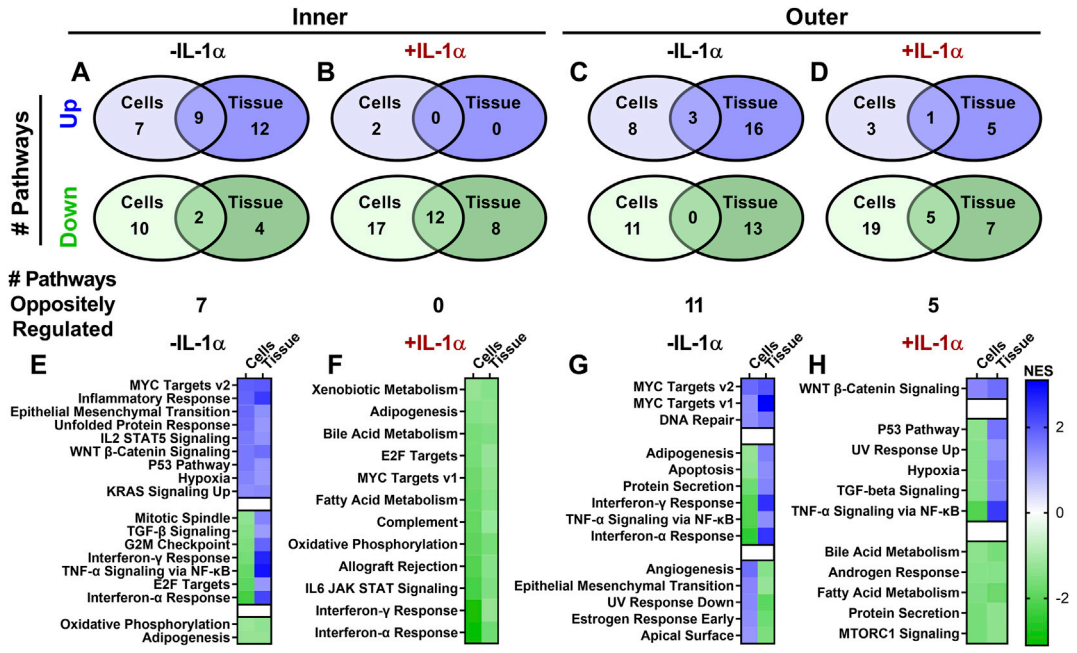

FIGURE 6 | Pathways altered by dynamic loading are more similar in inner zone than outer zone for cell stretch and tissue compression. Gene Set Enrichment Analysis (GSEA) revealed pathways up- (blue) or downregulated (green) with dynamic loading in the presence or absence of IL-1α. The number of pathways regulated by loading were compared between cell stretch and tissue compression for inner (**A**: –IL-1α, **B**: +IL-1α) and outer (**C**: –IL-1α, **D**: +IL-1α) zones. Normalized enrichment scores (NES) of pathways significantly regulated by loading in both models were compared for inner (**E**: –IL-1α, **F**: + IL-1α) and outer (**G**: –IL-1α, **H**: +IL-1α) zones.

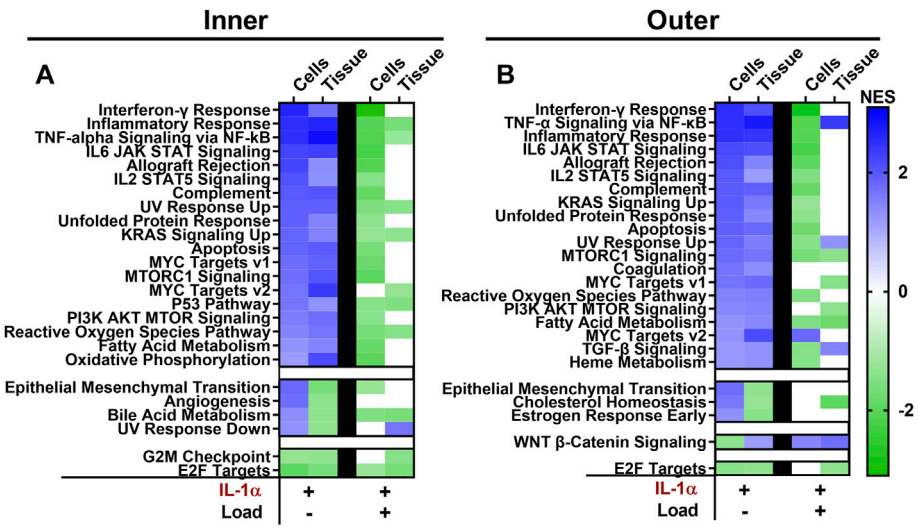

FIGURE 7 | The majority of pathways upregulated by IL-1α are downregulated by dynamic cell stretch in the presence of IL-1α. Pathways significantly differentially regulated with IL-1α stimulation are compared to significantly differentially regulated pathways with dynamic loading in the presence of IL-1α for inner **(A)** and outer **(B)** zones. Cell stretch and tissue compression normalized enrichment scores (NES) are shown in each column. A NES > 0 identifies upregulated (blue) pathways and a NES < 0 identifies downregulated (green) pathways. White boxes denote that the geneset did not meet the cutoff for significance (FDR < 0.25).

of meniscus cells. Dynamic tissue compression of meniscus tissue explants and dynamic tensile stretch of monolayer meniscus cells showed considerable concordance in RNA-sequencing results, although the degree of overlap varied based on the anatomic region and presence of an inflammatory stimulus. The highest concordance between loading models was seen in the inner zone IL-1 treated condition, where all the hallmark pathways identified by GSEA as significantly different by loading in the presence of

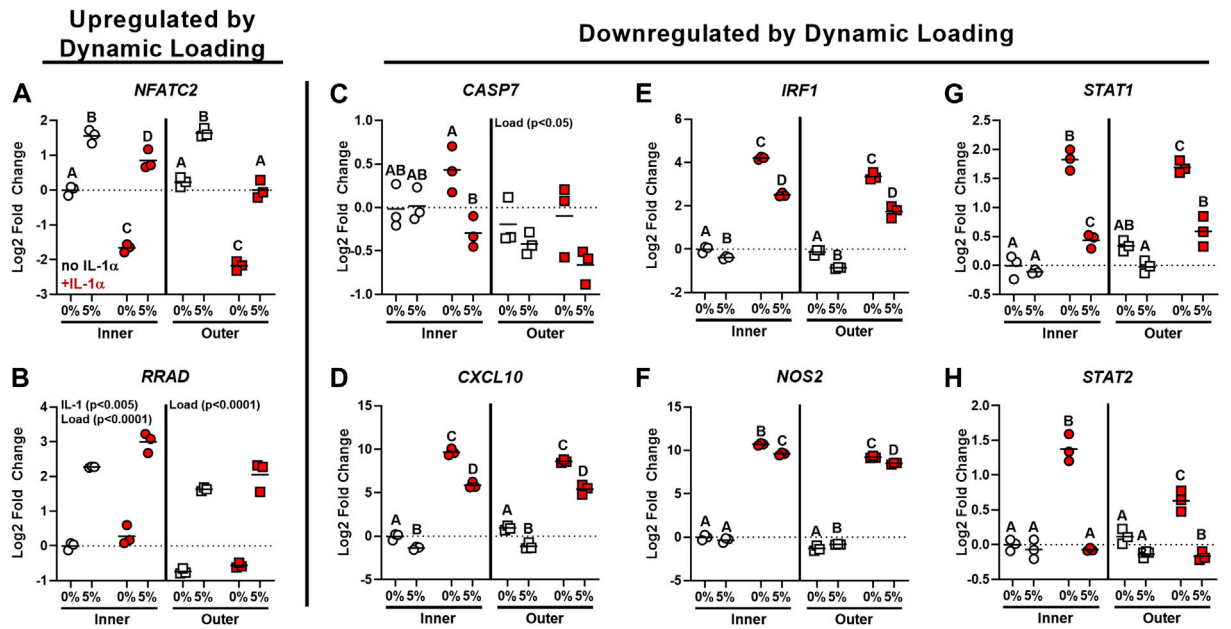

FIGURE 8 | RT-qPCR validated gene targets identified by RNA-sequencing for dynamic cell stretch. Gene targets upregulated by dynamic loading (**A**: *NFATC2*, **B**: *RRAD*) and downregulated by dynamic loading (**C**: *CASP7*, **D**: *CXCL10*, **E**: *IRF1*, **F**: *NOS2*, **G**: *STAT1*, **H**: *STAT2*) identified by RNA-sequencing were validated using RT-qPCR. Shape denotes zone (circle: inner, square: outer) and color identifies IL-1α stimulation (white: no IL-1α, red: + IL-1α). Results are presented as fold-change relative to the inner zone unloaded control group (indicated by the dashed line). Groups not sharing a letter are significantly different ($p < 0.05$). A significant main effect by load or IL-1 with no significant interaction between load and IL-1 is indicated by the factor name on the individual graph.

IL-1 for both models were downregulated and none showed opposite regulation. Overall, our findings reveal that dynamic mechanical loading mitigates the global inflammatory response of meniscus cells at the transcriptomic level.

In general, mechanical stimulation alone caused relatively few gene targets to be either up or downregulated for both loading models. The exception to this was outer zone tissue compression, which resulted in downregulation of numerous gene transcripts. We did not observe significant up-regulation of the anabolic genes *COL2A1*, *COL1A1*, or *ACAN* with dynamic loading in either model. Prior reports of the effect of dynamic loading on anabolic gene expression are mixed (Upton et al., 2003; Furumatsu et al., 2012), and the use of skeletally mature porcine tissue in this study may mean that these cells have limited anabolic capability due to age. Mechanical stimulation in the presence of IL-1 resulted in far more significantly differentially regulated genes than loading alone, and generally resulted in downregulation of many genes and upregulation of relatively few transcripts. Consistent with previous studies (Ferretti et al., 2006), *NOS2* expression was increased by IL-1 treatment and decreased by dynamic tensile stretch in the presence of IL-1 for both inner and outer zone cells, and the same effect was observed with dynamic compression of inner zone tissue. In addition to identifying individual genes of interest for meniscus research, this study reveals the global transcriptomic and pathway changes in both inner and outer zone meniscus cells in response to dynamic loading both in the presence and absence of the inflammatory stimulus IL-1.

Many of the hallmark pathways upregulated by IL-1 and downregulated by dynamic loading in the presence of IL-1 are inflammatory signaling pathways known to contribute to the development of OA, such as TNF-α signaling *via* NF-κB (Gao et al., 2020; Sueishi et al., 2020), interferon-γ (Otero et al., 2007), IL-6 JAK STAT signaling (Akeson and Malemud, 2017), and complement (Silawal et al., 2018). Genesets related to p53 and apoptosis, which are also known to play a role in the development of OA (Hwang and Kim, 2015; Xu et al., 2020), were also upregulated by IL-1 treatment and downregulated by dynamic loading in the presence of IL-1. Similarly, MTORC1 (Yang et al., 2020) and PI3K AKT MTOR (Sun et al., 2020) signaling pathways were also upregulated by IL-1 and downregulated by dynamic load. Interestingly, PI3K AKT MTOR signaling may play an important role in many processes known to be dysregulated in OA development, including apoptosis, proliferation, and metabolism (Zheng et al., 2021). Indeed, pathways related to proliferation and cell cycle regulation (KRAS signaling and MYC targets) were also identified by GSEA as being differentially regulated by dynamic loading in the presence of IL-1. Metabolic pathways, such as oxidative phosphorylation and fatty acid metabolism, were also upregulated by IL-1 and downregulated by dynamic load in the presence of IL-1. Due to the complex and often overlapping nature of these signaling pathways, determining the functional effects of dynamic mechanical stimulation will require considerable future work. However, these results demonstrate that dynamic loading has significant effects on diverse cellular functions related to tissue healing and OA development and dynamic loading seems to

oppose the effects of IL-1. These findings underscore the potential utility of developing therapies targeted to mechanotransduction pathways, which may have widespread effects not limited to a single aspect of OA development, such as inflammation or metabolism, but may be able to combat this multifactorial disease by modulating multiple critical pathways.

The function of many individual genes identified by RNA-seq and validated by RT-qPCR point to the exciting potential effects of the interaction between dynamic load and inflammation in meniscus cells. Targets that were upregulated by dynamic loading may have protective roles in meniscus cells. Expression of *NFATC2*, which is a calcium-responsive transcription factor, was downregulated by IL-1 treatment and upregulated by dynamic load for both inner and outer zone cells. NFATC2 has been shown to be protective against OA development, and knockdown of NFATC2 causes OA in a mouse model (Wang et al., 2009; Rodova et al., 2011; Greenblatt et al., 2013). *RRAD*, which was upregulated by dynamic loading, is protective against cellular senescence (Wei et al., 2019), and is an inhibitor of the NF-κB pathway (Hsiao et al., 2014). In addition to these upregulated targets, there were many genes in the RNA-seq dataset that were downregulated by dynamic loading in the presence of IL-1. *CASP7*, which is called the "executioner protein" for its role in apoptosis and is an outcome measure in many studies of potential OA therapeutics (Murakami et al., 2019), was downregulated by dynamic load in the presence of IL-1 for inner zone cells. The other 5 targets validated by qPCR are significantly upregulated by IL-1 treatment and downregulated by dynamic loading in the presence of IL-1. CXCL10 is a chemokine that stimulates monocytes and T cells and has elevated expression in the synovium and cartilage following articular fracture (Furman et al., 2018) and is evaluated in studies treating OA and joint inflammation (Wang et al., 2015). IRF1 is a transcription factor with roles related to inflammatory response, proliferation, and apoptosis, and has been linked to increased expression of MMP-3 and MMP-13 (Lu et al., 2014), which are mediators of meniscus tissue degeneration and prevent meniscus tissue repair *in vitro* (McNulty et al., 2009). *NOS2* encodes inducible nitric oxide synthase (iNOS), which is a key indicator of inflammatory response in meniscus cells and chondrocytes and has been linked to ECM degradation (LeGrand et al., 2001; Shin et al., 2003; Yang et al., 2010). Transcription factors STAT1 and STAT2 are activated by interferons and are common targets in studies of potential therapeutics for OA and rheumatoid arthritis (Li et al., 2001; Legendre et al., 2003; Millward-Sadler et al., 2006; Dai et al., 2018). Future work is needed to explore the significance of these gene expression changes on functional outcomes, such as cell survival, anabolic/catabolic balance, and cellular senescence, but these data clearly show the power of dynamic mechanical stimulation to mitigate IL-1-induced changes in expression of genes relevant to meniscus homeostasis and OA development.

RT-qPCR validation was performed only on samples from the cell stretch model, as this model showed much greater consistency of expression changes at the single gene level. This is evidenced by the order of magnitude difference in *p*-values observed between models of loading in the volcano plots (**Figure 4**) and clustering of samples in the PCA plots (**Figure 2**). There are a number of possible sources for the heterogeneity observed in the tissue compression dataset, including heterogeneity of tissue samples both between menisci (inter-individual) and between samples obtained from the same meniscus (intra-individual), as the variability of cellular phenotypes and ECM composition throughout the meniscus varies not only based on inner and outer regions, but also between anterior, posterior, and midbody regions (Mauck et al., 2007; Di Giancamillo et al., 2014). The cell stretch model allowed for greater control of donor and site variability as isolated cells were pooled from the entire inner or outer region of multiple menisci, reducing both inter- and intra-individual variability. Another potential contributing factor to differences between the two datasets is the RNA extraction procedure. RNA extraction from meniscus tissue required pulverization in a freezer mill for homogenization, followed by phenol/chloroform extraction, whereas high quality RNA from monolayer cells was easily isolated by column purification. High quality RNA (RIN > 6.5) was obtained for all meniscus tissue and monolayer samples used in this study. Any differences in RNA preparation should not affect the differential expression results presented here, as each sample type was sequenced and analyzed separately. However, it could be a contributing factor to the differences in variability observed between the loading models. Overall, both models are useful for studies of mechanotransduction and modulation of inflammatory response by mechanical stimulation based on the conservation of global transcriptomic trends and GSEA pathways; however, the cell stretch model yielded superior consistency and repeatability for individual gene expression analyses and is more amenable to isolation of high-quality RNA for transcriptomic studies.

The tissue compression model was designed to mimic physiologic loading as closely as possible, by using a strain level thought to correspond to physiologic *in vivo* loads (Upton et al., 2006b; Freutel et al., 2014) and a frequency of 1Hz, which corresponds to a brisk walking pace (Tudor-Locke and Rowe, 2012). Explants were subjected to three loading bouts of 4 h each on three consecutive days, as this has been shown to be sufficient time to detect mechanical loading effects on IL-1 induced tissue degeneration (McNulty et al., 2010). However, It is not entirely clear how macro-scale tissue strains are translated to cellular deformation, so the cell stretch parameters were chosen based on empirically-derived parameters found in the literature (Ferretti et al., 2006; Kanazawa et al., 2012). A 5% equibiaxial strain at 0.5Hz has pro-anabolic and anti-inflammatory effects on meniscal cells (Ferretti et al., 2006; Kanazawa et al., 2012), and 4 h of loading causes sustained anti-inflammatory effects (Ferretti et al., 2006). Therefore, a single loading bout was used for monolayer cells due to ongoing cellular proliferation in monolayer culture, which would have resulted in different cell densities at the time of loading if performed on multiple consecutive days. Furthermore, prior work using dynamically compressed agarose-embedded chondrocytes revealed that there was an initial response in gene expression that decays over time, and when repeated loading was performed each day for 3 days, as was done in the tissue explant model, the results were the same as the single loading bout (Nims et al., 2021). Despite the differences in loading protocols, the amount of overlap in observed responses is remarkable, suggesting that there

are conserved mechanisms of mechanotransduction activated by both cell stretch and tissue compression, and that both models of mechanical stimulation are useful for elucidating mechanisms by which meniscus cells sense and respond to their mechanical environment. However, the differences in loading protocols do limit the interpretation of our results and raise many additional interesting questions regarding the nature of mechanotransduction in meniscus cells.

Based on finite element modeling, 10% compression may represent physiologic loading for inner zone tissue but due to meniscus extrusion towards the periphery of the joint, outer zone tissue likely does not experience macroscale tissue compressive strains as high as 10% during normal physiologic loading (Upton et al., 2006b; Freutel et al., 2014). On the other hand, 5% cell stretch may be close to the magnitude of deformation experienced at the cellular level for both inner and outer zone cells (Upton et al., 2006b). Interestingly, it appears that the two loading regimes investigated in this study were comparable for the inner zone despite differences in loading parameters and cellular environment. It remains to be determined whether the differing response of outer zone cells to 10% tissue compression and 5% stretch is due to loading or environmental differences, such as differences in magnitude, frequency, type of load, duration of loading, or differences in the ECM and cell microenvironment. Further work is needed to elucidate the mechanisms of mechanosensation in meniscus cells, which could have implications for therapeutic targeting of mechanotransduction pathways to stimulate meniscus injury repair.

Little overlap was observed in GSEA pathways modulated by both models of loading between inner and outer zones. Only MYC Targets v2 was upregulated by both models across inner and outer zones. Interestingly, Interferon-γ Response, TNF-α Signaling *via* NF-κB, and Interferon-α Response pathways all showed the same pattern of expression, being upregulated by dynamic compression but downregulated by cell stretch in both inner and outer zone cells. In addition, very little agreement was observed between inner and outer zone response to loading in the presence of IL-1. Only the metabolic pathways Bile Acid Metabolism and Fatty Acid Metabolism are significantly regulated by both models of dynamic loading with IL-1 in both inner and outer zones. Inflammation related pathways IL6 JAK STAT Signaling and Interferon-γ Response were downregulated by both models of dynamic loading for inner zone samples in the presence of IL-1, and both of these pathways are downregulated by cell stretch of outer zone cells in the presence of IL-1, but not tissue compression. TNF-α Signaling via NF-κB, which is universally upregulated by IL-1 treatment alone, was also downregulated by both loading modalities for inner zone and by cell stretch of outer zone cells in the presence of IL-1, but upregulated by compression of outer zone tissue in the presence of IL-1. Generally, it appears that the anti-inflammatory effects of dynamic loading are well-conserved between inner and outer zone stretched monolayer cells and inner zone compressed tissue, but not outer zone compressed tissue. One explanation for this is that there may be ECM-dependent differences in mechanotransduction between zones, which could have important implications for targeting mechanotransduction pathways to stimulate injury healing. While it is beyond the scope of the analyses presented here to fully characterize the differences between inner and outer zone mechanoresponsiveness, interesting differences are apparent and warrant further investigation.

Overall, results from both models showed significant modulation of inflammation-related pathways with mechanical stimulation, supporting the potential of targeting mechanotransduction pathways as novel therapeutic targets to improve outcomes following meniscus injury. Anti-inflammatory effects of loading were well-conserved between the tissue compression and cell stretch models for inner zone, but the cell stretch model provided greater statistical power due to improved consistency between replicates and resulted in a larger number of significantly differentially regulated genes. Our findings on the global transcriptomic profiles of two models of mechanical stimulation lay the groundwork for future mechanistic studies of meniscus mechanotransduction, which may lead to the discovery of novel therapeutic targets for the treatment of meniscus injuries and the prevention of PTOA development.

DATA AVAILABILITY STATEMENT

The datasets presented in this study can be found in the NCBI Gene Expression Omnibus (GEO) under accession numbers GSE191175 (tissue compression) and GSE191321 (cell stretch). https://www.ncbi.nlm.nih.gov/geo/, GSE191175; GSE191321.

AUTHOR CONTRIBUTIONS

BA: conceptualization, investigation, formal analysis, writing—original draft. RI: conceptualization, investigation, formal analysis, visualization, writing—review and editing. IP and BH: resources, writing—review and editing. AM: conceptualization, supervision, funding acquisition, writing—review and editing.

FUNDING

Funding was provided in part by NIH grants AR073221, AR078245, and AR079184, Dr. Annunziato Amendola, and Duke Sports Medicine.

ACKNOWLEDGMENTS

We thank Drs. David Corcoran and Wei Chen from the Duke Genomic Analysis and Bioinformatics Core for assistance with the RNASeq analysis. We thank Drs. George Truskey and Adam Goode for helpful advice.

SUPPLEMENTARY MATERIAL

The Supplementary Material for this article can be found online at: https://www.frontiersin.org/articles/10.3389/fbioe.2022.837619/full#supplementary-material

REFERENCES

Agarwal, S., Deschner, J., Long, P., Verma, A., Hofman, C., Evans, C. H., et al. (2004). Role of NF-kappaB Transcription Factors in Antiinflammatory and Proinflammatory Actions of Mechanical Signals. *Arthritis Rheum.* 50 (11), 3541–3548. doi:10.1002/art.20601

Akeson, G., and Malemud, C. J. (2017). A Role for Soluble IL-6 Receptor in Osteoarthritis. *J. Funct. Morphol. Kinesiol.* 2 (3), 27. doi:10.3390/jfmk2030027

Andress, B., Kim, J. H., Cutcliffe, H. C., Amendola, A., Goode, A. P., Varghese, S., et al. (2021). Meniscus Cell Regional Phenotypes: Dedifferentiation and Reversal by Biomaterial Embedding. *J. Orthop. Res.* 39 (10), 2177–2186. doi:10.1002/jor.24954

Ballyns, J. J., and Bonassar, L. J. (2011). Dynamic Compressive Loading of Image-Guided Tissue Engineered Meniscal Constructs. *J. Biomech.* 44 (3), 509–516. doi:10.1016/j.jbiomech.2010.09.017

Bigoni, M., Sacerdote, P., Turati, M., Franchi, S., Gandolla, M., Gaddi, D., et al. (2013). Acute and Late Changes in Intraarticular Cytokine Levels Following Anterior Cruciate Ligament Injury. *J. Orthopaedic Res.* 31 (2), 315–321. doi:10.1002/jor.22208

Bigoni, M., Turati, M., Sacerdote, P., Gaddi, D., Piatti, M., Castelnuovo, A., et al. (2017). Characterization of Synovial Fluid Cytokine Profiles in Chronic Meniscal Tear of the Knee. *J. Orthop. Res.* 35 (2), 340–346. doi:10.1002/jor.23272

Burrage, P. S., Mix, K. S., and Brinckerhoff, C. E. (2006). Matrix Metalloproteinases: Role in Arthritis. *Front. Biosci.* 11, 529–543. doi:10.2741/1817

Cheung, H. S. (1987). Distribution of Type I, II, III and V in the Pepsin Solubilized Collagens in Bovine Menisci. *Connect. Tissue Res.* 16 (4), 343–356. doi:10.3109/03008208709005619

Clair, A. J., Kingery, M. T., Anil, U., Kenny, L., Kirsch, T., and Strauss, E. J. (2019). Alterations in Synovial Fluid Biomarker Levels in Knees with Meniscal Injury as Compared with Asymptomatic Contralateral Knees. *Am. J. Sports Med.* 47 (4), 847–856. doi:10.1177/0363546519825498

Dai, M., Liu, X., Wang, N., and Sun, J. (2018). Squid Type II Collagen as a Novel Biomaterial: Isolation, Characterization, Immunogenicity and Relieving Effect on Degenerative Osteoarthritis via Inhibiting STAT1 Signaling in Pro-inflammatory Macrophages. *Mater. Sci. Eng. C Mater. Biol. Appl.* 89, 283–294. doi:10.1016/j.msec.2018.04.021

Deschner, J., Wypasek, E., Ferretti, M., Rath, B., Anghelina, M., and Agarwal, S. (2006). Regulation of RANKL by Biomechanical Loading in Fibrochondrocytes of Meniscus. *J. Biomech.* 39 (10), 1796–1803. doi:10.1016/j.jbiomech.2005.05.034

Di Giancamillo, A., Deponti, D., Addis, A., Domeneghini, C., and Peretti, G. M. (2014). Meniscus Maturation in the Swine Model: Changes Occurring along with Anterior to Posterior and Medial to Lateral Aspect during Growth. *J. Cell. Mol. Med.* 18 (10), 1964–1974. doi:10.1111/jcmm.12367

Dobin, A., Davis, C. A., Schlesinger, F., Drenkow, J., Zaleski, C., Jha, S., et al. (2013). STAR: Ultrafast Universal RNA-Seq Aligner. *Bioinformatics* 29 (1), 15–21. doi:10.1093/bioinformatics/bts635

Eifler, R. L., Blough, E. R., Dehlin, J. M., and Haut Donahue, T. L. (2006). Oscillatory Fluid Flow Regulates Glycosaminoglycan Production via an Intracellular Calcium Pathway in Meniscal Cells. *J. Orthop. Res.* 24 (3), 375–384. doi:10.1002/jor.20028

Fermor, B., Jeffcoat, D., Hennerbichler, A., Pisetsky, D. S., Weinberg, J. B., and Guilak, F. (2004). The Effects of Cyclic Mechanical Strain and Tumor Necrosis Factor Alpha on the Response of Cells of the Meniscus. *Osteoarthritis Cartilage* 12 (12), 956–962. doi:10.1016/j.joca.2004.08.007

Ferretti, M., Madhavan, S., Deschner, J., Rath-Deschner, B., Wypasek, E., and Agarwal, S. (2006). Dynamic Biophysical Strain Modulates Proinflammatory Gene Induction in Meniscal Fibrochondrocytes. *Am. J. Physiol. Cel Physiol.* 290 (6), C1610–C1615. doi:10.1152/ajpcell.00529.2005

Freutel, M., Seitz, A. M., Galbusera, F., Bornstedt, A., Rasche, V., Knothe Tate, M. L., et al. (2014). Medial Meniscal Displacement and Strain in Three Dimensions under Compressive Loads: MR Assessment. *J. Magn. Reson. Imaging* 40 (5), 1181–1188. doi:10.1002/jmri.24461

Furman, B. D., Kent, C. L., Huebner, J. L., Kraus, V. B., McNulty, A. L., Guilak, F., et al. (2018). CXCL10 Is Upregulated in Synovium and Cartilage Following Articular Fracture. *J. Orthop. Res.* 36 (4), 1220–1227. doi:10.1002/jor.23735

Furumatsu, T., Kanazawa, T., Miyake, Y., Kubota, S., Takigawa, M., and Ozaki, T. (2012). Mechanical Stretch Increases Smad3-dependent CCN2 Expression in Inner Meniscus Cells. *J. Orthop. Res.* 30 (11), 1738–1745. doi:10.1002/jor.22142

Gallacher, P. D., Gilbert, R. E., Kanes, G., Roberts, S. N. J., and Rees, D. (2010). White on white Meniscal Tears to Fix or Not to Fix. *The Knee* 17 (4), 270–273. doi:10.1016/j.knee.2010.02.016

Gao, Y., Wang, S., He, L., Wang, C., and Yang, L. (2020). Alpinetin Protects Chondrocytes and Exhibits Anti-inflammatory Effects via the NF-Kb/ERK Pathway for Alleviating Osteoarthritis. *Inflammation* 43 (5), 1742–1750. doi:10.1007/s10753-020-01248-3

Ghazi Zadeh, L., Chevrier, A., Farr, J., Rodeo, S. A., and Buschmann, M. D. (2018). Augmentation Techniques for Meniscus Repair. *J. Knee Surg.* 31 (1), 99–116. doi:10.1055/s-0037-1602247

Greenblatt, M. B., Ritter, S. Y., Wright, J., Tsang, K., Hu, D., Glimcher, L. H., et al. (2013). NFATc1 and NFATc2 Repress Spontaneous Osteoarthritis. *Proc. Natl. Acad. Sci.* 110 (49), 19914–19919. doi:10.1073/pnas.1320036110

Grogan, S. P., Pauli, C., Lotz, M. K., and D'Lima, D. D. (2017). Relevance of Meniscal Cell Regional Phenotype to Tissue Engineering. *Connect. Tissue Res.* 58 (3-4), 259–270. doi:10.1080/03008207.2016.1268604

Gunja, N. J., and Athanasiou, K. A. (2010). Effects of Hydrostatic Pressure on Leporine Meniscus Cell-Seeded PLLA Scaffolds. *J. Biomed. Mater. Res. A.* 92 (3), 896–905. doi:10.1002/jbm.a.32451

Han, W. M., Heo, S.-J., Driscoll, T. P., Smith, L. J., Mauck, R. L., and Elliott, D. M. (2013). Macro- to Microscale Strain Transfer in Fibrous Tissues Is Heterogeneous and Tissue-specific. *Biophysical J.* 105 (3), 807–817. doi:10.1016/j.bpj.2013.06.023

Han, W. M., Heo, S. J., Driscoll, T. P., Boggs, M. E., Duncan, R. L., Mauck, R. L., et al. (2014). Impact of Cellular Microenvironment and Mechanical Perturbation on Calcium Signalling in Meniscus Fibrochondrocytes. *Eur. Cel Mater* 27, 321–331. doi:10.22203/ecm.v027a23

Hsiao, B. Y., Chang, T. K., Wu, I. T., and Chen, M. Y. (2014). Rad GTPase Inhibits the NFκB Pathway through Interacting with RelA/p65 to Impede its DNA Binding and Target Gene Transactivation. *Cell Signal* 26 (7), 1437–1444. doi:10.1016/j.cellsig.2014.03.003

Huber, W., Carey, V. J., Gentleman, R., Anders, S., Carlson, M., Carvalho, B. S., et al. (2015). Orchestrating High-Throughput Genomic Analysis with Bioconductor. *Nat. Methods* 12 (2), 115–121. doi:10.1038/nmeth.3252

Hwang, H. S., and Kim, H. A. (2015). Chondrocyte Apoptosis in the Pathogenesis of Osteoarthritis. *Int. J. Mol. Sci.* 16 (11), 26035–26054. doi:10.3390/ijms161125943

Kanazawa, T., Furumatsu, T., Hachioji, M., Oohashi, T., Ninomiya, Y., and Ozaki, T. (2012). Mechanical Stretch Enhances COL2A1 Expression on Chromatin by Inducing SOX9 Nuclear Translocalization in Inner Meniscus Cells. *J. Orthop. Res.* 30 (3), 468–474. doi:10.1002/jor.21528

Kapoor, M., Martel-Pelletier, J., Lajeunesse, D., Pelletier, J. P., and Fahmi, H. (2011). Role of Proinflammatory Cytokines in the Pathophysiology of Osteoarthritis. *Nat. Rev. Rheumatol.* 7 (1), 33–42. doi:10.1038/nrrheum.2010.196

Kersey, P. J., Staines, D. M., Lawson, D., Kulesha, E., Derwent, P., Humphrey, J. C., et al. (2012). Ensembl Genomes: an Integrative Resource for Genome-Scale Data from Non-vertebrate Species. *Nucleic Acids Res.* 40 (Database issue), D91–D97. doi:10.1093/nar/gkr895

Larsson, S., Englund, M., Struglics, A., and Lohmander, L. S. (2015). Interleukin-6 and Tumor Necrosis Factor Alpha in Synovial Fluid Are Associated with Progression of Radiographic Knee Osteoarthritis in Subjects with Previous Meniscectomy. *Osteoarthritis and Cartilage* 23 (11), 1906–1914. doi:10.1016/j.joca.2015.05.035

Legendre, F., Dudhia, J., Pujol, J.-P., and Bogdanowicz, P. (2003). JAK/STAT but Not ERK1/ERK2 Pathway Mediates Interleukin (IL)-6/Soluble IL-6R Down-Regulation of Type II Collagen, Aggrecan Core, and Link Protein Transcription in Articular Chondrocytes: ASSOCIATION with a Down-Regulation of SOX9 Expression. *J. Biol. Chem.* 278 (5), 2903–2912. doi:10.1074/jbc.M110773200

LeGrand, A., Fermor, B., Fink, C., Pisetsky, D. S., Weinberg, J. B., Vail, T. P., et al. (2001). Interleukin-1, Tumor Necrosis Factor Alpha, and Interleukin-17 Synergistically Up-Regulate Nitric Oxide and Prostaglandin E2 Production in Explants of Human Osteoarthritic Knee Menisci. *Arthritis Rheum.* 44 (9), 2078–2083. doi:10.1002/1529-0131(200109)44:9<2078:Aid-art358>3.0.Co;2-j

Li, W. Q., Dehnade, F., and Zafarullah, M. (2001). Oncostatin M-Induced Matrix Metalloproteinase and Tissue Inhibitor of Metalloproteinase-3 Genes Expression in Chondrocytes Requires Janus Kinase/STAT Signaling Pathway. *J. Immunol.* 166 (5), 3491–3498. doi:10.4049/jimmunol.166.5.3491

Liberzon, A., Birger, C., Thorvaldsdóttir, H., Ghandi, M., Mesirov, J. P., and Tamayo, P. (2015). The Molecular Signatures Database (MSigDB) Hallmark Gene Set Collection. *Cell Syst* 1 (6), 417–425. doi:10.1016/j.cels.2015.12.004

Liu, B., Goode, A. P., Carter, T. E., Utturkar, G. M., Huebner, J. L., Taylor, D. C., et al. (2017). Matrix Metalloproteinase Activity and Prostaglandin E2 Are Elevated in the Synovial Fluid of Meniscus Tear Patients. *Connect. Tissue Res.* 58 (3-4), 305–316. doi:10.1080/03008207.2016.1256391

Livak, K. J., and Schmittgen, T. D. (2001). Analysis of Relative Gene Expression Data Using Real-Time Quantitative PCR and the 2−ΔΔCT Method. *Methods* 25 (4), 402–408. doi:10.1006/meth.2001.1262

Lohmander, L. S., Englund, P. M., Dahl, L. L., and Roos, E. M. (2007). The Long-Term Consequence of Anterior Cruciate Ligament and Meniscus Injuries: Osteoarthritis. *Am. J. Sports Med.* 35 (10), 1756–1769. doi:10.1177/0363546507307396

Love, M. I., Huber, W., and Anders, S. (2014). Moderated Estimation of Fold Change and Dispersion for RNA-Seq Data with DESeq2. *Genome Biol.* 15 (12), 550. doi:10.1186/s13059-014-0550-8

Lu, H., Zeng, C., Zhao, H., Lian, L., and Dai, Y. (2014). Glatiramer Acetate Inhibits Degradation of Collagen II by Suppressing the Activity of Interferon Regulatory Factor-1. *Biochem. Biophysical Res. Commun.* 448 (3), 323–328. doi:10.1016/j.bbrc.2014.03.041

Madhavan, S., Anghelina, M., Sjostrom, D., Dossumbekova, A., Guttridge, D. C., and Agarwal, S. (2007). Biomechanical Signals Suppress TAK1 Activation to Inhibit NF-kappaB Transcriptional Activation in Fibrochondrocytes. *J. Immunol.* 179 (9), 6246–6254. doi:10.4049/jimmunol.179.9.6246

Mauck, R. L., Martinez-Diaz, G. J., Yuan, X., and Tuan, R. S. (2007). Regional Multilineage Differentiation Potential of Meniscal Fibrochondrocytes: Implications for Meniscus Repair. *Anatomical Rec.* 290 (1), 48–58. doi:10.1002/ar.20419

McHenry, J. A., Zielinska, B., and Donahue, T. L. (2006). Proteoglycan Breakdown of Meniscal Explants Following Dynamic Compression Using a Novel Bioreactor. *Ann. Biomed. Eng.* 34 (11), 1758–1766. doi:10.1007/s10439-006-9178-5

McNulty, A. L., Estes, B. T., Wilusz, R. E., Weinberg, J. B., and Guilak, F. (2010). Dynamic Loading Enhances Integrative Meniscal Repair in the Presence of Interleukin-1. *Osteoarthritis Cartilage/OARS, Osteoarthritis Res. Soc.* 18 (6), 830–838. doi:10.1016/j.joca.2010.02.009

McNulty, A. L., and Guilak, F. (2015). Mechanobiology of the Meniscus. *J. Biomech.* 48 (8), 1469–1478. doi:10.1016/j.jbiomech.2015.02.008

McNulty, A. L., Moutos, F. T., Weinberg, J. B., and Guilak, F. (2007). Enhanced Integrative Repair of the Porcine Meniscus *In Vitro* by Inhibition of Interleukin-1 or Tumor Necrosis Factor Alpha. *Arthritis Rheum.* 56 (9), 3033–3042. doi:10.1002/art.22839

McNulty, A. L., Rothfusz, N. E., Leddy, H. A., and Guilak, F. (2013). Synovial Fluid Concentrations and Relative Potency of Interleukin-1 Alpha and Beta in Cartilage and Meniscus Degradation. *J. Orthop. Res.* 31 (7), 1039–1045. doi:10.1002/jor.22334

McNulty, A. L., Weinberg, J. B., and Guilak, F. (2009). Inhibition of Matrix Metalloproteinases Enhances *In Vitro* Repair of the Meniscus. *Clin. Orthop. Relat. Res.* 467 (6), 1557–1567. doi:10.1007/s11999-008-0596-6

Millward-Sadler, S. J., Khan, N. S., Bracher, M. G., Wright, M. O., and Salter, D. M. (2006). Roles for the Interleukin-4 Receptor and Associated JAK/STAT Proteins in Human Articular Chondrocyte Mechanotransduction. *Osteoarthritis and Cartilage* 14 (10), 991–1001. doi:10.1016/j.joca.2006.03.013

Mootha, V. K., Lindgren, C. M., Eriksson, K.-F., Subramanian, A., Sihag, S., Lehar, J., et al. (2003). PGC-1α-responsive Genes Involved in Oxidative Phosphorylation Are Coordinately Downregulated in Human Diabetes. *Nat. Genet.* 34, 267. Available at: https://www.nature.com/articles/ng1180#supplementary-information. doi:10.1038/ng1180

Murakami, T., Otsuki, S., Okamoto, Y., Nakagawa, K., Wakama, H., Okuno, N., et al. (2019). Hyaluronic Acid Promotes Proliferation and Migration of Human Meniscus Cells via a CD44-dependent Mechanism. *Connect. Tissue Res.* 60 (2), 117–127. doi:10.1080/03008207.2018.1465053

Nielsen, A. B., and Yde, J. (1991). Epidemiology of Acute Knee Injuries: a Prospective Hospital Investigation. *J. Trauma* 31 (12), 1644–1648. doi:10.1097/00005373-199112000-00014

Nims, R. J., Pferdehirt, L., Ho, N. B., Savadipour, A., Lorentz, J., Sohi, S., et al. (2021). A Synthetic Mechanogenetic Gene Circuit for Autonomous Drug Delivery in Engineered Tissues. *Sci. Adv.* 7 (5), eabd9858. doi:10.1126/sciadv.abd9858

Otero, M., Lago, R., Gómez, R., Lago, F., Gomez-Reino, J. J., and Gualillo, O. (2007). Phosphatidylinositol 3-kinase, MEK-1 and P38 Mediate Leptin/interferon-Gamma Synergistic NOS Type II Induction in Chondrocytes. *Life Sci.* 81 (19), 1452–1460. doi:10.1016/j.lfs.2007.09.007

Puetzer, J. L., Ballyns, J. J., and Bonassar, L. J. (2012). The Effect of the Duration of Mechanical Stimulation and post-stimulation Culture on the Structure and Properties of Dynamically Compressed Tissue-Engineered Menisci. *Tissue Eng. Part. A.* 18 (13-14), 1365–1375. doi:10.1089/ten.TEA.2011.0589

Rath, E., and Richmond, J. C. (2000). The Menisci: Basic Science and Advances in Treatment. *Br. J. Sports Med.* 34 (4), 252–257. doi:10.1136/bjsm.34.4.252

Riera, K. M., Rothfusz, N. E., Wilusz, R. E., Weinberg, J. B., Guilak, F., and McNulty, A. L. (2011). Interleukin-1, Tumor Necrosis Factor-Alpha, and Transforming Growth Factor-Beta 1 and Integrative Meniscal Repair: Influences on Meniscal Cell Proliferation and Migration. *Arthritis Res. Ther.* 13 (6), R187. doi:10.1186/ar3515

Rodova, M., Lu, Q., Li, Y., Woodbury, B. G., Crist, J. D., Gardner, B. M., et al. (2011). Nfat1 Regulates Adult Articular Chondrocyte Function through its Age-dependent Expression Mediated by Epigenetic Histone Methylation. *J. Bone Miner Res.* 26 (8), 1974–1986. doi:10.1002/jbmr.397

Sanchez-Adams, J., Willard, V. P., and Athanasiou, K. A. (2011). Regional Variation in the Mechanical Role of Knee Meniscus Glycosaminoglycans. *J. Appl. Physiol.* 111 (6), 1590–1596. doi:10.1152/japplphysiol.00848.2011

Santamaria, S. (2020). ADAMTS-5: A Difficult Teenager Turning 20. *Int. J. Exp. Pathol.* 101 (1-2), 4–20. doi:10.1111/iep.12344

Scott, P. G., Nakano, T., and Dodd, C. M. (1997). Isolation and Characterization of Small Proteoglycans from Different Zones of the Porcine Knee Meniscus. *Biochim. Biophys. Acta (Bba) - Gen. Subjects* 1336 (2), 254–262. doi:10.1016/S0304-4165(97)00040-8

Shin, S. J., Fermor, B., Weinberg, J. B., Pisetsky, D. S., and Guilak, F. (2003). Regulation of Matrix Turnover in Meniscal Explants: Role of Mechanical Stress, Interleukin-1, and Nitric Oxide. *J. Appl. Physiol.* 95 (1), 308–313. doi:10.1152/japplphysiol.00131.2003

Silawal, S., Triebel, J., Bertsch, T., and Schulze-Tanzil, G. (2018). Osteoarthritis and the Complement Cascade. *Clin. Med. Insights Arthritis Musculoskelet. Disord.* 11, 1179544117751430. doi:10.1177/1179544117751430

Son, M., and Levenston, M. E. (2012). Discrimination of Meniscal Cell Phenotypes Using Gene Expression Profiles. *Eur. Cel Mater* 23, 195–208. doi:10.22203/ecm.v023a15

Subramanian, A., Tamayo, P., Mootha, V. K., Mukherjee, S., Ebert, B. L., Gillette, M. A., et al. (2005). Gene Set Enrichment Analysis: A Knowledge-Based Approach for Interpreting Genome-wide Expression Profiles. *Proc. Natl. Acad. Sci.* 102 (43), 15545–15550. doi:10.1073/pnas.0506580102

Sueishi, T., Akasaki, Y., Goto, N., Kurakazu, I., Toya, M., Kuwahara, M., et al. (2020). GRK5 Inhibition Attenuates Cartilage Degradation via Decreased NF-Kb Signaling. *Arthritis Rheumatol.* 72 (4), 620–631. doi:10.1002/art.41152

Sun, K., Luo, J., Guo, J., Yao, X., Jing, X., and Guo, F. (2020). The PI3K/AKT/mTOR Signaling Pathway in Osteoarthritis: a Narrative Review. *Osteoarthritis and Cartilage* 28 (4), 400–409. doi:10.1016/j.joca.2020.02.027

Tudor-Locke, C., and Rowe, D. A. (2012). Using Cadence to Study Free-Living Ambulatory Behaviour. *Sports Med.* 42 (5), 381–398. doi:10.2165/11599170-000000000-00000

Upton, M. L., Chen, J., Guilak, F., and Setton, L. A. (2003). Differential Effects of Static and Dynamic Compression on Meniscal Cell Gene Expression. *J. Orthopaedic Res.* 21 (6), 963–969. doi:10.1016/S0736-0266(03)00063-9

Upton, M. L., Chen, J., and Setton, L. A. (2006a). Region-specific Constitutive Gene Expression in the Adult Porcine Meniscus. *J. Orthopaedic Res.* 24 (7), 1562–1570. doi:10.1002/jor.20146

Upton, M. L., Gilchrist, C. L., Guilak, F., and Setton, L. A. (2008). Transfer of Macroscale Tissue Strain to Microscale Cell Regions in the Deformed Meniscus. *Biophys. J.* 95 (4), 2116–2124. doi:10.1529/biophysj.107.126938

Upton, M. L., Guilak, F., Laursen, T. A., and Setton, L. A. (2006b). Finite Element Modeling Predictions of Region-specific Cell-Matrix Mechanics in the Meniscus. *Biomech. Model. Mechanobiology* 5 (2), 140. doi:10.1007/s10237-006-0031-4

van den Berg, W. B., Joosten, L. A., and van de Loo, F. A. (1999). TNF Alpha and IL-1 Beta Are Separate Targets in Chronic Arthritis. *Clin. Exp. Rheumatol.* 17 (6 Suppl. 18), S105–S114.

Videman, T., Eronen, I., Friman, C., and Langenskiöld, A. (1979). Glycosaminoglycan Metabolism of the Medial Meniscus, the Medial Collateral Ligament and the Hip Joint Capsule in Experimental Osteoarthritis Caused by Immobilization of the Rabbit Knee. *Acta Orthopaedica Scand.* 50 (4), 465–470. doi:10.3109/17453677908989791

Wang, C. C., Lee, C. H., Peng, Y. J., Salter, D. M., and Lee, H. S. (2015). Platelet-Rich Plasma Attenuates 30-kDa Fibronectin Fragment-Induced Chemokine and Matrix Metalloproteinase Expression by Meniscocytes and Articular Chondrocytes. *Am. J. Sports Med.* 43 (10), 2481–2489. doi:10.1177/0363546515597489

Wang, J., Gardner, B. M., Lu, Q., Rodova, M., Woodbury, B. G., Yost, J. G., et al. (2009). Transcription Factor Nfat1 Deficiency Causes Osteoarthritis through Dysfunction of Adult Articular Chondrocytes. *J. Pathol.* 219 (2), 163–172. doi:10.1002/path.2578

Wei, Z., Guo, H., Qin, J., Lu, S., Liu, Q., Zhang, X., et al. (2019). Pan-senescence Transcriptome Analysis Identified RRAD as a Marker and Negative Regulator of Cellular Senescence. *Free Radic. Biol. Med.* 130, 267–277. doi:10.1016/j.freeradbiomed.2018.10.457

Wilusz, R. E., Weinberg, J. B., Guilak, F., and McNulty, A. L. (2008). Inhibition of Integrative Repair of the Meniscus Following Acute Exposure to Interleukin-1 *In Vitro*. *J. orthopaedic Res. : official Publ. Orthopaedic Res. Soc.* 26 (4), 504–512. doi:10.1002/jor.20538

Xu, M., Feng, M., Peng, H., Qian, Z., Zhao, L., and Wu, S. (2020). Epigenetic Regulation of Chondrocyte Hypertrophy and Apoptosis through Sirt1/P53/P21 Pathway in Surgery-Induced Osteoarthritis. *Biochem. Biophys. Res. Commun.* 528 (1), 179–185. doi:10.1016/j.bbrc.2020.04.097

Yang, H., Wen, Y., Zhang, M., Liu, Q., Zhang, H., Zhang, J., et al. (2020). MTORC1 Coordinates the Autophagy and Apoptosis Signaling in Articular Chondrocytes in Osteoarthritic Temporomandibular Joint. *Autophagy* 16 (2), 271–288. doi:10.1080/15548627.2019.1606647

Yang, S., Kim, J., Ryu, J. H., Oh, H., Chun, C. H., Kim, B. J., et al. (2010). Hypoxia-inducible Factor-2alpha Is a Catabolic Regulator of Osteoarthritic Cartilage Destruction. *Nat. Med.* 16 (6), 687–693. doi:10.1038/nm.2153

Zhang, Y., Wang, F., Bao, L., Li, J., Shi, Z., and Wang, J. (2019). Cyclic Hydrostatic Compress Force Regulates Apoptosis of Meniscus Fibrochondrocytes via Integrin Alpha5beta1. *Physiol. Res.* 68 (4), 639–649. doi:10.33549/physiolres.934088

Zheng, L., Zhang, Z., Sheng, P., and Mobasheri, A. (2021). The Role of Metabolism in Chondrocyte Dysfunction and the Progression of Osteoarthritis. *Ageing Res. Rev.* 66, 101249. doi:10.1016/j.arr.2020.101249

Zielinska, B., and Haut Donahue, T. L. (2005). 3D Finite Element Model of Meniscectomy: Changes in Joint Contact Behavior. *J. Biomechanical Eng.* 128 (1), 115–123. doi:10.1115/1.2132370

Conflict of Interest: The authors declare that the research was conducted in the absence of any commercial or financial relationships that could be construed as a potential conflict of interest.

Publisher's Note: All claims expressed in this article are solely those of the authors and do not necessarily represent those of their affiliated organizations, or those of the publisher, the editors and the reviewers. Any product that may be evaluated in this article, or claim that may be made by its manufacturer, is not guaranteed or endorsed by the publisher.

frontiers in Bioengineering and Biotechnology

ORIGINAL RESEARCH
published: 17 March 2022
doi: 10.3389/fbioe.2022.837554

Knee Joint Menisci Are Shock Absorbers: A Biomechanical *In-Vitro* Study on Porcine Stifle Joints

Andreas M. Seitz*, Jonas Schwer, Luisa de Roy, Daniela Warnecke, Anita Ignatius and Lutz Dürselen

Institute of Orthopedic Research and Biomechanics, Center of Trauma Research Ulm, Ulm University Medical Center, Ulm, Germany

The aim of this biomechanical *in vitro* study was to answer the question whether the meniscus acts as a shock absorber in the knee joint or not. The soft tissue of fourteen porcine knee joints was removed, leaving the capsuloligamentous structures intact. The joints were mounted in 45° neutral knee flexion in a previously validated droptower setup. Six joints were exposed to an impact load of 3.54 J, and the resultant loss factor (η) was calculated. Then, the setup was modified to allow sinusoidal loading under dynamic mechanical analysis (DMA) conditions. The remaining eight knee joints were exposed to 10 frequencies ranging from 0.1 to 5 Hz at a static load of 1210 N and a superimposed sinusoidal load of 910 N (2.12 times body weight). Forces (F) and deformation (l) were continuously recorded, and the loss factor (tan δ) was calculated. For both experiments, four meniscus states (intact, medial posterior root avulsion, medial meniscectomy, and total lateral and medial meniscectomy) were investigated. During the droptower experiments, the intact state indicated a loss factor of η = 0.1. Except for the root avulsion state (–15%, p = 0.12), the loss factor decreased (p < 0.046) up to 68% for the total meniscectomy state (p = 0.028) when compared to the intact state. Sinusoidal DMA testing revealed that knees with an intact meniscus had the highest loss factors, ranging from 0.10 to 0.15. Any surgical manipulation lowered the damping ability: Medial meniscectomy resulted in a reduction of 24%, while the resection of both menisci lowered tan δ by 18% compared to the intact state. This biomechanical *in vitro* study indicates that the shock-absorbing ability of a knee joint is lower when meniscal tissue is resected. In other words, the meniscus contributes to the shock absorption of the knee joint not only during impact loads, but also during sinusoidal loads. The findings may have an impact on the rehabilitation of young, meniscectomized patients who want to return to sports. Consequently, such patients are exposed to critical loads on the articular cartilage, especially when performing sports with recurring impact loads transmitted through the knee joint surfaces.

Keywords: knee, joint, meniscus, shock absorber, shock, impact, dynamic mechanic analysis (DMA), *in vitro*

OPEN ACCESS

Edited by:
Tarun Goswami,
Wright State University, United States

Reviewed by:
Rene Verdonk,
Ghent University, Belgium
Matteo Berni,
Rizzoli Orthopedic Institute (IRCCS), Italy

****Correspondence:***
Andreas M. Seitz
andreas.seitz@uni-ulm.de

Specialty section:
This article was submitted to Biomechanics, a section of the journal Frontiers in Bioengineering and Biotechnology

Received: *16 December 2021*
Accepted: *14 February 2022*
Published: *17 March 2022*

Citation:
Seitz AM, Schwer J, de Roy L, Warnecke D, Ignatius A and Dürselen L (2022) Knee Joint Menisci Are Shock Absorbers: A Biomechanical In-Vitro Study on Porcine Stifle Joints. Front. Bioeng. Biotechnol. 10:837554. doi: 10.3389/fbioe.2022.837554

1 INTRODUCTION

Patients suffering from anterior cruciate ligament (ACL) injuries (Gillquist and Messner, 1999; Lohmander et al., 2007; Bodkin et al., 2020), meniscus tears (Roos et al., 1998; Roos et al., 1999; Lohmander et al., 2007), or articular fractures of the knee (Weigel and Marsh, 2002; Buckwalter and Brown, 2004; Buckwalter et al., 2004) are up to 20 times more likely to develop post-traumatic osteoarthritis (PTOA) (Muthuri et al., 2011; Carbone and Rodeo, 2017; Thomas et al., 2017) compared to the healthy population. Traumatic meniscal tears are a frequent cause of disability and loss of work time (Mccann et al., 2009; Mcdermott, 2011; Badlani et al., 2013; Carbone and Rodeo, 2017), mostly affecting patients under 40 years of age (Ridley et al., 2017) and professional athletes (Majewski et al., 2006; Yeh et al., 2012; Snoeker et al., 2013). One of the superior goals of this active patient group is to return to work or sports as soon as possible. While arthroscopic suture repair provides a good prognosis for tears in the blood-supplied outer, so-called "red" and central "red-white" zone of the menisci, the healing potential for tears in the inner "white zone" is rather poor and remains a big clinical challenge (Bansal et al., 2021). Although being aware about the poor clinical long-term results (Andersson-Molina et al., 2002; Wachsmuth et al., 2003; Englund and Lohmander, 2004; Mcdermott and Amis, 2006; Intema et al., 2010; Salata et al., 2010), mechanically instable tears at the white zone are still mostly treated by partial meniscectomy, in order to obtain pain relief, avoid tear progression, and allow a faster return to different activities.

Besides biological alterations (Rai et al., 2019), biomechanical changes (Barton et al., 2017; Fischenich et al., 2017b) that are mainly related to the increased tibiofemoral contact pressure (Seitz et al., 2012; Sukopp et al., 2021) have been identified to be responsible for the amplification of PTOA progression after such meniscectomy procedures. Other than the main biomechanical function of tibiofemoral load transmission (Mcdermott et al., 2008), the frequently assigned shock-absorbing function of the menisci might also affect the knee joint homeostasis after meniscectomy. "The shocking truth about meniscus" by Andrews et al. (2011) revealed major flaws of the three most cited publications (Krause et al., 1976; Kurosawa et al., 1980; Voloshin and Wosk, 1983) that affiliate the meniscus with this shock-absorbing ability. Moreover, a recent commentary (Gecelter et al., 2021) came to the conclusion that based both on the mechanical properties and the evolutionary origin, the menisci are not shock absorbers. In contrast, there is evidence assigning a shock-absorbing function directly to the meniscus material itself (Pereira et al., 2014; Gaugler et al., 2015; Coluccino et al., 2017) and to the knee joint during activities of daily living (Winter, 1983; Ratcliffe and Holt, 1997). Therefore, the question remains whether the menisci play an active role as shock absorbers in the healthy, injured, and meniscectomized knee joints or not. Hence, the aim of this biomechanical *in vitro* study was to investigate the shock-absorbing function of the meniscus as an essential integrant of the knee joint during impact and repetitive loads.

Normal menisci have a highly anisotropic structure that is mainly composed of water (75%), collagen (23%), water-binding glycosaminoglycans (1%), and other matrix components leading to a time-dependent viscoelastic behavior (Herwig et al., 1984; Pereira et al., 2014; Seitz et al., 2021). While under static equilibrium conditions (Tibesku et al., 2004; Martin Seitz et al., 2013; Schwer et al., 2020) and repetitive loading (Kessler et al., 2006), the menisci exhibit considerable axial deformation, high impact, or shock loads, as seen, e.g., during jump landings, leading to an increase in their stiffness, and thus, to a decrease in the ability to reduce the transmitted stresses. Therefore, we hypothesize that the menisci contribute significantly to knee joint shock absorption during repetitive loads, while under impact loads, this shock absorption potential is absent.

2 METHODS

2.1 Study Design

The shock-absorbing potential of six porcine knee joints was investigated using a custom developed droptower setup, which provided one degree of freedom. After successful validation of the setup using defined damping materials, the joints were impacted with a total energy of 3.54 J. During the tests, only the meniscus states were successively varied to be able to relate the shock absorption potential directly to the menisci. These were intact, medial meniscus posterior root avulsion, medial meniscectomy, total lateral, and medial meniscectomy. The shock absorption was interpreted by the loss factor, which was calculated *via* the propagation time between two integrated load cells.

After modification of the test setup, a dynamic mechanical analysis (DMA) was conducted on eight porcine knees to investigate their shock-absorbing potential under repetitive, sinusoidal loads. For this purpose, a frequency scan including 10 different frequencies, ranging between 0.1–5 Hz at a constant load amplitude was performed while considering the four different meniscus states. The resultant shock absorption potential is calculated *via* the phase shift between force and displacement (strain) in order to draw conclusions about the influence of the meniscus on the damping in the knee joint.

2.2 Specimen Preparation

Fourteen fresh porcine hind limbs (liveweight ≈ 100 kg) were obtained for the experiments from a local butcher. The soft tissues were removed, leaving the capsuloligamentous knee joint structures intact. Before the tibial bone was shortened to a length of 4 cm in distance to the knee joint gap, the head of the fibula was secured using a setscrew. A precision miter screw allowed for plane parallel resection of the femoral bone in 5 cm distance to the joint gap and 45° neutral knee joint flexion (Proffen et al., 2012). During the preparation process, the tissues were kept moist using physiologic saline solution. After the preparation process, the specimens were wrapped in saline saturated gauze and stored at −20°C until the day of testing.

Both for the impact and for the repetitive (DMA) loading experiments, four meniscus states (intact, medial posterior root avulsion, medial meniscectomy, and total lateral and medial meniscectomy) were investigated to identify the shock-absorbing function of the meniscus (**Figure 1**). The meniscus

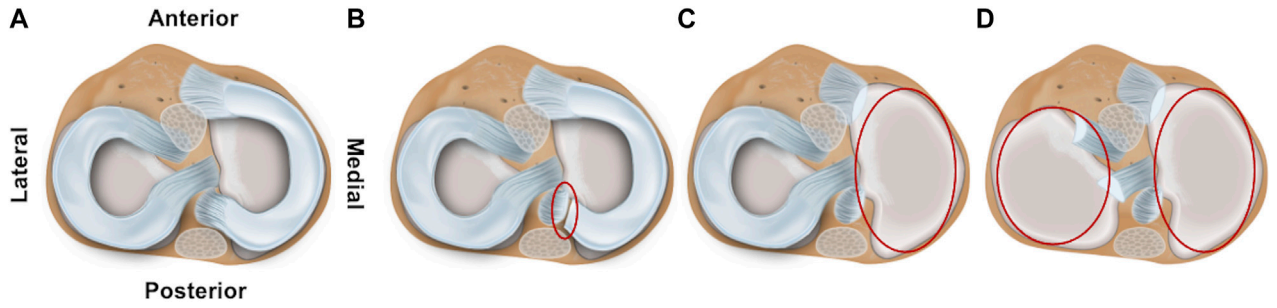

FIGURE 1 | Schematic drawing of the axial view on a tibial plateau of a left knee joint. The femur is removed to allow better visualization of the four investigated meniscal states: **(A)** intact, **(B)** avulsion of the posterior medial meniscus horn, **(C)** medial meniscectomy, and **(D)** total lateral and medial meniscectomy.

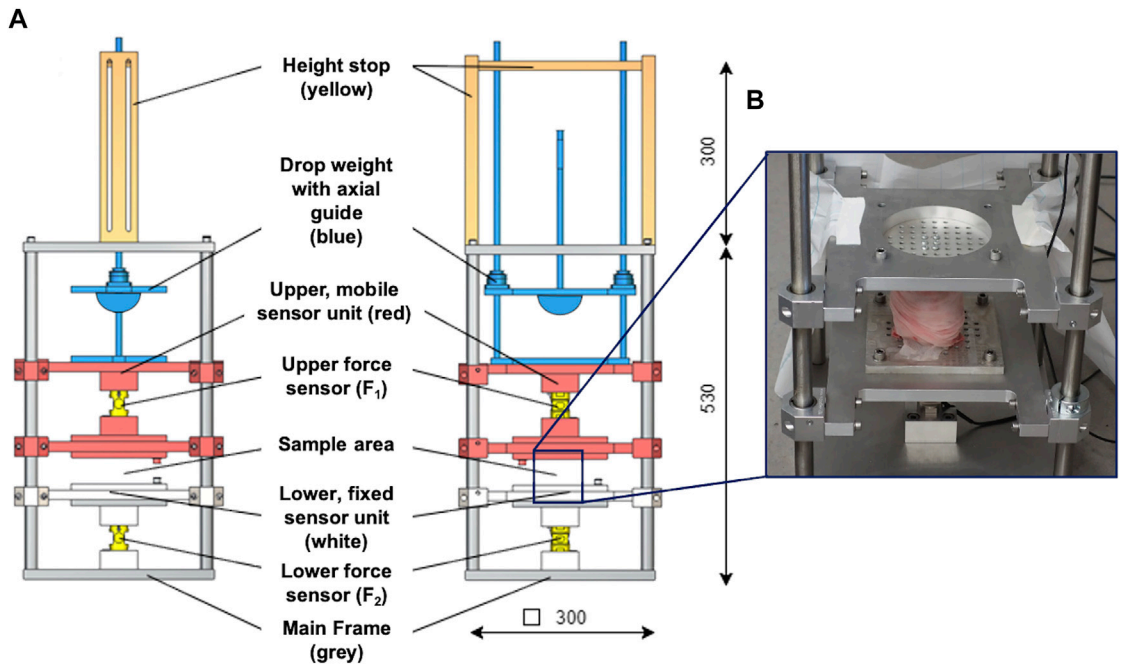

FIGURE 2 | (A) Technical drawing of the droptower setup in the side (left) and frontal (middle) view. The setup consisted of a height stop (ochre), which was directly connected to the axial guidance system of the drop weight. A hemisphere impactor (blue) was used to allow for pinpoint impact transmission. The upper, mobile sensor unit (red) is axially guided by eight axial ball bearings and incorporates the upper force sensor. It is further connected to an impact pad at its top end and to a sample holder at the lower end. The lower, fixed sensor unit (white) is also axially guided by four axial ball bearings and incorporates the lower force sensor. The lower end of this sensor unit is directly connected to the main frame. **(B)** Example of an installed porcine knee joint at the sample area at the droptower setup.

preparation steps were conducted as minimally invasive as possible by an orthopedic surgeon. During these preparation steps, the knee joints were kept in the respective testing setup to avoid a misplacement bias by disassembling and reassembling.

2.3 Test Setup and Validation

2.3.1 Droptower Setup

The droptower test setup configuration consisted of a weight-adjustable (up to 200 N), axially guided drop weight with a height stop and a hemispherical, stainless-steel impactor, which allows for pinpoint impact transmission (**Figure 2**). The drop weight hit the impact pad that was mounted to the mobile upper sensor unit containing a screwed-in 10 kN force sensor (KM30z, ME GmbH, Germany) to which the upper sample holder was connected with four knurled screws. Accurate and low-friction axial guidance of the upper sensor unit was ensured using eight linear ball bearings. The test sample was fixed between the two sample holders, while the lower sample holder was axially guided by four linear ball bearings. The lower sensor contained another screwed-in 10 kN force sensor (KM30z, ME GmbH, Germany) that was rigidly connected to the main frame. The test setup provided only one degree of freedom in the axial direction. This was guided by a total of twelve low-friction linear ball bearings, which were in contact with the stainless-steel main frame.

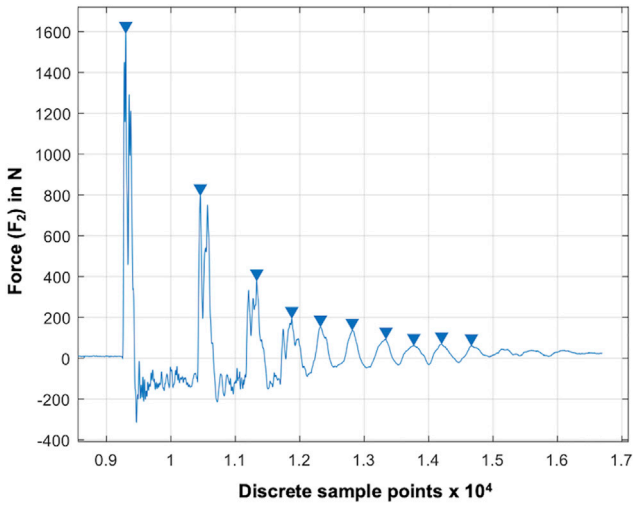

FIGURE 3 | Result graph of a droptower validation test using a known damping material (RF220). The blue arrows indicate automatically determined local maxima (x_n: blue arrows) at the lower force sensor (F_2). The force is given over the discrete sample points at a sampling rate of 20 kHz.

The two series-connected force sensors were used to determine the shock wave propagation by measuring the impact loads at the upper (F_1) and lower sensor (F_2) with the corresponding propagation time (Δt). The measurements were used to calculate the loss factor (η), which was used to interpret the damping behavior of the test sample. For damping materials, it can be assumed (Jäger et al., 2016) that

$$\eta \approx 2D \tag{1}$$

while for viscoelastic materials (e.g., articular cartilage or menisci), it can be assumed that

$$\eta = 2D\left|\sqrt{1-D^2}\right| \tag{2}$$

where D is the damping factor and calculated by

$$D = \frac{\Lambda}{\sqrt{4\pi^2+\Lambda^2}} \tag{3}$$

with Λ as the logarithmic decrement, while Λ can be determined by two consecutively measured maxima x_n:

$$x_{n+1}: \Lambda = \ln\left(\frac{x_n}{x_{n+1}}\right) \tag{4}$$

We used the maxima at the lower force sensor (F_2), as they equal to the reaction force, and thus, vary in accordance with the shock absorption ability of the test samples (**Figure 3**). Based on pretests identifying the potential impact frequencies and following the Nyquist theorem, the sampling rate was set to 30 kHz. Validation of the test setup was conducted using seven special damping materials made of polyurethane foam, indicating specific damping properties and a known loss factor (η) ranging from η = 0.11 (PUR RF220, REGUPOL BSW GmbH, Bad Berleburg, Germany) to η = 0.22 (PUR RF740). Each damping material was tested 60 times at two consecutive days by applying an impact of 3.54 J resulting from dropping 2.1 kg at a drop height of 172 mm, which is double of that used by Hoshino et al. (1.77 J) in their experiments (Hoshino and Wallace, 1987). Then, the experimental loss factor was compared to the given loss factor. The resultant Pearson's correlation coefficient (r = 0.93) indicated excellent correlations. Thus, successful validation of the droptower setup configuration was confirmed.

2.3.2 Dynamic Mechanical Analysis Setup

The modular design of the test setup allows for a fast removal of the height stop and drop weight assembly. This is necessary to allow for an integration of the test setup in the work space of a standard hydraulic dynamic materials testing machine (Instron 8871, Norwood MS, United States) with a total capacity of 10 kN. A multiaxial ball bearing was placed between the upper sensor unit and the actuator of the dynamic materials testing machine (**Figure 4**) to protect the load cell. The setup was centered and rigidly clamped to the base plate of the materials testing machine. An external high-precision laser length transducer (accuracy: ± 0.6 µm; optoNCDT 2201, Micro-Epsilon Eltrotec GmbH, Göppingen, Germany), which was installed at the lower sensor unit, was used together with its reflection plate counterpart that was firmly connected to the upper sensor unit to measure the sample deflection (l). During the DMA tests, the phase angle (δ), the applied oscillation input (force) amplitude ($F_{2,A}$), and the resultant oscillation output (deflection) amplitude (l_A) were continuously recorded (**Figure 5**). Based on these three parameters, the storage modulus (M') was determined (Ehrenstein et al., 2004) by

$$M' = \left(\frac{F_{2A}}{l_A}\right)cos\delta \tag{5}$$

while the loss modulus (M'') is calculated by

$$M'' = \left(\frac{F_{2A}}{l_A}\right)sin\delta \tag{6}$$

Based on both moduli, the loss factor (tan δ) can be calculated by

$$tan\,\delta = \frac{M''}{M'} \tag{7}$$

In addition, the complex modulus E^* results from the storage modulus (M') and the imaginary part (1) of the loss modulus (M''). It is also called dynamic modulus and indicates the behavior of stress to strain under oscillating loads:

$$M^* = M' + i * M'' = \frac{F_{2A}}{l_A} \tag{8}$$

Validation of the DMA test setup was conducted using the same seven damping materials (PUR RF, REGUPOL BSW GmbH, Bad Berleburg, Germany) as those for the droptower setup validation with a known loss factor (η = tanδ). Each damping material was tested three times at 5 Hz sinusoidal loading and a stroke length of ±1.25 mm for 20 cycles. During these validation experiments, the sampling rate was set to 1 kHz.

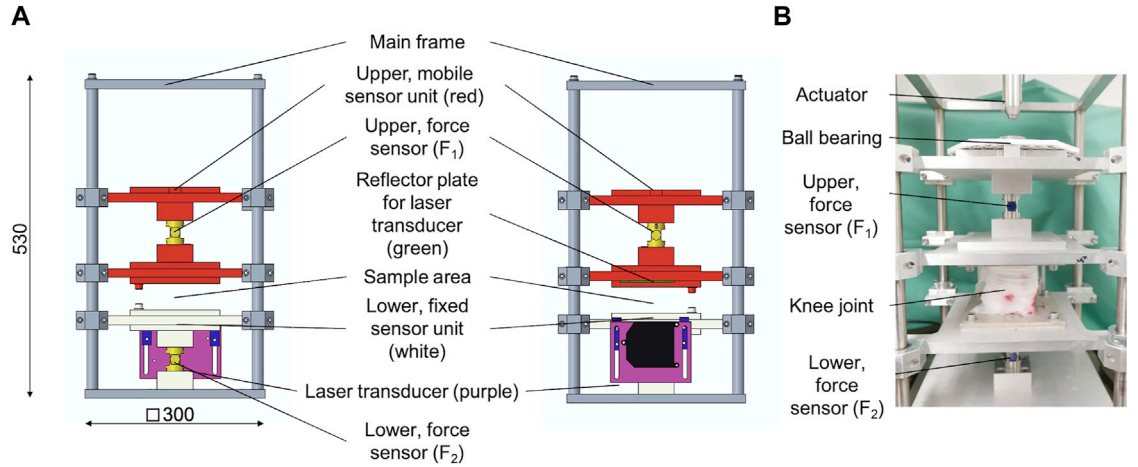

FIGURE 4 | (A) Technical drawing of the modified dynamic mechanical analysis (DMA) setup in side (left) and frontal (middle) view. The upper, mobile sensor unit (red) is axially guided by eight axial ball bearings and incorporates the upper force sensor. On its top, there is a multiaxial ball bearing to protect the load cell of the dynamic testing machine, while at the lower end, there is a reflector plate (green) for a laser transducer installed. The lower, fixed sensor unit (white) is axially guided by four axial ball bearings and incorporates the lower force sensor as well as an external, high-precision laser length transducer. The lower end of this sensor unit is directly connected to the main frame. **(B)** Example of an installed porcine knee joint at the sample area at the DMA setup.

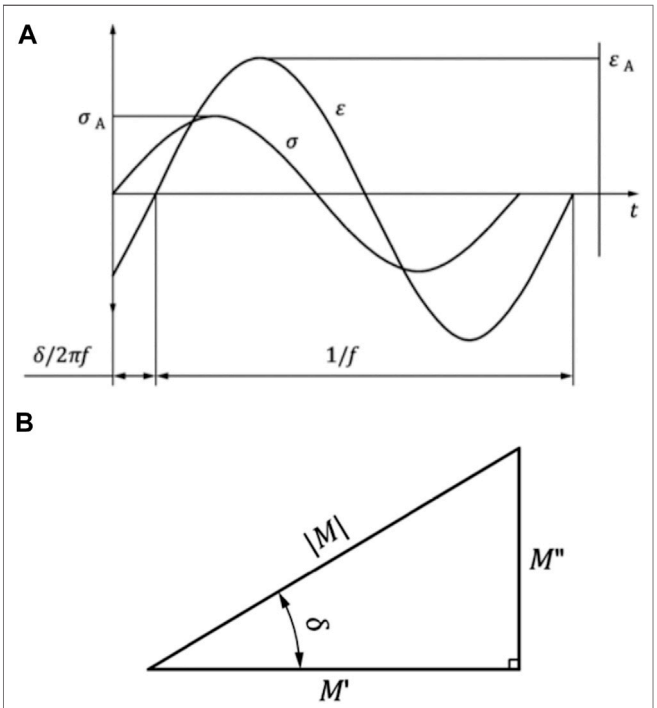

FIGURE 5 | (A) Representative force-induced sinusoidal oscillation (F) and the respective deflection response (l) of a viscoelastic material. The time-dependent, characteristic shift ($\delta/2\pi f$) of the force (F_A) versus the deflection (l_A) amplitudes are plotted over the time (t). **(B)** Relation between the storage modulus M′, the loss modulus M″, the phase angle δ, and the magnitude (*M*) of the complex modulus M*. Images are in accordance with DIN EN ISO 6721-1:2018-03.

Then, the experimental loss factor was compared to the given loss factor by the manufacturer. The resultant Pearson's correlation coefficient (r = 0.99) indicated excellent correlations. Thus, successful validation of the DMA setup configuration could be confirmed.

Synchronized data acquisition for both the droptower (F_1, F_2, Δt) and DMA (F_1, F_2, l, and force/displacement output of the materials testing machine) setup measurements was achieved using a USB data acquisition card (USB-6218, NI Corp., Austin TX, United States) and a customized LabVIEW software (LabVIEW 2019; NI Corp., Austin TX, United States). Subsequent data postprocessing was performed using customized MATLAB scripts (MATLAB 2019b; The MathWorks Inc., Natick MA, United States).

2.4 Droptower Experiments

Based on the results of a study investigating the impact-absorbing properties of a healthy and meniscectomized knee joint (Hoshino and Wallace, 1987), an *a priori* sample size calculation [G*Power 3.1.9.2 (Faul et al., 2007): α = 0.05, Power (1 – β) = 0.95, effect size (dz) = 2.79, n = 4] was performed to ensure sufficient statistical power [Actual power = 0.98] of the study. In order to be able to identify differences after simulating a meniscus tear, the sample size was increased to n = 6.

At the day of testing, the joints were thawed at room temperature and subsequently centrally mounted between the two sample holders using 4–6 proximal and eight distal screws in 45° neutral knee joint flexion (Proffen et al., 2012). To account for the viscoelastic behavior of the knee soft tissues, the joints were loaded 12 min prior to testing with 120 N, following an established protocol (Maher et al., 2017). During preconditioning, the drop height was adjusted to 172 mm and the drop weight was adjusted to 2.1 kg, resulting in an impact energy of 3.54 J, which is double of that used by Hoshino et al. (1.77 J) (Hoshino and Wallace, 1987). After application of the impact and successful

crosscheck of the data recording, the joint was unloaded and allowed to undergo relaxation for 12 min. The tests were repeated three times, resulting in a total test time of 90 min for each meniscus state. The mean values of these three measurements were used for further analyses. Then, the next meniscus preparation step was performed and the experiments were repeated. After each preparation step the joint capsule incision was fixed by surgical sutures. The sampling rate during the droptower experiments was set to 30 kHz. During the tests, the joints were kept moist by constantly misting physiological saline solution.

2.5 Dynamic Mechanical Analysis

Based on the results of a similar study performing a DMA on human menisci (Pereira et al., 2014), an *a priori* sample size calculation [G*Power 3.1.9.2 (Faul et al., 2007): $\alpha = 0.05$, Power $(1-\beta) = 0.80$, effect size (dz) = 1.15, $n = 7$] was performed to ensure sufficient statistical power [Actual power = 0.85] of the study. Comparators to determine the effect size dz were tan δ values (mean ± SD) of the anterior medial menisci and mid body medial menisci values. In order to be able to identify differences after simulating meniscus pathologies, the sample size was increased to $n = 8$.

At the day of testing, the porcine knee joints were thawed and centrally applied in the modified DMA test setup in 45° neutral knee joint flexion (Proffen et al., 2012). A total of 8–12 screws were used to secure the specimen against translation. Taylor et al. (2006) identified an axial knee joint loading of 2.12 times body weight (BW) during the stance phase and 0.3 times BW during the swing phase of normal gait in sheep knees. Since sheep and pigs are similar in their neutral knee position and gait (Proffen et al., 2012), these values were transferred to the forces in the porcine knee, resulting in a static load of 1,210 N and a superimposed sinusoidal load of 910N, which was applied to the porcine knee joints. As a result, peak loads of 2120 N and minimum loads of 300 N were identified for the sinusoidal DMA tests. Additionally, the joints were loaded 12 min prior to testing with 300 N to account for the viscoelastic behavior of the knee soft tissues (Maher et al., 2017). A total of ten frequencies (0.1, 0.2, 0.4, 0.6, 0.8, 1, 2, 3, 4, and 5 Hz) were arranged randomly for each knee and scanned directly one after the other, in accordance with this randomized sequence. The frequency range was adapted from Pereira et al. (2014) and cropped to the frequencies that match best to those observed during gait, running, and other daily activities (Danion et al., 2003; Simoni et al., 2021). The sampling rate was adapted to the respective frequency in a way that 1,000 values were recorded per single sinusoidal oscillation, resulting in a total of 10,000 measurement points per DMA run. After the intact meniscus state investigation, the joints were allowed to undergo relaxation for 12 min. Then, the next meniscus preparation step was performed and the experiments were repeated. After each preparation step, the joint capsule incision was fixed by surgical sutures. During the tests, the joints were continuously kept moist by constantly misting physiological saline solution.

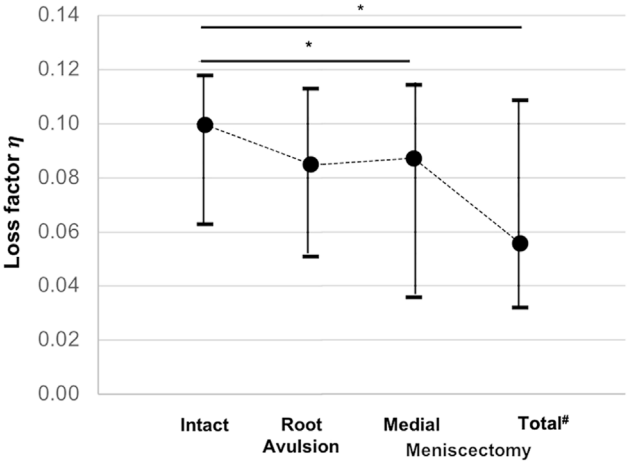

FIGURE 6 | Minimum, median, and maximum loss factor (η) values compared at the four investigated meniscus states: intact, root avulsion at the posterior horn of the medial meniscus, medial meniscectomy and total lateral and medial meniscectomy. The dotted line indicates the progression of the consecutively investigated meniscus states. #The total meniscectomy state was statistically lower than any of the other states; *Wilcoxon test: $^{*,\#}p < 0.05$; $n = 6$.

2.6 Statistical Analysis

Gaussian distribution of the results data was tested using the Shapiro–Wilk test, resulting in non-normally distributed data for the droptower and normally distributed data for the DMA experiments. Thus, non-parametric (droptower) and parametric (DMA) statistical analyses were performed using a statistical software package (SPSS v24, IBM Corp., Armonk, NY, United States).

In detail, for the droptower experiments, F_2 and η were elaborated by comparing the four meniscus states using a Friedman test followed by a Wilcoxon test, in which significant differences were observed. For the DMA experiments, tan δ was elaborated by comparing the four meniscus states by means of a one-way ANOVA followed by Duncan post-hoc testing, in which significant differences were observed. In general, $p = 0.05$ was considered significant, while p-value Bonferroni correction was applied where necessary.

3 RESULTS

3.1 Droptower Experiments

Friedman testing revealed significant differences in both the force maxima at the lower force sensor (F_2; $p = 0.02$) and the loss factor (η; $p = 0.002$). For the intact state, a median F_2 of 1187 N was measured. Furthermore, a significant F_2 increase of 9% after medial meniscectomy (Wilcoxon: $p = 0.46$) and of 24% after total meniscectomy (Wilcoxon: $p = 0.014$) was identified. These findings were completed by the results of the loss factor (**Figure 6**): The intact state possessed a medial loss factor of $\eta = 0.1$. Friedman testing revealed significant differences of the loss factor (η) for the meniscus states ($p = 0.002$). In detail, except

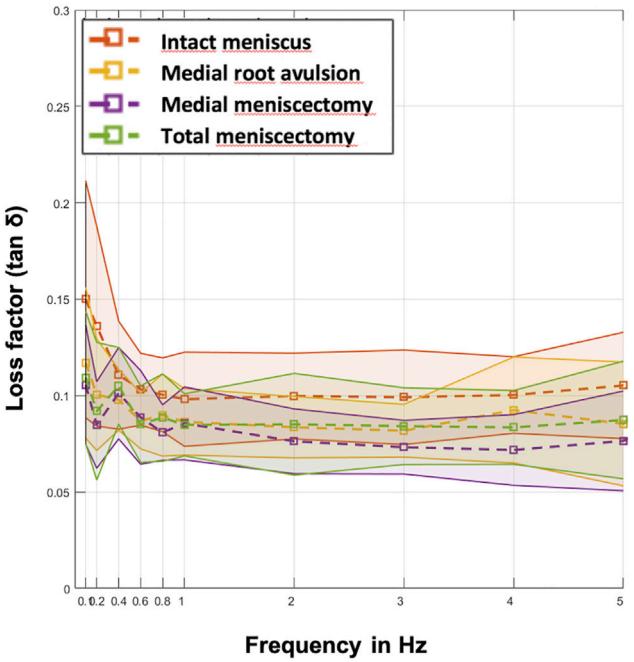

FIGURE 7 | Mean values (dashed lines) of the loss factor (tan δ) ± SD (represented by the envelope in the same color) plotted over the ten investigated frequencies (0.1, 0.2, 0.4, 0.6, 0.8, 1, 2, 3, 4, and 5 Hz) at the four meniscal states (red: intact menisci; yellow: avulsion of the posterior medial meniscus horn; purple: medial meniscectomy; green: total lateral and medial meniscectomy). n = 8.

for the root avulsion state (−15%, Wilcoxon: p = 0.12), the loss factor significantly decreased (Wilcoxon: p < 0.046) by a maximum of −68% for the total meniscectomy state (Wilcoxon: p = 0.028) when compared to the intact state. The loss factor of the total meniscectomy state was always statistically lower (Wilcoxon p = 0.028) than those of any other state. However, there was no loss factor difference for the comparison between the posterior root avulsion and the medial meniscectomy state (Wilcoxon p = 0.054).

3.2 Dynamic Mechanical Analysis

Parametric statistical analyses revealed that knees with an intact meniscus had the highest loss factors, ranging from tan δ = 0.10 to tan δ = 0.15 throughout all investigated frequencies (**Figure 7**). Each consecutive simulated meniscus deterioration lowered the loss factor. Thus, after posterior medial root avulsion, the mean value of the loss factor (tan δ) was reduced by 15%, while medial meniscectomy resulted in a reduction of 24%. The resection of both the lateral and medial menisci resulted in a reduction of 18% compared to the intact meniscus state. When comparing the meniscal states at specific frequencies in detail (**Figure 8**), one-way ANOVA with Duncan post-hoc testing indicated significant differences for the comparisons of the intact state and the medial meniscectomy at 0.1, 0.2, 2, 3, and 4 Hz (p < 0.04) and for the comparisons of the intact meniscus state and the total meniscectomy at 0.2 Hz (p = 0.02).

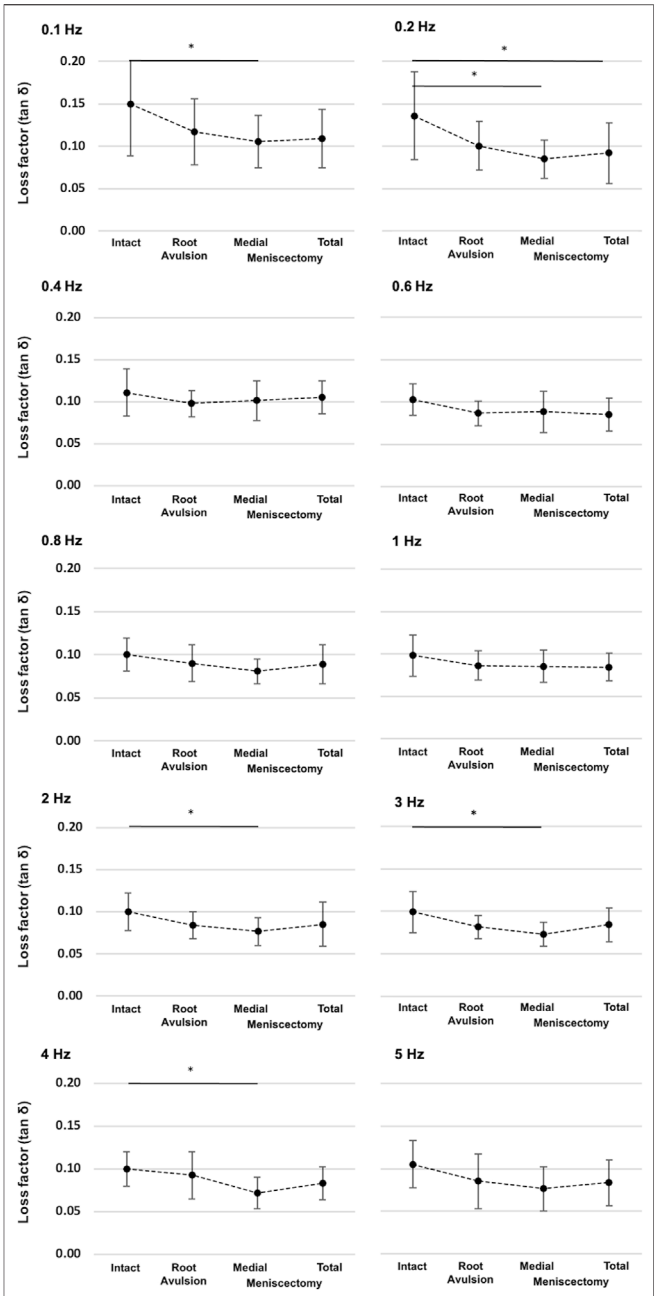

FIGURE 8 | Detailed representation of the loss factor (tan δ) ± SD at the ten investigated frequencies (0.1–5 Hz) and under the four investigated meniscus states: intact, root avulsion at the posterior horn of the medial meniscus, medial meniscectomy, and total lateral and medial meniscectomy. The dotted line indicates the progression of the consecutively investigated meniscus states. *One-way ANOVA with post-hoc Duncan test: *p < 0.05; n = 8.

4 DISCUSSION

In this biomechanical *in vitro* study, we investigated the shock-absorbing potential of the menisci inside porcine knee joints during impact loading and repetitive sinusoidal loads by applying a DMA. The test setup was successfully validated for both

applications. Both during the impact loads and during the DMA analysis, the loss factor (η) and the loss factor (tan δ), respectively, were the highest for the intact meniscus state. During impact loading, the loss factor and, thus, the shock-absorbing potential of the menisci were reduced the more meniscus tissue was resected. Therefore, this study suggests that the menisci contribute to the shock absorption inside porcine knee joints under impact loads. During repetitive sinusoidal loads, the loss factor was lowest for the medial meniscectomy state, followed by the total lateral and medial meniscectomy state. However, both meniscectomy states indicated significantly lower loss factors compared to the intact meniscus state. Hence, it can be concluded that under sinusoidal loads in a frequency range from 0.1 Hz up to 5 Hz, the menisci significantly contribute to the knee joint shock absorption. In summary, the results of the present study suggest that the menisci contribute to the shock absorption during both repetitive and impact loading, refuting our hypothesis.

Hoshino and Wallace (1987) investigated the shock absorption potential of human menisci in 20 knee joints and found a comparable reaction force increase of 21% for the comparison between the intact and the total meniscectomized knee joint. Also, for the root avulsion and medial meniscectomy conditions, our relative values were in a very similar range (108–109%). Regarding the force at the lower sensor (F_2), Hoshino et al. determined forces of up to 1600 N, thus being 400 N higher compared to the F_2 forces of the present study. This might be due to the more pronounced curvature of the porcine tibial, potentially resulting in higher shear forces, which might be transmitted to other joint structures in the porcine knee. Chu et al. (1986) investigated the shock wave propagation during dynamic loading in six human lower limbs using accelerometers and force transducers. They measured an average increase in impulse force of 11% at the tibia and 23% at the femur, after total meniscectomy and removal of the articular cartilage. In the present study, F_2 increased by 24% only after total meniscectomy. In contrast, Chu et al. also removed cartilage structures. Articular cartilage has been shown to possess a 40-times higher complex modulus (E*) (Temple et al., 2016) compared to the menisci (Pereira et al., 2014; Fischenich et al., 2017a). This might be interpreted in a way that the menisci seem to be more responsible for the increased tibial forces in the Chu study (Chu et al., 1986). Therefore, the results of Chu et al. differ by only 1% to the results of the present study. In their work, Kurosawa et al. (1980) examined a total of 14 human knee joints under quasi-static loads of 500, 1,000, and 1,500 N at a loading rate of 5 mm/min. They observed higher energy dissipation in meniscectomized knee joints than intact knee joints at all loading levels. These findings are in contrast to the ones obtained in the present study and to those from Hoshino and Wallace (1987) and Chu et al. (1986). However, compared to the other studies, the transmitted energy during the loading reached only 0.023 J at a load of 1500 N. Thus, the results from Kurosawa are difficult to compare with the present study and are more likely to reflect the energy absorption potential during creep loading of all viscoelastic knee joint structures.

Pereira et al. (2014) investigated in their study the viscoelastic response of isolated human meniscus tissue at a frequency range of 0.1–10 Hz under displacement-controlled conditions. They subdivided the menisci into their anatomical regions (anterior horn, pars intermedia, posterior horn) and determined variations of the loss factor (tan δ) at 1 Hz from 0.12 at the posterior lateral meniscus to 0.18 in the anterior medial meniscus. In accordance to the findings of the present study, Pereira also showed a frequency dependent response: while at low frequencies (0.1–0.6 Hz) high loss factor values (~0.2) and a loss factor minimum at 1 Hz were observed, high frequencies (>3 Hz) again led to high loss factor values. Gaugler et al. (2015) investigated in their study on isolated meniscus tissue both sinusoidal loads at a frequency of 0.1 Hz and impact loads and found loss factors of 0.3 for sinusoidal and 0.17 for impact loads. The findings of our study are within the same range as those from Gaugler et al. and indicate the same ratio when comparing sinusoidal and impact loads. Additionally, Coluccino et al. (2017) investigated the viscoelastic response of bovine meniscus explants and found both similar ranges of the loss factor (tan δ) of, e.g., 0.17 at 0.1 Hz and a similar frequency dependency of the damping response of the meniscus within the range from 0.1 to 5 Hz.

Limitations should be considered when interpreting the results of the present *in vitro* study. First, due to the very good availability and standardized phenotype, we used a porcine knee joint model in our study investigation. Although the porcine knee showed only acceptable appearance congruence for the ACL and lateral menisci (Proffen et al., 2012) and differences in the viscoelastic properties (Sandmann et al., 2013) when compared to the human knee joint, the relative comparisons were in a similar range than those observed in a human cadaver study, both for the impact (Hoshino and Wallace, 1987) and the DMA conditions investigating isolated menisci [tan δ ~ 0.2; (Pereira et al., 2014)]. Furthermore, the test setup provided only one translational degree of freedom in the axial direction. However, during pretests, we experienced significant evasive rotational movement of the porcine knee joint under compressive loads, especially after the two meniscectomy states. In consequence, the obtained shock absorption results were significantly biased by these evasive movements and the resultant influence of the viscoelastic response of the surrounding soft tissues, while providing more physiological degrees of freedom.

5 CONCLUSION AND OUTLOOK

The results of this biomechanical *in vitro* study indicate that the meniscus significantly contributes to the shock absorption of the porcine knee joint both under impact loads and under more moderate, sinusoidal loads at different frequencies. The findings may have an impact on the rehabilitation of young, meniscectomized patients that want to return to sports as soon as possible. Such patients are exposed to critical loads carried by the articular cartilage, when performing shock intensive sports like skiing, volleyball, etc. In summary, a partial meniscectomy leads not only to a reduced tibiofemoral contact area, but also to an inhibited shock-absorbing potential of

the meniscus and, thus, to an increased contact pressure. Consequently, during the meniscectomy procedure, care should be taken to save as much meniscal tissue as possible, underlining the clinical findings to save the meniscus (Lubowitz and Poehling, 2011; Seil and Becker, 2016; Lee et al., 2019; Pujol and Beaufils, 2019)—also from a shock absorption point of view. A meniscus allograft transplantation (MAT) procedure is able to biomechanically restore the injured or (partially) meniscectomized knee joint to the original, healthy state (Koh et al., 2019; Seitz and Durselen, 2019; Zaffagnini et al., 2019). However, not only from a biomechanical point of view, but also from a clinical point of view, especially when patients present persisting post-meniscectomy syndromes, does MAT represent a viable option to decrease pain, improve knee joint function, and, thus, delay the onset of PTOA after meniscus injury (Zaffagnini et al., 2016; De Bruycker et al., 2017).

DATA AVAILABILITY STATEMENT

The raw data supporting the conclusion of this article will be made available by the authors, without undue reservation.

ETHICS STATEMENT

Ethical review and approval was not required for the animal study because the porcine knee joints were received from a local butcher.

AUTHOR CONTRIBUTIONS

AS and JS performed the specimen preparation, data analysis, and statistics. AS drafted the manuscript. DW and LdR conducted the mechanical testing. AI and LD participated in the design and coordination of the study. LD conceived the study. All authors read and approved the final manuscript.

ACKNOWLEDGMENTS

We thank K. Kreienbaum and L. Wächter from the Technische Hochschule Ulm for their technical support and Patrizia Horny from the Institute of Orthopedic Research and Biomechanics Ulm for her art design support.

REFERENCES

Andersson-Molina, H., Karlsson, H., and Rockborn, P. (2002). Arthroscopic Partial and Total Meniscectomy. *Arthrosc. J. Arthroscopic Relat. Surg.* 18, 183–189. doi:10.1053/jars.2002.30435

Andrews, S., Shrive, N., and Ronsky, J. (2011). The Shocking Truth about Meniscus. *J. Biomech.* 44, 2737–2740. doi:10.1016/j.jbiomech.2011.08.026

Badlani, J. T., Borrero, C., Golla, S., Harner, C. D., and Irrgang, J. J. (2013). The Effects of Meniscus Injury on the Development of Knee Osteoarthritis. *Am. J. Sports Med.* 41, 1238–1244. doi:10.1177/0363546513490276

Bansal, S., Floyd, E. R. M., Kowalski, M., Elrod, P., Burkey, K., Chahla, J., et al. (2021). Meniscal Repair: The Current State and Recent Advances in Augmentation. *J. Orthop. Res.* 39, 1368–1382. doi:10.1002/jor.25021

Barton, K. I., Shekarforoush, M., Heard, B. J., Sevick, J. L., Vakil, P., Atarod, M., et al. (2017). Use of Pre-clinical Surgically Induced Models to Understand Biomechanical and Biological Consequences of PTOA Development. *J. Orthop. Res.* 35, 454–465. doi:10.1002/jor.23322

Bodkin, S. G., Werner, B. C., Slater, L. V., and Hart, J. M. (2020). Post-traumatic Osteoarthritis Diagnosed within 5 Years Following ACL Reconstruction. *Knee Surg. Sports Traumatol. Arthrosc.* 28, 790–796. doi:10.1007/s00167-019-05461-y

Buckwalter, J. A., and Brown, T. D. (2004). Joint Injury, Repair, and Remodeling. *Clin. Orthop. Relat. Res.* 423, 7–16. doi:10.1097/01.blo.0000131638.81519.de

Buckwalter, J. A., Saltzman, C., and Brown, T. (2004). The Impact of Osteoarthritis. *Clin. Orthop. Relat. Res.* 427, S6–S15. doi:10.1097/01.blo.0000143938.30681.9d

Carbone, A., and Rodeo, S. (2017). Review of Current Understanding of post-traumatic Osteoarthritis Resulting from Sports Injuries. *J. Orthop. Res.* 35, 397–405. doi:10.1002/jor.23341

Chu, M. L., Yazdani-Ardakani, S., Gradisar, I. A., and Askew, M. J. (1986). An *In Vitro* Simulation Study of Impulsive Force Transmission along the Lower Skeletal Extremity. *J. Biomech.* 19, 979–987. doi:10.1016/0021-9290(86)90115-6

Coluccino, L., Peres, C., Gottardi, R., Bianchini, P., Diaspro, A., and Ceseracciu, L. (2017). Anisotropy in the Viscoelastic Response of Knee Meniscus Cartilage. *J. Appl. Biomater. Funct. Mater.* 15, e77–e83. doi:10.5301/jabfm.5000319

Danion, F., Varraine, E., Bonnard, M., and Pailhous, J. (2003). Stride Variability in Human Gait: the Effect of Stride Frequency and Stride Length. *Gait & Posture* 18, 69–77. doi:10.1016/s0966-6362(03)00030-4

De Bruycker, M., Verdonk, P. C. M., and Verdonk, R. C. (2017). Meniscal Allograft Transplantation: a Meta-Analysis. *SICOT-J* 3, 33. doi:10.1051/sicotj/2017016

Ehrenstein, G. W., Riedel, G., and Trawiel, P. (2004). Dynamic Mechanical Analysis (DMA). *Carl Hanser Verlag Gmbh Co. KG* 1, 236–299. doi:10.3139/9783446434141.006

Englund, M., and Lohmander, L. S. (2004). Risk Factors for Symptomatic Knee Osteoarthritis Fifteen to Twenty-Two Years after Meniscectomy. *Arthritis Rheum.* 50, 2811–2819. doi:10.1002/art.20489

Faul, F., Erdfelder, E., Lang, A.-G., and Buchner, A. (2007). G*Power 3: a Flexible Statistical Power Analysis Program for the Social, Behavioral, and Biomedical Sciences. *Behav. Res. Methods* 39, 175–191. doi:10.3758/bf03193146

Fischenich, K. M., Boncella, K., Lewis, J. T., Bailey, T. S., and Haut Donahue, T. L. (2017a). Dynamic Compression of Human and Ovine Meniscal Tissue Compared with a Potential Thermoplastic Elastomer Hydrogel Replacement. *J. Biomed. Mater. Res.* 105, 2722–2728. doi:10.1002/jbm.a.36129

Fischenich, K. M., Button, K. D., Decamp, C., Haut, R. C., and Donahue, T. L. H. (2017b). Comparison of Two Models of post-traumatic Osteoarthritis; Temporal Degradation of Articular Cartilage and Menisci. *J. Orthop. Res.* 35, 486–495. doi:10.1002/jor.23275

Gaugler, M., Wirz, D., Ronken, S., Hafner, M., Göpfert, B., Friederich, N. F., et al. (2015). Fibrous Cartilage of Human Menisci Is Less Shock-Absorbing and Energy-Dissipating Than Hyaline Cartilage. *Knee Surg. Sports Traumatol. Arthrosc.* 23, 1141–1146. doi:10.1007/s00167-014-2926-4

Gecelter, R. C., Ilyaguyeva, Y., and Thompson, N. E. (2021). The Menisci Are Not Shock Absorbers: A Biomechanical and Comparative Perspective. *Anat. Rec. (Hoboken)* 1, 1. doi:10.1002/ar.24752

Gillquist, J., and Messner, K. (1999). Anterior Cruciate Ligament Reconstruction and the Long Term Incidence of Gonarthrosis. *Sports Med.* 27, 143–156. doi:10.2165/00007256-199927030-00001

Herwig, J., Egner, E., and Buddecke, E. (1984). Chemical Changes of Human Knee Joint Menisci in Various Stages of Degeneration. *Ann. Rheum. Dis.* 43, 635–640. doi:10.1136/ard.43.4.635

Hoshino, A., and Wallace, W. (1987). Impact-absorbing Properties of the Human Knee. *The J. Bone Jt. Surg. Br. volume* 69-B, 807–811. doi:10.1302/0301-620x.69b5.3680348

Intema, F., Hazewinkel, H. A. W., Gouwens, D., Bijlsma, J. W. J., Weinans, H., Lafeber, F. P. J. G., et al. (2010). In Early OA, Thinning of the Subchondral Plate Is Directly Related to Cartilage Damage: Results from a Canine ACLT-Meniscectomy Model. *Osteoarthritis and Cartilage* 18, 691–698. doi:10.1016/j.joca.2010.01.004

Jäger, H., Mastel, R., and Knaebel, M. (2016). *Technische Schwingungslehre.* Wiesbaden: Springer Vieweg.

Kessler, M. A., Glaser, C., Tittel, S., Reiser, M., and Imhoff, A. B. (2006). Volume Changes in the Menisci and Articular Cartilage of Runners. *Am. J. Sports Med.* 34, 832–836. doi:10.1177/0363546505282622

Koh, Y.-G., Lee, J.-A., Kim, Y.-S., and Kang, K.-T. (2019). Biomechanical Influence of Lateral Meniscal Allograft Transplantation on Knee Joint Mechanics during the Gait Cycle. *J. Orthop. Surg. Res.* 14, 300. doi:10.1186/s13018-019-1347-y

Krause, W., Pope, M., Johnson, R., and Wilder, D. (1976). Mechanical Changes in the Knee after Meniscectomy. *J. Bone Jt. Surg.* 58, 599–604. doi:10.2106/00004623-197658050-00003

Kurosawa, H., Fukubayashi, T., and Nakajima, H. (1980). Load-Bearing Mode of the Knee Joint. *Clin. Orthopaedics Relat. Res.* 149, 283–290. doi:10.1097/00003086-198006000-00039

Lee, W. Q., Gan, J. Z., and Lie, D. T. T. (2019). Save the Meniscus - Clinical Outcomes of Meniscectomy versus Meniscal Repair. *J. Orthop. Surg. (Hong Kong)* 27, 2309499019849813. doi:10.1177/2309499019849813

Lohmander, L. S., Englund, P. M., Dahl, L. L., and Roos, E. M. (2007). The Long-Term Consequence of Anterior Cruciate Ligament and Meniscus Injuries. *Am. J. Sports Med.* 35, 1756–1769. doi:10.1177/0363546507307396

Lubowitz, J. H., and Poehling, G. G. (2011). Save the Meniscus. *Arthrosc. J. Arthroscopic Relat. Surg.* 27, 301–302. doi:10.1016/j.arthro.2010.12.006

Maher, S. A., Wang, H., Koff, M. F., Belkin, N., Potter, H. G., and Rodeo, S. A. (2017). Clinical Platform for Understanding the Relationship between Joint Contact Mechanics and Articular Cartilage Changes after Meniscal Surgery. *J. Orthop. Res.* 35, 600–611. doi:10.1002/jor.23365

Majewski, M., Susanne, H., and Klaus, S. (2006). Epidemiology of Athletic Knee Injuries: A 10-year Study. *The Knee* 13, 184–188. doi:10.1016/j.knee.2006.01.005

Mccann, L., Ingham, E., Jin, Z., and Fisher, J. (2009). Influence of the Meniscus on Friction and Degradation of Cartilage in the Natural Knee Joint. *Osteoarthritis and Cartilage* 17, 995–1000. doi:10.1016/j.joca.2009.02.012

Mcdermott, I. D., and Amis, A. A. (2006). The Consequences of Meniscectomy. *J. Bone Jt. Surg. Br. volume* 88-B, 1549–1556. doi:10.1302/0301-620x.88b12.18140

Mcdermott, I. D., Masouros, S. D., and Amis, A. A. (2008). Biomechanics of the Menisci of the Knee. *Curr. Orthopaedics* 22, 193–201. doi:10.1016/j.cuor.2008.04.005

Mcdermott, I. (2011). Meniscal Tears, Repairs and Replacement: Their Relevance to Osteoarthritis of the Knee. *Br. J. Sports Med.* 45, 292–297. doi:10.1136/bjsm.2010.081257

Muthuri, S. G., Mcwilliams, D. F., Doherty, M., and Zhang, W. (2011). History of Knee Injuries and Knee Osteoarthritis: a Meta-Analysis of Observational Studies. *Osteoarthritis and Cartilage* 19, 1286–1293. doi:10.1016/j.joca.2011.07.015

Pereira, H., Caridade, S. G., Frias, A. M., Silva-Correia, J., Pereira, D. R., Cengiz, I. F., et al. (2014). Biomechanical and Cellular Segmental Characterization of Human Meniscus: Building the Basis for Tissue Engineering Therapies. *Osteoarthritis and Cartilage* 22, 1271–1281. doi:10.1016/j.joca.2014.07.001

Proffen, B. L., Mcelfresh, M., Fleming, B. C., and Murray, M. M. (2012). A Comparative Anatomical Study of the Human Knee and Six Animal Species. *The Knee* 19, 493–499. doi:10.1016/j.knee.2011.07.005

Pujol, N., and Beaufils, P. (2019). Save the Meniscus Again!. *Knee Surg. Sports Traumatol. Arthrosc.* 27, 341–342. doi:10.1007/s00167-018-5325-4

Rai, M. F., Brophy, R. H., and Sandell, L. J. (2019). Osteoarthritis Following Meniscus and Ligament Injury: Insights from Translational Studies and Animal Models. *Curr. Opin. Rheumatol.* 31, 70–79. doi:10.1097/bor.0000000000000566

Ratcliffe, R. J., and Holt, K. G. (1997). Low Frequency Shock Absorption in Human Walking. *Gait & Posture* 5, 93–100. doi:10.1016/s0966-6362(96)01077-6

Ridley, T. J., Mccarthy, M. A., Bollier, M. J., Wolf, B. R., and Amendola, A. (2017). Age Differences in the Prevalence of Isolated Medial and Lateral Meniscal Tears in Surgically Treated Patients. *Iowa Orthop. J.* 37, 91–94.

Roos, E. M., Roos, H. P., and Lohmander, L. S. (1999). WOMAC Osteoarthritis Index-additional Dimensions for Use in Subjects with post-traumatic Osteoarthritis of the Knee. *Osteoarthritis and Cartilage* 7, 216–221. doi:10.1053/joca.1998.0153

Roos, H., Lauren, M. r., Adalberth, T., Roos, E. M., Jonsson, K., and Lohmander, L. S. (1998). Knee Osteoarthritis after Meniscectomy: Prevalence of Radiographic Changes after Twenty-One Years, Compared with Matched Controls. *Arthritis Rheum.* 41, 687–693. doi:10.1002/1529-0131(199804)41:4<687::aid-art16>3.0.co;2-2

Salata, M. J., Gibbs, A. E., and Sekiya, J. K. (2010). A Systematic Review of Clinical Outcomes in Patients Undergoing Meniscectomy. *Am. J. Sports Med.* 38, 1907–1916. doi:10.1177/0363546510370196

Sandmann, G. H., Adamczyk, C., Garcia, E. G., Doebele, S., Buettner, A., Milz, S., et al. (2013). Biomechanical Comparison of Menisci from Different Species and Artificial Constructs. *BMC Musculoskelet. Disord.* 14, 324. doi:10.1186/1471-2474-14-324

Schwer, J., Rahman, M. M., Stumpf, K., Rasche, V., Ignatius, A., Dürselen, L., et al. (2020). Degeneration Affects Three-Dimensional Strains in Human Menisci: *In Situ* MRI Acquisition Combined with Image Registration. *Front. Bioeng. Biotechnol.* 8, 582055. doi:10.3389/fbioe.2020.582055

Seil, R., and Becker, R. (2016). Time for a Paradigm Change in Meniscal Repair: Save the Meniscus!. *Knee Surg. Sports Traumatol. Arthrosc.* 24, 1421–1423. doi:10.1007/s00167-016-4127-9

Seitz, A. M., and Dürselen, L. (2019). Biomechanical Considerations Are Crucial for the success of Tendon and Meniscus Allograft Integration-A Systematic Review. *Knee Surg. Sports Traumatol. Arthrosc.* 27, 1708–1716. doi:10.1007/s00167-018-5185-y

Seitz, A. M., Galbusera, F., Krais, C., Ignatius, A., and Dürselen, L. (2013). Stress-relaxation Response of Human Menisci under Confined Compression Conditions. *J. Mech. Behav. Biomed. Mater.* 26, 68–80. doi:10.1016/j.jmbbm.2013.05.027

Seitz, A. M., Lubomierski, A., Friemert, B., Ignatius, A., and Dürselen, L. (2012). Effect of Partial Meniscectomy at the Medial Posterior Horn on Tibiofemoral Contact Mechanics and Meniscal Hoop Strains in Human Knees. *J. Orthop. Res.* 30, 934–942. doi:10.1002/jor.22010

Seitz, A. M., Osthaus, F., Schwer, J., Warnecke, D., Faschingbauer, M., Sgroi, M., et al. (2021). Osteoarthritis-Related Degeneration Alters the Biomechanical Properties of Human Menisci before the Articular Cartilage. *Front. Bioeng. Biotechnol.* 9, 659989. doi:10.3389/fbioe.2021.659989

Simoni, L., Scarton, A., Macchi, C., Gori, F., Pasquini, G., and Pogliaghi, S. (2021). Quantitative and Qualitative Running Gait Analysis through an Innovative Video-Based Approach. *Sensors* 21, 1. doi:10.3390/s21092977

Snoeker, B. A. M., Bakker, E. W. P., Kegel, C. A. T., and Lucas, C. (2013). Risk Factors for Meniscal Tears: a Systematic Review Including Meta-Analysis. *J. Orthop. Sports Phys. Ther.* 43, 352–367. doi:10.2519/jospt.2013.4295

Sukopp, M., Schall, F., Hacker, S. P., Ignatius, A., Dürselen, L., and Seitz, A. M. (2021). Influence of Menisci on Tibiofemoral Contact Mechanics in Human Knees: A Systematic Review. *Front. Bioeng. Biotechnol.* 9, 1. doi:10.3389/fbioe.2021.765596

Taylor, W. R., Ehrig, R. M., Heller, M. O., Schell, H., Seebeck, P., and Duda, G. N. (2006). Tibio-femoral Joint Contact Forces in Sheep. *J. Biomech.* 39, 791–798. doi:10.1016/j.jbiomech.2005.02.006

Temple, D. K., Cederlund, A. A., Lawless, B. M., Aspden, R. M., and Espino, D. M. (2016). Viscoelastic Properties of Human and Bovine Articular Cartilage: a Comparison of Frequency-dependent Trends. *BMC Musculoskelet. Disord.* 17, 419. doi:10.1186/s12891-016-1279-1

Thomas, A. C., Hubbard-Turner, T., Wikstrom, E. A., and Palmieri-Smith, R. M. (2017). Epidemiology of Posttraumatic Osteoarthritis. *J. Athl Train.* 52, 491–496. doi:10.4085/1062-6050-51.5.08

Tibesku, C. O., Mastrokalos, D. S., Jagodzinski, M., and Pässler, H. H. (2004). [MRI Evaluation of Meniscal Movement and Deformation *In Vivo* under Load Bearing Condition]. *Sportverletz Sportschaden* 18, 68–75. doi:10.1055/s-2004-813001

Voloshin, A. S., and Wosk, J. (1983). Shock Absorption of Meniscectomized and Painful Knees: a Comparative *In Vivo* Study. *J. Biomed. Eng.* 5, 157–161. doi:10.1016/0141-5425(83)90036-5

Wachsmuth, L., Keiffer, R., Juretschke, H.-P., Raiss, R. X., Kimmig, N., and Lindhorst, E. (2003). *In Vivo* contrast-enhanced Micro MR-Imaging of Experimental Osteoarthritis in the Rabbit Knee Joint at 7.1T11This Work Is Supported by BMBF, Leitprojekt Osteoarthrose. *Osteoarthritis and Cartilage* 11, 891–902. doi:10.1016/j.joca.2003.08.008

Weigel, D. P., and Marsh, J. L. (2002). High-energy Fractures of the Tibial Plateau. *The J. Bone Jt. Surgery-American Volume* 84, 1541–1551. doi:10.2106/00004623-200209000-00006

Winter, D. A. (1983). Energy Generation and Absorption at the Ankle and Knee during Fast, Natural, and Slow Cadences. *Clin. Orthopaedics Relat. Res.* 175, 147–154. doi:10.1097/00003086-198305000-00021

Yeh, P. C., Starkey, C., Lombardo, S., Vitti, G., and Kharrazi, F. D. (2012). Epidemiology of Isolated Meniscal Injury and its Effect on Performance in Athletes from the National Basketball Association. *Am. J. Sports Med.* 40, 589–594. doi:10.1177/0363546511428601

Zaffagnini, S., Di Paolo, S., Stefanelli, F., Dal Fabbro, G., Macchiarola, L., Lucidi, G. A., et al. (2019). The Biomechanical Role of Meniscal Allograft Transplantation and Preliminary *In-Vivo* Kinematic Evaluation. *J. Exp. Ortop* 6, 27. doi:10.1186/s40634-019-0196-2

Zaffagnini, S., Grassi, A., Marcheggiani Muccioli, G. M., Benzi, A., Serra, M., Rotini, M., et al. (2016). Survivorship and Clinical Outcomes of 147 Consecutive Isolated or Combined Arthroscopic Bone Plug Free Meniscal Allograft Transplantation. *Knee Surg. Sports Traumatol. Arthrosc.* 24, 1432–1439. doi:10.1007/s00167-016-4035-z

Conflict of Interest: The authors declare that the research was conducted in the absence of any commercial or financial relationships that could be construed as a potential conflict of interest.

frontiers in Bioengineering and Biotechnology

ORIGINAL RESEARCH
published: 21 March 2022
doi: 10.3389/fbioe.2022.835730

A Morphological Study of the Meniscus, Cartilage and Subchondral Bone Following Closed-Joint Traumatic Impact to the Knee

T. L. Haut Donahue[1], G. E. Narez[2], M. Powers[2], L. M. Dejardin[3], F. Wei[4] and R. C. Haut[4]*

[1]Department of Biomedical Engineering, University of Memphis, Memphis, TN, United States, [2]Department of Biomedical Engineering, University of Massachusetts Amherst, Amherst, MA, United States, [3]Department of Small Animal Clinical Sciences, Michigan State University, East Lansing, MI, United States, [4]Orthopaedic Biomechanics Laboratories, College of Osteopathic Medicine, Michigan State University, East Lansing, MI, United States

Post-traumatic osteoarthritis (PTOA) is a debilitating disease that is a result of a breakdown of knee joint tissues following traumatic impact. The interplay of how these tissues influence each other has received little attention because of complex interactions. This study was designed to correlate the degeneration of the menisci, cartilage and subchondral bone following an acute traumatic event that resulted in anterior cruciate ligament (ACL) and medial meniscus tears. We used a well-defined impact injury animal model that ruptures the ACL and tears the menisci. Subsequently, the knee joints underwent ACL reconstruction and morphological analyses were performed on the menisci, cartilage and subchondral bone at 1-, 3- and 6-months following injury. The results showed that the morphological scores of the medial and lateral menisci worsened with time, as did the tibial plateau and femoral condyle articular cartilage scores. The medial meniscus was significantly correlated to the medial tibial subchondral bone at 1 month (p = 0.01), and to the medial tibial cartilage at 3 months (p = 0.04). There was only one significant correlation in the lateral hemijoint, i.e., the lateral tibial cartilage to the lateral tibial subchondral bone at 6 months (p = 0.05). These data may suggest that, following trauma, the observed medial meniscal damage should be treated acutely by means other than a full or partial meniscectomy, since that procedure may have been the primary cause of degenerative changes in the underlying cartilage and subchondral bone. In addition to potentially treating meniscal damage differently, improvements could be made in optimizing treatment of acute knee trauma.

Keywords: impact injury, meniscus, cartilage, subchondral bone, knee

OPEN ACCESS

Edited by:
Nicola Francesco Lopomo, University of Brescia, Italy

Reviewed by:
Matteo Berni, Rizzoli Orthopedic Institute (IRCCS), Italy
Gregorio Marchiori, Rizzoli Orthopedic Institute (IRCCS), Italy

****Correspondence:***
T. L. Haut Donahue
thdonahu@gmail.com

Specialty section:
This article was submitted to Biomechanics, a section of the journal Frontiers in Bioengineering and Biotechnology

Received: *14 December 2021*
Accepted: *22 February 2022*
Published: *21 March 2022*

Citation:
Haut Donahue TL, Narez GE, Powers M, Dejardin LM, Wei F and Haut RC (2022) A Morphological Study of the Meniscus, Cartilage and Subchondral Bone Following Closed-Joint Traumatic Impact to the Knee. Front. Bioeng. Biotechnol. 10:835730. doi: 10.3389/fbioe.2022.835730

INTRODUCTION

Menisci are fibrocartilaginous tissues in the knee joint that aid in load distribution and act to protect the underlying articular cartilage from excessive joint loads. Menisci are frequently torn either in isolated injuries or in combination with damage to the anterior cruciate ligament (ACL). It is well documented that following traumatic damage to the ACL and meniscus, 78–83% of patients will develop post-traumatic osteoarthritis (PTOA) 10–14 years post-injury, regardless of treatment modality (surgical reconstruction or conservative interventions) (Fink et al., 2001; von Porat

et al., 2004). More recently, clinical studies have indicated that PTOA can develop as early as 3 years post-injury (Whittaker et al., 2015; Wang et al., 2020).

Knee PTOA is a disease that affects all tissues within the joint including menisci, articular cartilage, subchondral bone, synovium, fat pad and ligaments. The interplay of these tissues and how they affect each other is difficult to study and hence has received limited attention to date. In the Framingham OA study of 913 knees, meniscal damage in a given location was associated with higher regional tibial subchondral bone mineral density (BMD) (Lo et al., 2008). Human clinical studies have shown that there is a strong association between meniscal damage and cartilage loss (Hunter et al., 2006; Sharma et al., 2008), with less meniscal coverage and lower meniscal height increasing the risk of cartilage loss. Few studies, however, have analyzed all three major tissues in the joint, i.e., menisci, cartilage and subchondral bone, and investigated how the degree of degradation correlates with the development of osteoarthritis in the joint.

We have developed a closed-joint impact injury animal model that mimics the clinical development of PTOA following a traumatic insult. This model has been used to document the natural history of PTOA following closed-joint trauma (Fischenich et al., 2015; Pauly et al., 2015; Fischenich et al., 2017a). This model demonstrates degradative changes in the material properties of the menisci, articular cartilage and bone. These changes in our model include increased cartilage fissuring, decreased glycosaminoglycan content in both the cartilage and meniscus, as well as decreases in bone volume (BV) and BMD. However, the previous studies using our model did not attempt to correlate the degradation of the menisci, cartilage and subchondral bone to each other. More recently, our closed-joint impact injury model was combined with surgical reconstruction of the ACL (Narez et al., 2021a; Wei et al., 2021; Wei et al., 2022). Despite reconstruction of the ACL, decreases in the material properties of the menisci and the articular cartilage were still present, but minimal changes were documented in subchondral bone quality and morphometry. Again, there was no attempt to correlate the changes in the subchondral bone to those in the menisci or articular cartilage.

The goals of the current study were to document the degree of damage to menisci, cartilage and subchondral bone in a closed-joint impact injury animal model with ACL surgical reconstruction and determine if there was a potential correlation between the degree of damage in these joint tissues. It was hypothesized there would be a correlation between the level of meniscal degeneration with both the underlying cartilage and the subchondral bone within a given hemijoint.

METHODS

All animal procedures for this study were approved by the Institutional Animal Care and Use Committee at Michigan State University (IACUC #05/16-073–00 and #PROTO201900255). Eighteen skeletally mature Flemish Giant rabbits (6.34 ± 0.75 kg, aged 6–9 months) were held in individual cages (32 × 32 × 28 in). The animals, a mix of male (n = 10) and female (n = 8), were anesthetized using standard protocols including 2% isoflurane in oxygen. The right hindlimb of each rabbit was shaved to expose the knee joint. The animals were then positioned into a rigid custom fixture in a servo-hydraulic testing system (Instron Corp, Norwood, MA) (**Figure 1**) (Isaac et al., 2010a; Fischenich et al., 2015; Pauly et al., 2015; Fischenich et al., 2017a; Fischenich et al., 2017b; Narez et al., 2021a; Wei et al., 2021; Wei et al., 2022). Using controlled impact with a 400 N preload, the actuator compressed the tibia downward 3.5 mm. This motion resulted in an anterior drawer of the knee where the tibia moved anteriorly with respect to the femur, causing ACL rupture. An auto-stop program was developed and used so that the test stopped automatically when there was an approximately 330 N load drop within 30 ms, which was indicative of a soft tissue (ACL) failure. ACL failure was confirmed by a board-certified veterinary surgeon (LMD) *via* a manual anterior drawer test of the joint. Force, time and displacement data were collected at 5 kHz. The left knee served as a contralateral control. We have previously shown that this impact injury animal model more closely mimics the clinical scenario following ACL rupture than the commonly used ACL surgical transection model, exhibiting many characteristics seen in human PTOA patients (Fischenich et al., 2017b). These animals were part of a much larger study with a total of 96 rabbits that investigated the efficacy of a surgical intervention and a pharmaceutical intervention in mitigating post-traumatic osteoarthritis (Narez et al., 2021a; Narez et al., 2021b; Wei et al., 2021; Narez et al., 2022; Wei et al., 2022). An animal model was necessary to recreate a true ACL/meniscus longitudinal injury study. Animals smaller than a rabbit often develop a calcified meniscus at an early age, hence the choice of the lapine model. The minimum number of animals was used

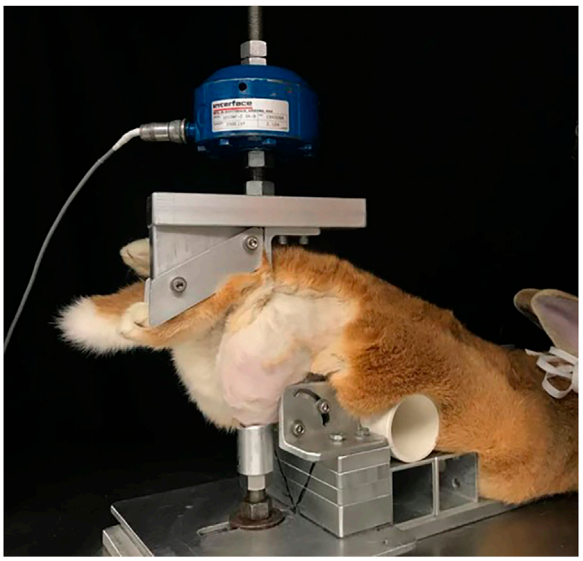

FIGURE 1 | Injurious impact of rabbit knee set-up. In prone position (belly down) the rabbit's hind paw was supported directly below the actuator of a servo-hydraulic machine. The knee was supported to prevent lateral and medial motion (with permission from Narez et al., 2021a).

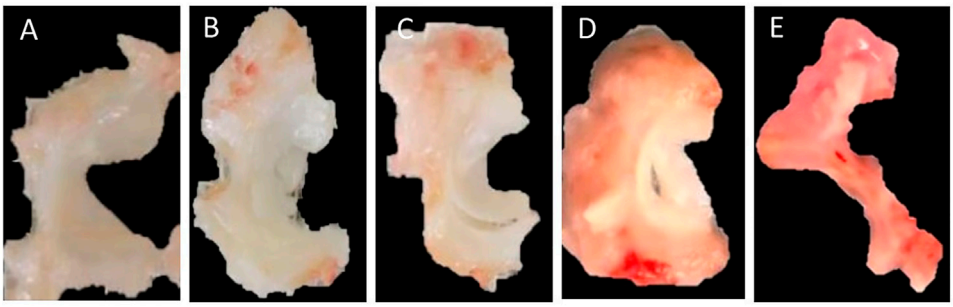

FIGURE 2 | Morphological scoring of the meniscus. **(A)** 0 = normal, **(B)** 1 = surface fibrillation, **(C)** 2 = undisplaced tears, **(D)** 3 = displaced tears, **(E)** 4 = tissue maceration.

such that a reasonable power (80%) was still obtained. No inhumane procedures were applied to the animals and they all experienced regular gait within 3 days after the intervention. Hence, this animal study fits the 3R's principle (Hubrecht and Carter, 2019).

Approximately 2 weeks post-impact, a board-certified veterinary surgeon (LMD), performed a reconstruction of the torn ACL (Wei et al., 2021). Through a medial parapatellar arthrotomy, the condition of the ACL and meniscus was examined in more detail. If meniscal damage was evident, it was noted and treated with a partial or full meniscectomy. For a partial meniscectomy, only the injured or torn regions were removed. For extensive damage to the meniscus, a full meniscectomy was performed where the entire damaged medial meniscus was removed. Following meniscal debridement, to repair the torn ACL, the musculotendinous junction of the semitendinosus tendon (ST) was transected leaving the tibial attachment intact. At the ACL footprint, a 2.7 mm diameter tibial bone tunnel and a 3.2 mm diameter femoral tunnel were drilled. The ST free end was passed under the medial collateral ligament and through the tunnels via a suture loop. Tension was applied to the ST as it was secured to the femoral bone tunnel with a custom PEEK interference fit screw. To ensure the joint's stability, post-reconstruction, an anterior drawer test was performed on the reconstructed knee. Postoperatively, the animals were monitored by a licensed veterinary nurse and randomly assigned to one of 3 groups. Rabbits were euthanized at 1-, 3- or 6-months post-trauma, with $n = 6$ in each time-point group. These timepoints were chosen to correspond to what others have done in the literature studying PTOA (Coleman et al., 2018; Lisee et al., 2021). Based on our previous studies using this animal model, and evaluation of mechanical properties of the cartilage and meniscus, an n = 6 in each group provides 80% power in the study (Narez et al., 2021a; Wei et al., 2022).

MORPHOLOGY ANALYSIS

Meniscus

Following euthanasia, morphology grading of meniscal tissues was conducted by four separate blinded graders using a scoring system used by previous studies (Matyas et al., 2004; Pauli et al., 2011; Fischenich et al., 2014; Narez et al., 2021a). Each region of the meniscus (anterior, central and posterior) was scored. However, due to the fact that some knees had partial or full meniscectomies, regions were averaged to create one score for the lateral meniscus and one score for the medial meniscus. For both menisci, a score of 0 indicated normal tissue, a score of 1 indicated surface fibrillation, a score of 2 indicated un-displaced tears, a score of 3 indicated displaced tears, and a score of 4 indicated tissue maceration (**Figure 2**).

Cartilage Morphological Assessment

Morphology of the articular cartilage was assessed within 2 h following euthanasia. The surfaces of the tibial plateau and femoral condyles were stained with India ink to highlight surface fissures and other tissue irregularities. A blind morphological assessment (Yoshioka et al., 1996) was conducted by three independent graders with the following numerical grading scale: 1 = intact cartilage with the surface appearing normal, 2 = a few surface lesions that retained ink, 3 = moderate fibrillation retaining intense black patches of ink and 4 = full thickness erosion exposing underlying subchondral bone (**Figure 3**).

Subchondral Bone

Following euthanasia, bones were placed into a 10% neutral-buffered formalin solution. The limbs were decalcified in a 10% formic acid solution and sectioned to isolate regions of interest. The femoral condyles were sectioned along the parasagittal plane, passing through the medial and lateral condyles in a crani-caudal orientation, while the tibia was sectioned in the frontal plane, just anterior to the midline of the tibial plateau. Samples were processed, paraffin-embedded and sectioned at 7 μm. Sections were deparaffinized and stained with Hematoxylin, Saf-O and FG. Slides were imaged with a bright field microscope (Leica Microsystems Inc., Buffalo Grove, IL) and an Olympus DP25 camera (Olympus, Center Valley, PA). Three blind graders evaluated the subchondral bone morphology, using an OARSI score. Scores were reported and averaged before statistical analysis occurred. Scoring: 0 = normal, 1 = small spaces <50% of the length of condyle or plateau, 2 = Moderate spaces/some splits <50% of the length, 3 = moderate spaces/splits >50% of the

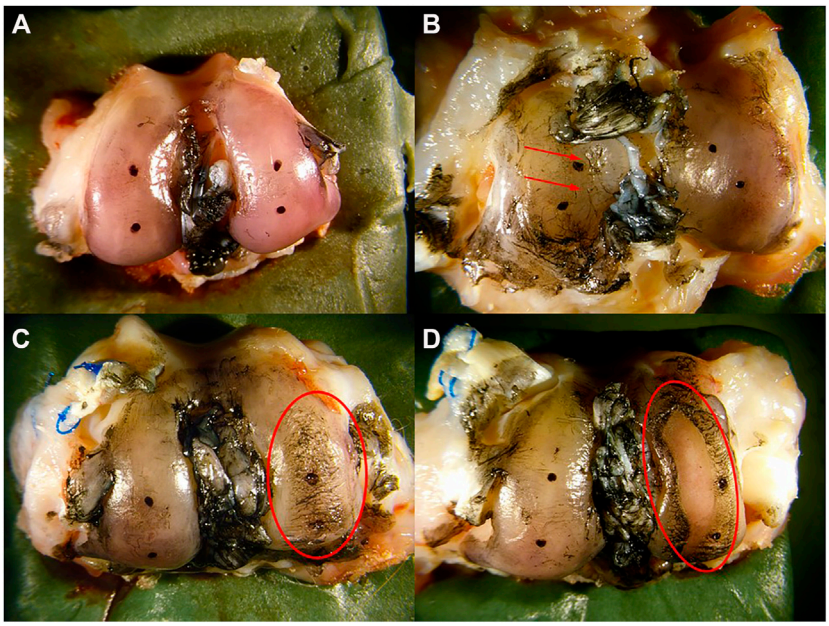

FIGURE 3 | Morphological scoring of cartilage. **(A)** intact cartilage with the surface appearing normal was assigned a score of 1, **(B)** a few surface lesions (red arrows) that retain ink was assigned a score of 2, **(C)** moderate fibrillation retaining intense black patches of ink (red circle) was assigned a score of 3, and **(D)** full thickness erosion exposing underlying bone (red circle) was assigned a score of 4.

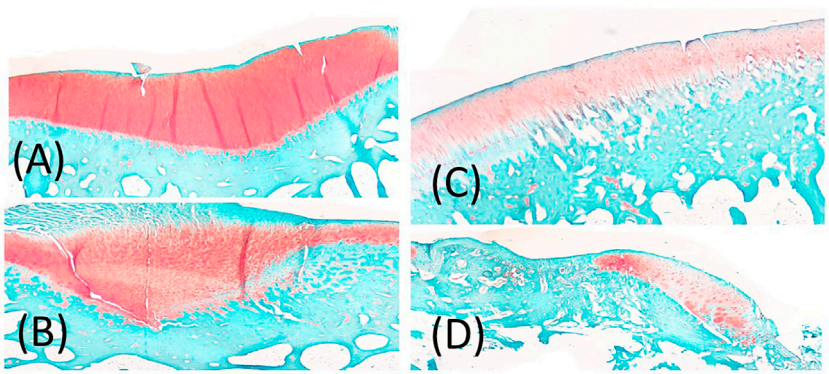

FIGURE 4 | (A) representation of Score 1 = small spaces <50% of the length of condyle or plateau, **(B)** representation of 2 or 3 score depending on 2 = Moderate spaces/some splits <50% of the length, 3 = moderate spaces/splits >50% of the length, **(C)** 4 = numerous splits <50% of the length, **(D)** 5 = numerous splits >50% of the length.

length, 4 = numerous splits <50% of the length, 5 = numerous splits >50% of the length (Gerwin et al., 2010) (**Figure 4**).

Statistical Analysis

Comparisons were only made within a hemijoint, not across hemijoints. Spearman Rank correlations were made between a) medial meniscus and medial cartilage of the tibial plateau, b) medial meniscus and medial cartilage of the femoral condyle, c) medial meniscus and medial tibial plateau subchondral bone, d) medial meniscus and medial femoral condyle subchondral bone, e) medial cartilage of the tibia and the medial tibial plateau subchondral bone, f) medial femoral cartilage and subchondral bone, g) lateral meniscus and lateral cartilage of the tibial plateau, h) lateral meniscus and lateral cartilage of the femoral condyle, i) lateral meniscus and the lateral tibial plateau subchondral bone, j) lateral meniscus and the lateral femoral condyle subchondral bone, k) lateral tibial plateau cartilage and subchondral bone, l) lateral femoral condyle cartilage and subchondral bone, m) lateral tibial cartilage and lateral femoral cartilage, and n) medial tibial cartilage and medial femoral cartilage. These correlations were made at 1, 3 and 6 months for a total of 42 correlations. Statistical significance was set as p-value <0.05.

TABLE 1 | Average morphological scores for all tissues studied.

	1 month	3 months	6 months
Medial Meniscus (scored 0–3)	2.19 ± 0.61	2.51 ± 0.45	2.49 ± 0.32
Lateral Meniscus (scored 0–3)	1.21 ± 0.27	2.04 ± 0.50	2.22 ± 0.29
Medial Tibial Plateau Cartilage (scored 1–4)	3.03 ± 0.17	3.77 ± 0.15	3.85 ± 0.15
Lateral Tibial Plateau Cartilage (scored 1–4)	3.18 ± 0.36	3.41 ± 0.35	3.79 ± 0.21
Medial Femoral Condyle Cartilage (scored 1–4)	2.93 ± 0.34	3.34 ± 0.34	3.53 ± 0.38
Lateral Femoral Condyle Cartilage (scored 1–4)	1.98 ± 0.33	2.07 ± 0.36	2.46 ± 0.36
Medial Tibial Plateau Subchondral Bone (scored 0–5)	1.50 ± 1.03	2.88 ± 1.56	2.13 ± 0.75
Lateral Tibial Plateau Subchondral Bone (scored 0–5)	2.25 ± 0.50	2.18 ± 1.14	1.43 ± 0.69
Medial Femoral Condyle Subchondral Bone (scored 0–5)	1.08 ± 0.30	2.79 ± 0.90	2.00 ± 1.78
Lateral Femoral Condyle Subchondral Bone (scored 0–5)	1.79 ± 0.51	1.46 ± 0.95	1.50 ± 0.64

TABLE 2 | Statistical values for all correlations between menisci, cartilage and subchondral bone for all comparisons at 1 month (mon), 3 and 6 months.

	Lateral meniscus	Medial meniscus	Lateral tibial cartilage	Medial tibial cartilage	Lateral femoral cartilage	Medial femoral cartilage
Lateral tibial cartilage	1 mon $p = 0.12$ 3 mon $p = 0.09$ 6 mon $p = 0.33$	N/A	N/A	N/A	See Other	N/A
Lateral femoral cartilage	1 mon $p = 0.07$ 3 mon $p = 0.39$ 6 mon $p = 0.11$	N/A	1 mon $p = 0.21$ 3 mon $p = 0.35$ 6 mon $p = 0.14$	N/A	N/A	N/A
Lateral tibial bone	1 mon $p = 0.25$ 3 mon $p = 0.21$ 6 mon $p = 0.09$	N/A	1 mon $p = 0.20$ 3 mon $p = 0.38$ **6 mon $p = 0.05$**	N/A	N/A	N/A
Lateral femoral bone	1 mon $p = 0.36$ 3 mon $p = 0.30$ 6 mon $p = 0.35$	N/A	N/A	N/A	1 mon $p = 0.15$ 3 mon $p = 0.15$ 6 mon $p = 0.10$	N/A
Medial tibial cartilage	N/A	1 mon $p = 0.39$ **3 mon $p = 0.04$** 6 mon $p = 0.09$	N/A	N/A	N/A	See Other
Medial femoral cartilage	N/A	1 mon $p = 0.10$ 3 mon $p = 0.13$ 6 mon $p = 0.13$	N/A	1 mon $p = 0.13$ 3 mon $p = 0.48$ **6 mon p = 0.02**	N/A	N/A
Medial tibial bone	N/A	**1 mon p = 0.01** 3 mon $p = 0.21$ 6 mon $p = 0.38$	N/A	1 mon $p = 0.38$ 3 mon $p = 0.39$ 6 mon $p = 0.10$	N/A	N/A
Medial femoral bone	N/A	1 mon $p = 0.19$ 3 mon $p = 0.19$ 6 mon $p = 0.33$	N/A	N/A	N/A	1 mon $p = 0.31$ 3 mon $p = 0.28$ 6 mon $p = 0.21$

Bolded values represent significant correlations between row and column.

RESULTS

All animals experienced ACL failure and were reconstructed. Of the 18 rabbits enrolled in the study, three rabbits had a full medial meniscectomy and 7 received a partial medial meniscectomy based on the level of damage observed in the medial meniscus. None of the animals had lateral meniscal damage that was noted during surgical reconstruction of the joint. The average morphological scores for the medial and lateral hemijoints, meniscus, femoral and tibial cartilage as well as tibial plateau and femoral condyle subchondral bone are presented in **Table 1**. Both the medial and lateral menisci tended to worsen with time, and the medial scores were higher than lateral scores. It is important to note that the lateral menisci had no indication of damage during reconstructive surgery, so the damage that developed to raise the scores over 6 months developed after reconstructive surgery. A similar trend was seen for the medial and lateral, tibial plateau and femoral condyle cartilage. Scores worsened with time, with 6 months scores being the highest. The subchondral bone of the tibial plateau and femoral condyles did not worsen with time and tended to show no consistent trends.

Of the 42 possible correlations, only 4 were significant (**Table 2**). The medial meniscus was significantly correlated to the medial tibial subchondral bone at 1 month ($p = 0.01$) and the medial meniscus was significantly correlated to the medial tibial cartilage at 3 months ($p = 0.04$). There was only one significant correlation in the lateral hemijoint, the lateral tibial cartilage to the lateral tibial subchondral

bone at 6 months ($p = 0.05$). The medial tibial cartilage significantly correlated to medial femoral cartilage at 6 months.

DISCUSSION

The study showed that significant correlations occurred between 1) the tibial plateau subchondral bone and cartilage in the lateral hemijoint, and 2) between the meniscus and tibial cartilage in the medial hemijoint, 3) between the meniscus and tibial subchondral bone in the medial hemijoint, and 4) between femoral and tibial cartilage in the medial hemijoint. There were no significant correlations between the femoral condyle cartilage and femoral subchondral bone. Hence, in the medial hemijoint, when the meniscus was damaged, the cartilage and subchondral bone were also significantly damaged as early as 1 month. This finding confirms that the menisci likely play a significant role in protecting the cartilage and bone (Fox et al., 2012; Abusara et al., 2018). However, in the lateral compartment, where no meniscal damage was noted during reconstructive surgery, no strong association between the meniscus and either the articular cartilage and underlying subchondral bone damage was noted. Interestingly, at later time points (6 months), the lateral tibial cartilage and tibial plateau bone were correlated. While there was no significant damage acutely to the lateral meniscus, morphological score worsened with time. We hypothesize that perhaps there was either a change in joint kinematics following reconstruction that affected the lateral compartment, or the medial meniscus damage changed the loading in the lateral hemijoint resulting in increased damage. Future studies will need to further investigate possible causes for this result.

Few studies have previously attempted to document correlations between the integrity of the three tissues studied here; meniscus, cartilage and subchondral bone. One previous study, using magnetic resonance imaging did show that meniscal extrusion predicts increases in subchondral bone lesions, expansion of subchondral bone and bone cysts, and is associated with decreases in tibial articular cartilage volume as well as increases in tibial plateau area (Wang et al., 2010). That study, however, did not report the degree of degeneration of the main body of the meniscus, only that it was extruded. Meniscal extrusion has also been associated with the development of osteophytes (Miller et al., 1997; Lerer et al., 2004). While these studies are interesting, they do not report the cause of meniscal extrusion, whether it be due to meniscal attachment laxity or degenerative changes in the main body of the meniscus.

Previous studies using the same animals as in this current study documented changes in the histological and biomechanical behavior of the cartilage, meniscus and bone (Narez et al., 2021a; Wei et al., 2022). Compared to their contralateral controls, reconstructed limbs showed osteoarthritic changes to both the lateral and the medial menisci, articular cartilage and subchondral bone as early as 1-month post-trauma. The degeneration progressed in all tissues over time up to 6-months. Overall, the medial compartments had more tissue damage than their corresponding lateral counterparts. The damage that was present in these rabbits mimics clinical observations of patients suffering ACL injury and undergoing reconstruction (Felson, 2004; Goldring and Goldring, 2016). There were overall decreases in the cartilage fiber modulus and matrix modulus, and an increase in the cartilage tissue permeability when comparing the reconstructed to the control limbs. Decreases in both the instantaneous and equilibrium modulus were documented in both menisci. Minimal changes were found in bone quality and morphometry; however, bones from the reconstructed limbs showed large volumes of osteophyte formations, with an increase in volume over time. (Narez et al., 2021a; Wei et al., 2022). The reconstructed limbs demonstrated increases in cartilage fissuring and subchondral bone spaces or splits, as well as decreases in cartilage glycosaminoglycan (GAG) staining and tidemark integrity, therefore generally exhibiting more tissue damage than their contralateral control limbs. The analyses of the subchondral bone thickness (SCBT) showed a general trend of thickening of the underlying bone following ACL injury and reconstruction at all three time-points (except for the lateral compartments of the femur and tibia at 6-months), with a significant increase of the SCBT in the medial compartment of the tibia at 6-months post-trauma. GAG coverage analyses found a significant decrease in coverage of the medial meniscus at the 1- month time point. In the lateral meniscus, there was a documented decrease in coverage at both 3 and 6-months. Cortical and trabecular microstructure worsened in the reconstructed limbs with time compared to contralateral limbs. These data indicate that reconstruction alone does not prevent osteoarthritic changes. Taken together with the data from this study correlating the cartilage, menisci and bone morphology, it is likely that there is a complex interplay amongst joint tissues and future work should investigate all joint tissues in a PTOA study and attempt to elude the starting point of damage to explore targeting early interventions to slow or prevent the onset and progression of PTOA.

The importance of subchondral bone in the development of OA has been well characterized in a review by (Li et al., 2013). This review documents the commonly seen subchondral bone sclerosis as a hallmark of OA in addition to microdamage, bone marrow edema-like lesions and bone cysts. Lacourt et al., 2012 studied the relationship between cartilage and subchondral bone in a racehorse model that is a natural model of repetitive trauma-induced osteoarthritis (Lacourt et al., 2012). While that study showed that cartilage damage was associated with bone degeneration, the meniscus was not investigated. In a guinea pig model of spontaneous OA, Zamli et al., 2014 showed that subchondral bone thickening preceded chondrocyte apoptosis and cartilage degradation (Zamli et al., 2014). Wang et al., 2013 showed that subchondral bone changes (i.e., increased thickness, bone mineral density and a decrease in porosity) occurred prior to cartilage degeneration (Wang et al., 2013). While these studies suggest that subchondral bone changes precede cartilage changes in spontaneous OA (Wang et al., 2013; Zamli et al., 2014), which tissue is first affected and potentially induces pathological changes in other joint structures after acute trauma has yet to be elucidated. If the order or sequence of degeneration were

known, better therapeutic interventions could be investigated, improving the outcome of ACL replacement surgery or joint treatment following a traumatic impact event.

The current study strongly suggested that 1) early meniscal damage in the medial hemijoint resulted in subsequent damage to the medial cartilage and underlying tibial subchondral bone and 2) early medial meniscal damage likely affected the lateral hemijoint. Our model delivered a single injurious impact to the knee joint that resulted in ACL failure and either no or partial medial meniscal damage. Based on observable structural damage, partial or full medial meniscectomy was performed at the time of ACL reconstructive surgery. Degenerative changes in the medial meniscus, femoral and tibial articular cartilage and subchondral bone were correlated in a first attempt to help understand potential relationships between these three joint tissues after a single blunt joint impact. The study was limited by the fact that not all animals had meniscal damage requiring a meniscectomy and by the relatively small sample size (n = 6) in each group. Another limitation is that we did not apply a fixed pre-tension to the ACL reconstruction in the current study. However, clinically a fixed pre-tension is not used, and further, the pre-tension of the native tissue is not known, so what pre-tension to use remains unclear. Despite these limitations, these data suggested that, following trauma, the observed medial meniscal damage should be treated acutely by means other than a full or partial meniscectomy, since that procedure may have been the primary cause of degenerative changes in the underlying cartilage and subchondral bone. In fact, a clinical study confirms that repairs of meniscal damage are more favorable than meniscectomies (Lutz et al., 2015). Meniscal repair and substitution are becoming more commonplace and future research should continue to optimize these techniques (Paxton et al., 2011; Zaffagnini et al., 2011). Additionally, perhaps other improvements that aim to optimize acute knee trauma should be explored, such as treatment with Poloxamer 188 (P188) which acts to reseal cell membranes following traumatic rupture (Serbest et al., 2006; Natoli and Athanasiou, 2008; PascualGarrido et al., 2009; Bajaj et al., 2010; Isaac et al., 2010b; Coatney et al., 2015; Narez et al., 2021b). And yet, the current study also showed degenerative changes in the lateral cartilage and underlying bone without early observed damage to the overlying lateral meniscus post-trauma. Thus, while PTOA in the joint was likely induced by structural tissue changes in the medial hemijoint, there were likely other pathological processes at play.

DATA AVAILABILITY STATEMENT

The original contributions presented in the study are included in the article/Supplementary Material, further inquiries can be directed to the corresponding author.

ETHICS STATEMENT

The animal study was reviewed and approved by the Institutional Animal Care and Use Committee at Michigan State University (IACUC #05/16-073-00 and #PROTO201900255).

AUTHOR CONTRIBUTIONS

GN, FW, and MP oversaw data collection and analysis, and compiled all data. LD carried out all animal surgeries FW, RH and TH designed the study and oversaw all work. TH prepared the manuscript. All authors reviewed and edited the manuscript. All authors have read and approved the final submitted manuscript.

FUNDING

Research reported in this publication was supported by the U.S. Department of Defense under Grant Numbers W81XWH-16-1-0734 and W81XWH-16-1-0735.

ACKNOWLEDGMENTS

The authors would like to acknowledge Clifford Beckett and Patrick Vaughn for technical support, and Dr. Maria Dolores Porcel Sanchez and Heather DeFore for surgical assistance during this study.

REFERENCE

Abusara, Z., Andrews, S. H. J., von Kossel, M., and Herzog, W. (2018). Menisci Protect Chondrocytes from Load-Induced Injury. *Sci. Rep.* 8 (1), 1–11. doi:10.1038/s41598-018-32503-1

Bajaj, S., Shoemaker, T., Hakimiyan, A. A., Rappoport, L., Pascual-Garrido, C., Oegema, T. R., et al. (2010). Protective Effect of P188 in the Model of Acute Trauma to Human Ankle Cartilage: The Mechanism of Action. *J. Orthop. Trauma* 24 (9), 571–576. doi:10.1097/BOT.0b013e3181ec4712

Coatney, G. A., Abraham, A. C., Fischenich, K. M., Button, K. D., Haut, R. C., and Haut Donahue, T. L. (2015). Efficacy of P188 on Lapine Meniscus Preservation Following Blunt Trauma. *J. Mech. Behav. Biomed. Mater.* 47, 57–64. doi:10.1016/j.jmbbm.2015.03.008

Coleman, M. C., Goetz, J. E., Brouillette, M. J., Seol, D., Willey, M. C., Petersen, E. B., et al. (2018). Targeting Mitochondrial Responses to Intra-Articular Fracture to Prevent Posttraumatic Osteoarthritis. *Sci. Transl. Med.* 10 (427), eaan5372. doi:10.1126/SCITRANSLMED.AAN5372

Felson, D. T. (2004). An Update on the Pathogenesis and Epidemiology of Osteoarthritis. *Radiologic Clin. North America* 42 (1), 1–9. doi:10.1016/s0033-8389(03)00161-1

Fink, C., Hoser, C., Hackl, W., Navarro, R. A., and Benedetto, K. P. (2001). Long-Term Outcome of Operative or Nonoperative Treatment of Anterior Cruciate Ligament Rupture -Is Sports Activity a Determining Variable? *Int. J. Sports Med.* 22 (4), 304–309. doi:10.1055/s-2001-13823

Fischenich, K. M., Button, K. D., Coatney, G. A., Fajardo, R. S., Leikert, K. M., Haut, R. C., et al. (2015). Chronic Changes in the Articular Cartilage and Meniscus Following Traumatic Impact to the Lapine Knee. *J. Biomech.* 48 (2), 246–253. doi:10.1016/j.jbiomech.2014.11.038

Fischenich, K. M., Button, K. D., DeCamp, C., Haut, R. C., Donahue, T. L. H., and Donahue, H. (2017). Comparison of Two Models of Post-Traumatic Osteoarthritis; Temporal Degradation of Articular Cartilage and Menisci. *J. Orthop. Res.* 35 (3), 486–495. doi:10.1002/JOR.23275

Fischenich, K. M., Coatney, G. A., Haverkamp, J. H., Button, K. D., DeCamp, C., Haut, R. C., et al. (2014). Evaluation of Meniscal Mechanics and Proteoglycan Content in a Modified Anterior Cruciate Ligament Transection Model. *J. biomechanical Eng.* 136 (7), 0710011–0710018. doi:10.1115/1.4027468

Fischenich, K. M., Pauly, H. M., Button, K. D., Fajardo, R. S., DeCamp, C. E., Haut, R. C., et al. (2017). A Study of Acute and Chronic Tissue Changes in Surgical and Traumatically-Induced Experimental Models of Knee Joint Injury Using Magnetic Resonance Imaging and Micro-Computed Tomography. *Osteoarthritis and Cartilage* 25 (4), 561–569. doi:10.1016/j.joca.2016.10.010

Fox, A. J. S., Bedi, A., and Rodeo, S. A. (2012). The Basic Science of Human Knee Menisci. *Sports Health* 4 (4), 340–351. doi:10.1177/1941738111429419

Gerwin, N., Bendele, A. M., Glasson, S., and Carlson, C. S. (2010). The OARSI Histopathology Initiative - Recommendations for Histological Assessments of Osteoarthritis in the Rat. *Osteoarthritis and cartilage* 18 (Suppl. 3), S24–S34. doi:10.1016/J.JOCA.2010.05.030

Goldring, S. R., and Goldring, M. B. (2016). Changes in the Osteochondral Unit during Osteoarthritis: Structure, Function and Cartilage-Bone Crosstalk. *Nat. Rev. Rheumatol.* 12 (11), 632–644. doi:10.1038/NRRHEUM.2016.148

Hubrecht, R. C., and Carter, E. (2019). The 3Rs and Humane Experimental Technique: Implementing Change. *Animals* 9 (10), 754. doi:10.3390/ANI9100754

Hunter, D. J., Zhang, Y. Q., Niu, J. B., Tu, X., Amin, S., Clancy, M., et al. (2006). The Association of Meniscal Pathologic Changes with Cartilage Loss in Symptomatic Knee Osteoarthritis. *Arthritis Rheum.* 54 (3), 795–801. doi:10.1002/ART.21724

Isaac, D. I., Golenberg, N., and Haut, R. C. (2010). Acute Repair of Chondrocytes in the Rabbit Tibiofemoral Joint Following blunt Impact Using P188 Surfactant and a Preliminary Investigation of its Long-Term Efficacy. *J. Orthop. Res.* 28 (4), 553–558. doi:10.1002/jor.21022

Isaac, D. I., Meyer, E. G., and Haut, R. C. (2010). Development of a Traumatic Anterior Cruciate Ligament and Meniscal Rupture Model with a Pilot *In Vivo* Study. *J. biomechanical Eng.* 132 (6), 064501. doi:10.1115/1.4001111

Lacourt, M., Gao, C., Li, A., Girard, C., Beauchamp, G., Henderson, J. E., et al. (2012). Relationship between Cartilage and Subchondral Bone Lesions in Repetitive Impact Trauma-Induced Equine Osteoarthritis. *Osteoarthritis and Cartilage* 20, 572–583. doi:10.1016/j.joca.2012.02.004

Lerer, D. B., Umans, H. R., Hu, M. X., and Jones, M. H. (2004). The Role of Meniscal Root Pathology and Radial Meniscal Tear in Medial Meniscal Extrusion. *Skeletal Radiol.* 33 (10), 569–574. doi:10.1007/s00256-004-0761-2

Li, G., Yin, J., Gao, J., Cheng, T. S., Pavlos, N. J., Zhang, C., et al. (2013). Subchondral Bone in Osteoarthritis: Insight into Risk Factors and Microstructural Changes. *Arthritis Res. Ther.* 15 (6), 223. Available at: http://arthritis-research.com/content/15/6/223. doi:10.1186/ar4405

Lisee, C., Spang, J. T., Loeser, R., Longobardi, L., Lalush, D., Nissman, D., et al. (2021). Tibiofemoral Articular Cartilage Composition Differs Based on Serum Biochemical Profiles Following Anterior Cruciate Ligament Reconstruction. *Osteoarthritis and cartilage* 29 (12), 1732–1740. doi:10.1016/J.JOCA.2021.09.005

Lo, G. H., Niu, J., McLennan, C. E., Kiel, D. P., McLean, R. R., Guermazi, A., et al. (2008). Meniscal Damage Associated with Increased Local Subchondral Bone Mineral Density: A Framingham Study. *Osteoarthritis and Cartilage* 16 (2), 261–267. doi:10.1016/J.JOCA.2007.07.007

Lutz, C., Dalmay, F., Ehkirch, F.-P., Cucurulo, T., Laporte, C., Le Henaff, G., et al. (2015). Meniscectomy Versus Meniscal Repair: 10years Radiological and Clinical Results in Vertical Lesions in Stable Knee. *Orthopaedics Traumatol. Surg. Res.* 101 (8), S327–S331. doi:10.1016/J.OTSR.2015.09.008

Matyas, J. R., Atley, L., Ionescu, M., Eyre, D. R., and Poole, A. R. (2004). Analysis of Cartilage Biomarkers in the Early Phases of Canine Experimental Osteoarthritis. *Arthritis Rheum.* 50 (2), 543–552. doi:10.1002/art.20027

Miller, T. T., Staron, R. B., Feldman, F., and Çepel, E. (1997). Meniscal Position on Routine MR Imaging of the Knee. *Skeletal Radiol.* 26, 424–427. doi:10.1007/s002560050259

Narez, G. E., Brown, G., Herrick, A., Ek, R. J., Dejardin, L., Wei, F., et al. (2021). Assessment of Changes in the Meniscus and Subchondral Bone in a Novel Closed-Joint Impact and Surgical Reconstruction Lapine Model. *J. Biomech.* 126, 110630. doi:10.1016/J.JBIOMECH.2021.110630

Narez, G. E., Brown, G., Herrick, A., Ek, R. J., Dejardin, L., Wei, F., et al. (2022). Evaluating the Efficacy of Combined P188 Treatment and Surgical Intervention in Preventing Post-Traumatic Osteoarthritis Following a Traumatic Knee Injury. *J. Biomech. Eng.* 144 (4), 041003. doi:10.1115/1.4052564

Narez, G. E., Wei, F., Dejardin, L., Haut, R. C., and Haut Donahue, T. L. (2021). A Single Dose of P188 Prevents Cell Death in Meniscal Explants Following Impact Injury. *J. Mech. Behav. Biomed. Mater.* 117, 104406. doi:10.1016/j.jmbbm.2021.104406

Natoli, R. M., and Athanasiou, K. A. (2008). P188 Reduces Cell Death and IGF-I Reduces GAG Release Following Single-Impact Loading of Articular Cartilage. *J. Biomech. Eng.* 130 (4), 41012. doi:10.1115/1.2939368

Pascual Garrido, C., Hakimiyan, A. A., Rappoport, L., Oegema, T. R., Wimmer, M. A., and Chubinskaya, S. (2009). Anti-Apoptotic Treatments Prevent Cartilage Degradation after Acute Trauma to Human Ankle Cartilage. *Osteoarthritis and Cartilage* 17 (9), 1244–1251. doi:10.1016/j.joca.2009.03.007

Pauli, C., Grogan, S. P., Patil, S., Otsuki, S., Hasegawa, A., Koziol, J., et al. (2011). Macroscopic and Histopathologic Analysis of Human Knee Menisci in Aging and Osteoarthritis. *Osteoarthritis and Cartilage* 19 (9), 1132–1141. doi:10.1016/j.joca.2011.05.008

Pauly, H. M., Larson, B. E., Coatney, G. A., Button, K. D., DeCamp, C. E., Fajardo, R. S., et al. (2015). Assessment of Cortical and Trabecular Bone Changes in Two Models of Post-Traumatic Osteoarthritis. *J. Orthop. Res.* 33 (12), 1835–1845. doi:10.1002/jor.22975

Paxton, E. S., Stock, M. V., and Brophy, R. H. (2011). Meniscal Repair Versus Partial Meniscectomy: A Systematic Review Comparing Reoperation Rates and Clinical Outcomes. *Arthrosc. J. Arthroscopic Relat. Surg.* 27 (9), 1275–1288. doi:10.1016/J.ARTHRO.2011.03.088

Serbest, G., Horwitz, J., Jost, M., and Barbee, K. A. (2006). Mechanisms of Cell Death and Neuroprotection by Poloxamer 188 after Mechanical Trauma. *FASEB j.* 20 (2), 308–310. doi:10.1096/fj.05-4024fje

Sharma, L., Eckstein, F., Song, J., Guermazi, A., Prasad, P., Kapoor, D., et al. (2008). Relationship of Meniscal Damage, Meniscal Extrusion, Malalignment, and Joint Laxity to Subsequent Cartilage Loss in Osteoarthritic Knees. *Arthritis Rheum.* 58 (6), 1716–1726. doi:10.1002/art.23462

von Porat, A., Roos, E. M., and Roos, H. (2004). High Prevalence of Osteoarthritis 14 Years after an Anterior Cruciate Ligament Tear in Male Soccer Players: A Study of Radiographic and Patient Relevant Outcomes. *Ann. Rheum. Dis.* 63 (3), 269–273. doi:10.1136/ard.2003.008136

Wang, L.-J., Zeng, N., Yan, Z.-P., Li, J.-T., and Ni, G.-X. (2020). Post-Traumatic Osteoarthritis Following ACL Injury. *Arthritis Res. Ther.* 22, 57. doi:10.1186/s13075-020-02156-5

Wang, T., Wen, C.-Y., Yan, C.-H., Lu, W.-W., and Chiu, K.-Y. (2013). Spatial and Temporal Changes of Subchondral Bone Proceed to Microscopic Articular Cartilage Degeneration in Guinea Pigs with Spontaneous Osteoarthritis. *Osteoarthritis and Cartilage* 21, 574–581. doi:10.1016/j.joca.2013.01.002

Wang, Y., Wluka, A. E., Pelletier, J. P., Martel-Pelletier, J., Abram, F., Ding, C., et al. (2010). Meniscal Extrusion Predicts Increases in Subchondral Bone Marrow Lesions and Bone Cysts and Expansion of Subchondral Bone in Osteoarthritic Knees. *Rheumatology* 49 (5), 997–1004. doi:10.1093/rheumatology/keq034

Wei, F., Haut Donahue, T., Haut, R. C., Porcel Sanchez, M. D., and Dejardin, L. M. (2021). Reconstruction of the Cranial Cruciate Ligament Using a Semitendinosus Autograft in a Lapine Model. *Vet. Surg.* 50 (6), 1326–1337. doi:10.1111/vsu.13643

Wei, F., Powers, M. J. F., Narez, G. E., Dejardin, L. M., Haut Donahue, T., and Haut, R. C. (2022). Post-Traumatic Osteoarthritis in Rabbits Following Traumatic Injury and Surgical Reconstruction of the Knee. *Ann. Biomed. Eng.* 50, 169–182. doi:10.1007/S10439-022-02903-6

Whittaker, J. L., Woodhouse, L. J., Nettel-Aguirre, A., and Emery, C. A. (2015). Outcomes Associated with Early Post-Traumatic Osteoarthritis and Other Negative Health Consequences 3-10 Years Following Knee Joint Injury in Youth Sport. *Osteoarthritis and Cartilage* 23 (7), 1122–1129. doi:10.1016/J.JOCA.2015.02.021

Yoshioka, M., Coutts, R. D., Amiel, D., and Hacker, S. A. (1996). Characterization of a Model of Osteoarthritis in the Rabbit Knee. *Osteoarthritis and Cartilage* 4 (2), 87–98. doi:10.1016/s1063-4584(05)80318-8

Zaffagnini, S., Marcheggiani Muccioli, G. M., Lopomo, N., Bruni, D., Giordano, G., Ravazzolo, G., et al. (2011). Prospective Long-Term Outcomes of the Medial Collagen Meniscus Implant Versus Partial Medial Meniscectomy. *Am. J. Sports Med.* 39 (5), 977–985. doi:10.1177/0363546510391179

Zamli, Z., Robson Brown, K., Tarlton, J. F., Adams, M. A., Torlot, G. E., Cartwright, C., et al. (2014). Subchondral Bone Plate Thickening Precedes Chondrocyte Apoptosis and Cartilage Degradation in Spontaneous Animal Models of Osteoarthritis. *Biomed. Res. Int.* 2014, 1–10. doi:10.1155/2014/606870

Conflict of Interest: The authors declare that the research was conducted in the absence of any commercial or financial relationships that could be construed as a potential conflict of interest.

Publisher's Note: All claims expressed in this article are solely those of the authors and do not necessarily represent those of their affiliated organizations, or those of the publisher, the editors, and the reviewers. Any product that may be evaluated in this article, or claim that may be made by its manufacturer, is not guaranteed or endorsed by the publisher.

Advantages of publishing in Frontiers

OPEN ACCESS
Articles are free to read for greatest visibility and readership

FAST PUBLICATION
Around 90 days from submission to decision

HIGH QUALITY PEER-REVIEW
Rigorous, collaborative, and constructive peer-review

TRANSPARENT PEER-REVIEW
Editors and reviewers acknowledged by name on published articles

Frontiers
Avenue du Tribunal-Fédéral 34
1005 Lausanne | Switzerland

Visit us: www.frontiersin.org
Contact us: frontiersin.org/about/contact

REPRODUCIBILITY OF RESEARCH
Support open data and methods to enhance research reproducibility

DIGITAL PUBLISHING
Articles designed for optimal readership across devices

FOLLOW US
@frontiersin

IMPACT METRICS
Advanced article metrics track visibility across digital media

EXTENSIVE PROMOTION
Marketing and promotion of impactful research

LOOP RESEARCH NETWORK
Our network increases your article's readership